

**RHEOLOGICAL BEHAVIOR OF
NANOCRYSTALLINE/SUBMICRON CERAMIC
POWDER DISPERSIONS**

**A Thesis Submitted to
the Graduate School of Engineering and Sciences of
İzmir Institute of Technology
in Partial Fulfillment of the Requirements for the Degree of**

DOCTOR OF PHILOSOPHY

in Chemical Engineering

**by
Özlem Çağlar DUVARCI**

February, 2009

We approve the thesis of Özlem Çağlar DUVARCI

Prof. Dr. Muhsin ÇİFTÇİOĞLU
Supervisor

Prof. Dr. Devrim BALKÖSE
Committee Member

Prof. Dr. Mustafa DEMİRCİOĞLU
Committee Member

Assoc. Prof. Dr. Funda TIHMINLIOĞLU
Committee Member

Assoc. Prof. Dr. Sedat AKKURT
Committee Member

12 February 2009

Prof. Dr. Devrim BALKÖSE
Head of the Chemical Engineering
Department

Prof. Dr. Hasan BÖKE
Dean of the Graduate School of
Engineering and Science

ACKNOWLEDGEMENT

Sincere gratitude is expressed to my advisor, Prof. Dr. Muhsin Çiftçiođlu, for providing the opportunity to research on such an important subject, rheology, and his inexhaustible effort in advising, ideas and the guidance in the preparation of this manuscript. I would like to acknowledge the Head of Chemical Engineering Department, Prof. Dr. Devrim Balköse for her support at the beginning and during my PhD education. I would like to express my gratitude to Prof. Dr. Mustafa Demirciođlu, Assoc. Prof. Dr. Funda Tıhmınlıođlu, and Assoc. Prof. Dr. Sedat Akkurt for their precious contributions. I ought to thank to Assoc. Prof. Dr. Erol Őeker for supplying me data analysis software. I would like to thank to Melek Malkoç for her precious help in purchasing the Rheometer and technical support she provided.

Special thanks to my colleagues and roommates Yelda Akdeniz , Filiz Ömürlü and Berna Topuz for their interest, contributions, sincere friendship, and endless understanding at desperate times. I would like to thank to Deniz ŐimŐek for his precious contributions, time saving advices, and friendship. I am very grateful to Nesrin Tatlıdil for her sincere friendship and support. Without them, I'm sure my thesis would not have been completed in such an enjoyable or efficient manner.

I would like to express my gratitude to all members of my family, for their patience, understanding, and support all throughout the study. My special thanks to my husband, Yavuz Duvarcı, and my mother, Sabahat Çađlar for their encouragement and patient devotion.

ABSTRACT

RHEOLOGICAL BEHAVIOR OF NANOCRYSTALLINE/SUBMICRON CERAMIC POWDER DISPERSIONS

Several rheometric techniques were applied to submicron and nano ceramic powder dispersions systematically in this study. The rheological behavior of the dispersions was determined by steady shear and dynamic shear rheology. Dynamic shear rheological techniques are scarcely used for the characterization of ceramic powder dispersions contrary to polymers.

The flow behaviors of the submicron and nano dispersions were found to be dependent on the solids content and fructose concentration. The submicron alumina, nano alumina, and nano titania dispersions in fructose solution showed shear thinning behavior and were fitted to the Herschel-Bulkley model.

The dynamic shear rheology measurements showed that the solid part of the dispersions was dominant over the liquid part for both submicron and nano powder dispersions. The elastic modulus was higher than the viscous modulus in stress and frequency sweep measurements. The elastic moduli of the dispersions with solids content lower than 40 vol% were dependent on the angular frequency which indicated a gel-like behavior. However, the elastic moduli of the dispersions with 40 vol% solids were independent of angular frequency which indicated a solid like behavior. Further increase in fructose content had significant effects on both steady shear and dynamic shear rheological behavior of the dispersions regardless of particle size. The submicron and nano ceramic powder dispersions can be prepared by using fructose for the regulation of the rheological behavior of ceramic powder dispersions. The characterization of powder surfaces is essential for the effective adsorption of fructose.

ÖZET

NANOKRİSTAL/MİKRONALTI SERAMİK TOZ DAĞITIMLARININ REOLOJİK DAVRANIŞI

Nano ve mikronaltı seramik toz dağıtımlarına çeşitli reometrik teknikler sistematik olarak uygulanmıştır. Dağıtımların reolojik davranışı, kararlı kayma ve dinamik kayma reolojisi ile belirlenmiştir. Dinamik kayma reolojik teknikler seramik toz dağıtımlarının karakterizasyonunda polimerlerin aksine kullanılmıştır.

Mikronaltı ve nano dağıtımların akma davranışları katı içeriğine ve früktoz konsantrasyonuna bağlı olduğu görülmüştür. Früktoz solüsyonunda mikronaltı ve nano alüminyum oksit ve nano titan dağıtımların kayma incelen davranışı göstermiş ve Herschel-Bulkley modeline uymuştur.

Dinamik kayma reolojisi ölçümleri hem mikronaltı hem de nano toz dağıtımlarında katı kısmının sıvı kısmına göre daha baskın olduğunu göstermiştir. Gerilim ve frekans tarama testlerinde, elastik modül, akma modülünden daha yüksektir. Hacimsel katı içeriği %'si 40'dan az olan dağıtımların elastik modülleri açısal frekansa bağlıdır, bu da jel gibi bir davranışa işaret etmektedir. Ancak, hacimsel katı içeriği %40 olan dağıtımların elastik modülü açısal frekanstan bağımsız olup katı gibi bir davranışa işaret etmektedir. Früktoz konsantrasyonunun fazla artışı hem yatışkan hem de dinamik kayma reolojisinin parçacık boyutuna bağlı olmaksızın önemli ölçüde etkilemiştir. Mikronaltı ve nano seramik toz dağıtımlarının hazırlanmasında, seramik toz dağıtımlarının reolojik davranışının ayarlanması için früktoz kullanılabilir. Tozların yüzey karakterizasyonu früktozun etkili adsorpsiyonunda esastır.

TABLE OF CONTENTS

LIST OF TABLES.....	ix
LIST OF FIGURES.....	x
LIST OF SYMBOLS/ABBREVIATIONS.....	xvi
CHAPTER 1. INTRODUCTION.....	1
CHAPTER 2. CERAMIC POWDER DISPERSIONS.....	4
2.1. The Use of Saccharides as Dispersant in Ceramic Powder Dispersions.....	18
2.1.1. Monosaccharides.....	19
2.1.2. Adsorption Mechanism of Monosaccharides.....	21
CHAPTER 3. RHEOLOGICAL BEHAVIOR OF DISPERSIONS.....	23
3.1. The Types of Rheometers.....	41
3.2. Sources of Error in Rheological Experiments.....	43
3.3. Recent Studies on the Rheological Behavior of Ceramic Dispersions.....	45
CHAPTER 4. EXPERIMENTAL STUDY.....	52
4.1. Powder Preparation.....	52
4.2. Specifications of Materials.....	53
4.3. Preparation of Dispersions.....	54
4.4. Characterization Methods.....	54
4.4.1. Rheological Methods.....	55
4.4.2. Consolidation of Submicron Alumina and Nano Alumina Dispersions.....	56
4.4.3. The FTIR study of Submicron Alumina, Nano Alumina and Nano Titania Dispersions.....	57

CHAPTER 5. RESULTS AND DISCUSSION.....	59
5.1. The Characterization of the Materials.....	59
5.2. The Techniques for Rheological Measurements of the Dispersions.....	83
5.2.1. The Effect of Successive Experiments on Thixotropy of the Dispersions.....	87
5.3. Rheological Measurements of the Fructose Solutions.....	89
5.4. The Rheological Behavior of Submicron Alumina Dispersions.....	92
5.4.1. The Effect of Solids Content and Fructose Concentration on the Steady Shear Rheology of the Submicron Alumina Dispersions.....	92
5.4.2. The Effect of Solids Content and Fructose on the Dynamic Shear Rheology of the Submicron Alumina Dispersions.....	100
5.4.2.1. The Effect of Preshear on the Determination of LVER of the Submicron Alumina Dispersions.....	100
5.5. The Rheological Behavior of Nano Alumina Dispersions.....	113
5.5.1. The Effect of Solids Content and Fructose Concentration on the Steady Shear Rheology of the Nano Alumina Dispersions.....	113
5.5.2. The Effect of Solids Content and Fructose on the Dynamic Shear Rheology of the Nano Alumina Dispersions.....	120
5.6. The Rheological Behavior of Nano Titania Dispersions.....	125
5.6.1. The Effect of Solids Content and Fructose Concentration on the Steady Shear Rheology of the Nano Titania Dispersions.....	126
5.6.2. The Effect of Solids Content and Fructose on the Dynamic Shear Rheology of the Nano Titania Dispersions.....	138
5.7. The Comparison of Dynamic Shear Rheological Behavior Submicron Alumina, Nano Alumina and Nano Titania Dispersions.....	147

5.8. The Densification Behavior of Freeze Dried Submicron Alumina and Nano Alumina Dispersion	150
CHAPTER 6. CONCLUSION	156
REFERENCES	160
APPENDICES	165
APPENDIX A. IMPORTANT PARAMETERS IN RHEOLOGICAL MEASUREMENTS OF CERAMIC POWDER DISPERSION	165
APPENDIX B. THE RHEOLOGICAL BEHAVIOR OF SUBMICRON ALUMINA DISPERSIONS	170
APPENDIX C. THE RHEOLOGICAL BEHAVIOR OF NANO ALUMINA DISPERSIONS	194
APPENDIX D. THE RHEOLOGICAL BEHAVIOR OF NANO TITANIA DISPERSIONS	218

LIST OF TABLES

<u>Table</u>	<u>Page</u>
Table 2.1. Nonretarded Hamaker Constants for Ceramic Materials Interacting under Vacuum and across Water at 298 K [Lewis, 2000].	6
Table 2.2. General information on commonly known sugars	19
Table 3.1. Rheological models relating shear stress and shear rate [Hunter, 2000].	29
Table 4.1. The specification of the powders used in the thesis	53
Table 4.2. The conditions of the rheological tests	56
Table 5.1. The location of the IR peaks of D-fructose and related functional groups [Ibrahim et. al. 2006]	80
Table 5.2. The calculated thixotropic areas of 25 vol% α -Al ₂ O ₃ in 1.3 wt% fructose solution.	89
Table 5.3. The viscosities, Reynolds Number at 100 and 200 1/s, and the data consistency of Newtonian model of Fructose Solutions	90
Table 5.4. The model parameters of Herschel-Bulkley Model ($\tau = \tau_o + K\dot{\gamma}^n$) calculated for the submicron alumina dispersions.	94
Table 5.5. The model parameters of Herschel-Bulkley Model ($\tau = \tau_o + K\dot{\gamma}^n$) calculated for the nano alumina dispersions.	114
Table 5.6. The model parameters of Herschel-Bulkley Model ($\tau = \tau_o + K\dot{\gamma}^n$) calculated for the nano titania dispersions without pH adjustment	127
Table 5.7. The model parameters of Herschel-Bulkley Model ($\tau = \tau_o + K\dot{\gamma}^n$) calculated for the nano titania dispersions with pH adjustment	128
Table 5.8. The green body and sintered body densities of submicron and nano alumina	150

LIST OF FIGURES

<u>Figure</u>	<u>Page</u>
Figure 2.1. Schematic illustration of the forces defined in the DLVO theory with respect to particle separation.....	5
Figure 2.2. The schematic representation of the electrical double layer around negatively charged particle.....	7
Figure 2.3. The DLVO curve for two charged particles approaching to each other.....	8
Figure 2.4. Schematic illustration between suspension microstructure and interparticle forces.....	9
Figure 2.5. Schematic illustration of two particles covered by polymer layer resulted in a repulsive force.....	11
Figure 2.6. Schematic illustration of electrosteric stabilization: (a) charged particles with nonionic polymers; (b) polyelectrolytes attached to uncharged particles.....	12
Figure 2.7. Representative schematic illustration of nanoparticle haloing behavior.....	16
Figure 2.8. Hypothetical derivation of D-Fructose starting from Dihydroxyacetone by adding secondary alcohol group.....	20
Figure 3.1. Types of rheological behavior exhibited by colloidal dispersions: (a) Newtonian flow; (b) shear thinning (pseudoplastic); (c) shear thickening; (d) Bingham plastic; and (e) pseudoplastic with a yield stress.....	26
Figure 3.2. Stress response, τ , versus time for a step input in strain of (a) the Hookean solid, (b) the Newtonian fluid, (c) viscoelastic solid or liquid.....	30
Figure 3.3. The creep recovery of a material.....	32
Figure 3.4. The schematic diagram for oscillatory movement.....	33
Figure 3.5. (a) the Hookean Solid and (b) the Newtonian Liquid.....	34
Figure 3.6. The schematic diagram of the Kelvin-Voigt model.....	35
Figure 3.7. The schematic diagram of the Maxwell model.....	37
Figure 3.8. A schematic diagram for an oscillating strain and the stress	

response of a material which is viscoelastic with respect to time.....	38
Figure 3.9. Schematic diagram of different type of rheometers, measurements, and geometries.....	41
Figure 3.10. Typical testing geometries for rheometers a) concentric cylinder (couette), b) cone and plate, and c) parallel plates.....	42
Figure 4.1. The schematic illustration of experimental set-up for the preparation of nano-TiO ₂ particles.....	53
Figure 4.2. The schematic diagram for the preparation of consolidated bodies from dispersions.....	56
Figure 5.1. The TGA curve of D-fructose.....	60
Figure 5.2. The TGA curve of submicron alumina powder.	60
Figure 5.3. The TGA curve of nano alumina powder.....	61
Figure 5.4. The TGA curve of the titania precipitate.....	62
Figure 5.5. The variation of zeta potential of submicron alumina with pH.....	63
Figure 5.6. The variation of zeta potential of nano alumina with pH.....	63
Figure 5.7. The variation of zeta potential of nano titania with pH.....	64
Figure 5.8. The XRD pattern of D-Fructose.....	65
Figure 5.9. The XRD patterns of submicron alumina powder.....	65
Figure 5.10. The XRD pattern of nano alumina.....	66
Figure 5.11. The XRD patterns of the titania powders heated to (a) 70, 90, 200, 225, 250, 300, 350, 400, (b), 425-450, 475, 500, 550, 600, 650, 700, and 800 °C.....	67
Figure 5.12. The variation of density (◆) and w _R , % rutile, (□) with respect to temperature.....	68
Figure 5.13. The N ₂ physisorption isotherm of submicron alumina.	70
Figure 5.14. The N ₂ physisorption isotherm of nano alumina.....	70
Figure 5.15. The N ₂ physisorption isotherm of nano titania.....	71
Figure 5.16. The variation of crystal size based on Scherer Equation (◆) and the calculated particle size based on BET surface area (□) with respect to temperature.....	71
Figure 5.17. The variation of BET surface area (●) and pore size based on BJH desorption (□) with respect to temperature.....	72
Figure 5.18. The particle size distribution of submicron alumina powder.....	73

Figure 5.19. The particle size distribution of nano alumina powder.	74
Figure 5.20. The particle size distribution of nano titania powder.	75
Figure 5.21. The SEM micrograph of submicron alumina powder.	76
Figure 5.22. The SEM micrographs of nano alumina powder (a) before and (b) after ballmilling.	77
Figure 5.23. The SEM micrographs of nano titania powder (a) as precipitated and (b) after heat treatment at 425°C for 2 hours.	78
Figure 5.24. The FT-IR spectrum of D-fructose.	79
Figure 5.25. The FT-IR spectra of (a) submicron alumina, (b) nano alumina, and (c) nano titania powders.	80
Figure 5.26. The FTIR spectra of (a) submicron alumina, (b) nano alumina, and (c) nano titania powders which were recovered from 5 vol% dispersions in 10 wt% fructose solutions by centrifugation.	81
Figure 5.27. The FTIR spectra of (a) submicron alumina, (b) nano alumina, and (c) nano titania powders which were obtained by washing recovered powders with water and centrifuged second time.	82
Figure 5.28. Schematic diagrams of protection tool used for steady shear experiments.	83
Figure 5.29. The results of stress sweep tests of 40 vol% α -Al ₂ O ₃ dispersion with 3 wt% polyacrylic acid based on dry weight of submicron alumina.	84
Figure 5.30. Schematic diagrams of protection tool used for steady shear experiments.	84
Figure 5.31. Time sweep tests of the dispersions having (a) 35 vol% α -Al ₂ O ₃ and in 10wt% fructose solution and (b) 45 vol% α -Al ₂ O ₃ in 14 wt% fructose solution.	85
Figure 5.32. The influence of oil around sample on viscosity measurement of 40 vol% α -Al ₂ O ₃ in 2.6 wt% fructose solution.	86
Figure 5.33. The effect of successive measurements on (a) the same sample and on (b) fresh samples on the thixotropic behavior of 25 vol% α -Al ₂ O ₃ in 1.3 wt% fructose solution.	88
Figure 5.34. A typical thixotropic loop test [Barnes, 1997].	89
Figure 5.35. The viscosities of fructose solutions at 100 1/s.	90

Figure 5.36. The flow curves of (a) 4, 10, 15 and 20 wt%, (b) 30, 40, 50 and 60 wt%, (c) 70, 80 wt% fructose solutions.	91
Figure 5.37. The variation of HB yield stress of the submicron alumina dispersions with solids content in semi-logarithmic distribution.	95
Figure 5.38. The variation of consistency coefficient, K , of submicron alumina dispersions with solids content in semi-logarithmic distribution.	96
Figure 5.39. The variation of flow index, n , of submicron alumina dispersions with in semi-logarithmic distribution.	97
Figure 5.40. The viscosities of the submicron dispersions at a shear rate of (a) 50 1/s and (b) 100 1/s.	98
Figure 5.41. The variation of thixotropic loop areas of the submicron alumina dispersions with solids content.	100
Figure 5.42. The results of stress sweep tests done for three times successively to 20 vol% submicron alumina with 1 wt% fructose solution without preshearing.	101
Figure 5.43. The results of stress sweep tests done for three times subsequently to 20 vol% submicron alumina in 1 wt% fructose solution which was presheared at 50 1/s and let to rest for 0, 300, 600, and 900 s.	102
Figure 5.44. The results of stress sweep tests done for three times subsequently to 20 vol% submicron alumina in 1 w% fructose solution which was presheared at 100 1/s and let to rest for 0, 300, 600, and 900 s.	103
Figure 5.45. The results of stress sweep tests done for three times subsequently to 20 vol% submicron alumina in 1 w% fructose solution which was presheared at 200 1/s and let to rest for 0, 300, 600, and 900 s.	104
Figure 5.46. The results of stress sweep tests done for three times subsequently to 20 vol% submicron alumina in 1 w% fructose solution which was presheared at 300 1/s and let to rest for 0, 300, 600, and 900 s.	104
Figure 5.47. The variation of (a) G' and (b) G'' of the submicron alumina dispersions at a shear stress of 0.01 Pa.	107
Figure 5.48. The variation of (a) G' and (b) G'' of the submicron alumina dispersions at an angular frequency of 628 rad/s.	110

Figure 5.49. The variation of (a) G' and (b) G'' of the submicron alumina dispersions at an angular frequency of 6.28 rad/s.....	111
Figure 5.50. The variation of (a) G' and (b) G'' of the submicron alumina dispersions at an angular frequency of 0.0628 rad/s.....	112
Figure 5.51. The variation of HB yield stress of the nano alumina dispersions with solids content in semi-logarithmic distribution.....	115
Figure 5.52. The variation of consistency coefficient, K , of nano alumina dispersions with solids content in semi-logarithmic distribution.....	116
Figure 5.53. The variation of flow index, n , of nano alumina dispersions with in semi-logarithmic distribution.....	117
Figure 5.54. The viscosities of the nano alumina dispersions at a shear rate of (a) 50 1/s and (b) 100 1/s.....	118
Figure 5.55. The variation of thixotropic loop areas of the nano alumina dispersions with solids content.....	119
Figure 5.56. The variation of (a) G' and (b) G'' of the nano alumina dispersions at an angular frequency of 628 rad/s.....	122
Figure 5.57. The variation of (a) G' and (b) G'' of the nano alumina dispersions at an angular frequency of 6.28 rad/s.....	123
Figure 5.58. The variation of (a) G' and (b) G'' of the nano alumina dispersions at an angular frequency of 0.0628 rad/s.....	124
Figure 5.59. The variation of HB yield stress of the nano titania dispersions with solids content in semi-logarithmic distribution (a) without pH adjustment and with pH adjustment.....	129
Figure 5.60. The variation of consistency coefficient, K , of the nano titania dispersions with solids content in semi-logarithmic distribution (a) without pH adjustment and with pH adjustment.....	131
Figure 5.61. The variation of flow index, n , of the nano titania dispersions with solids content in semi-logarithmic distribution (a) without pH adjustment and with pH adjustment.....	132
Figure 5.62. The viscosities of the nano titania dispersions at a shear rate of (a) 50 1/s and (b) 100 1/s.....	134

Figure 5.63. The viscosities of the nano titania dispersions at a shear rate of (a) 50 1/s and (b) 100 1/s with pH adjustment.....	135
Figure 5.64. The variation of thixotropic loop areas of the nano titania dispersions with solids content (a) without pH adjustment and (b) with pH adjustment.....	137
Figure 5.65. The variation of (a) G' and (b) G'' of the nano titania dispersions without pH adjustment at a angular frequency of 628 rad/s.....	140
Figure 5.66. The variation of (a) G' and (b) G'' of the nano titania dispersions without pH adjustment at a angular frequency of 6.28 rad/s.....	141
Figure 5.67. The variation of (a) G' and (b) G'' of the nano titania dispersions without pH adjustment at a angular frequency of 0.0628 rad/s.....	142
Figure 5.68. The variation of (a) G' and (b) G'' of the nano titania dispersions with pH adjustment at a angular frequency of 628 rad/s.....	144
Figure 5.69. The variation of (a) G' and (b) G'' of the nano titania dispersions with pH adjustment at a angular frequency of 6.28 rad/s.....	145
Figure 5.70. The variation of (a) G' and (b) G'' of the nano titania dispersions with pH adjustment at a angular frequency of 0.0628 rad/s.....	146
Figure 5.71. The variation of the G' and (b) G'' of the dispersions at 628 rad/s with surface area available in 1 mL dispersion.....	148
Figure 5.72. The variation of the G' and (b) G'' of the dispersions at 6.28 rad/s with surface area available in 1 mL dispersion.....	149
Figure 5.73. The variation of the G' and (b) G'' of the dispersions at 0.0628 rad/s with surface area available in 1 mL dispersion.....	149
Figure 5.74. The shrinkage curves of submicron alumina, nano alumina and nano titania powders.....	151

LIST OF SYMBOLS/ABBREVIATIONS

B	half maximum of the diffraction peak
D	diameter/crystal size in Scherer Equation
De	Deborah number, the ratio of material's stress relaxation time to the characteristic flow time
D_{50}	median particle size of the powder
IEP	isoelectric point
J	Compliance
J_R	recoverable compliance
f	Frequency
G	relaxation modulus/ shear modulus/ spring modulus
G'	elastic/storage modulus
G''	viscous/loss modulus
G^*	complex modulus
HB	Herschel Bulkley
PSD	particle size distribution
K	the consistency index
n	flow index
SA	surface area
SEM	scanning electron microscope
s	Second
LVER	linear viscoelastic region
TGA	thermal gravimetric analysis
R	Radius
r	the distance between particles
V_{vdW}	the attractive potential energy due to long-range van der Waals interactions between particles
V_{elect}	the repulsive potential energy resulting from electrostatic interactions between like-charged particle surfaces
V_{steric}	the repulsive potential energy resulting from steric interactions between particle surfaces coated with adsorbed polymeric species

$V_{\text{structural}}$	the potential energy resulting from the presence of nonadsorbed species in solution
V_T	the total interparticle force
V_R	the sum of the repulsive electrostatic forces
V_A	attractive van der Waals forces
XRD	Xray diffraction
t	time
t_c	material's characteristic flow time

Greek Letters

ψ	surface potential
ϕ	stern potential
ζ	zeta potential
λ	material's stress relaxation time, xray wavelength in Scherer Equation
γ	deformation
γ_o	applied strain (constant)
γ_C	creep region
γ_R	recovery region
γ_E	the strain in elastic region (Hookean Solid)
$\dot{\gamma}$	shear rate
$\dot{\gamma}_V$	the applied shear rate in viscous region (Newtonian Liquid)
τ	shear stress
τ_o	yield stress/ applies stress (constant)
τ_e	equilibrium stress for viscoelastic solid
τ_E	the shear stress in elastic region (Hookean Solid)
τ_V	the shear stress in viscous region (Newtonian Liquid)
η	viscosity
η_o	zero shear viscosity
η_∞	infinite shear viscosity
η'	elastic viscosity (dynamic viscosity component)
η''	loss viscosity (dynamic viscosity component)
η^*	complex (dynamic) viscosity

α	model parameter (for Ellis and Meter Models)
ω	radial frequency
δ	the phase angle
θ	Bragg diffraction angle
ρ	density

CHAPTER 1

INTRODUCTION

Colloidal processing of ceramics is a well-known process among various powder processing techniques. It offers an improvement of the reliability and strength of the ceramics by reducing heterogeneities such as agglomerates, organic and inorganic inclusions, etc (Lange, 1998). The basic steps of the colloidal processing can be summarized as the preparation of particles and dispersion in a liquid medium, consolidation, removal of the liquid phase, and densification (Lewis, 2000). The ceramic dispersions are prepared by dispersing solid particles in an aqueous or non-aqueous medium. Among various alternative liquid mediums, water is preferable due to environmental issues (Li and Akınç, 2005).

The colloidal processing of nanopowders gained attention over the past few years, because the production of nanopowders becomes available from various synthesis routes and the use of nanopowders in various applications has received a significant interest due to their unique and interesting properties (Bowen, 2002). Their mechanical, chemical, optical, magnetic, and electrical properties are related with the high density of grain boundaries and interfaces which are resulted from their nanoscale microstructure.

The forming processes of nanopowders such as spin and dip coating, injection molding, extrusion and gelcasting are generally necessitate the use of aqueous and pseudoplastic dispersions with low viscosity which may lead to the formation of crack free and reliable grain/fired structures (Lange, 1998 and Lewis, 2000). Such dispersions require an accurate control of its rheological behavior. Controlling rheological behavior of the dispersion relies on the understanding of interactions of particles and the liquid medium because such multiphase content shows wide variety of behaviors and make them difficult to process. As the particle size gets smaller, the specific interactions become more important, because the contact area between particles and dispersing medium and the number of particles increases significantly so that the dispersion of particles becomes more difficult. The observation of the rheological behavior of submicron alumina dispersions may constitute a basis for quantifying and comparing material properties regarding the particle interactions with dispersant as particle size of

the powder approaches to nano size. Therefore, the better understanding of the rheological behavior of nanopowders dispersions can be provided.

Generally, the rheological behavior of nanopowder dispersions is non-Newtonian and measuring its steady shear rheology would not be sufficient to characterize its flow properties. Because, the non-Newtonian dispersions may have both liquid like (viscous) and solid like (elastic) properties at the same time. The viscous and elastic properties of the dispersions can be differentiated by determining dynamic shear rheology. The dynamic shear rheology of nanoparticle dispersions is scarcely studied compared to polymers. This thesis addresses the rheological behavior of aqueous dispersions having nano and submicron particles and paying more attention to the effect of particle size and number of particles in the dispersions on the rheological behavior of ceramic powder dispersions.

The rheological techniques related with steady shear rheology involve the determination of flow curves, viscosity and thixotropy. The dynamic experiments are stress sweep and frequency sweep tests, which may allow understand the relations between particles and the liquid medium more closely.

The relations between particles and liquid medium are regulated by the use of dispersants. The dispersants commonly can be several organic compounds such as organic acids (polyacrylic acid, stearic acid glycolic acid, and etc.), organic salts (ammomium salt of polyacrylic acid, and etc.) and organic materials (polymers, polysaccharides and etc.). The use of the polysaccharides as a dispersant has recently gained attention due to environmental concerns. The earlier research have shown that the addition of polysaccharides in ceramic powder dispersions can reduce the viscosity and provide stable and highly concentrated dispersions. However, the use of polysaccharides with high molecular weight has a reverse effect on viscosity of the dispersions (Schilling et al., 2002a, Sikora et al., 2004). The use of polysaccharides with low molecular weight is preferable. Hence, monosaccharides such as fructose can be used for dispersing nano and submicron ceramic powders.

Addition of fructose in to ceramic powder dispersions caused short range, steric repulsion forces. The decrease in viscosity occurred by the removal of water molecules adsorbed on the surface of the particles (Li and Akinç, 2004). This enhances the mobility of water molecules and their contribution to flow. They mainly focused on the steady shear rheology (the determination of viscosity of the dispersions) however; the dynamic shear rheology provides more detailed information on the relations between

particles and the dispersing medium which are undetectable by steady shear rheology. This thesis focuses on the effect of fructose on the rheology of nano and submicron ceramic powders considering viscous and elastic parts of the suspensions by investigating both steady shear and dynamic shear rheology.

CHAPTER 2

CERAMIC POWDER DISPERSIONS

According to the International Union of Pure and Applied Chemistry (IUPAC), the term *colloid* refers to a state of subdivision, implying that the molecules or polymolecular particles dispersed in a medium have, at least in one direction, a dimension roughly between 1 nm and 1 μm , or that in a system discontinuities are found at distances of that order.

A dispersion is a system in which particle size of any nature (e.g. solid, liquid or gas) are dispersed in a continuous phase of a different composition (or state). The dispersed phase for the particles refers to particles that have essentially the properties of a bulk phase of the same composition. The dispersion of solid-liquid system (the solid particles in liquid medium) is the concerned area in this report. This system is described as a *colloidal suspension* by IUPAC in which the size of the particles lies in the colloidal range.

The lower limit for the size of the particles for colloidal dispersions is around 1 nm because smaller particles would be indistinguishable from the solution. The upper limit would be normally set at a radius of 1 μm (Hunter, 2001). The surface area of such particles is relatively high with respect to the micron-sized particles. The contact area between the dispersed particle and dispersion medium is relatively large and so does the energy associated with this interface. Colloidal processing of materials mainly relies on this feature.

Interparticle (or surface) forces between particles become more important in processing of colloidal dispersions as the size of the particles becomes smaller. The sum of these forces set the stability of the suspension. One of the main issues of colloidal processing is the stability of the colloidal suspension. The terms stable and stability are used to describe the particles that do not aggregate at a significant rate in this report. Generally, an aggregate is a group of particles (which may be atoms or molecules) held together in any way. Actually, a colloidal particle itself may be regarded as an aggregate. More specifically, aggregate is used to describe the structure formed by the cohesion of colloidal particles. This process is also called as aggregation (Hunter, 2001).

Colloidal particles in a dispersed state in a liquid medium always undergo Brownian motion (due to heat) and they will be continuously colliding with one another. The particles will remain as individual particles if those collisions do not result in aggregates. The stability of colloids is then determined by the interaction between the particles during such a collision. There are two basic interactions: one is attractive and the other is repulsive. When attraction dominates, the particles will adhere with each other and finally, the entire dispersion may coalesce. When repulsion dominates, the system will be stable and remain in a dispersed state for a certain time.

The stability of the bulk colloidal suspension is determined by the outcome of individual particle collisions and is dominated by surface forces acting between the particles as they approach each other. According to the classical theory developed by Derjaguin, Landau, Verwey and Overbeek, known as DLVO theory, the total interparticle force (V_T) is the sum of the repulsive electrostatic forces (V_R) and attractive van der Waals forces (V_A) as it is given in equation 2.1. The schematic representation for the forces acting on a particle due to DLVO theory is given in Figure 2.1.

$$V_T = V_R + V_A \quad (2.1)$$

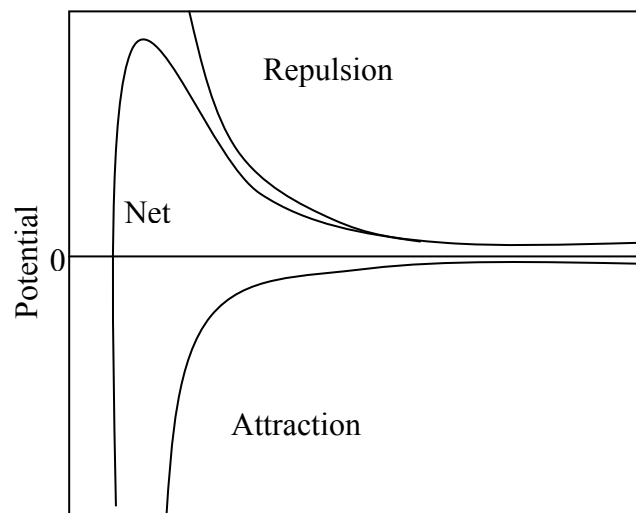


Figure 2.1. Schematic illustration of the forces defined in the DLVO theory with respect to particle separation (Source: Shanefield, 1996).

The van der Waals Force between atoms and molecules is the sum of three different forces:

- (i) The Keesom force which is the interaction between two permanent dipoles.
- (ii) The Debye force which is the interaction between one permanent dipole and one induced dipole.
- (iii) The London or dispersion force which is the interaction between two induced dipoles.

All of these forces are proportional to $1/r^6$ (r is the distance between the atoms or molecules).

The van der Waals force is a result of electric and magnetic polarization and propagation of the electric field. One possible way of assessing the magnitude of van der Waals interaction is to know the value of Hamaker constant which depends on the material and medium (see Table 2.1). (Shanefield, 1996).

Table 2.1 Nonretarded Hamaker Constants for Ceramic Materials Interacting under Vacuum and across Water at 298 K (Source: Lewis, 2000).

Material	Crystal Structure	Hamaker Constant ($\times 10^{-20}$ J)	
		Under Vacuum	Across Water
α -Al ₂ O ₃	Hexagonal	15.2	3.67
SiO ₂ (quartz)	Trigonal	8.86	1.02
SiO ₂	Amorphous	6.5	0.46
TiO ₂	Hexagonal	15.3	5.35
3Y-ZrO ₂	Tetragonal	20.3	7.23

When a colloid is immersed in water a charge may develop on the surface due to either a preferential affinity of ions in solution to the surface, a preferential physical restriction of ions within the surface to dissolution, or the ionization of surface groups.

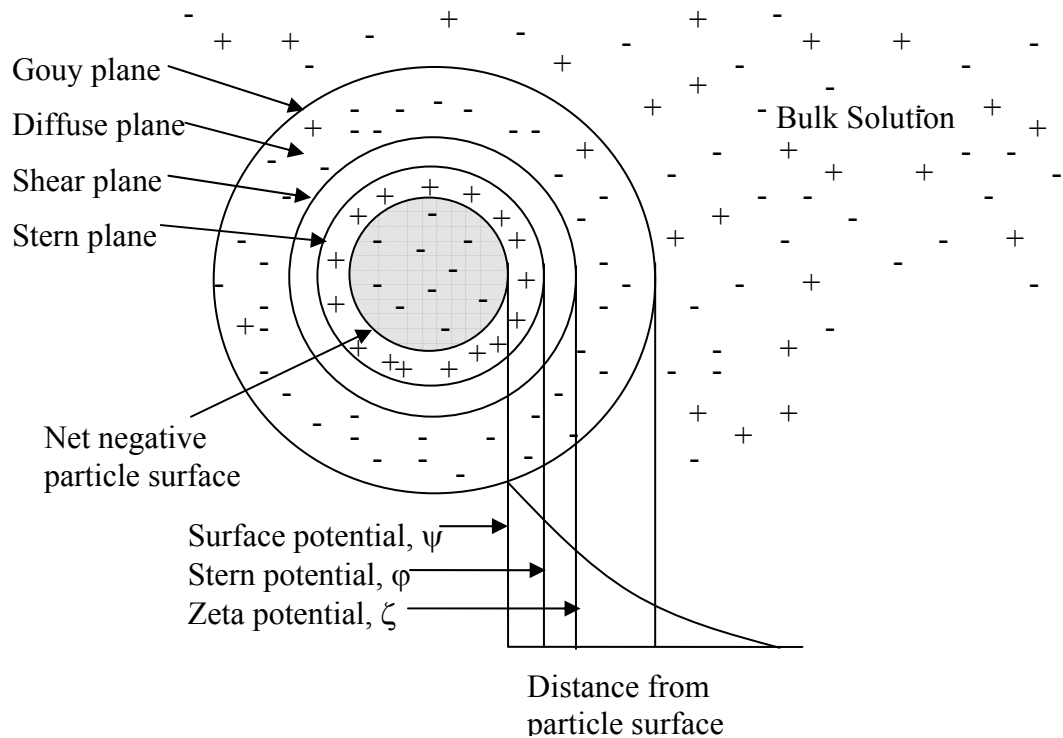


Figure 2.2. The schematic representation of the electrical double layer around negatively charged particle.

When a net positive or negative surface charge is present, counter ions in the water of opposite charge will accumulate at the surface. Because of thermal motion of the water molecules, this layer of counter ions diffuses, with the concentration of counter ions decaying exponentially away from the surface. Since the overall balance of charge within the solution must be maintained, the net charge on the surface is balanced by the net charge in the diffuse layer. The arrangement of charge on the colloid surface, and counter ions in the diffuse layer, is known as the electrical double layer as shown in Figure 2.2.

When two charged surfaces in solution come into close proximity, the diffuse layers of counter ions projecting from each surface overlap. If the charge on the particles is of the same sign, this overlap causes an increase in the concentration of counter ions in the intervening gap, and results in an osmotic pressure between the surfaces. Due to this repulsive force, energy must be expended to bring the surfaces together, and this forms the basis of the electrostatic repulsion energy term.

A cloud of counterions around a charged particle renders the particle neutral at large distances. The thickness of the counterion cloud is defined as Debye length, and is

the measure of the range of repulsion (Franks and Lange, 1999). The repulsion force is proportional to the inverse of distance squared.

Two particles having the same charge will repel each other. However, as the particles approach to each other at nanometer distances, the van der Waals forces are going to be dominant and there will be a net attraction until contact is made. The contact point is called as “primary minimum” (Shanefield, 1996; Franks and Lange, 1999). As the particles become slightly farther away from each other, the van der Waals attraction decreases sharply and electrostatic repulsion becomes dominant. In other words, this phenomenon appears when the counterion concentration is low and thus, when the Debye length is large. The suspensions under this condition are defined as “dispersed” (Franks and Lange, 1999). Addition of salt causes the reduction in Debye length and an increase in counterion concentration so that the separation distance becomes large and the surface charge of the particle remains constant. When the separation distance becomes large enough, another low potential energy will be reached in some cases and this is called as the “secondary minimum” (Shanefield, 1996; Franks and Lange, 1999). Through secondary minimum, the range of repulsive potential will decrease sufficiently and van der Waals attraction dominates the system again. The particle network becomes weakly attractive and the particles sit apart in the secondary minimum. Figure 2.3 shows the DLVO curve for two charged particles approaching each other.

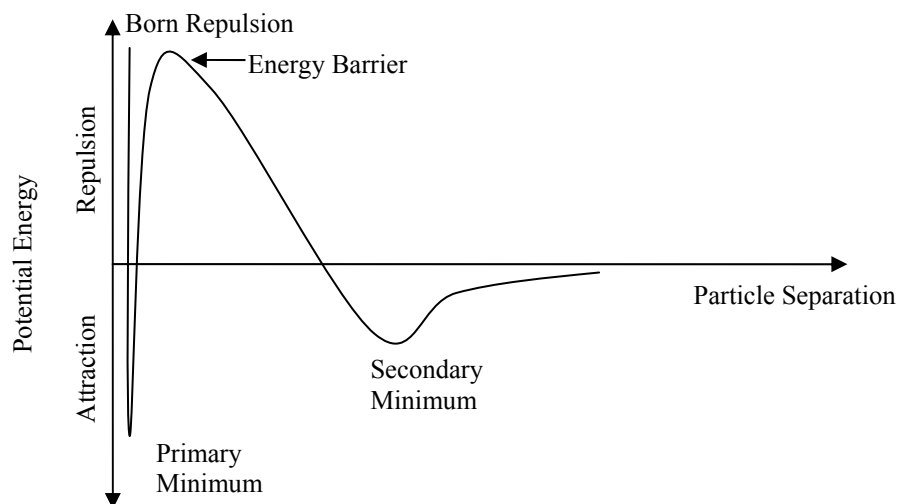


Figure 2.3. The DLVO curve for two charged particles approaching to each other (Source: Shanefield, 1996).

This phenomenon associates with the pH of suspension. Knowing pH of a suspension will be helpful to describe “the state” of the suspension. The pH at which the zeta potential is zero at diffuse layer is known as the isoelectric point (IEP). In other words, IEP is the pH value, at which a molecule carries no net electrical charge. An oxide can be also characterized by its “point of zero charge”. Point of zero charge (PZC) can be defined as the pH at which surface charge density is zero. If there are no ions other than H^+ and OH^- , IEP and PZC will be equal to each other. However, in presence of non-potential ions will cause a shift in PZC and IEP relative to each other. At IEP, the majority of surface sites are neutral and the net charge on the surface is zero. At pH conditions away from the isoelectric point the net surface charge is either positive (at lower pH) or negative (at higher pH) reflecting the exchange of protons with the surface hydroxyl groups. At IEP, there is no repulsive potential. Instead of this, van der Waals attraction pulls the particles together to form a strong touching network, which is called as flocculated (Franks and Lange, 1999).

As a result, the DLVO theory predicts the stability of the colloidal particles suspended in polar liquids (Lewis, 2000) and a careful investigation and fine-tuning through interparticle forces can facilitate the preparation of suspensions in dispersed or, weakly or strongly flocculated states (see Figure 2.4).

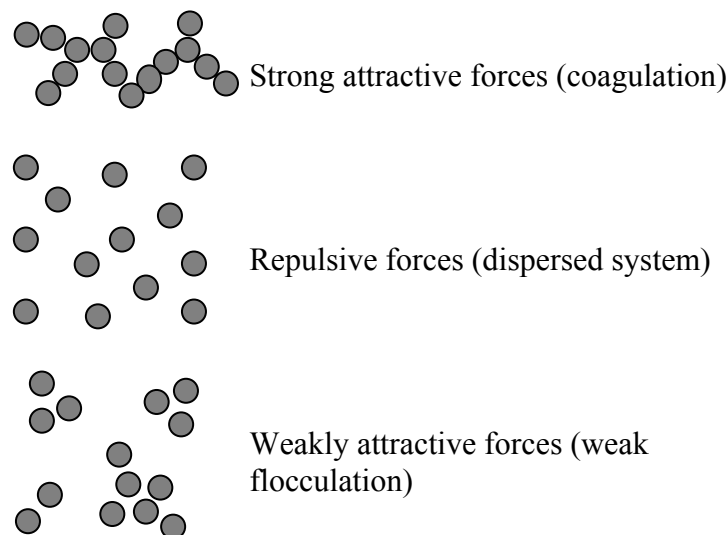


Figure 2.4. Schematic illustration between suspension microstructure and interparticle forces (Source: Sigmund et al., 2000).

Brownian motion must have been taken under consideration because it has an important effect on the stability of dispersion. A suspension of particles having relatively small electric charges (hence low repulsion) are going to have enough thermal motion kinetic energy after any given time to approach to the primary minimum as shown in Figure 2.3. Then, the particles will stay together. When temperature is raised, fast agglomeration will occur.

For a stable suspension at room temperature, the potential energy peak next to the primary minimum must be at least ~ 25 mV because thermal energy available for Brownian motion corresponds to 25 mV at 20°C (Shanefield, 1996). Hence, suspensions having high potential energies will be highly dispersed and considered as stable because agglomeration rate will be slow. The stability ratio of a suspension would be determined which represents valuable information on the assessment of their long-term physical stability.

Due to the random nature of each collision there will be a distribution of collision energies for a colloidal system. For a given energy barrier, only a proportion of collisions will have sufficient kinetic energy to overcome the energy barrier and form an aggregate. The stability ratio is therefore strongly influenced by the height of the energy barrier, increasing dramatically with small increases in the height of the barrier.

The height of the energy barrier is highly sensitive to factors affecting the attractive van der Waals and repulsive electrostatic forces. In terms of the van der Waals forces, this includes the Hamaker constant of the surfaces and the intervening medium. For the electrostatic force, factors such as surface potential, electrolyte concentration and electrolyte valency are important.

An alternative way to prepare a highly dispersed stable suspension would be the use of polymeric dispersants. The presence of suitable polymeric dispersants can also be helpful for the preparation of dispersed colloidal suspensions. The polymeric additives cover the surface of the particles by adsorption. The interpenetration of polymer layer results in a repulsive force (or steric stabilization) when two such particles approach (see Figure 2.5).

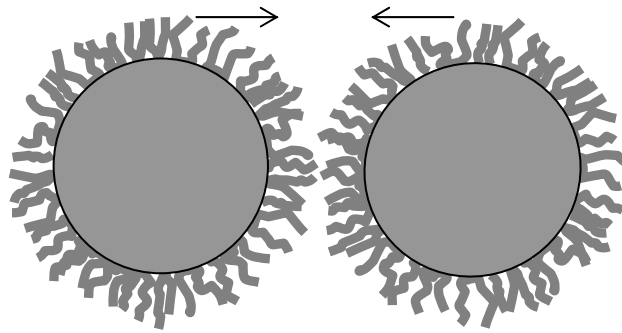


Figure 2.5. Schematic illustration of two particles covered by polymer layer resulted in a repulsive force (Source: Lewis, 2000).

Sigmund et al. stated some requirements for steric stabilization (Sigmund et al., 2000). According to them, the thickness of the adsorbed layers, the affinity of the polymer, the adsorbed amount, and the solvency of the polymer in the media are strongly interrelated. Lewis (2000) reported that one must consider the adsorbed layers' thickness and density to overcome the van der Waals attraction between particles and to prevent bridging flocculation.

The term of electrosteric stabilization is used when addition of polyelectrolyte maintains dispersion (Sigmund et al., 2000). Polyelectrolytes serve a combined effect of a pure electrostatic repulsion and a polymeric repulsion (steric stabilization). The origin of the electrostatic component may be a net charge on the particle surface (see Figure 2.6.a) and/or charges associated with the polymer attached to the surface (see Figure 2.6.b). The dominant effect will be assigned by the segment density profile at the interface. Electrosteric effect becomes more important when the polyelectrolyte is highly charged and the particle surface oppositely charged (Lewis, 2000; Sigmund, 2000; Pettersson et al., 2000; Bowen, 2005).

Solvent conditions (e.g. pH and ionic strength of polyelectrolyte) should be taken into consideration because the adsorption behavior and conformation of polyelectrolyte will be changed. For an anionic polyelectrolyte, the thickness of adsorbed layer will be thinner and massive and the resulted degree of ionization will be lower when the pH is set at lower values (Pettersson et al., 2000; Lewis, 2000; Desset et al., 2001; Liufu et al., 2005).

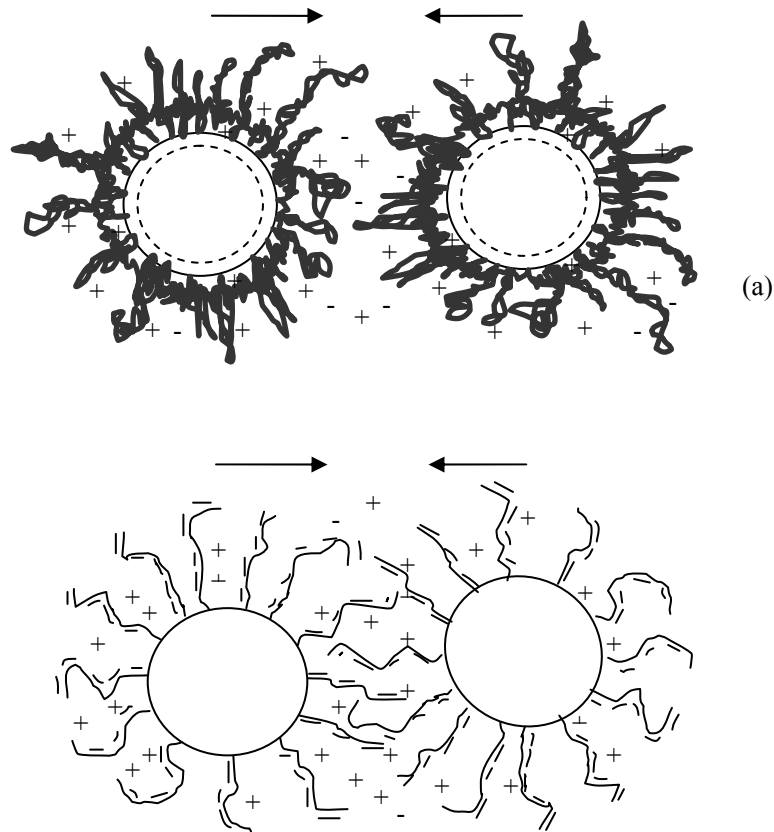


Figure 2.6. Schematic illustration of electrosteric stabilization: (a) charged particles with nonionic polymers; (b) polyelectrolytes attached to uncharged particles.

Adsorption process will take place between particle surface and polyelectrolyte itself when polyelectrolyte is added into the suspension. The chemical and physical properties of the solid surfaces and the solvent medium have important effects on the adsorption of polyelectrolytes. When the system consists of oppositely charged polyelectrolyte/particle pairs the adsorption is always strong due to the ionic interaction, and destabilization of the suspension may occur as a result of polymer bridging or charge neutralization of powder particles by the adsorbed polyelectrolytes (Pettersson et al., 2000). At small adsorbed amounts, such species can promote flocculation either via surface charge neutralization or bridging mechanisms. One possible reason of this result would be the incomplete coverage of the surface. The particles loosely attach to each other to minimize the uncovered surface. Liu (1998b) considered that this kind of flocculation formation can be used to determine the minimum amount of polyelectrolyte required for the stabilization of suspension. At higher adsorbed amounts, particle

stability increases because of long-range repulsive forces resulting from electrosteric interactions.

As a summary, the non-DLVO forces (means not expressed in DLVO theory) can also facilitate the adjustment of the state of suspension. According to Lewis (2000), total interparticle forces which govern the colloidal stability can be expressed as

$$V_{total} = V_{vdW} + V_{elect} + V_{steric} + V_{structural} \quad (2.2)$$

where, V_{vdW} is the attractive potential energy due to long-range van der Waals interactions between particles, V_{elect} the repulsive potential energy resulting from electrostatic interactions between like-charged particle surfaces, V_{steric} the repulsive potential energy resulting from steric interactions between particle surfaces coated with adsorbed polymeric species, and $V_{structural}$ the potential energy resulting from the presence of nonadsorbed species in solution that may either increase or decrease suspension stability (Lewis, 2000).

Meanwhile, Tari et al. (Tari et al.,1998) studied on the dispersion of alumina powders with particles in 0.1-1 μm range. Their aim was to study the influence of particle size distribution (PSD) on the colloidal processing of alumina. The total solid content of the dispersed alumina slips was maximized and their rheological properties were correlated to the packing ability during slip casting. The concentrations of the prepared suspensions were varied between 40-70 wt% which were dispersed by using polyacrylic acid (PAA) as polyelectrolyte. They reported that the tape-cast green bodies reached to 78% of theoretical density. Recently, Liufu et al. (2005) studied with PAA for the dispersion of titania nanoparticles (20 ± 5 nm). The solid content was kept constant at 10 wt% while the molecular weight of PAA was changed. They observed that zeta potential decreases with increase in the adsorption density of PAA. High molecular weight PAA (120,000 g/mol) was found to cause flocculation due to the bridging of long macromolecular chains. Finally, they concluded that PAA was appropriate dispersant under described conditions in the article.

Pettersson et al. (2000) aimed to investigate the mechanisms of eight anionic polyelectrolytes to stabilize single oxide systems of $\alpha\text{-Al}_2\text{O}_3$, ZrO_2 and 3Y-ZrO_2 . The Na^+ and NH_4^+ salts of polyacrylic acid and polymethacrylic acids with different molecular weights were used. They focused on the distribution of charges and the

resulting potentials around the particles for a better understanding of the influence of polyelectrolyte dispersants on the stability, rheology, and many other properties of colloidal sized solids dispersed in liquids. They also considered the degree of dissociation of polyelectrolytes, which varied with pH of the solutions, by potentiometric titrations. The particle sizes of the α -Al₂O₃, ZrO₂ and 3Y-ZrO₂ were 2.3, 0.3 and 0.41 μ m respectively. The solid contents were changed between 1-30 wt%. They observed that destabilization (or lowering zeta potential) occurs at low pH as a result of charge neutralization upon adsorption and then polymer bridging occurred. Polyacrylates with Na⁺ induce relatively higher surface charges and higher adsorption with respect to polyacrylates with NH₄⁺. However, for polymethacrylates the opposite was observed. The adsorbed layer was thicker when the particles and polymers have equal charge. Finally, the authors concluded that polyacrylates and polymethacrylates were efficient polyelectrolytes for the dispersion of α -Al₂O₃, ZrO₂ and 3Y-ZrO₂ suspensions. The zeta potentials of these suspensions were about 40 mV or higher.

Singh et al. (2005) pointed out that there was a need to study the higher solids content carefully because dispersants which provide good dispersion for low solids content may not work for high solid contents. They used dibasic ammonium citrate (DAC) and albumin (prepared from white portion of fresh egg) to disperse alumina powder having 0.72 μ m particles in size. The solid contents of the suspensions were changed between 1.47-50 wt% and the further pH adjustments were done by HCl and NaOH. While the concentrations of dispersants were not clearly stated, the authors reported optimum concentrations as 5250 and 150 ppm for albumin and DAC respectively. The surface of the alumina particles were negatively charged when dispersants were added. Moreover, albumin had more impact on the surface charge. They claimed that these dispersants would have similar impact at high solid contents as well as low solid contents since the surface charge did not change significantly for all conditions described in the article. Later on, Singh et al. (2005) used an anionic dispersant, ammonium salt of polycarboxylate, to disperse alumina powder (having particles 0.6 μ m) for suspensions having 5-12.85 wt-% solid contents.

Lebrette et al. (2004) used Tiron and a strong base, (C₂H₅)₄NOH, to disperse titania particles 0.4 μ m for suspensions having 3 and 49 wt% solid contents. The article reported the influence of ethanol amount to titania dispersion. The concluded that the presence of ethanol may facilitate the preparation of titania suspensions up to 49 wt-% solid content.

Redispersion of alumina powder was studied by Desset et al. (2001). They used five different ligands such as citric acid, polyacrylic acid, 1,2-dihydroxy 3,5-dibenzene disulfonic acid, 1,2,3,4-butane-tetra-carboxylic acid, and glycolic acid. Their aim was to measure the stabilizing, peptizing, and protecting effects of these ligands for alumina suspension (10 wt%) having particles 0.2 μm in size. The pH of the suspensions was adjusted by adding NaOH or HNO₃. Redispersion studies were performed by dispersing of the powder in water by using ultrasound and the addition of a ligand and subsequent drying. The authors claimed that the sequence during preparation of suspensions has an importance: The addition of ligands into aqueous suspensions will cause stabilizing effect while addition of bare powder into water containing ligands will cause peptizing effect. When one needs protecting effect then, the suspension can be prepared by the addition of powder containing ligand(s) into water. Finally, the authors reported that if one considers the redispersion of the powders made of aggregated colloidal particles, then careful attention must be given to keep the powder surface hydrated during aggregation and drying stages.

Large colloidal particles can be stabilized by depletion forces as a third alternative way (Lewis, 2000; Tohver et al., 2001). These forces occur when colloidal particles are introduced to a solution containing nonadsorbing, smaller species, such as polymers, polyelectrolytes, or much smaller colloidal particles as see in Figure 2.7. These species are defined as depletants which may promote flocculation *or* stabilization of primary colloidal particles. Theoretically, the smaller species may lead to flocculation of a stable suspension. However, the following study showed that the charged species in solution may influence the stability of the uncharged bigger particles by segregating around them. Tohver et al. (2001) studied on stabilization of large particles by adding much smaller charged particles into solution and introduced the term “nanoparticle haloing”. In their study, charged hydrous zirconia nanoparticles of average radius 3 nm was added to a suspension of (marginally charged) colloidal silica spheres of radius 285 nm in deionized water. The concentration of charged particles increased and the following behavior was observed:

- At low nanoparticle concentrations: the silica spheres aggregate, driven by the generic van der Waals attractions (Figure 2.8.a).
- At intermediate nanoparticle concentrations, the dispersion becomes stable (Figure 2.8.b).
- At higher concentrations the silica spheres aggregate again (Figure 2.8.c).

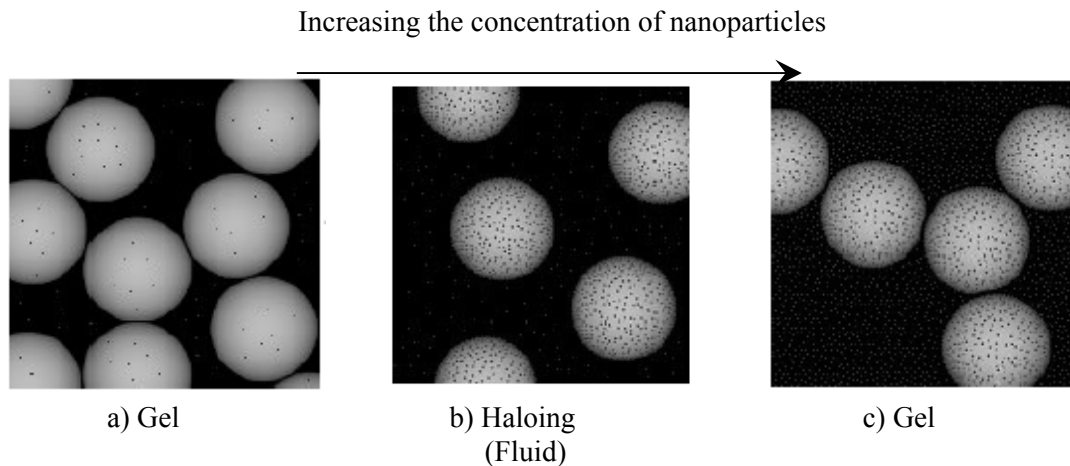


Figure 2.7. Representative schematic illustration of nanoparticle haloing behavior (Source: Tohver et al., 2001).

The observation made showed that there are two critical values of concentration of nanoparticles which are defined as lower and upper critical values by Tohver et al. (2001). These two values introduced three regions in phase diagram: (i) a colloidal gel composed of silica microspheres at nanoparticle volume fractions below a lower critical value, (ii) a homogenous fluid composed of stabilized silica microspheres and nanoparticles at intermediate nanoparticle volume fractions, and (iii) a colloidal gel composed of silica microspheres at nanoparticle volume fractions above an upper critical value. They stated that the system began in non-equilibrium state in the absence of nanoparticles. They concluded that nanoparticle haloing could be driven solely by highly repulsive interactions between nanoparticles in solution. Hence, this can generate a substantial zeta potential on colloidal microspheres suspended near their isoelectric point. For highly charged nanoparticles, this type of charge amplification can occur at extremely low nanoparticle volume fractions ($<10^{-3}$). The stabilization of colloidal suspensions by using an electrolyte has been widely studied. Lim et al. (1997) studied on the stabilization of alumina powders in water by adding HCl and its impact on greenbody density and sintered density of the compacts which are consolidated by means of centrifugation. Powder suspensions of 7, 15 and 30 vol% of alumina were prepared in an HCl solution of optimum pH value of 2.4. Initially the particle size of the powders was $0.18 \pm 0.034 \mu\text{m}$. They concluded that colloidal processing is an efficient way to eliminate agglomeration problem (Lim et. al., 1997).

Meanwhile, Evanko et al. (1997) studied the effects of pH, electrolyte concentration and solids concentration on the surface charge characteristics, viscosity and stability of concentrated alumina dispersions (1-10 wt%). The study considered the relationships between these properties of the dispersions. The particle size of the alumina powder reported as 1 μm . NaCl is used as electrolyte solution. pH, electrolyte concentration, and solids content had a strong influence on the surface charge and therefore the viscosity and stability of concentrated dispersions of alumina in water.

Bae et al. (2003) aimed to investigate the dispersion stability of titania powder, which was prepared by homogenous precipitation at low temperature (named as HPPLTed in the article), in pure aqueous and organic media by adding different electrolytes to consider the effect of valence of cation on titania. The electrolytes were CsCl, CaCl₂, FeCl₃, and ZrCl₄. Commercial powders (MT-500 HD and P-25) were dispersed under same conditions for comparisons. The synthesized titania powder has an appearance that the primary particles are acicular or needle-shaped with a thickness of 3-7 nm. The authors reported that the surface area of HPPLTed (180 m²/g) was much higher than the commercial ones (40-50 m²/g) which lead to higher H⁺ adsorption on the powder surface and thus, much lower isoelectric point (pH_{IEP}= 2.31). Electrolytes having higher valence cation led to increase in zeta potential. The addition of electrolytes into both aqueous and organic solvents caused to a common charge reversal from negative to positive at the surface of TiO₂.

One of the recent studies on the stability of titania particles in high purity water was conducted by Snoswell et al. (2005). In their study, the primary particles had a diameter of approximately 150 nm and were composed of smaller crystallites with a size on the order of 10 nm. They used KCl as electrolyte and set the pH by using KOH. The stability ratio was calculated by collecting data of the change in light scattering intensity (or turbidity) for fast regime and for slow regime. The fast and slow regimes were determined from the initial gradient of the turbidity-time curve. However, they reported that the calculation of the halftime of aggregation for non-spherical, porous particles would be problematic because the initial number of particles must be estimated from the solids content. They assumed that the particles were monodisperse. Finally, they reported that an increase in both the gradient and critical coagulation concentration of the stability curves were observed as pH increases. Titania particles became negatively charged at higher pH and hence, the surface potential increased.

2.1. The Use of Saccharides as Dispersant in Ceramic Powder Dispersions

Polysaccharides are naturally occurring biopolymers and are complex carbohydrates, made up of multiple sugar molecules. These polymers are used as food energy sources and construction materials of livings. The commonly known sugars are listed in Table 2.2. The sugar molecules linked together may be glucose, galactose, or any of the many other sugar molecules. The most abundant examples of polysaccharides are starch and cellulose. Due to their ability to alter the basic properties of water, polysaccharides have been used in many industries such as food, textile, paper, adhesive, paint, pharmaceuticals, cosmetics, etc. The functions of polysaccharides in these applications can be emulsification, stabilization, encapsulation, flocculation, film formation, binding and coating (Liu and Laskowski, 2002).

The structure of polysaccharides can be very complex. Polysaccharides are built of many different types of such monomers joined together in different ways by glycosidic linkages. A glycosidic bond is a certain type of functional group that joins a carbohydrate (sugar) molecule to an alcohol, which may be another carbohydrate. Two monosaccharides can form a disaccharide by glycosidic bond. For example, fructose and glucose are joined together to form sucrose. More complicated polysaccharides such as starch, glycogen, cellulose or chitin consist of numerous monosaccharide units joined by glycosidic bonds. Starch and cellulose are formed entirely of glucose molecules linked together.

When all the constituent monosaccharides are of the same type, they are termed as *homopolysaccharides*; when more than one type of monosaccharide is present they are termed as *heteropolysaccharides*. Cellulose, chitin, chitosan, and, glycogen are the examples for homopolysaccharides. Glucomannan, galactoglycomannan, hyaluronic acid and alginic acid are the examples for heteropolysaccharides.

Saccharides in aqueous solution can exist commonly in cyclic or rarely in linear form and these forms readily interconvert. Only the cyclic forms have an anomeric carbon and can form a glycosidic bond; once the bond has formed, the saccharide unit can no longer attain the linear form.

Table 2.2. General information on commonly known sugars.

Sugar	Carbohydrate	Monosaccharide or disaccharide	Additional information
Beet sugar (cane sugar)	Sucrose	Disaccharide (fructose and glucose)	Similar to white and powdered sugar, but varied degree of purification
Brown sugar	Sucrose	Disaccharide (fructose and glucose)	Similar to white and powdered sugar, but varied degree of purification
Corn syrup	Glucose	Monosaccharide	Very sweet Very sweet and inexpensive Added to soft drinks and canned or frozen fruits
Fruit sugar	Fructose	Monosaccharide	
High-fructose corn syrup	Fructose	Monosaccharide	
Honey	Fructose and glucose	Monosaccharides	
Malt sugar	Maltose	Disaccharide (glucose and glucose)	Formed by the hydrolysis of starch, but sweeter than starch
Maple syrup	Sucrose	Disaccharide (fructose and glucose)	
Milk sugar	Lactose	Disaccharide (glucose and galactose)	Made in mammary glands of most lactating animals
Powdered sugar	Sucrose	Disaccharide (fructose and glucose)	Similar to white and brown sugar, but varied degree of purification
White sugar (Table Sugar)	Sucrose	Disaccharide (fructose and glucose)	Similar to brown and powdered sugar, but varied degree of purification

2.1.1. Monosaccharides

Monosaccharides are colorless substances and soluble in water, lower alcohols, acetic acid and pyridine. They can be also recrystallized by removing the solvents and most monosaccharides are obtained in a crystalline form (Stanek et al., 1963 and Collins and Ferrier, 1995). The term monosaccharides describes the sugars that on hydrolysis yield no further lower sugars (Stanek et al., 1963). Monosaccharides are simple sugars and can have different number of carbon atoms. They have free aldehyde or keto groups and can be combined to form disaccharides and polysaccharides. In general, monosaccharides can be defined as polyhydroxyaldehydes (aldose) or polyhydroxyketones (ketose). The simplest monosaccharides according to this definition were glyceraldehyde and dihydroxyacetone. These monosaccharides are assigned to trioses

group which means that the monosaccharides have three carbon atoms. The monosaccharide containing four carbon atoms is named as tetroses, five as pentoses and further series are hexoses, heptoses etc.

The monosaccharides generally have a pair of optical antipodes. If the projection formula of a monosaccharide is oriented so that the aldehydic group is on top then in the formula, the hydroxyl group at the asymmetric carbon atom on the left side (called as laevo rotary) or on the right side (called as dextro rotary). The laevo rotary antipode is denoted by L- and the dextro rotary is denoted by D-.

D-fructose belongs to the series of D-ketoses. The characteristic D-ketose series can be derived from dihydroxyacetone by hypothetically added a secondary alcohol group between carbonyl and $-\text{CH}_2\text{OH}$ groups. By repeating this procedure, D-Fructose is obtained (Stanek et al., 1963) The hypothetical derivation of D-fructose starting from Dihydroxyacetone by adding secondary alcohol group is given in see Figure 2.8.

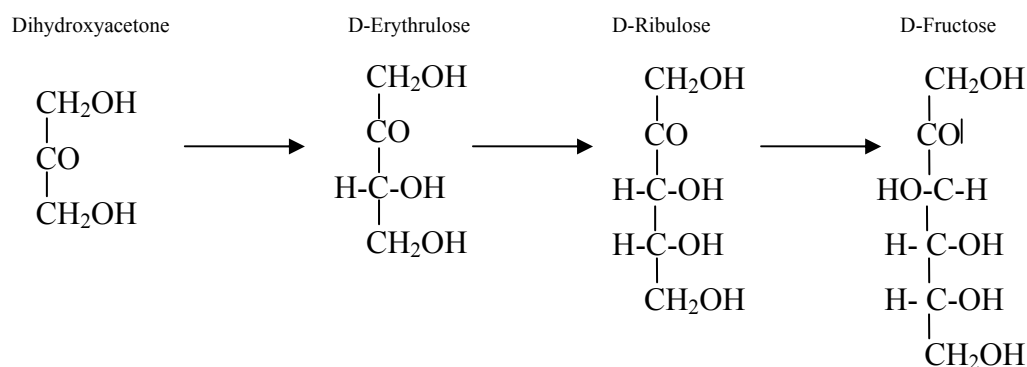


Figure 2.8. Hypothetical derivation of D-Fructose starting from Dihydroxyacetone by adding secondary alcohol group.

D-Fructose occurs in free state mainly in fruit juices such as apples and tomatoes. It can be produced by hydrolysis of sucrose or inulin which is a polysaccharide containing D-Fructose and D-glucose.

The reactivity of the individual hydroxyl groups in the monosaccharide molecule and the relative reactivity are not known very much. Aqueous dilute solutions of inorganic acids at normal temperatures do not cause a noticeable change in the structure of monosaccharides. When D-glucose is subjected to the action of acids, D-mannose and D-fructose are formed. The high concentration of organic acids caused

decomposition of monosaccharides to furan derivatives (ending up with a cyclic form by dehydration).

2.1.2. Adsorption Mechanism of Monosaccharides

The primary adsorption mechanism of polysaccharides to the surfaces may be the hydrogen bonding and the other is chemical complexation (Liu and Laskowski, 2002). Polysaccharides contain large number of –OH groups and these groups are the only polar groups. The polar groups interact with surfaces and the hydrophobic radicals point towards the aqueous phase, making the surfaces hydrophobic. However, the hydrogen bonding mechanism may be postulated due to the –OH groups on the material surfaces in aqueous medium. The material and polysaccharides form hydrogen bond with water molecules. For the adsorption of polysaccharides through hydrogen bonding, the two existing hydrogen bonds must be broken down to form hydrogen bonding between material surface and polysaccharide.

The chemical complexation was detected by FTIR studies. The appearance of a broad O-H stretching band centering at about 3370 cm^{-1} , a weak peak at 957 cm^{-1} , minor shifts in the band at 935 cm^{-1} due to ring formation and a shift of 848 cm^{-1} (equatorial $C_1\text{-H}$ deformation) to 893 cm^{-1} (axial $C_1\text{-H}$ deformation) were the indicators of polysaccharides attachment on to metal oxide surfaces. (Liu and Laskowski, 2002).

It is reported that the presence of metallic sites on the mineral surfaces enhance the polysaccharide adsorption (Liu and Laskowski, 2002). For example, it was found that the quartz sample adsorbed more polysaccharides when it was covered by Pb metallic sites with respect to the sample without Pb sites. The pH of the medium affected the adsorption of polysaccharides because of the hydroxylation of metallic sites on the surfaces is pH dependent. It was observed that the isoelectric point (IEP) of the materials can be a good indicator of the adsorption of polysaccharides. High IEP indicates a basic surface and a low IEP indicates an acidic surface. It was reported that the oxides/hydroxides of lead, nickel and magnesium have high IEPs (between 10 and 12) and strongly adsorbed polysaccharides such as dextrin, starch or guar gum. However, polysaccharides have not been found to interact with metal cations or bare metallic surfaces which are known as Lewis acids (electron acceptors). This behavior is evaluated as the indication of the acidic characteristic of -OH groups in polysaccharides

during their interaction with mineral surfaces. Liu and Laskowski (2002) mention a study on the adsorption of glucose onto alumina. Two alumina samples were considered; one with high concentrations of surface basic –OH groups and one without. It was found that the glucose adsorption was much higher on the alumina sample with high basic –OH groups.

CHAPTER 3

RHEOLOGICAL BEHAVIOR OF DISPERSIONS

Solid/liquid dispersions (suspensions) are present in many forms: polymers, foods, paints, inks, biological materials, pharmaceuticals, agrochemicals, ceramics, dyestuffs, paper coatings, cosmetics, etc. These suspensions involve aqueous or non-aqueous media and organic or inorganic disperse phase. Such multiphase content shows wide variety of behaviors and make them difficult to process. As the particle size gets smaller, dispersion of particles becomes more difficult and the dispersion of nanometer scale particles is quite critical in these emerging technologies.

Processing of a suspension usually requires identification of flow characteristics because its rheological behavior gives important information about the suspension properties. These properties can be controlled by manipulating the forces acting on the particles.

Rheology is described as the science of the *deformation* and *flow* of matter and is used in the evaluation of the processability of materials to provide information on flow and deformation properties. In other words, the utility of materials is assessed due to their rheological behavior. In the early 1920's the behavior of clays and paints initially promoted by Bingham to introduce rheology as a new scientific field. However, the main developments in this field progressed when polymers have been concerned (Barnes, 1989, Coussert, 2005). Besides polymers, there is a vast variety of materials composed of emulsions, foam, and suspensions of solid particles. When the concentration of suspended material is low, then the rheological response is very close to the interstitial liquid which is generally Newtonian. However, when the concentration is sufficiently high the suspended materials develop specific interactions. This kind of fluids generally display a non-Newtonian behavior.

To understand non-Newtonian behavior of a suspension, dispersion of particles must be taken into consideration, which is mainly based on changing surface characteristics. One of the traditional methods is to disperse particles by creating electrostatic repulsion. However, much larger surface potential is needed as the particle size decreases and solids content increases. The other common method is using

polymeric dispersants. Larger polymeric dispersants may lead to an increase in viscosity for concentrated suspensions. Having a compact layer of polymer around a particle results in an increase in the effective volume fraction of a suspension and, hence, its viscosity. The use of alternative dispersants is necessary due to these limitations. Smaller dispersants with controlled adsorption to the surface of particles can provide a viable way for dispersing concentrated nanoparticle suspensions.

Preparation of a suspension having desired flow properties and maintaining sufficient stability against sedimentation, aggregation and agglomeration can be achieved by understanding its rheological behavior. One of the important issues is to establish criteria for controlling rheological properties and physical stability. Therefore, it is very important to provide a basis for quantifying and comparing material properties during each phase of the manufacturing process (beginning from the raw materials to final product) to enhance the reliability of the products. Hence, measurements and standards play an important role for manufacturing reliable products.

In the scope of this thesis work, the ultimate goal is to prepare suspensions having a low viscosity which is insensitive to temperature variations with high solids content and showing pseudoplastic behavior. However, suspensions involving submicron and nano particles can display different rheological properties including shear thinning, shear thickening, yielding and thixotropy. These complex rheological responses are the result of the magnitude of interparticle forces.

Many materials can be classified as solids, liquids, and fluids. Each of them has different rheological responses. In order to understand rheological behavior of materials, intermolecular forces should be taken into account to control material behavior. The other important issue is the importance of the time scale of our observations. Hence, it is important to consider the time scale of measurements with respect to its characteristic time of the material which is given by Deborah number.

Deborah number (De) was introduced by Maxwell, which is defined as the ratio of material's stress relaxation time, λ , to the characteristic flow time, t_c (Goodwin and Hughes, 2000). When a material is subjected to an instantaneous deformation, the molecules jump to a higher energy state. If the material was hold at this state for a while, the molecules diffuse to reach a lower energy state which is equal to the initial state. Thus, the original shape of the material has been lost and a viscous flow has occurred. Hence, materials can be classified into three categories by considering this number. If the Deborah number of a material is higher than unity, the material is defined as a solid

like material. If the Deborah number of a material is lower than unity, the material is defined as a liquid like material. The materials are classified as viscoelastic materials when the Deborah number is in the order of 1.

$De \ll 1$	$De \approx \text{order of } 1$	$De \gg 1$
Liquid-like	Viscoelastic	Solid-like

It is valuable to note that all liquids show elastic properties under appropriate conditions even if these conditions are extreme. The elastic properties for liquids can be observed at a short enough time or a high enough frequency.

The ideal solids and ideal liquids are described by Hooke's and Newton's laws, respectively. In this chapter, theoretical approach for rheological characterization of viscoelastic and liquid-like materials will be given because dilute suspensions behave like a liquid, while concentrated suspensions may have viscoelastic properties.

The ideal case of liquid like materials represented by Newtonian fluids whose viscosity is independent of shear rate (Figure 3.1.a). The relation between shear stress (τ) and shear rate ($\dot{\gamma}$) is represented by the following equation;

$$\tau = \eta \frac{d\gamma}{dt} = \eta \dot{\gamma} \quad (3.1)$$

where γ is the deformation, η is the viscosity and t is time. For non-Newtonian materials, viscosity is a function of shear rate. Generally, non-Newtonian materials behave as Newtonian fluids at low shear rates but then display steadily decreasing viscosity as shear rate increases. These materials are known as shear-thinning or pseudoplastic (Figure 3.1.b) materials. A few materials show Newtonian behavior at low shear rates and then steadily increasing viscosity as shear rate increases. These materials are called as shear-thickening or dilatant (Figure 3.1.c) materials. If the relationship (above a corresponding yield stress) is linear between shear stress and shear rate, the flow behavior is called as Bingham plastic (Figure 3.1.d). Some materials do not flow to any practical extent until a certain stress threshold is reached. These materials are described as having a yield stress (Figure 3.1.e).

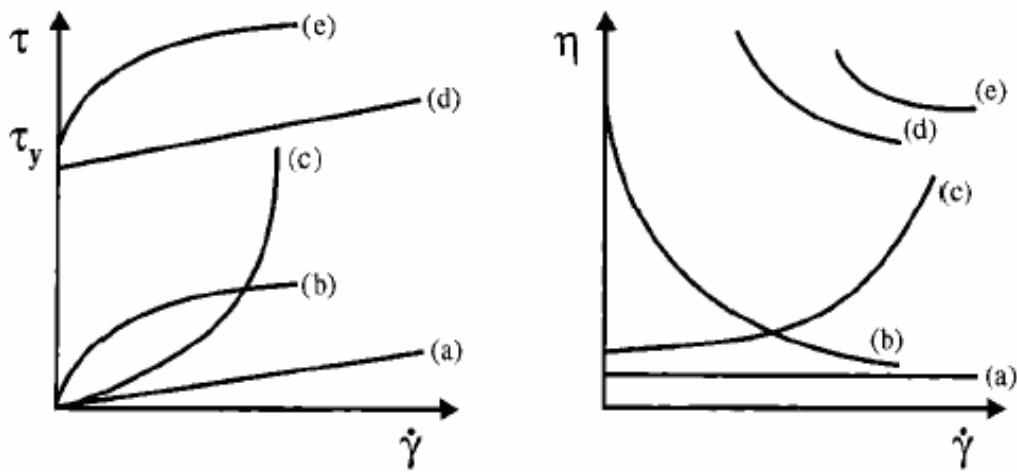


Figure 3.1. Types of rheological behavior exhibited by colloidal dispersions: (a) Newtonian flow; (b) shear thinning (pseudoplastic); (c) shear thickening; (d) Bingham plastic; and (e) pseudoplastic with a yield stress (Source: Lewis, 2000).

Yield stress is defined as the minimum shear stress required initiating flow. It can also be defined as the stress below which a material will not exhibit a fluid-like behavior. In other words, the material which is subjected to stresses less than its yield stress shows a nonpermanent deformation or a slow creeping motion over the time scale of the experiment. The higher the yield value, the more readily a medium will maintain particles in suspension with minimal sedimentation. Thus, the magnitude of the static yield value may be used as one of the criteria for controlling sedimentation during storage and the ease of using or processing a product.

Some systems exhibit a time dependent rheological behavior which is called as thixotropic behavior, which is the change over time in shear stress response of a material due to structural breakdown or formation. In this case, viscosity of fluid decreases (called as thixotropic material) or increases (called as rheopectic material) with time while a constant shear rate is applied. Thixotropic behavior describes degradation of structure of the system and viscosity reduction with time. Therefore, a thixotropic material shows shear-thinning behavior because the orientation of the particles or molecules changes to align flow direction. When the external force is removed, the structure recovers in portion or completely in time. The time taken for the structure to re-assemble itself may range from seconds to hours. A thixotropic loop provides qualitative information about its time dependence, thus the loop area indicates

how fast the structure recovers after the force is removed. This type of experiments provide valuable information about suspension fluidity and time required for rebuilding of disturbed structure upon resting for certain applications like film formation.

The non-Newtonian rheological behaviors were described with different equations. When a material behaves like solid for small applied stress and then flows with a constant differential viscosity for higher shear stresses, it is called as Bingham plastic material;

$$\tau = \tau_o + \eta\dot{\gamma} \quad (3.2)$$

where τ is shear stress, τ_o is yield stress, η is viscosity and $\dot{\gamma}$ is shear rate. A concentrated coal suspension and some food products exhibit this kind of behavior. The deviation from ideality is often negligible for these systems. Power law relation represents varying differential viscosity with a negligible yield value. This model is also known as Oswald-de Waele model;

$$\tau = K\dot{\gamma}^n \quad (3.3)$$

The power law equation has two parameters to fit to experimental data: the exponent of shear rate, n , which is the slope of $\log \tau$ versus $\log \dot{\gamma}$. The second parameter is consistency index (K) and $\log K$ is the y-intercept of the $\log \tau$ versus $\log \dot{\gamma}$ plot, which is related to the magnitude of the viscosity (Morrison, 2000).

Usually, non-linear relationship between shear stress and shear rate above the yield value is observed. The simplest model for this kind of behavior is the Herschel-Bulkley model which is given by;

$$\tau = \tau_o + K\dot{\gamma}^n \quad (3.4)$$

This behavior would be detected by plotting $\log(\tau - \tau_o)$ versus $\log \dot{\gamma}$. This is a linear relationship and its slope gives “ n ” and must be different than unity. This model is an empirical model. This model explains the physical behavior of fluids having three dimensional structure and a sufficient resistance to flow. When fluid is subjected to

shear stress which is high enough, break down of structure progresses non-linearly unlike to Bingham plastic flow. The flow units become smaller as the breakdown progresses and the aligned streamlines become closer as shear rate increases. Thus, a differential viscosity results with increasing shear rate.

More detailed studies showed that shear stress-shear rate curves are mostly linear at very low and very high shear rates. This is recognized and studied by many researchers (see Table 3.1). Ellis, de Haven, and Meter models defined two limiting viscosities;

$$\lim_{\dot{\gamma} \rightarrow 0} \frac{\tau}{\dot{\gamma}} = \eta_o \quad \text{zero shear viscosity} \quad (3.5)$$

$$\lim_{\dot{\gamma} \rightarrow \infty} \frac{\tau}{\dot{\gamma}} = \eta_\infty \quad \text{infinite shear viscosity} \quad (3.6)$$

and the apparent viscosity is between η_o and η_∞ . For Ellis and Meter models, α is often close to 2 and τ_i can be roughly defined as corresponding shear stress where η_o decreases to the half of its final value. The Table 3.1 summarizes the rheological models for Newtonian and non-Newtonian fluids.

If a material is Newtonian, measuring its viscosity would be sufficient to characterize its flow properties. However, non-Newtonian materials may have both liquid like (viscous) and solid like (elastic) properties at the same time. For this kind of materials, Deborah number is in the order of 1. This kind of materials is called as viscoelastic materials. In macroscopic point of view, the material is considered as a continuum (stores energy). However, its properties are considered as dynamic (losses energy) in microscopic point of view. Hence, the properties depends on the balance between elastic (storage of energy) and viscous (loss of energy) parts.

Viscoelastic properties can be determined by applying a constant strain (stress relaxation), or a constant stress (creep), or sinusoidal oscillations which are oscillating strain (deformation sinusoidally) and oscillating stress (applying stress which varies sinusoidally) at a given frequency.

Table 3.1. Rheological models relating shear stress and shear rate (Source: Hunter, 2001).

Model	Equation	Empirical Parameters
Newton	$\tau = \eta \frac{d\gamma}{dt} = \eta \dot{\gamma}$	η
Bingham	$\tau = \tau_0 + \eta_{PL} \dot{\gamma}$	η_{PL}, τ_0
Power Law, 1926	$\tau = K \dot{\gamma}^n$	K, n
Herschel-Bulkley	$\tau = \tau_0 + K \dot{\gamma}^n$	τ_0, K, n
Ellis	$\frac{\tau}{\dot{\gamma}} = \eta = \frac{\eta_0}{\left(1 + (\tau/\tau_i)^{\alpha-1}\right)}$	η_0, τ_i, α
de Haven, 1959	$\frac{\tau}{\dot{\gamma}} = \eta = \frac{\eta_0}{\left(1 + C \tau^n\right)}$	η_0, C, n
Prandtl-Eyring, 1926	$\tau = A \cdot \text{arcsinh}[\dot{\gamma}/B]$	A, B
Powell-Eyring, 1936	$\tau = C \dot{\gamma} + B^{-1} A \cdot \text{arcsinh}[\dot{\gamma}/A]$	A, B, C
Meter, 1964	$\frac{\tau}{\dot{\gamma}} = \eta = \eta_\infty + \frac{\eta_0 - \eta_\infty}{1 + (\tau/\tau_i)^{\alpha-1}}$	$\eta_0, \eta_\infty, \alpha, \tau_i$
Krieger, 1972	$\frac{\eta - \eta_\infty}{\eta_0 - \eta_\infty} = \left[1 + \frac{ \tau }{\tau_i}\right]^{-1}$	$\eta_0, \eta_\infty, \tau_i$
Carreau, 1968	$\frac{\eta - \eta_\infty}{\eta_0 - \eta_\infty} = [1 + (\lambda \dot{\gamma})]^{(n-1)/2}$	$\eta_0, \eta_\infty, \lambda, n$

Stress relaxation is a measure of time dependent response of viscoelasticity. The Hookean solid shows no stress relaxation when it is subjected to a constant strain (Figure 3.2.a.). However, a Newtonian liquid relaxes instantly to zero as soon as the strain becomes constant (Figure 3.2.b.). A viscoelastic solid or liquid shows stress relaxation over a significant time. In viscoelastic liquid the stress relaxes to zero, while it asymptotically approaches to an equilibrium stress, τ_e for viscoelastic solid (Figure 3.2.c.) (Macosko, 1994).

Figure 3.2. Stress response, τ , versus time for a step input in strain of (a) the Hookean solid, (b) the Newtonian fluid, (c) viscoelastic solid or liquid (Source: Macosko, 1994).

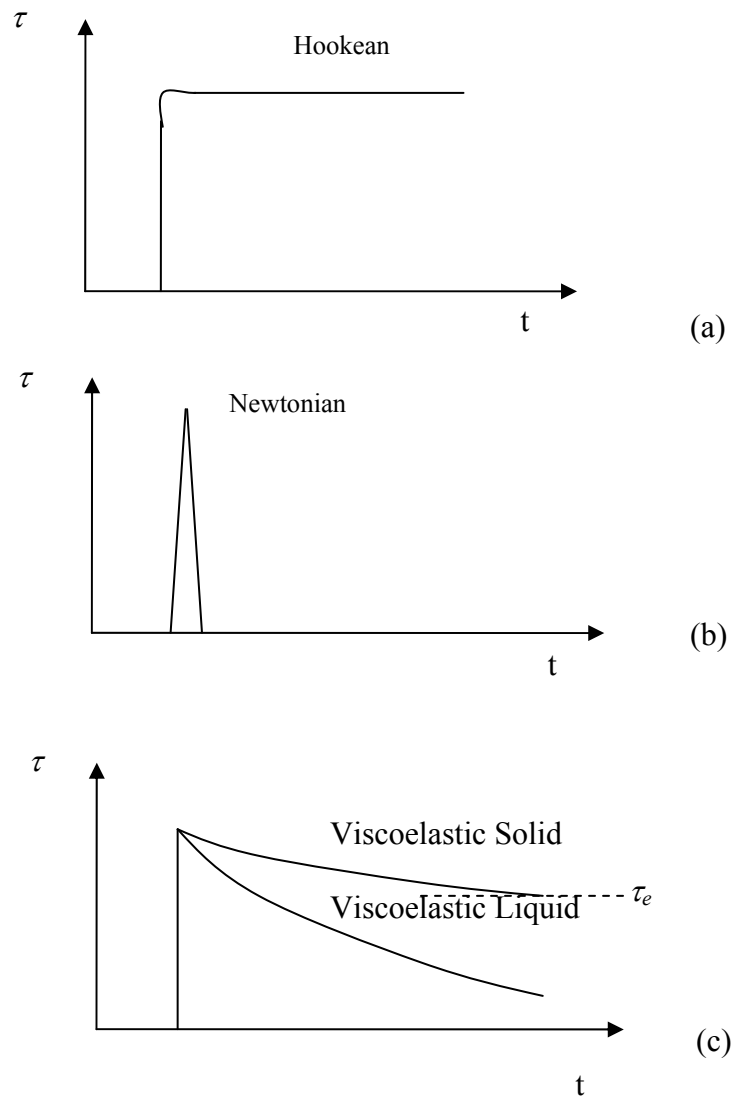


Figure 3.2. Stress response, τ , versus time for a step input in strain of (a) the Hookean solid, (b) the Newtonian fluid, (c) viscoelastic solid or liquid (Source: Macosko, 1994).

The stress relaxation data can be converted to a relaxation modulus (G) by the following equation;

$$G(t) = \frac{\tau(t)}{\gamma_o} \quad (3.7)$$

where γ_o is the applied strain which is constant (Macosko, 1994).

Dilute solutions or suspensions show complete stress relaxation in very short times. However, concentrated suspensions show short relaxation time followed by a constant modulus at very low strain values.

Creep experiments are done by applying a constant stress and by determining strain which increases with time. The ratio of strain per stress defines the compliance (J) of the material,

$$J(t) = \frac{\gamma(t)}{\tau_o} \quad (3.8)$$

where τ_o is the applied stress which is constant.

A highly compliant material exhibits a large strain for small applied stresses. The reverse of the ratio (resulting stress per applied strain) gives rigidity of the material. A highly rigid material exhibits high stresses with respect to applied small strain (Macosko, 1994). The compliance sometimes is called creep compliance.

If a constant stress is applied for a while (t_1) and then removed, there may be no flow and strain maybe recovered completely. If there is a flow, the recovery can not be completed. This is another type of experiment often done in conjunction with creep and called as creep and recovery test. Creep region (γ_C) and recovery region (γ_R) are given by,

$$\gamma_C = \tau_o J(t) \quad (3.9)$$

and

$$\gamma_R = \tau_o [J(t_1) - J(t - t_1)] \quad (3.10)$$

In general, there are three regions present in the creep compliance-time curve as it is given in Figure 3.3. The bonds between the primary structural units stretch elastically in the region of instantaneous compliance (curve AB). Curve BC represents the time-dependent retarded elastic region with compliance J_R . The linear region with steady-state compliance J is the curve CD. The time required to reform the ruptured bonds is in excess of the test period. After the stress is removed, a recovery occurs, which is represented by DF. The magnitude of the instantaneous elastic recovery (DE) is the same as AB. It is followed by a retarded elastic recovery which is equivalent to the retarded region of the creep curve. The original structure is never recovered completely,

since some bonds are irreversibly broken in the creep region. The degree of recovery is represented by the recoverable compliance J_R , which is equal to $AH (J_c)$.

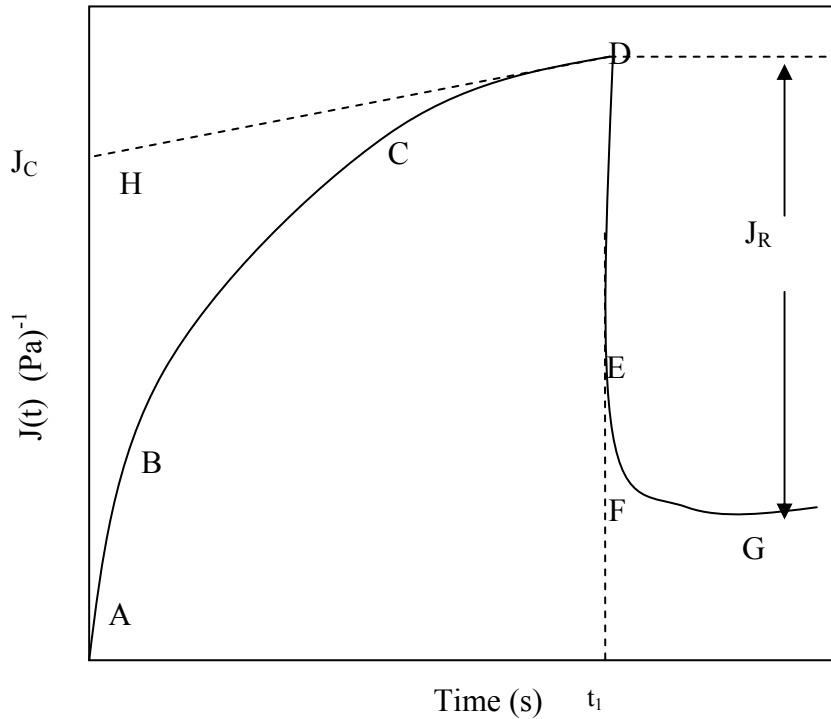


Figure 3.3. The creep recovery of a material.

The significance of oscillatory measurements lies on the resulted non-destructive measurements that are delivered in terms of discrete components of materials such as viscosity or shear modulus. The Figure 3.4. shows the oscillatory movement that material experiences. Generally, viscoelastic materials display time and temperature dependent properties. By analyzing with oscillatory measurements, the viscosity and shear modulus of a viscoelastic material can be resolved into “viscous” and “elastic” components (Goodwin and Hughes, 2000). The basic idea is to apply a sine wave shaped strain (or stress) and to measure, the response of the material, stress (or strain).

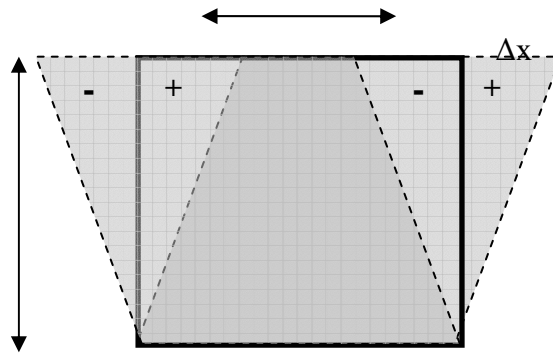


Figure 3.4. The schematic diagram for oscillatory movement.

The oscillating stress with time at constant frequency gives a response of material as oscillating strain. If strain is being oscillating, the response will be oscillating stress. This behavior is approached by combining Hookean spring and Newtonian dashpots. Hookean spring obeys the Hooke's law and the response of the spring can be described by shear modulus (G) (see Figure 3.5.a). The Newtonian dashpot is composed of a cup filled with Newtonian oil having a viscosity η and a piston placed in the oil (see Figure 3.5.b).

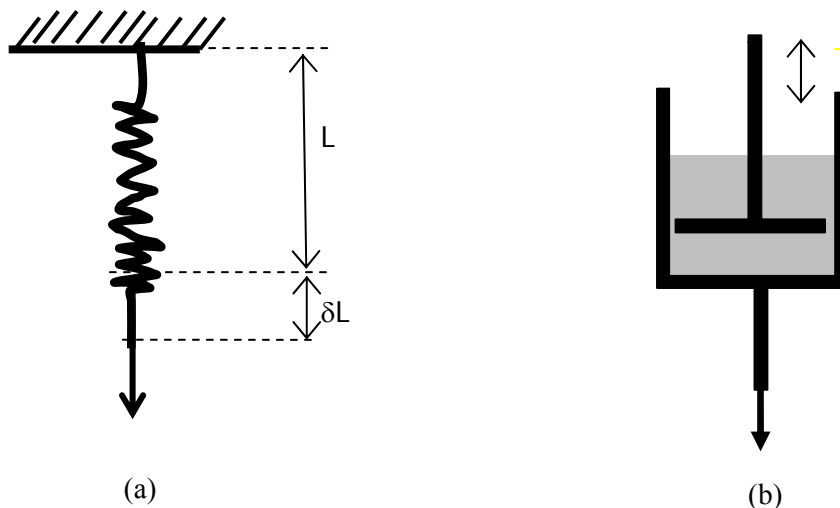


Figure 3.5. (a) the Hookean Solid and (b) the Newtonian Liquid.

The Hookean solid is perfectly elastic and the deformation is proportional to any force applied. This relationship is given in the following equation;

$$\tau_E = G\gamma_E \quad (3.11)$$

where τ_E is the shear stress, G is the spring modulus and γ_E is the strain.

The dashpot contains the Newtonian liquid and the relationship between shear stress and shear rate is expressed mathematically as;

$$\tau_V = \eta\dot{\gamma}_V \quad (3.12)$$

where τ_V is the shear stress and $\dot{\gamma}_V$ is the applied shear rate and η is viscosity. The shear rate is derived by taking the derivative of the strain with respect to time,

$$\dot{\gamma} = d\gamma / dt \quad (3.13)$$

a) The Kelvin-Voigt Model

According to the Kelvin model, the linear stresses are added to visualize viscoelastic response due to combination of the Hookean solid and the Newtonian liquid by arranging them in parallel as seen in Figure 3.6,

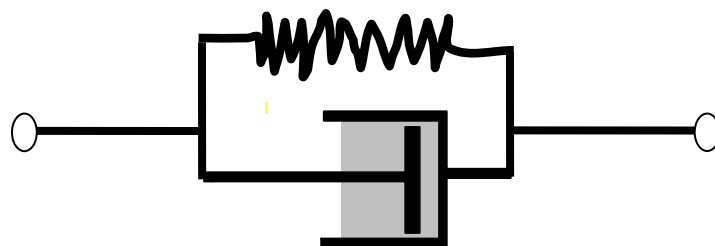


Figure 3.6. The schematic diagram of the Kelvin-Voigt model.

Any strain applied to the system is the same strain being applied to the spring and the dashpot,

$$\gamma = \gamma_E = \gamma_V \quad (3.14)$$

The total stress is equal to the spring stress plus the dashpot stress,

$$\tau = \tau_E + \tau_V \quad (3.15)$$

Hence, the constitutive equation describing the Kelvin-Voigt model becomes,

$$\tau = G\gamma_E + \eta\dot{\gamma}_V = G\gamma + \eta \frac{d\gamma}{dt} \quad (3.16)$$

A sinusoidally varying strain (γ) applied to the material is expressed as,

$$\gamma = \gamma_o \sin(\omega t) \quad (3.17)$$

where γ_o is the strain amplitude, ω is the radial frequency of strain, and t is time.

The radial frequency is defined by,

$$\omega = 2\pi f \quad (3.18)$$

f is applied frequency measured in Hertz. When the strain expression is inserted to the shear stress acting on the spring, the stress equation becomes,

$$\tau_E = G\gamma_o \sin(\omega t) \quad (3.19)$$

It can be said that the applied strain (γ) and the resulted shear stress on the spring (τ_E) are “in-phase” because both of them are sine wave.

The strain rate is obtained by differentiating the strain equation with respect to time,

$$\frac{d\gamma}{dt} = \dot{\gamma} = \omega\gamma_o \cos(\omega t) \quad (3.20)$$

The resulted stress acting on the dashpot can be expressed as,

$$\tau_v = \eta\omega\gamma_o \cos(\omega t) \quad (3.21)$$

The applied strain and the resulted shear stress on the dashpot are 90° out-of-phase, because the strain is a sine wave and the stress is cosine wave. Finally, the total stress response (τ) of material according to the Kelvin-Voigt model can be expressed as a sum of in phase and out-of-phase components,

$$\tau = G\gamma_o \sin(\omega t) + \eta\omega\gamma_o \cos(\omega t) \quad (3.22)$$

Here, it is seen that the resulted stress consists of two kinds of stresses: the first one is “in-phase” which is elastic component, and the second one is “out-of-phase” which is the viscous component.

If a Newtonian liquid is subjected to oscillating strain, the peak stress is out of phase because the peak stress is proportional to the rate of strain. For a viscoelastic material, some energy is stored and some energy is dissipated, hence, the stored contribution is in phase and the dissipated contribution is out of phase.

b) The Maxwell Model

The strain rates are added according to the Maxwell model due to combination of the Hookean solid and the Newtonian liquid by arranging in series (see Figure 3.7.),

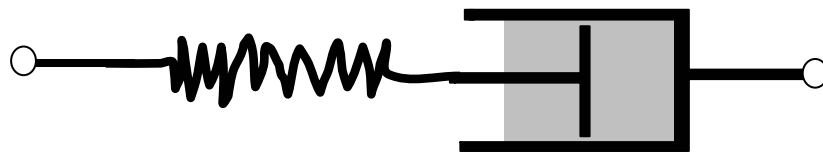


Figure 3.7. The schematic diagram of the Maxwell model.

The total stress resulted on this system is the same stress resulted on the spring and the dashpot,

$$\tau = \tau_E = \tau_V \quad (3.23)$$

The total strain is equal to the spring strain plus the dashpot strain,

$$\gamma = \gamma_E + \gamma_V \quad (3.24)$$

The strain rate is expressed as,

$$\frac{d\gamma}{dt} = \frac{d\gamma_E}{dt} + \frac{d\gamma_V}{dt} \quad (3.25)$$

and, the constitutive equation of Maxwell model is,

$$\dot{\gamma} = \frac{1}{G} \left(\frac{d\tau}{dt} \right) + \frac{\tau}{\eta} \quad (3.26)$$

When the equation 3.20 is inserted to the equation 3.26, the Maxwell model becomes,

$$\omega\gamma_o \cos(\omega t) = \frac{1}{G} \left(\frac{d\tau}{dt} \right) + \frac{\tau}{\eta} \quad (3.27)$$

The steady state solution of this first order differential equation is,

$$\tau = \frac{G(\lambda\omega)^2 \gamma_o}{1 + (\lambda\omega)^2} \sin(\omega t) + \frac{G\lambda\omega\gamma_o}{1 + (\lambda\omega)^2} \cos(\omega t) \quad (3.28)$$

The term of λ is the relaxation time and is defined as,

$$\lambda = \eta/G \quad (3.29)$$

Again, the resulted stress consists of two stresses: the first term is “in-phase” which is elastic component, and the second term is “out-of-phase” which is the viscous component.

Both of these models describe viscoelastic behavior. More complex combinations of the Hookean solid and the Newtonian liquid models may yield more complex equations which can better describe more complex rheological profiles.

When a constant strain is applied to a material, the angular velocity and the strain amplitude are assigned parameters (see Figure 3.8).

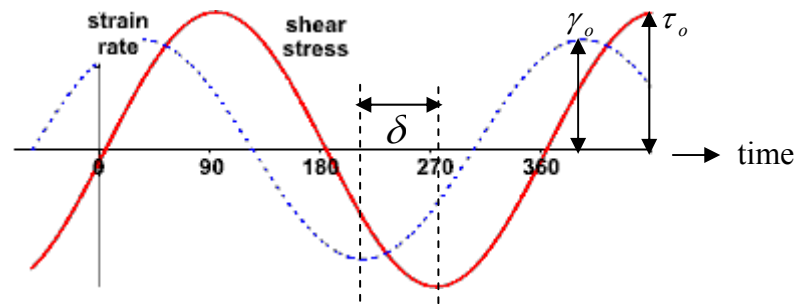


Figure 3.8. A schematic diagram for an oscillating strain and the stress response of a material which is viscoelastic with respect to time.

The assigned strain and the measured shear stress are given as,

$$\gamma = \gamma_o \sin(\omega t) \quad (3.30)$$

$$\tau = \tau_o \sin(\omega t + \delta) \quad (3.31)$$

where δ is the phase angle, γ_o and τ_o is the strain and the shear stress amplitude respectively. The shear stress expression can be expanded as,

$$\tau = \tau_o [\cos \delta \cdot \sin(\omega t) + \sin \delta \cdot \cos(\omega t)] \quad (3.32)$$

Both the Kelvin-Voigt and the Maxwell model have two contributions corresponding to the elastic (G') and the viscous (G'') components.

$$G'(\omega) = \frac{\tau_o}{\gamma_o} \cos(\delta) \quad (3.33)$$

$$G''(\omega) = \frac{\tau_o}{\gamma_o} \sin(\delta) \quad (3.34)$$

where G' is elastic or storage modulus is the stress that is in phase with the strain and is a measure of the solid-like or structured nature (*i.e.*, energy storage) of a material. The viscous or loss modulus G'' is the stress that is 90° out of phase with the strain. It is a measure of the liquid-like nature (*i.e.*, viscous dissipation) of a material. The ratio of viscous modulus to elastic modulus gives the phase angle,

$$\tan(\delta) = \frac{G''}{G'} \quad (3.35)$$

Thus, G' and G'' provide information on the microstructure of a material by decoupling its elastic and viscous properties. The complex modulus is given as,

$$G^* = G'(\omega) + iG''(\omega) \quad (3.36)$$

where i is equal to $\sqrt{-1}$. When the testing material is purely elastic, then the phase angle and viscous modulus equal to zero and the complex modulus equals to storage modulus. However, for purely viscous material, the phase angle equals to 90° and, the storage modulus becomes zero and the complex modulus equals to the viscous modulus.

The storage viscosity and the dynamic viscosity of the material are defined by using following equations,

$$\eta' = \frac{G''}{\omega} = \frac{\tau_o''}{\dot{\gamma}_o} = \left(\frac{\tau_o}{\gamma_o} \omega \right) \sin(\delta) \quad (3.37)$$

$$\eta'' = \frac{G'}{\omega} = \frac{\tau_o'}{\dot{\gamma}_o} = \left(\frac{\tau_o}{\gamma_o} \omega \right) \cos(\delta) \quad (3.38)$$

and the complex viscosity is,

$$|\eta^*| = (\eta'^2 + \eta''^2)^{1/2} = \left[\left(\frac{G''}{\omega} \right)^2 + \left(\frac{G'}{\omega} \right)^2 \right]^{1/2} = \frac{1}{\omega} |G^*| \quad (3.39)$$

The stress response of the material, can be written both in terms of moduli and in terms of viscosities,

$$\tau = G' \gamma_o \sin(\omega t) + G'' \gamma_o \cos(\omega t) \quad (3.40)$$

$$\tau = \eta'' \gamma_o \omega \sin(\omega t) + \eta' \gamma_o \omega \cos(\omega t) \quad (3.41)$$

The aim of oscillating strain sweep test is to measure the point where the stiffness or the strength of a material is initially affected by the amount of strain. This test may be used to determine linear viscoelastic region and critical strain. When the moduli and phase angle remain constant as a function of strain in a certain range of strain, the material classified as linear-viscoelastic in that range and the test considered being non-destructive. The critical strain, at which the material becomes non-linear viscoelastic, indicates the minimum energy required to disrupt the structure, which is dependent on the dispersion quality. The higher the critical strain the better the system is dispersed.

An alternative method of monitoring storage, viscous, and complex modulus, and complex viscosity with respect to frequency is to apply a sinusoidally varying stress and measure the sinusoidal strain output.

These components of bulk viscosity or modulus have specific meanings in context of bulk properties of material. Each of them is very sensitive to specific events happening in the morphology or microstructure or even in nanostructure of the material. These structural variations are often invisible when traditional viscometers are used.

3.1. The Types of Rheometers

The most basic and widely used form of rheometers is the steady shear viscometer. There are a wide variety of existing devices which have been developed for

the measurement of steady shear viscosity specific to certain applications (Figure 3.9). The common goal of all these devices is to determine the bulk viscosity of a material as it flows in a steady shear or continuous fashion. However, in order to make a comparison between materials, simple shear viscosity measurements becomes limited in use.

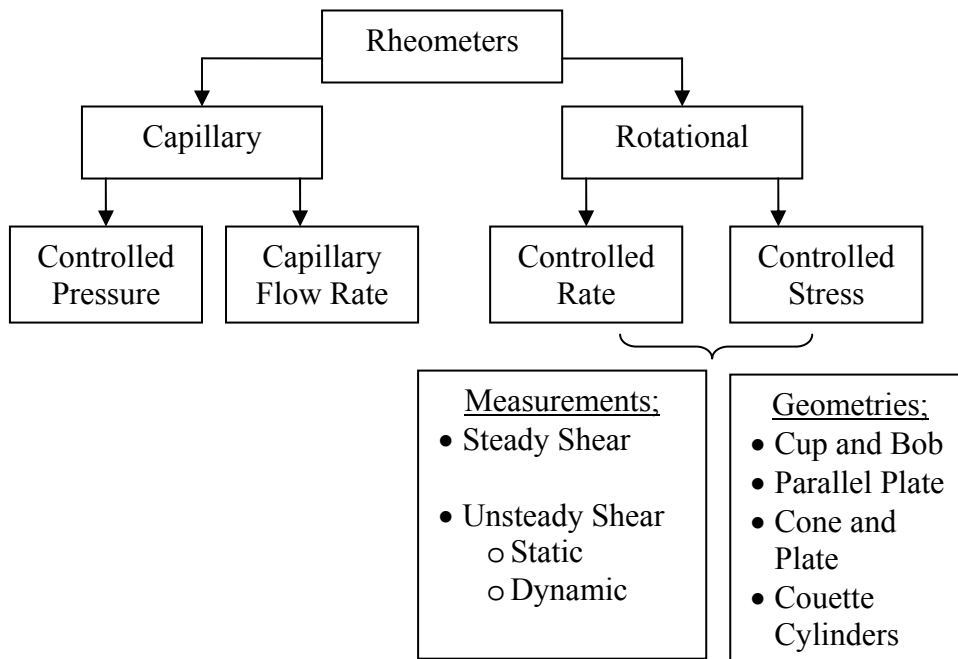


Figure 3.9. Schematic diagram of different type of rheometers, measurements, and geometries.

The ability of applying small deformations constantly or dynamically may allow visualizing dynamic shear testing. In dynamic (oscillatory) measurements, the sample is being vibrated between two parallel plates or concentric cylinders as opposite to being sheared continuously. Here the controlling oscillation at controlled temperature play important role to determine materials behavior. A sinusoidal stress or strain is applied and the induced response is determined in the oscillation technique. By this way, the sample continuously excites but never exceeds a strain large enough to destroy structure. Thus linear viscoelastic region can be observed. When the sample is overstrained the elastic structure will be destroyed.

The common geometries used to observe steady shear rheology and dynamic shear rheology are given in Figure 3.10. The appropriate geometry is dictated primarily

by the properties of sample material and by the desire to simulate a process or in situ application.

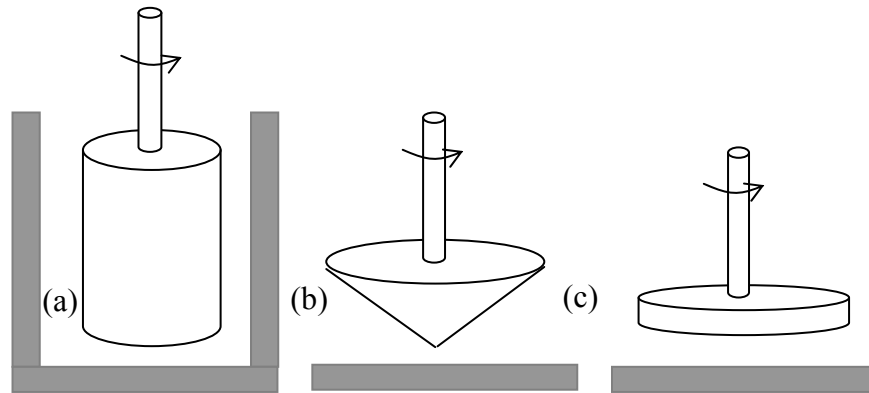


Figure 3.10. Typical testing geometries for rheometers a) concentric cylinder (couette), b) cone and plate, and c) parallel plates.

Different processes and the influence on product properties or changes in formulations can be simulated by using rheological studies. These measurements can be used to examine material structure for quality control of raw material, and/or process control such as consistency, reliability, shear and/or storage stability against sedimentation. Since, every application requires its own specialized characterization tests, sometimes it is difficult to observe and optimize small differences during process. However, rheological measurements can reveal all these small variations. These measurements can also be of help in the development of new products, giving better understanding of the processes governing the final properties.

It can be said that rheological behavior can be observed under either extensional or shear deformation. Shear deformation take into account due to its relevance to the scope of this thesis. Shear rheology can be divided into steady shear or dynamic shear. Steady shear rheology experiments can be used to obtain information on viscosity as a function of steady shear rate. Dynamic shear rheology experiments can be conducted in two different ways. The first one is called as static because a small strain or stress is applied to the sample which is stress relaxation and creep and recovery tests, respectively. The second one is called as dynamic. The corresponding tests are time, amplitude, frequency, temperature sweep tests, in which the measurements are performed at low strain amplitudes. The definitions of rheological property

determination methods in the following part are associated with the capabilities of Haake Mars II Advanced Rheometer System.

3.2. Sources of Error in Rheological Experiments

There are several sources of error which may affect the rheological measurements seriously. During application of a rheological technique, one should be aware of the sources of error which may be based on instrument, measurement system and/or based on sample instabilities.

Poor calibration and machining or alignment of the instrument might be an important source of error. The errors based on measurement system might be caused by inertial contribution of fluid (Fluid inertia), by the difference between the measured and the calculated shear rate at the edge of measurement system (edge effects), by viscous dissipation of heat during flow. The errors based on sample instabilities involve sample fracturing, centrifugal expulsion and the material itself (Collyer and Clegg, 1998).

The inertial contribution of fluid is needed to be neglected for satisfying the conservation of linear momentum. The presence of fluid inertia has two effects for rheological measurements with cone and plate and parallel plate geometries: contribution to pressure gradient to the stress distribution along the measurement gap and contribution to actual flow field by creating inner flow towards the apex of cone and outflow along the plate. The contribution of the flow inertia can produce shear thickening effect. This inertia driven secondary flow can be negligible if the $N_{RE} < 40$ for parallel plate measurement system and if $0.15 N_{RE}^2 < 1$ for cone and plate measurement system with small cone angles. The Reynolds number is calculated by the following equation,

$$N_{RE} = \frac{\rho \Omega R^2}{\eta} \quad (3.42)$$

where ρ is density of the material (kg/m^3), Ω is the angular velocity (1/s), R is the radius of the measurement apparatus (m) and η is the viscosity (Pa.s). The error in measured torque due to flow geometry may be caused by edge effects. The edge effect means the difference between measured and calculated (ideal) shear rate at the edge.

The edge effects become significant for cone and plate measurement system if the cone angle is greater than 4° . The edge effect becomes larger if the material has non-Newtonian rheological behavior. There is a greater tendency to deviate from ideal flow at edge for non-Newtonian fluids than Newtonian. If the distance of gap over diameter (h/D) is less than 0.075, the error in measured torque becomes less than 2% for parallel plate measurement system.

The energy generation due to flow can produce changes in temperature and may lead deviation in measured viscosity values. Viscous heating effect becomes greater at high shear rates and for highly viscous materials.

Sample fracturing is an inward propagation of a crack from the edge (sample air interface) in cone and plate and parallel plate measurement systems. This is caused by secondary normal forces. The centrifugal expulsion arises due to centrifugal forces. Sample fracturing and centrifugal expulsion limits the highest shear rate applied. The nature of the material may cause severe experimental difficulties. The difficulties may be slippage at fluid-solid interface, inhomogeneity of the sample, shear induced particle migration, particle bridging across the gap, sedimentation, presence of air bubbles, and sample evaporation. The thin layer of liquid at the top of the suspension which has lower viscosity may cause the slippage. The serrated surfaces may disrupt this layer. Shear induced particle migration may be caused by the non-uniform shear field. The particles are accumulate in the center of the sample due to shear forces. The particle bridging mostly occurs in the cone and plate geometry. The presence of several particles having the similar size with the gap between the apex and the plate may cause asymmetric torque measurements. Sedimentation will have a significant effect when the density difference between particle and suspending medium is large. The sedimentation of the particle may be eliminated or postponed if double cup and bob or concentric cylinder geometries is used. The presence of air bubbles may cause phase separation at the top. If the samples are subjected to vacuum, the bubbles can be removed. The rheological behavior of highly concentrated suspensions or solutions will be easily affected by evaporation of medium or solute, even in small amounts. One method to control evaporation is to coat the sample-air interface with a layer of a low volatility, relatively non-viscous oil. Humidifying the sample environment and/or eliminating the direct air-flow through the measurement space may be helpful methods to prevent evaporation.

3.3. Recent Studies on the Rheological Behavior of Ceramic Dispersions

The use of rheometric techniques to characterize ceramic suspensions was scarcely investigated when compared with molten polymeric materials. The use of rheometric techniques could allow us to observe and understand the regarding materials and the interactions with additives such as dispersants and binders. The understanding of rheology of ceramic suspensions is fundamental in applications and optimization of products and properties.

The rheological behavior of suspensions prepared with sub-micron or micron sized particles were investigated widely. Cesarano and Aksay (1988) investigated the stability and rheology of α -alumina suspensions with polyacrylic acid and Na^+ salt of polymethacrylic acid as a function of pH, solids loading, and molecular weight. They used high purity, sub-micron size α -alumina powders (0.2 and 1.0 μm in size) whose surface areas were 4.5 and 6.8 m^2/g . The suspension pH was varied between 4.5 and 10.0. They found that as the volume percent of solids increases, the viscosity increases with narrower pH intervals where the lowest viscosity is obtained. The polyelectrolyte became fully charged at pH 8.8 and the viscosity had the lowest value for all cases. Above pH 9, adsorption of polyelectrolyte did not occur. The amount of water was small and the concentration of excess polyelectrolyte in solution became appreciable which led to an increase in viscosity. Excess amount of polyelectrolyte led to depletion flocculation. Below pH 9, the repulsive barrier decreases because of a decrease in the negative charge characteristics and led to an increase in viscosity. They reported that 62 vol % alumina suspensions with 0.42 μm particles in size had viscosities below 0.5 Pa.s.

Ferrira and Olhero (2004) investigated the effect of particle size and distribution on the rheological behavior of silica suspensions which were prepared by mixing powders having different particle sizes (2.2, 6.5, and 19 μm) with finer powder (fumed silica) having a particle size of 0.07 μm . They reported that the presence of fine powder (0.07 μm) caused shear thinning behavior for slurries prepared with 2.2 μm sized powder. In contrast, shear thickening behavior was observed for slurries prepared with 10 μm sized powder.

Liu (1998c) investigated the stability and rheological behavior of 3Y-ZrO₂ having 95 nm powders with the addition of polyacrylic acid. The suspensions were

formed by slip casting and densities of greenbodies were taken into account. Suspensions having 45-55 vol% solids content were prepared and it was observed that yield stress of suspensions increased with the increase of solid content.

Schilling and his colleagues (Kim et al., 2000; Schilling et al., 2002a; Schilling et al., 2002b) worked on the rheological behavior of suspensions having sub-micron and nano sized alumina particles with addition of mono and polysaccharides. Generally, the addition of saccharides having different molecular weights led to a decrease in the viscosity and the yield stress of suspensions. In one of their studies, they prepared a suspension of sub-micron α -alumina powder with and without the addition of polysaccharides. The addition of high molecular weight polysaccharides led to thixotropic behavior. However, the authors observed that suspensions showed a Newtonian like rheological behavior with the addition of polysaccharides in general. However results of another study conducted by the authors revealed that the presence of nano sized particles, the rheological behavior of suspensions fitted to Herschel-Bulkley model.

A similar powder-medium was investigated by Tseng and Wu (2003). They investigated the rheological behavior of aqueous suspensions having sub-micron sized α -alumina powder. In contrast to other referred studies, they prepared suspensions with 1-15 vol% solids content without addition of dispersants. They considered the microstructure of sintered thick sheets which were prepared by electrophoretic deposition method. They observed more porous structure from concentrated suspension with respect to lower ones. In another study (Tseng and Lin, 2003), nano titania particles (7-20 nm) were suspended in water without addition of any dispersants. The rheological behavior was observed. To determine the yield stress, they investigated the aggregation of the particles. They stated that the formation of agglomerates would be taking place which was related to the diffusion limited cluster-cluster model.

Tari et al. (1998) investigated the flow characteristics of several alumina suspensions with a particle size ranging from submicron (0.1 μm) to micron range (1 μm). They observed that suspension of high solids content exhibited shear thinning behavior. The shear thinning is attributed to the release of immobilized water present in the flocculates. They stated that as the shear rate increased the network of flocculates were broken and the “entrapped” water was released and hence, lower viscosity was observed. Moreover, as the particle size decreased, the effect of the entrapped water might be more significant.

Li and Akinç (2005) reported the study on the nature (and hence the mobility) of water in aqueous suspensions of nanometric alumina particles and the rheological properties. The suspensions have various solids contents and fructose concentrations. They set their primary purpose as the understanding of the role of mono- and disaccharides for altering the rheology of nanoparticle suspensions. They stated that the influence of water adsorption on rheology of suspensions was twofold: it restricts the mobility of water molecules and reduces the fraction of free water contributing to the flow and the overlap of the bound water layers leads to dipole interaction between particles, hence increased resistance to flow. They concluded that as the particle size approaches nanoscale, the role of adsorbed layers becomes quite significant.

In the last ten years, the rheometric techniques rather than the determination of flow behavior and viscosity such as dynamic measurements were used to understand suspension behavior. Kirby et al. (2005) worked on the effect of polyethyleneimine (PEI) on the rheological behavior of aqueous mullite and barium strontium aluminosilicate (BSAS) suspensions to optimize a dip-coating process. The suspensions having 20-45 vol% of particles were subjected to ultrasonic treatment for 5 min, presheared at a stress of 200 Pa and allowed to equilibrate prior to measurement for 15 minutes. Furthermore, a specially designed solvent trap was used to minimize the evaporation of water. In this way, variations in sample handling were minimized to ensure reproducibility of the data. Stress viscometer measurements were carried out on concentrated mullite and BSAS suspensions (45 vol% solids loading at pH 7) of varying PEI concentration. They found that the critical PEI concentrations to minimize linear elastic moduli and yield stress were 0.2 mg/mm^2 of mullite and 0.4 mg/mm^2 of BSAS, respectively. Above the critical PEI concentration of each system, the apparent viscosity increased and shear-thinning flow behavior intensified with increasing PEI concentration. Such effects typically stem from an increasing fraction of polymer that does not adsorb to the ceramic particles, but is dissolved in the solution medium.

Wolthers et al. (1996) investigated on the rheological behavior of depletion flocculated dispersion of silica particles by using two different rheometers, a controlled stress and a harmonic rheometer. The authors divided the viscoelastic measurements into three sections: retardation, relaxation and harmonic experiments. They defined retardation experiments as application of small amount of stress and observation of deformation with respect to time. In contrast to retardation experiments, relaxation experiments involve application of small amount of deformation and observation of

stress with respect to time. Harmonic experiments were described as the measure of the frequency dependency of the material. The suspensions were characterized by retardation and harmonic experiments. The solids content of the suspensions differed from 8 to 16.1 vol%. The particles were coated with stearyl and dispersed in cyclohexane. When adequate polystyrene was added to the system depletion flocculation occurred. Aggregating systems are notorious for their experimental problems, they had often strongly shear thinning behavior and in addition their rheological properties can be a function of the shear history. The experiments were repeated three times with fresh samples. However, the errors of the repeated measurements were within 50% systematic error. Increase in volume fraction increases the error. The authors ascribe these systematic errors to differences in shear history, which may occur during the filling of the rheometer.

One of the main problems in rheological measurements of the suspensions was to reset the shear history. Schmidt and Münstedt (2002) worked on the concentrated monodisperse suspensions as a function of preshear conditions and temperature. They used two different glass spheres (0.27 and 1.18 μm in size) which were dispersed in polyisobutylenes having different molecular weights. The volume fractions of the suspensions were ranging between 0.20 and 0.35. The study focused on the microstructural changes during preshearing. The preshear experiments were done at constant shear stress (0.19 Pa) and only the time period of preshear was differed. The viscosity and dynamic-mechanical experiments (dynamic shear experiments) of the suspensions were conducted after preshearing. They found that the influence of preshear time on the stress dependence of the shear viscosity was less pronounced at low volume fractions. They observed an increase in shear viscosity at small stresses during preshearing which was attributed to the formation of a particle network due to particle diffusion. The viscosity reached to η_{∞} which were not affected by the preshear history. The dynamic experiments showed that viscous modulus was dominant over storage modulus. Both the G' and the G'' values increased as the frequency (ω) increased. The suspensions transformed from viscoelastic liquid to viscoelastic solid as frequency was decreased. There were decrease of the G'' with ω and the G' with ω^2 at high frequencies and decrease of both G' and G'' with ω at low frequencies. The measurement temperature has an effect on the behavior of the G' . When the experiment was done at 31.3°C the G' increased with frequency and reached a plateau. However,

increasing the temperature to 40°C caused the G' have a shoulder between high and low frequency or a plateau at intermediate frequencies.

Aoki et al. (2003) worked on the rheology of carbon black suspensions. The carbon black suspensions were used as an additive for pigmentation, UV protection, and in plastics, inks and coatings to control rheological behavior. The average particle and the aggregate size of the carbon black particles were 76 nm and 230 nm, respectively. The suspending mediums were 20 wt% polystyrene in dibutyl phthalate (PS-DBP) and two varnishes: a rosin-modified phenol resin (Varnish-1) and an alkyd resin (Varnish-2). The solids loading of the suspensions were between 0 and 35 wt%. They found that three different rheological behaviors were observed for these three different suspending media. When the carbon black particles were mixed with PS-DBP, the affinity of the suspending medium towards carbon black particles was described as low and the polystyrene partially was adsorbed onto particles. The frequency sweep tests have shown that the G' was dominant over the G'' . The G' and the G'' were increased with the increase of solids loading and were insensitive to angular frequency. This behavior was explained as the reflection of the solid like character of agglomerated network under small strain. When Varnish-1 was used as a suspending medium, the affinity of the suspending medium was described as moderate. The G' was dominant over the G'' and the G' and the G'' were increased with the increase of solids loading and angular frequency. This behavior denoted a gel-like, self-similarly branched fractal network. The dependency of the G' and the G'' on angular frequency was power law type ($G' \approx G''(\omega)/\tan\delta \propto \omega^n$). The critical gelation point was observed at $n=0.71$ at $\tan(\pi n/2)$ for the suspension having 35 vol% carbon black. The affinity of the Varnish-2 was the highest among the other mediums. The particles were randomly dispersed to form no large agglomerates.

Lu and Kessler (2006) worked on the effects of polyacrylic acid (PAA) and ammonium-poly (methacrylic acid) (PMAA) on dispersion and rheology of nano-alumina suspensions. First of all, 10 wt% glycerol solution was prepared and ball-milled for 5 min. The particles were added incrementally (10 g) and homogenized by ball-milling for 12 hours after each addition. The pH of the suspension was kept at 1.5 by HCl addition to promote the adsorption PAA or ammonium PMAA. Then, the pH of the suspension was adjusted to 9.5 by NH_4OH addition. The final suspension was mixed for 24 hours. They found that when particle size decreased from 0.2 μm to 38 nm, the

required amount of PAA became 20 times higher. They stated that more PAA was needed and the efficiency of PAA adsorption became lower when the particle size approaches to nano. The increase in viscosity of the nano- Al_2O_3 suspensions with respect to the Al_2O_3 suspensions having 0.2 μm particles under the same conditions might be due to the increase of the overlapping areas between the particles. The presence of PMAA- NH_4 suspension instead of PAA caused higher viscosity and shear stress at all shear rates compared to the PAA suspension due to longer chains which resulted in thicker electrical double layer and larger overlapping area.

Lu (2007) worked on the rheological behavior of carbon nano tube (CNT) and alumina particle dispersion system. The average particle size of the alumina particles was found as 27.5 nm. The CNTs were multi-walled with 1-30 nm in diameter and 0.5-40 μm in length. The surface areas of alumina and CNTs were 45 and 40-300 m^2/g , respectively. The disperse medium was aqueous glycerol solution (10 wt%) and polyacrylic acid was used as a dispersant. The suspensions were prepared by following the same procedure described in Lu and Kessler's study (Lu and Kessler 2006). The volume fractions of pure nano-alumina suspensions were ranging between 20 and 45 vol%. The solids loading of the nano-alumina-CNT co-dispersions were 40 vol% and contained 0- 2.6 vol% of CNTs. The CNTs were added in small amounts and the suspension was ball-milled for 1 hour after each addition. The samples were presheared at 0.6 Pa for 60 s and then, dynamic measurements were done for three times. The viscosities of pure nano-alumina suspensions having 20-45 vol% solids loading were between 0.03 and 4.35 Pa.s at a shear rate of 30 $1/\text{s}$. The flow behaviors of the suspensions were described by Herschel-Bulkley model. The dynamic steady shear measurements showed that the G' was dominant at higher angular frequencies and there was a crossover point of G' and G'' as the angular frequency decreased. This behavior denoted the transition of the suspension structure from more elastic (at high angular frequencies) to more viscoplastic (at low angular frequencies). The interaction of adsorbed PAA layers arises as the solids loading increases. When the angular frequency ω approaches zero, G' represents the energy storage capability of a suspension under "undisturbed conditions". The G'' became negligible at angular frequency close to zero for 20 vol% nano-alumina suspensions, which means the suspension has a little viscoplastic behavior under static conditions. The G' and the G'' moduli became higher (150 and 120 Pa respectively) as angular frequency approaches to zero when the solids

loading was increased to 40 vol%. It was considered as the experienced fundamental structural reorganization during the oscillatory test of the suspension having 40 vol% solids. The structural change was not restored after the oscillatory shear. The addition of CNTs in small amounts (below 1.3 vol%) did not change the rheological behavior of nano-alumina suspensions. The CNTs may be far apart and may not be in contact with each other. However, when the solids contents of CNTs were above 1.3 vol%, yield stress of the suspensions increased and the G' became higher than the G'' at all angular frequencies.

CHAPTER 4

EXPERIMENTAL STUDY

4.1. Powder Preparation

The preparation of titania particles was performed by the hydrolysis of titanium isopropoxide by introducing into ethanol-water mixture at room temperature. The schematic illustration of the experimental set-up was given in Figure 4.1. Titanium (IV) isopropoxide was diluted by ethanol (TiISP/EtOH=0.45) in a glass bottle and led to be mixed for an hour by a magnetic stirrer to reach to equilibrium. An ethanol-water mixture (EtOH/H₂O=1) was prepared in a beaker and placed in an ultrasonic bath. Mixing was provided by a laboratory-type mixer. While the ethanol-water mixture (400 mL) was mixed and subjected to the sonification at the same time, titanium (IV) isopropoxide-ethanol mixture (100 mL) was added drop-wise by using a peristaltic pump (6 mL/min). The white precipitates were seen immediately as the titanium (IV) isopropoxide was introduced to the ethanol-water mixture. The precipitates were collected by using centrifuge (at 3500 rpm for 30 min) and led to dry at 70°C in an oven for 12 hours. The dried precipitates were ground in a mortar and screened. The powder was heated to different temperatures (90-800°C). The heating rate, soaking time and cooling rate were 10 °C/min, 120 min and 15°C/min respectively. The powder was calcined at 425°C for 2 hours and ballmilled with zirconia balls for 12 hours in ethanol medium. The ball milled powder was dried in an oven at 70 °C for 12 hour.

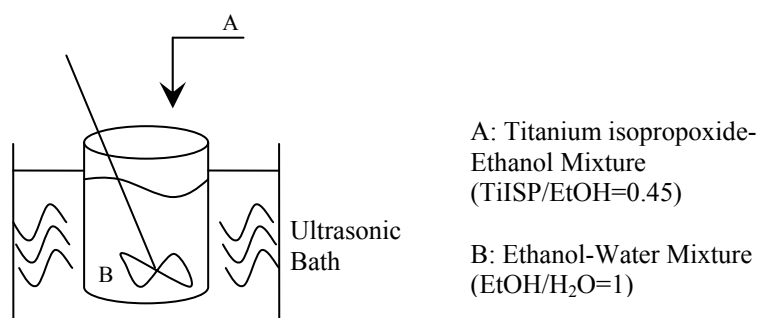


Figure 4.1. The schematic illustration of the experimental set-up for the preparation of nano-TiO₂ particles.

4.2. Specifications of Materials

The submicron alumina powder coded as AC (99.99% purity) was supplied from Sumitomo Chemicals Co., Ltd., Japan. The nano alumina powder coded as NA (99.95% purity) was supplied from Alfa Aesar GmbH & Co, Germany. The nano titania powder coded as NT was prepared via chemical precipitation method by using Titanium (IV) isopropoxide. The specifications of the powders used in this thesis were tabulated in Table 4.1. D-fructose (99% purity) and polyacrylic acid (99% purity) were used as dispersant in this thesis and were supplied from Fluka and Merck, respectively. The average particle size of the powders were calculated from surface area by assuming that the particles were monodisperse and spherical.

Table 4.1. The specification of the powders used in the thesis.

Code	Name	Density (g/cm ³)	Surface Area (BET, m ² /g)	Average Particle Size calculated from BET (nm)	Crystal Phase
AC	Alumina	3.98	12.3	122	alpha
NA	Alumina	3.65	36.2	45	70:30 Delta:Gamma
NT*	Titania	3.61	146.6	11	anatase

(*) The given values were based on the measurements on the powder which was heat treated at 425°C

4.3. Preparation of Dispersions

The dispersions were prepared as follows: the predetermined amount of water was placed in a plastic bottle and fructose was added and dissolved in water. The predetermined amount of powder was added in small amounts to fructose solution while the dispersion was mixed by hand in an ultrasonic bath for an hour. The dispersions were let to reach equilibrium at room temperature for three days. Dispersions had paste like appearance at the beginning of the resting period. After three days, the dispersions became much more fluid like. The samples were subjected to ultrasonic treatment for 10 minutes before placing the sample onto the measuring space for rheological experiments.

The dispersions prepared by submicron alumina, nano alumina and nano titania were coded as AC, NA, and NT, respectively. The number of the code of the powder indicated the volume percent of the solids content in the dispersion. The dispersants used were fructose and polyacrylic acid and were coded as F and PAA, respectively. The number next to dispersant code indicated the weight percent of the dispersant present in the dispersion.

The solids content of the dispersions having submicron alumina and nano alumina was varied between 5 and 40 vol%. The powders were dispersed in fructose solutions whose concentration was varied between 1 and 40 wt%. The solids content of the dispersions having nano titania were varied between 5 and 20 vol%. The dispersions at higher solids content were paste like and did not flow. The pH adjustment of the suspensions was done by adding required amounts fructose and the powder into nitric acid solution which was previously adjusted to pH~3.

4.4. Characterization Methods

The powders were characterized by X-Ray diffraction Analyzer (XRD-Philips Expert Pro), Scanning Electron Microscope (SEM-Philips XL-30S FEG), Accelerated Surface Area and Porosimeter (ASAP-Micromeritics 2000), Sedigraph (PSA-Micromeritics Instruments Corp.), ZetaSizer 3000 HSA (Malvern Instruments) Thermal Gravimetric Analyzer, (TGA- Shimadzu, TG-51), and Helium Picnometer. The rheological behaviors of the dispersions were determined by using a rotational rheometer (Haake Mars II, Advanced rheometer System).

The XRD patterns of the materials were measured between 20-60° of 2 θ . The samples for SEM micrographs were prepared by dispersing the material in ethanol by using sonification. The dispersed material was dropped onto stamp and led to dry at 70°C. The BET surface area of the powders was determined by N₂ adsorption. The surface analysis has two steps: first degassing and second N₂ adsorption at -196°C. The degassing can be done at temperatures ranging between room temperature and 300°C. The degassing of samples of nano titania powder which were heat treated at 70 and 200°C were done at 50°C and 150°C. The other nano titania samples which were heated to the temperature above 200°C were degassed at 250°C. The particle size distribution of the sub micron alumina was determined by using Sedigraph. The sample for

measurement was prepared by adding 1 g of submicron alumina into 50 mL ultrapure water and the pH was adjusted to about 4 by addition of nitric acid solution. The dispersion was subjected to ultrasonic treatment for half of hour before measurement. The particle size distributions of nano alumina and nano titania powders were determined by using ZetaSizer. The sample for the measurement was prepared by adding about 0.5 mg of powder into UV cuvette and necessary amount of ultrapure water. The dilution was done if the sample was too blurry. The dispersion was subjected to ultrasonic treatment for half of hour and ultrasonic treatment was repeated if necessary. The zeta potentials of the powders at different pH values were measured by using ZetaSizer. The pH adjustments were done by adding dilute nitric acid or ammonia solution. The TGA curves of the powders (AC, NA, NT and DT) and D-fructose were obtained by heating to 600 and 1000 °C under N₂ atmosphere with a heating rate of 10 °C/min. The density measurements were done at 25°C and about 3-6 g of the sample was used. All rheological measurements were performed by using parallel plate measurement apparatus with a diameter of 35 mm and 1 mL of the dispersion was used for each experiment.

4.4.1. Rheological Methods

The rheological behavior of the dispersions was determined by steady shear and dynamic shear rheology measurements. The measurements were done at 20°C and repeated for three times. The average of these three measurements was reported. Before applying dynamic rheology tests, the samples were sheared at 0.1 Pa for 30 s and rested for 300 s. The rheological methods were tabulated in Table 4.2. The rheological behavior of the fructose solutions was determined. The fructose solutions were prepared by mixing predetermined amount of fructose and water by a magnetic stirrer in a plastic bottle.

Table 4.2. The conditions of the rheological tests.

Rheological Method	Preshear	Details
Flow Curve	-	$\dot{\gamma}=0-500$ 1/s in 100 s (ramp)
Viscosity	-	$\dot{\gamma}=0-500$ 1/s, (stepwise)
Thixotropy	-	$\dot{\gamma}=0-400$ 1/s in 100 s $\dot{\gamma}=400-0$ 1/s in 100 s
Stress Sweep	$\tau=0.1$ Pa for 30 s $\tau=0.1$ Pa for 300 s	$\tau=0.003-30.0$ Pa, $f=1$ Hz
Frequency sweep	$\tau=0.1$ Pa for 30 s $\tau=0.1$ Pa for 300 s	$f=0.01-100.0$ Hz, τ due to stress sweep test.

4.4.2. Consolidation of Submicron Alumina and Nano Alumina Dispersions

The dispersions were consolidated by using a freeze dryer. The dispersions were placed in hollow tubes as it is shown in Figure 4.2.

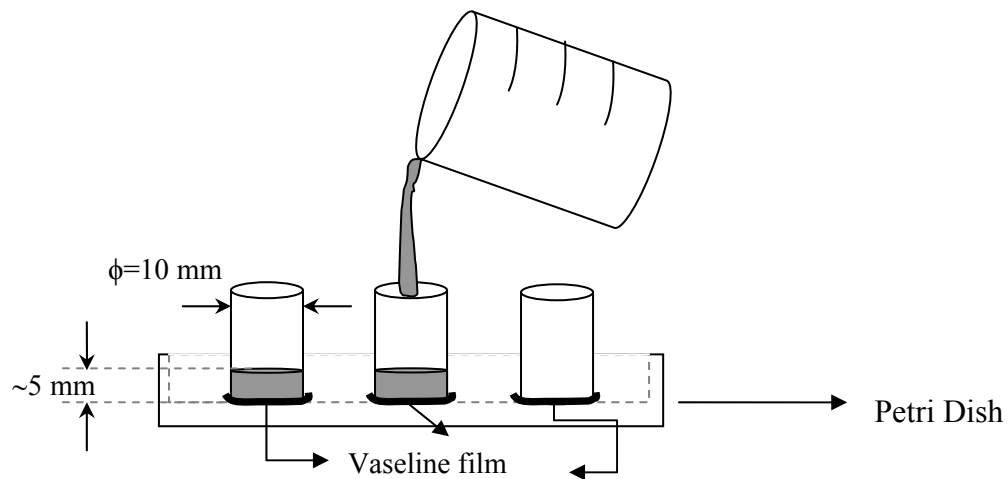


Figure 4.2. The schematic diagram for the preparation of consolidated bodies from dispersions.

Liquid nitrogen was placed around the hollow tubes to freeze them for approximately ten minutes. The bodies were placed in freeze dryer and dried for 4 hours. The dried bodies were kept at 70°C until the sintering was done.

The heating rate, soaking time and cooling rate were 10 °C/min, 120 minutes and 10°C/min, respectively. The sintering of submicron alumina and nano alumina were conducted 1400 and 1200°C, respectively. In order to compare the densities of the sintered bodies, powders were dry pressed in stainless steel die having a diameter of 10 mm. The pressure of dry pressing was 37.5 MPa.

The densities of the bodies before sintering were calculated by using dimensions of the bodies. The density of the sintered bodies was measured by using Archimedes' Principle. Sortorius Density measurement kit was used for the density measurements. The samples were weighed first (W_A) and then placed in beaker filled with ultrapure water and heated on a heater. The sample in water was boiled for 5 hours. Then, the sample was let to cool down to room temperature. The excess water on the sintered body was removed by a wet tissue. The sintered body was weighed again (W_S) and the weight in water (W_{SS}) by using density measurement kit. The collected data was used to calculate density of the sintered body by using the following equation,

$$\rho = \frac{W_A \times \rho_{H_2O}}{W_S - W_{SS}} \quad (4.1)$$

The measurements were done at 20°C and the density of water (ρ_{H_2O}) was taken as 0.9982 g/cm³.

4.4.3. The FTIR study of Submicron Alumina, Nano Alumina and Nano Titania Dispersions

The FTIR spectra of the D-fructose and powders were obtained by using Shimadzu FTIR spectrophotometer (8400S). KBr was used in the sample preparation for the analysis. The pellets for samples were prepared by following the steps of mixing with KBr in certain amounts (3 mg sample in 150 mg KBr-sample mixture), keeping at 120°C overnight, ground in a mortar and pressing. The dispersions of submicron alumina, nano alumina and nano titania having 5 vol% solids in 10 wt% fructose

solution were prepared for FTIR analyses. The dispersions were centrifuged at 7500 rpm for 15 minutes in order to recover the powders. The supernatants were removed and the powder was dried at 80°C for 12 hours. After FTIR analyses of the powders were done, water was added and the powder dispersed again by ultrasonic treatment. The powder was recovered again by centrifugation and the powder was dried at 80°C.

CHAPTER 5

RESULTS AND DISCUSSION

5.1. The Characterization of the Materials

The materials used in experimental study were characterized by different characterization methods. The weight loss of the materials was calculated from TGA. The IEP of the powders was determined by measuring zeta potential. The crystal size and crystal structure of the materials were observed by XRD patterns. The He Pycnometer was used to measure density of the powders. N₂ adsorption data was used to calculate surface area of the powders by using Brunauer-Emmett-Teller (BET) approximation. The pore size distribution was determined from desorption data by using Barrett-Joiner-Halenda (BJH) approximation. The particle sizes of the powders were determined by using Sedigraph and Zeta Sizer. The particle morphology was observed from SEM micrographs.

D-Fructose was used as received and the TGA curve is given in Figure 5.1. D-fructose lost 98.5% of its weight and decomposes completely when it is heated to 650°C.

The TGA curves of the submicron alumina, nano alumina and nano titania powders are given in Figure 5.2. The submicron alumina powders were used as received. The powder lost 0.2% of its weight when it was heated to 600 °C. Nano alumina particles were ball milled for 12 hours with zirconia balls in ethanol medium. The nano alumina powder lost 2.1% of its weight when it was heated to 800°C. The TGA curve of the titania precipitate which was previously dried at 70 °C is given in Figure 5.2. The powder lost 12.5% of its weight when it was heated to about 425 °C. No further significant weight loss was detected after 425°C. The weight loss may occur due to desorption of physical adsorbed water, loss of hydroxyl groups, removal of chemically adsorbed water, decomposition of remaining ethanol. The calcination temperature of the titania powder was chosen as 425°C. The calcined powder was ball-milled for 12 hours with zirconia balls in ethanol media.

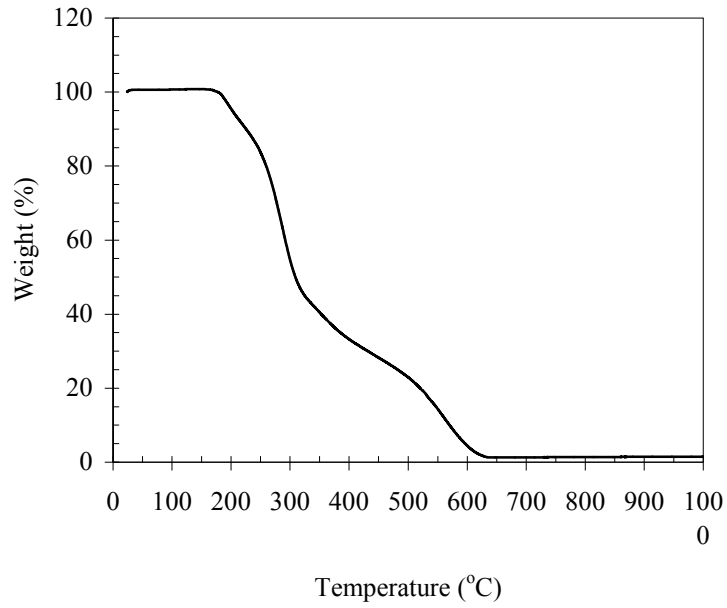


Figure 5.1. The TGA curve of D-fructose.

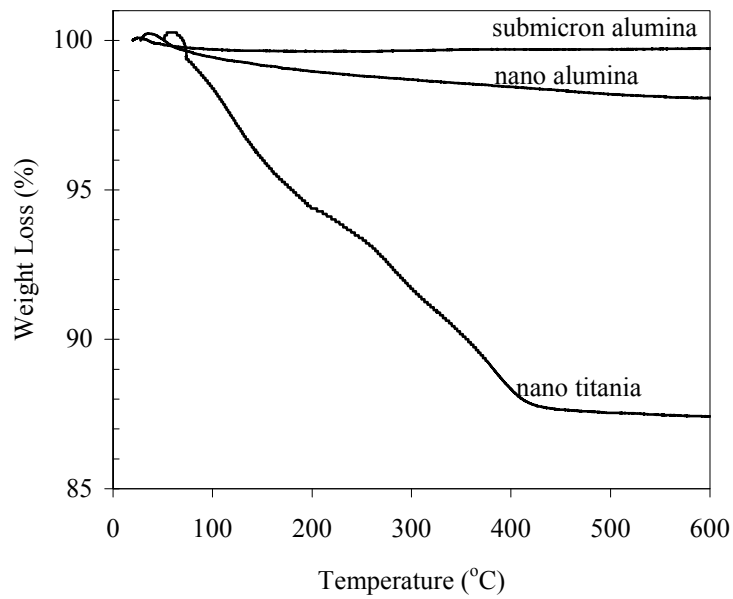


Figure 5.2. The TGA curves of submicron alumina, nano alumina, and nano titania powders.

Zeta potentials of the submicron alumina, nano alumina, and nano titania powders with respect to pH are given in Figure 5.3. The point of zero charge of submicron alumina was located at pH of about 8.2. Small changes in pH changed zeta

potential of submicron alumina significantly. The zeta potential rapidly increased/decreased to about +20/-20 mV as the pH was adjusted to 8.1/8.5. Further increase or decrease in pH made the zeta potential increase to +30 mV or -30 mV. It can be concluded that the dispersion of submicron alumina was quite stable for a wide range of pH. For nano alumina powder, the powder had zero zeta potential at pH of 8.8. Small increase/decrease in pH did not affect the zeta potential significantly. However, zeta potential reached much higher values (45 mV) as the pH was about 7.1 compared to submicron alumina. Zeta potential was about -31 when the pH was equal to 10.1. This indicated that the system will be more stable in acidic media. The IEP of the nano titania powder was at about pH of 5. The system can be considered as unstable in the range of pH=4 to pH=6 due to small values of zeta potential. Zeta potential reached much higher values when the pH was increased to about 7 or decreased about 3. The zeta potential of nano titania at a pH of 2.9 and 8.1 was about 23 and -30 mV, respectively.

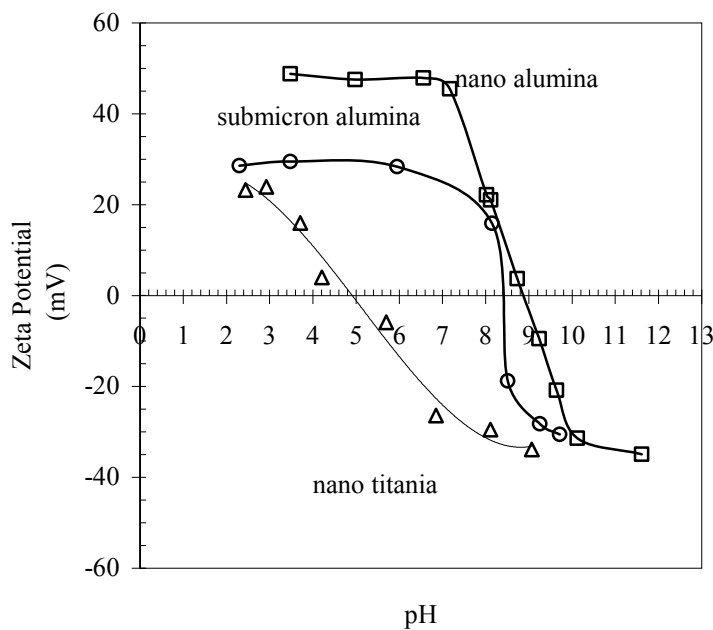


Figure 5.3. The variation of zeta potential of submicron alumina, nano alumina, and nano titania with pH.

The XRD pattern of D-Fructose is given in Figure 5.4. The XRD pattern of D-fructose showed its typical peaks related with its crystalline form. The pattern was similar to standard XRD diffraction pattern of D-fructose as published by JCPDS (39-

1839). The main peaks were located at 12.84, 13.90, 16.88, 19.11, 19.89, 20.45, 20.65, 28.12, 29.80, 34.18, 34.70, 35.62, 38.95, 39.81, and 40.91 of 2θ .

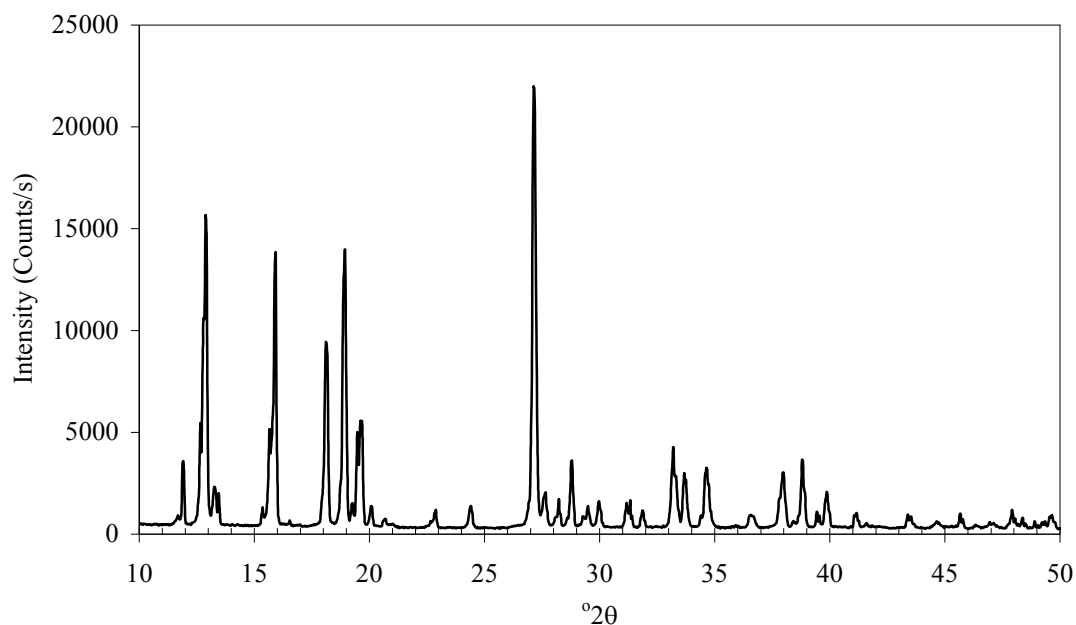


Figure 5.4. The XRD pattern of D-Fructose.

The XRD pattern of submicron alumina is given in Figure 5.5 and has same diffraction pattern of standard α -alumina whose diffraction pattern number published by JCPDS was 11-0661. The main diffraction peaks were located at 25.51, 35.04, 37.74, 52.43, 57.39, 66.37, 68.13, 76.73 and 77.01 of 2θ . The crystallite size of the powder was calculated as 50 nm at 24.48 of 2θ by Scherer equation.

The XRD pattern of nano alumina is given in Figure 5.6. The manufacturer stated that the powder is in delta and gamma phase of alumina in (70:30) ratio and it was confirmed by the XRD pattern. The standard diffraction pattern numbers for gamma and delta alumina published by JCPDS are 50-0741 and 04-0877, respectively. Most of the peaks overlaid with each other due to the complex crystal structure. The crystallite size of the powder was calculated by using the peak located at 33.32 of 2θ because it was the only peak without overlay. The crystallite size was calculated as 20 nm by Scherer equation.

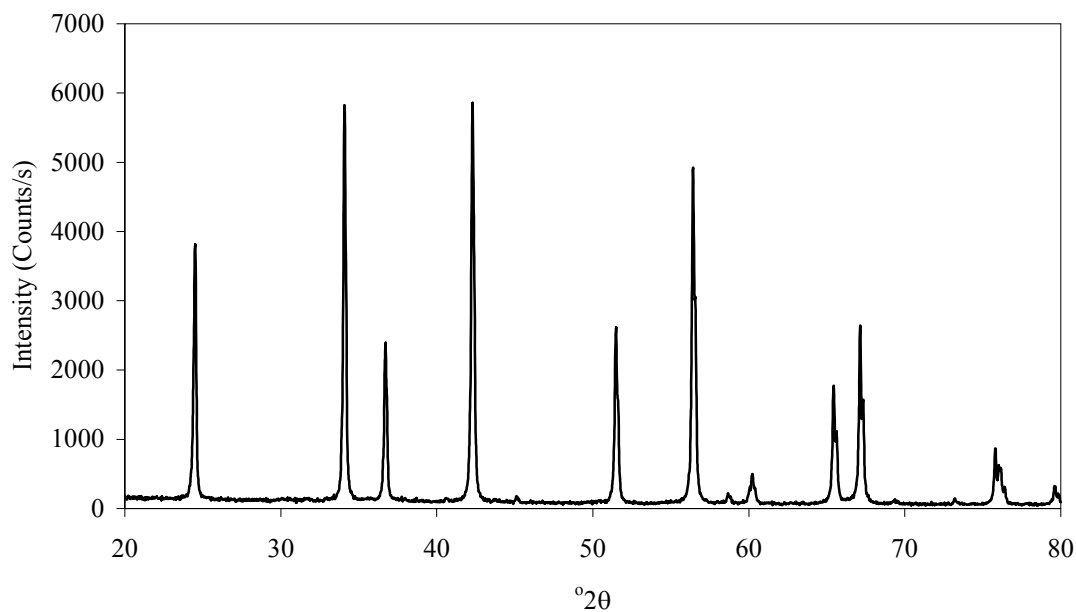


Figure 5.5. The XRD patterns of submicron alumina powder.

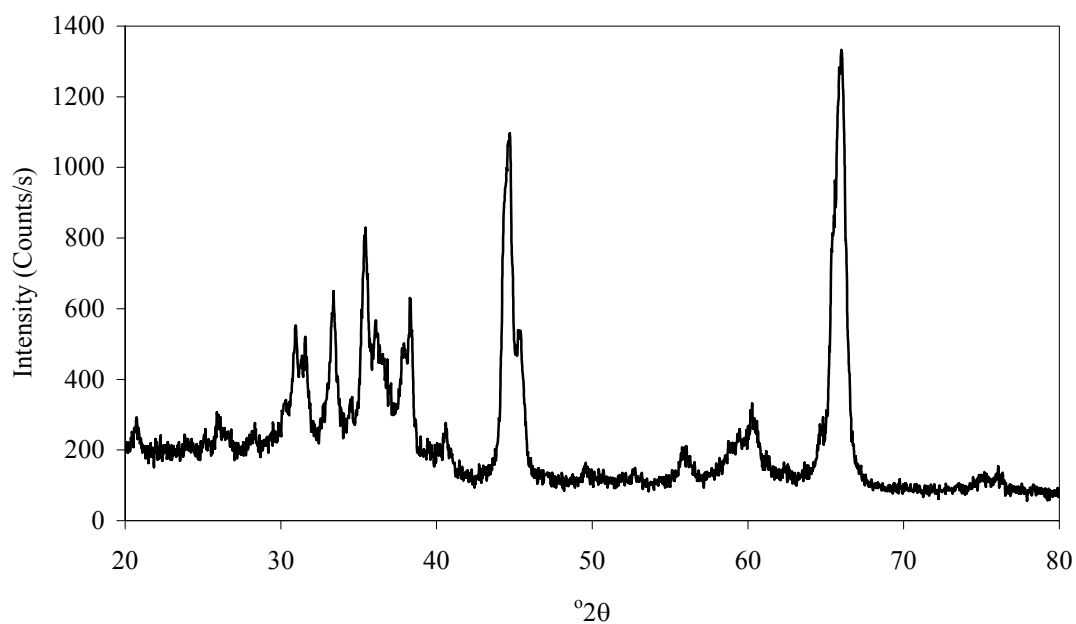


Figure 5.6. The XRD pattern of nano alumina.

The XRD patterns of the titania powders which were heated to different temperatures are shown in Figure 5.7 and Figure 5.8. The powder dried at 70°C has broad anatase peaks which are located at about 24.8, 37.5, 47.1, 53.9 and 54.8 of 2θ°. The anatase peaks became sharper, reach to higher intensities, and were shifted in small

amounts at higher temperatures. The anatase peaks were denoted with “A” on Figure 5.7. and located at 25.1, 37.7, 48.1, 54.9 and 56.1 of $^{\circ}2\theta$ for the sample heated to 400°C. The peaks related with rutile phase were denoted by “R” on Figure 5.8. and located at 27.2, 35.8, 41.0, 43.8, 54.1, and 56.4 of $2\theta^{\circ}$. The numbers of the standard XRD patterns for anatase and rutile crystal phases published by JCPDS are 84-1286 and 88-1175, respectively.

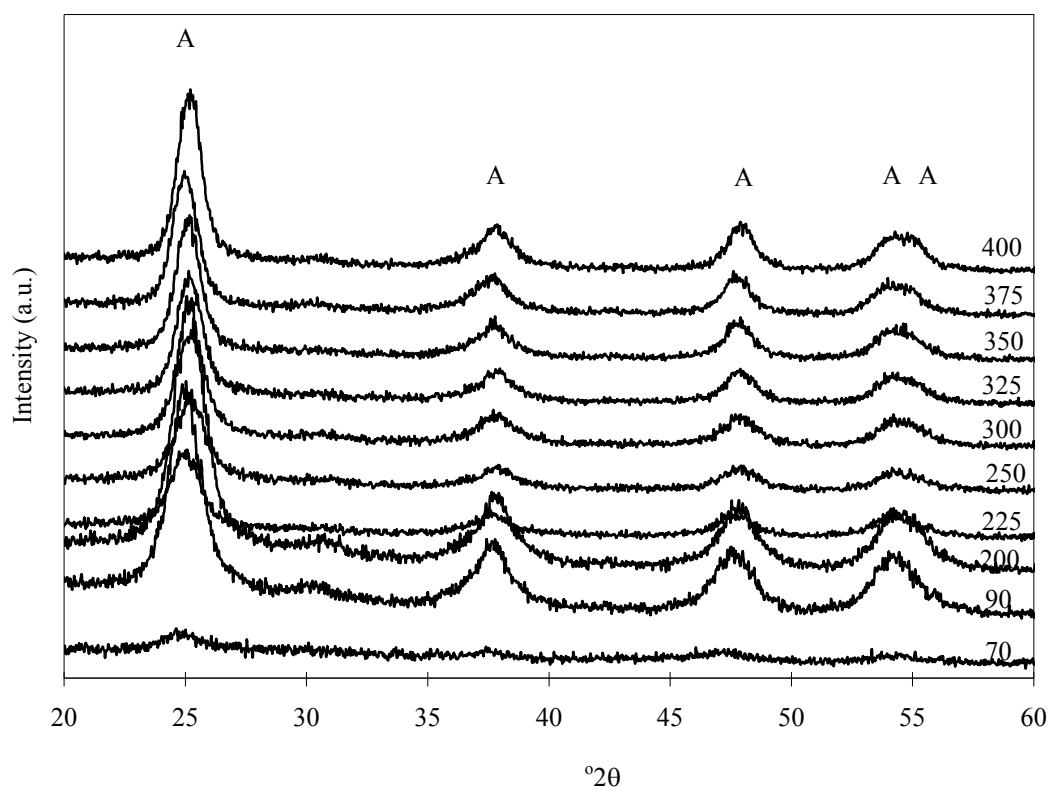


Figure 5.7. The XRD patterns of the titania powders heated to 70, 90, 200, 225, 250, 300, 350, 400.

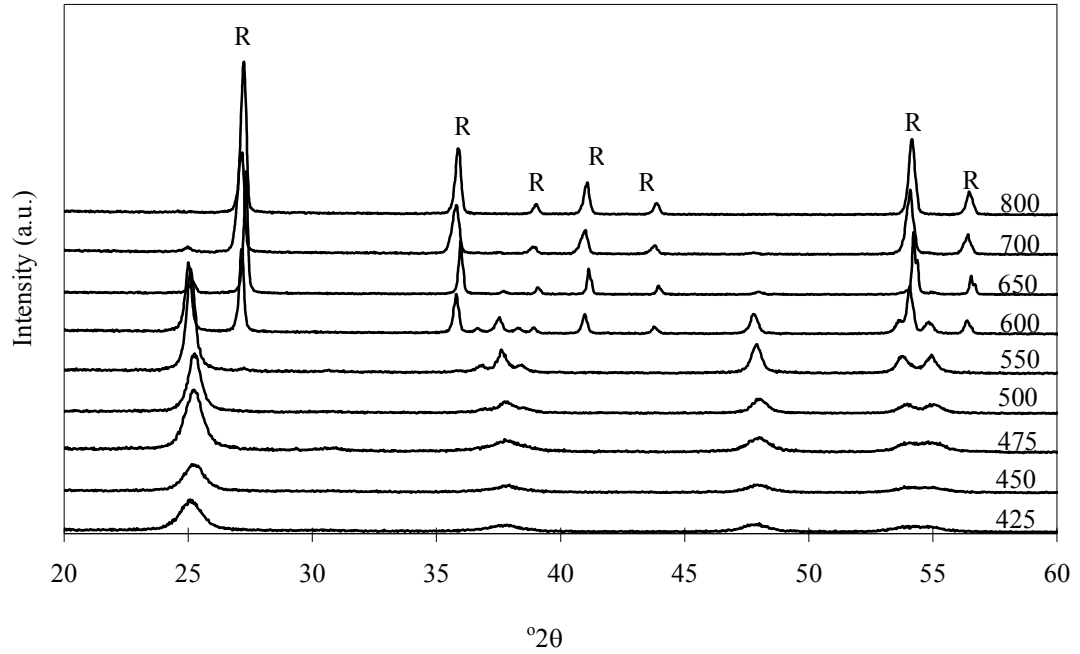


Figure 5.8. The XRD patterns of the titania powders heated to 425-450, 475, 500, 550, 600, 650, 700, and 800 °C.

The weight percent of rutile to anatase during phase transformation of nano titania were calculated by Spurr-Myers equation (Spurr and Myers, 1957) which follows as,

$$w_R \% = \frac{100}{1 + 0.8(I_A/I_R)} \quad (5.1)$$

where w_R is weight percent of rutile in the sample, I_A is the peak intensity of strongest anatase peak (the reflection of (101) plane) and I_R is the peak intensity of strongest rutile peak (the reflection of (110) plane). The anatase to rutile phase transformation detected when the nano titania was heated to 550°C. The range of temperatures for the anatase-rutile phase transformation was observed between 550 and 700°C and completed between 700 and 800°C. The strongest peak of anatase and rutile phases appeared at 25.1 and 27.2 of 2θ , respectively. The weight percent of rutile in the samples heated at 550, 600, 650 and 700°C was calculated as 2.6, 59.9, 93.2 and 94.6 wt%, respectively. The density of the titania powder at 70, 425 and 800°C was measured as 3.19, 3.61 and 4.13 g/cm³, respectively. The variation of density of nano titania powder and the weight percent of rutile is given in Figure 5.9.

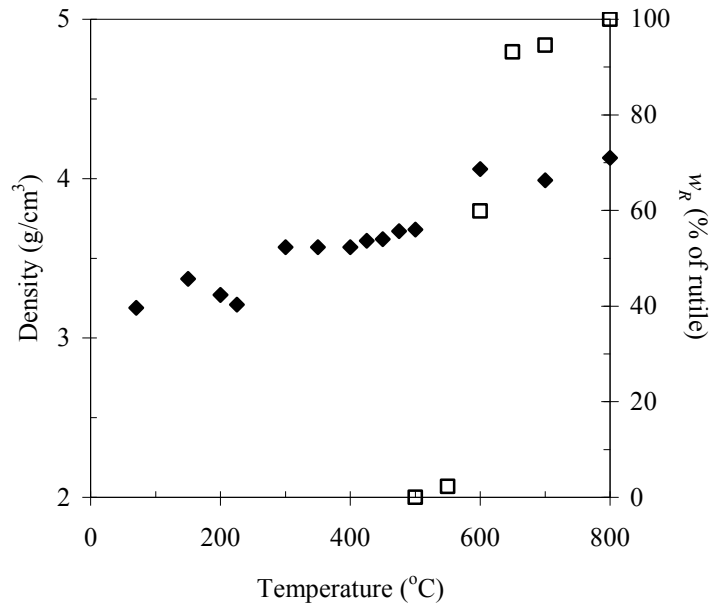


Figure 5.9. The variation of density of nano titania (◆) and w_R , % rutile, (□) with respect to temperature.

The crystal size of the titania powder heated at different temperatures were calculated from strongest peaks of anatase and rutile phases by using Scherer Equation which follows as,

$$D = \frac{0.9\lambda}{B \cos \theta} \quad (5.2)$$

where D , λ , B , and θ are crystal size in nm, xray wavelength (1.5405 Å for CuK $_{\alpha}$), the full width at half maximum of the diffraction peak, and Bragg diffraction angle, respectively. The crystal size of the titania powder heated at 70°C was calculated as 5.1 nm. The crystal size increased to 9.7 nm and 40.5 at 425 and 800 °C, respectively. The crystal size increased at temperatures where phase transformation occurred. The other particle size calculation was done based on surface area. The particles were assumed as spherical and the equation 5.3. was used.

$$D = 2R = \frac{6000}{\rho(SA)} \quad (5.3)$$

where D , R , ρ and SA are diameter of particle in nm, radius of particle in nm, density of the particles at that temperature and BET surface area of the powder at that temperature, respectively.

The N_2 physisorption isotherms of submicron alumina, nano alumina and nano titania are given in Figures 5.10-12. The submicron alumina and nano alumina showed Type II isotherms which indicates characteristics of non-porous or macroporous structures. The mesoporous structures was showed the Type IV isotherm for the nano titania powder with H3 hysteresis loop which is given by the aggregates of platy particles or adsorbents containing slit shaped pores (Rouquerol et al., 1999).

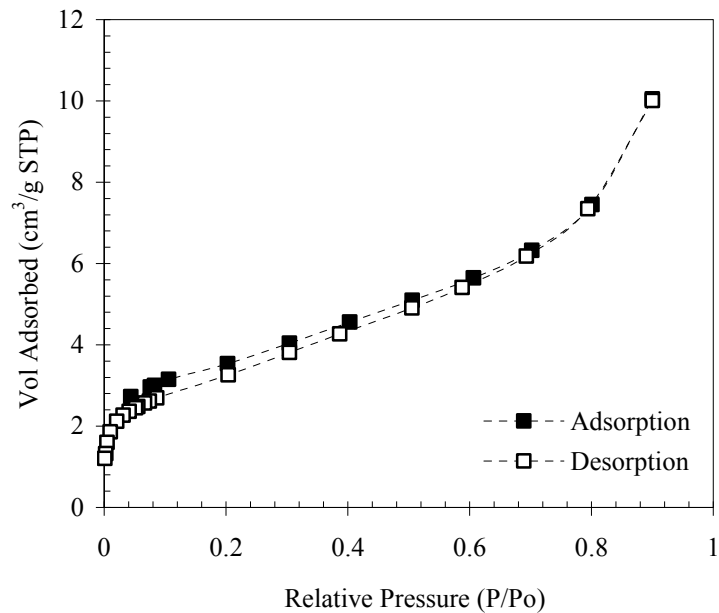


Figure 5.10. The N_2 physisorption isotherm of submicron alumina.

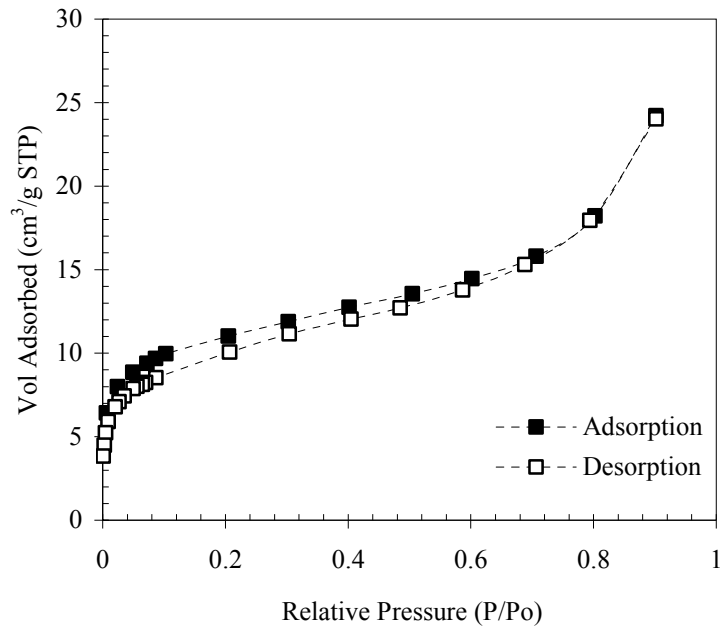


Figure 5.11. The N₂ physisorption isotherm of nano alumina.

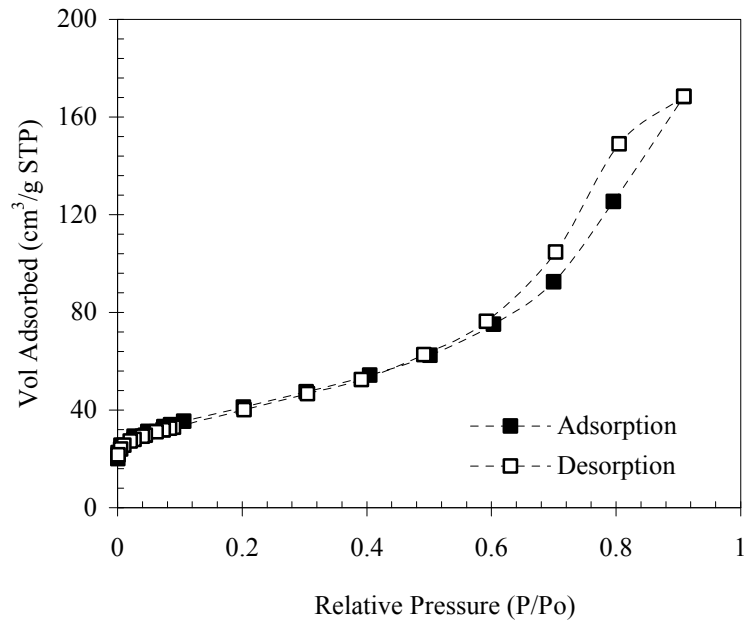


Figure 5.12. The N₂ physisorption isotherm of nano titania.

The calculated particle size from BET surface area was very close to the calculated crystal size based on Scherer Equation. The variation of crystal size based on Scherer Equation and the calculated particle size based on BET surface area with respect to temperature is given in Figure 5.13.

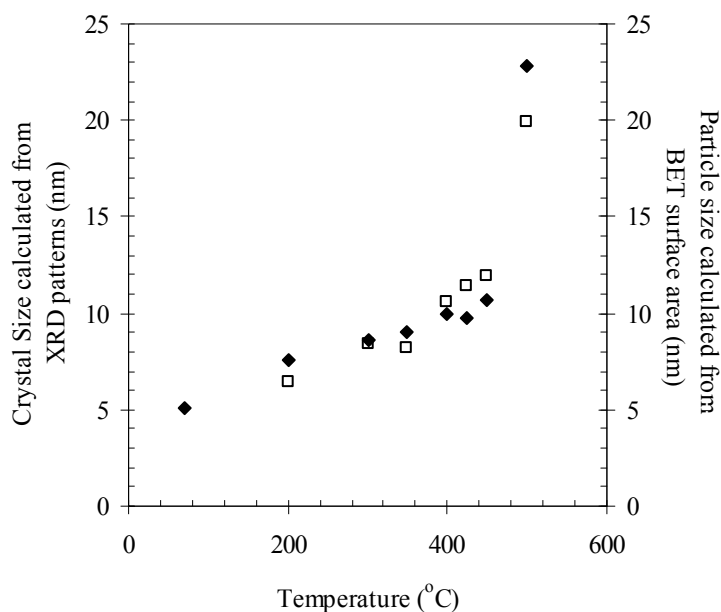


Figure 5.13. The variation of crystal size calculated from Scherer Equation (◆) and the particle size calculated from BET surface area (□) with respect to temperature.

The variation of BET surface area and BJH desorption pore size with respect to temperature is given in Figure 5.14. The BET surface area of the titania powder decreased as the temperature was increased. The surface area of the titania powder dried at 200°C was measured as 287 m²/g. The surface area was almost linearly decreased with increasing temperature. The surface area of the powder was 82 m²/g at 500°C. The pore size based on BJH desorption data increased as the temperature was increased. The pore size increased from 5.2 to 5.4 nm as temperature was increased from 200 to 500°C.

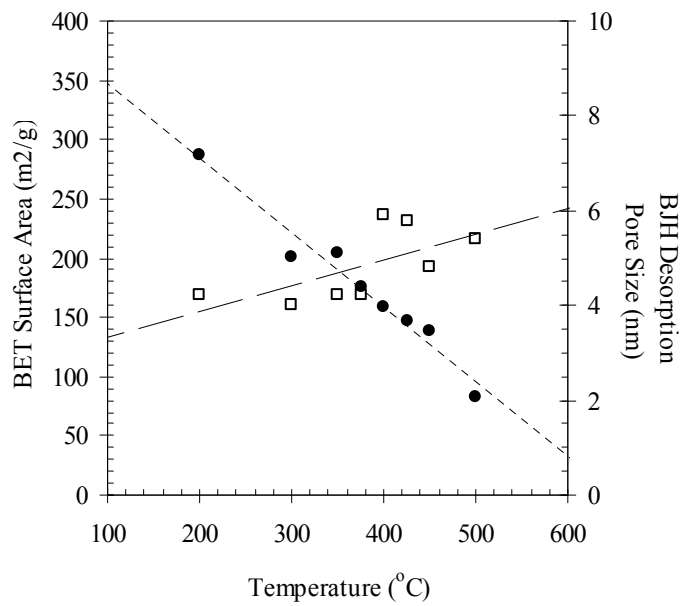


Figure 5.14. The variation of BET surface area (●) and pore size based on BJH desorption (□) with respect to temperature.

The particle size distribution (PSD) of submicron alumina is given in Figure 5.15. About 94 wt% of the alumina particles were below 1 μm and an important part of the particles (90 wt%) were below 0.5 μm . About 18 wt % of the particles were below 0.1 μm and the D_{50} (median) particle size of the alumina was 0.185 μm . The average particle size of the powder was also calculated from its surface area as 0.122 μm . These two results were comparable and the difference would be based on the assumption of being monodisperse and spherical particles which was made during calculation.

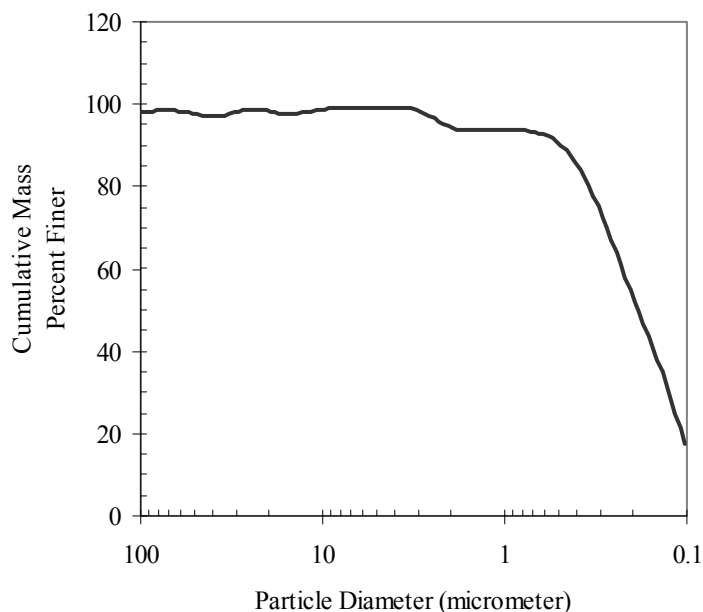


Figure 5.15. The particle size distribution of submicron alumina powder.

The PSDs of nano alumina and nano titania powder were determined by using static light scattering measurement technique. The PSD of nano alumina is given in Figure 5.16. The PSD was narrow and the particle size of the powder was about 20 nm which is indicated by a sharp peak when the distribution by number was taken into consideration. The same result was determined from XRD pattern. The crystallite size was 20 nm. The PSD is much broader regarding the volumetric distribution. The average particle sizes calculated from surface area and the particle size measurement were comparable with the reported value by manufacturer. The average particle size by number and by volume was about 26 nm and 50 nm, respectively. The surface area of the powder determined from N₂ adsorption data was 36.2 m²/g. The reported average particle size and surface area by manufacturer are 45 nm and 35 m²/g, respectively.

The PSD of nano titania is given in Figure 5.17. The peaks located at 90 and 280 nm represented the particle size of the powder determined from number and volumetric based distributions, respectively. However, the particle size calculated from surface area and X-Ray peaks were much lower than these values. The particle size of the powder observed from SEM micrograph supported these calculated particle sizes. The reason behind this difference in measured and calculated average particle size may rely on the assumptions and the operating principle of the static light scattering instrument.

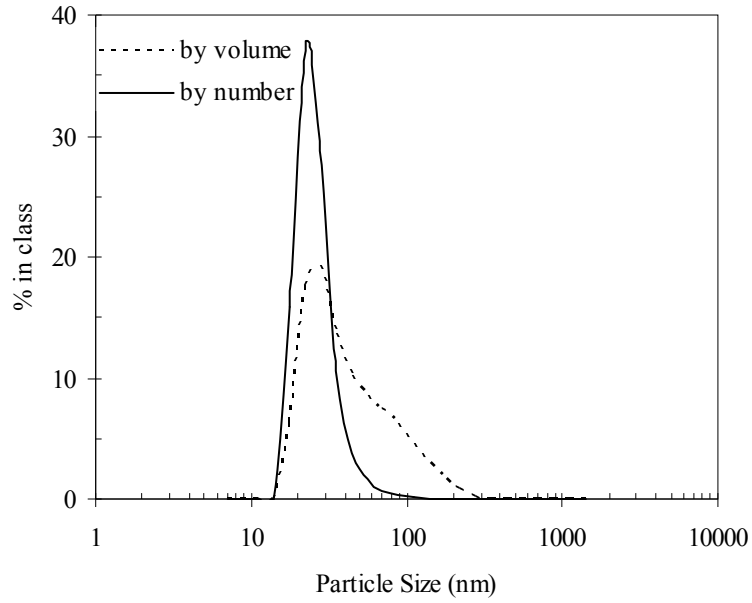


Figure 5.16. The particle size distribution of nano alumina powder.

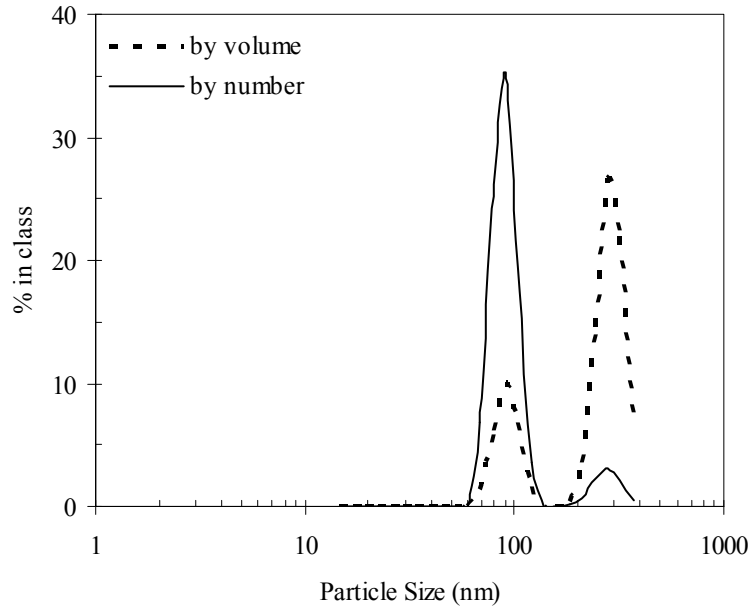


Figure 5.17. The particle size distribution of nano titania powder.

It is assumed in particle size measurement by light scattering that the particles are homogenous, non absorbing spherical particles in a dilute suspension. The operating principle of the instrument was based on the difference in the reflective indices of the

colloid and the solvent. The electric field of an incident light beam induces an oscillating dipole in the colloid, which causes scattering of light in all directions. The electric vector of the incident light with wavelength is polarized perpendicular to the scattering plane, and the scattered photons were detected with the same polarization at an angle (Lyklema, 2005). The static light scattering measurement uses the time averaged scattering. The presence of aggregates, adsorbing species, and contaminants such as dust and bubble changes the scattering intensity, so does the particle size.

The particles of nano titania were not perfectly spherical like the nano alumina particles which were determined from the SEM micrographs. It was observed that the sequential particle size measurements were different from each other for the nano titania powder. The large surface area may favor the agglomeration during measurement. The violation of the assumptions for the PSD measurement by static light scattering may result in much bigger average particle size than expected.

The SEM micrograph of the submicron alumina is given in Figure 5.18. The smallest and biggest sizes of the particles observed from the micrograph were 80 and 450 nm. The particles were irregularly shaped and nonporous.

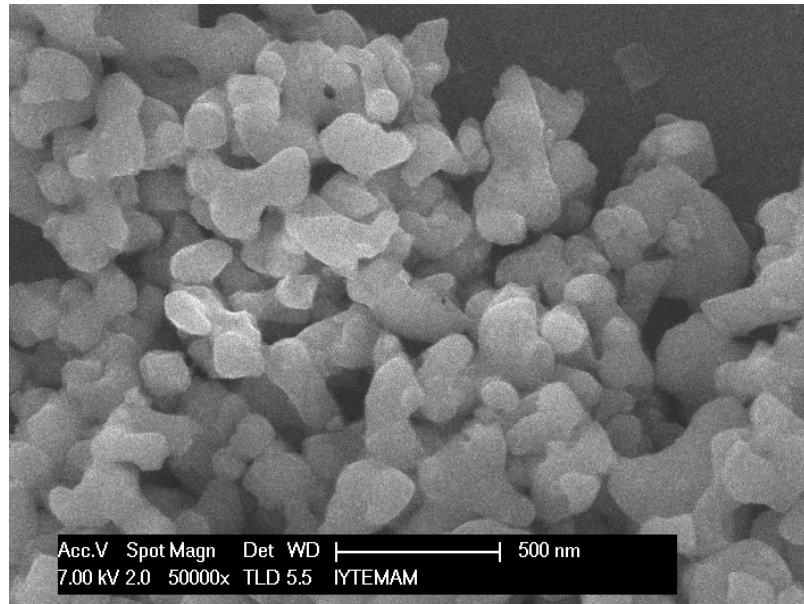
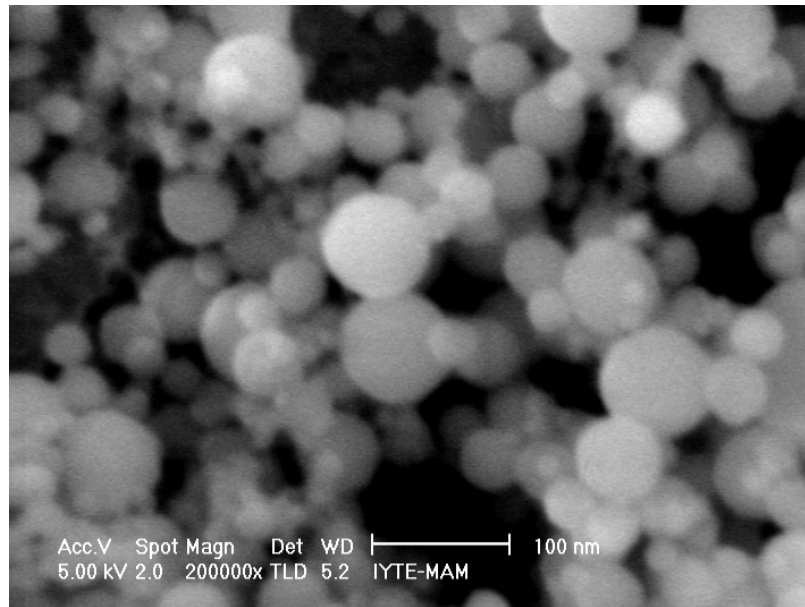
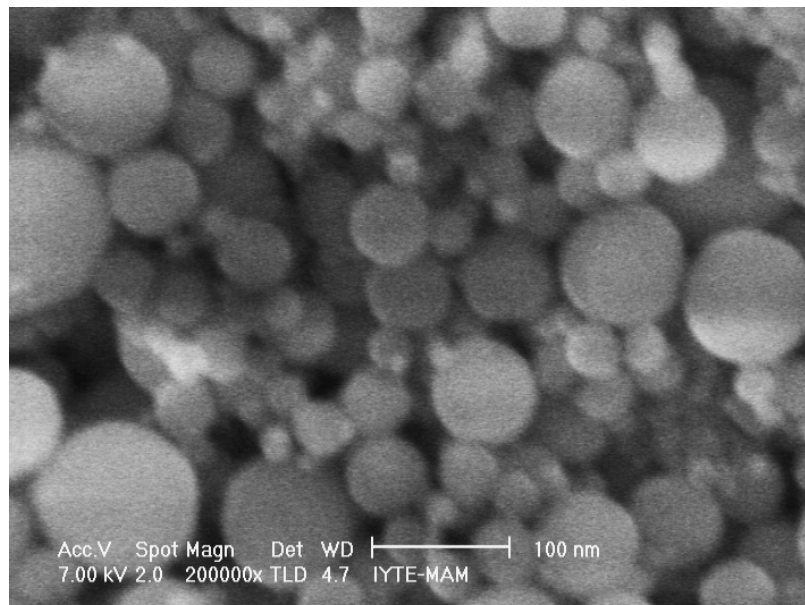


Figure 5.18. The SEM micrograph of submicron alumina powder.

The nano alumina particles were spherical and in various particle sizes. The biggest and smallest particle size in Figure 5.19.a. was about 120 nm and 10 nm, respectively. The SEM micrograph given in Figure 5.19.b. was taken after ball milling for 12 hours. Ball milling process did not change the morphology of the powder.



(a)



(b)

Figure 5.19. The SEM micrographs of nano alumina powder (a) before and (b) after ballmilling.

The SEM micrographs of nano titania powder are given in Figure 5.20. It was seen that titania particles as precipitated were irregularly shaped and agglomerated. The

titania particles became slightly greater than the precipitated particles after heat treatment at 425°C.

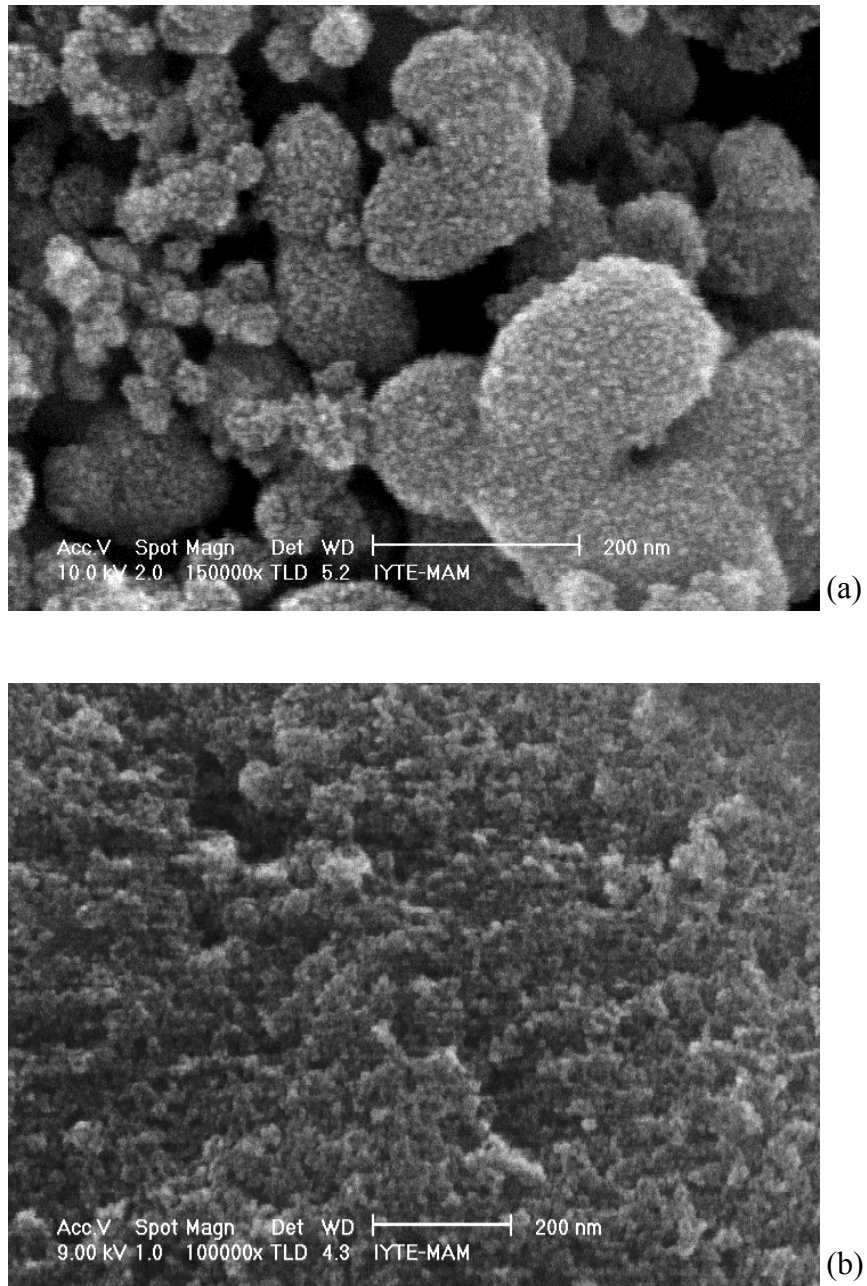


Figure 5.20. The SEM micrographs of nano titania powder (a) as precipitated and (b) after heat treatment at 425°C for 2 hours.

The chemical formula of D-fructose is $C_6H_{12}O_6$ and contains 4 carbon atoms between two methyl groups CH_2OH . The schematic representation of D-fructose is given in Figure 5.21. The second carbon atom has a double bond with oxygen. The carbon atoms except the second carbon atom are carrying hydrogen atoms and hydroxyl groups. The FT-IR spectrum of D-fructose is given in Figure 5.22. The strong IR peaks of D-fructose were a broad peak related with $-OH$ vibrational stretching located in the range of 3876 and 3005 $1/cm$ and a sharp peak related with CH_x-OH , C-O stretching located at 1058 $1/cm$. The functional groups related with peaks observed from FT-IR spectrum of D-fructose are given Table 5.1.

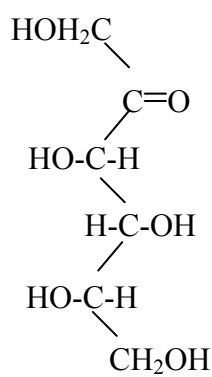


Figure 5.21. The schematic representation of D-fructose (Source: Stanek et al., 1963).

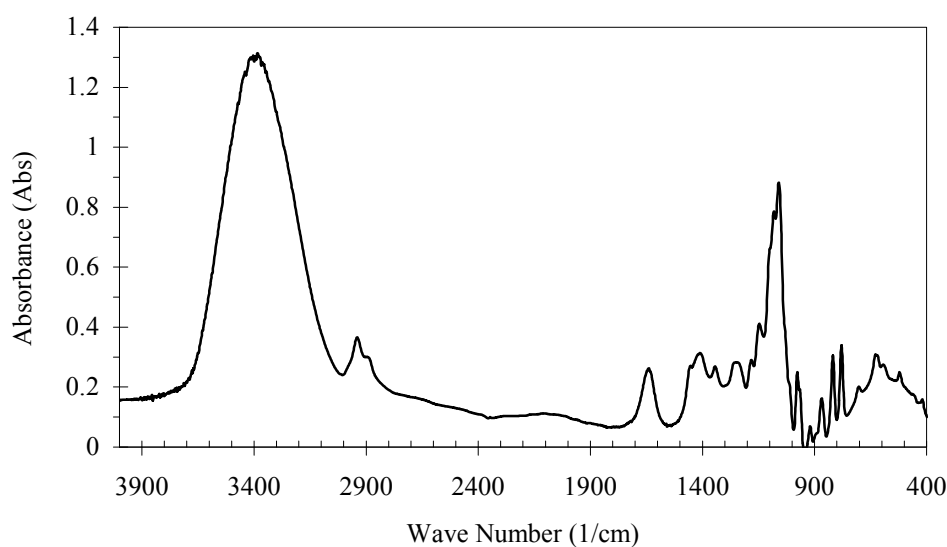


Figure 5.22. The FT-IR spectrum of D-fructose.

Table 5.1. The location of the IR peaks of D-fructose and related functional groups
(Source: Ibrahim et al. 2006).

Peak (cm^{-1})	Group	Peak Assignment
990	$\text{CH}=\text{CH}_2$	CH_2 out-of-plane deformation
1058.68	$\text{CH}_x\text{-O-H}$ in alcohols	C-O stretch
from 1191 to 995		A band of C-O and C-C stretching
1225	C-O-C in vinyl ethers or esters	C-O-C antisymmetric stretch
from 1362 to 1191		C-H and O-H deformation
from 1526 to 1347	O-C-H, C-O-H	combination band of OCH and COH deformation
from 1849 to 1634	C=O	C=O stretching
2950-2850	C-H	C-H stretching in aliphatics
from 3876 to 3005	O-H	OH vibrational stretching

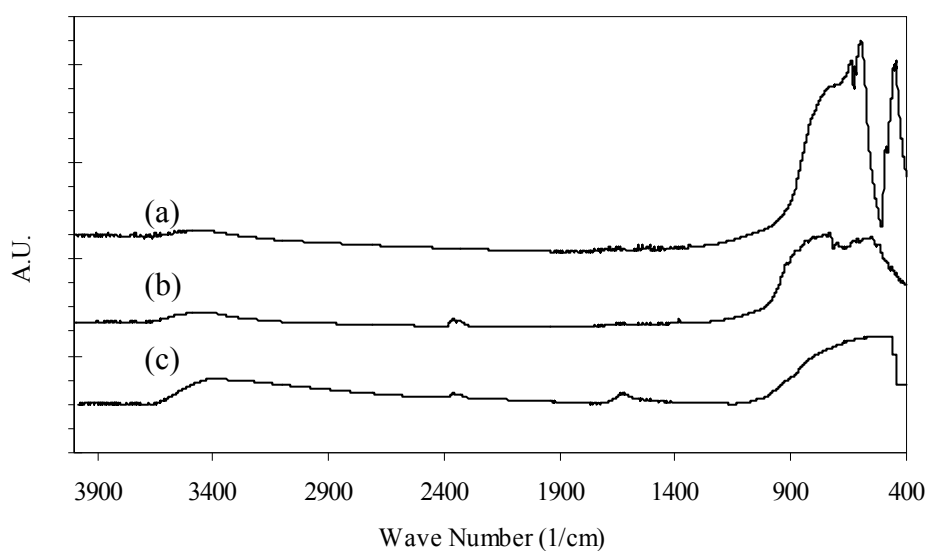


Figure 5.23. The FT-IR spectra of (a) submicron alumina, (b) nano alumina, and (c) nano titania powders.

The IR peaks of the submicron alumina, nano alumina and nano titania are given in Figure 5.23. The FT-IR spectra of the powders shows broad peak which is –OH vibrational stretching located in the range of 3876 and 3005 1/cm and a broad peak located in the range of 900 and 400 1/cm. The peak located at about 2350 1/cm was related with the chemisorbed CO₂ on powder's surface at 25°C.

In order to observe the adsorbed D-fructose onto powder surfaces, the dispersions of submicron alumina, nano alumina and nano titania having 5 vol% solids in 10 wt% fructose solution were prepared and kept at room temperature for 3 days to reach equilibrium. Then the dispersion was centrifuged, the recovered powder was dried. The FT-IR spectra of the recovered powders are given in Figure 5.24. The IR peaks of O-H vibrations at about 3450 1/cm and C-O stretching at 1058 1/cm were seen which were related with D-fructose.

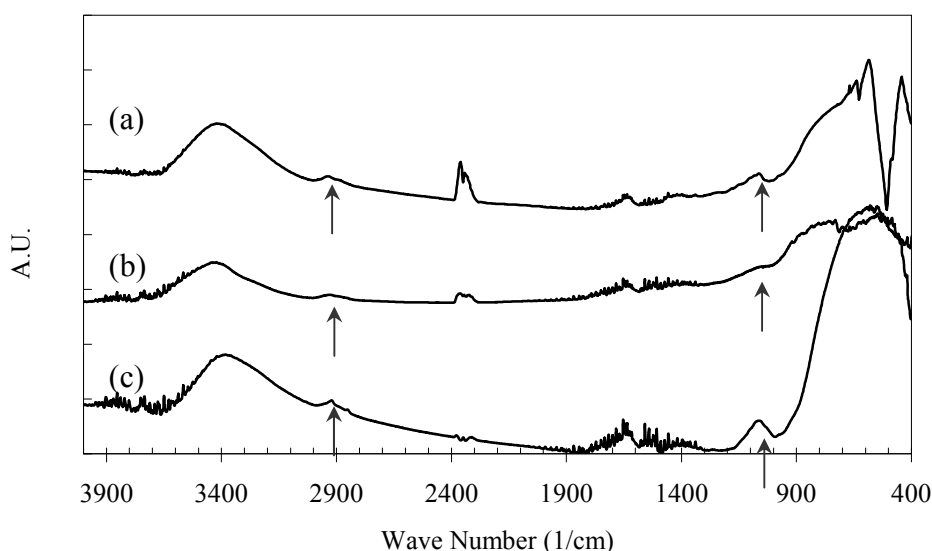


Figure 5.24. The FTIR spectra of (a) submicron alumina, (b) nano alumina, and (c) nano titania powders which were recovered from 5 vol% dispersions in 10 wt% fructose solutions by centrifugation.

The recovered powders were re-dispersed, centrifuged and dried at 80°C. The FT-IR spectra of the powders are given in Figure 5.25. The washed submicron alumina and nano alumina powders did not show the peaks related with O-H and C-H vibrations and C-O stretching which were observed for the recovered powders. This indicated that there was no D-fructose on the surface detectable by IR. However, IR spectrum of nano titania showed peaks at 2925, 2855 and a broad peak at about 1053 1/cm. These peaks

can be evaluated as the chemisorbed species related with D-fructose on nano titania or the D-fructose molecules entrapped in the pores of the titania powder which has mesoporous pore structure.

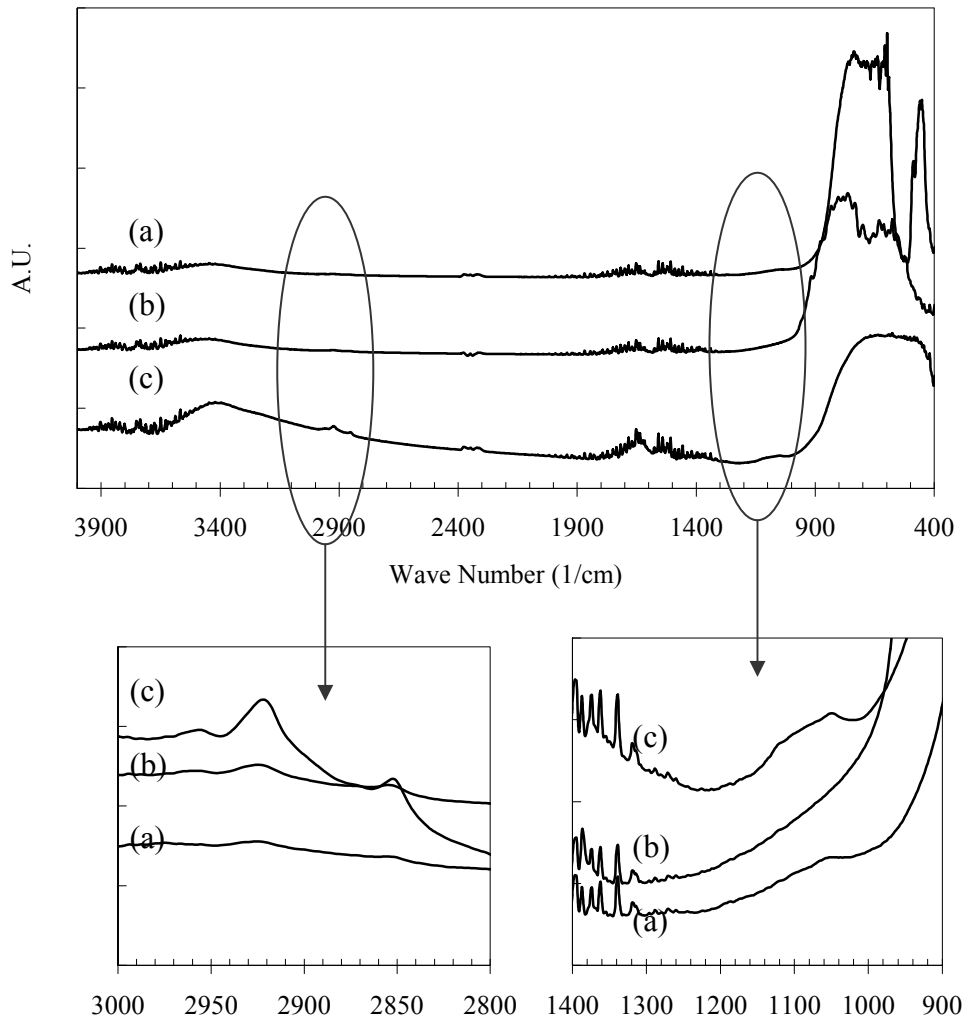


Figure 5.25. The FTIR spectra of (a) submicron alumina, (b) nano alumina, and (c) nano titania powders which were obtained by washing recovered powders with water and centrifuged second time.

5.2. The Techniques for Rheological Measurements of the Dispersions

One of the most important problems on rheological measurements of the dispersions was the evaporation of the dispersed medium from the edge of the measurement space. The solids content at edges increased rapidly during measurement and led to inaccurate measurements. As the measurement time extended, the problem

became more serious. Drying problem was avoided by using several protection tools. A circular shaped wet tissue was placed around the measurement space. After sample was loaded on the measurement space, a hemisphere cup made of a plastic material was placed to cover the measurement space. The water vapor from wet tissue provided a water-saturated environment. Therefore, the rate of evaporation from sample was so slow that at least two of the steady shear experiments can be done. The schematic diagram of the described drying protection tool is given in Figure 5.26.

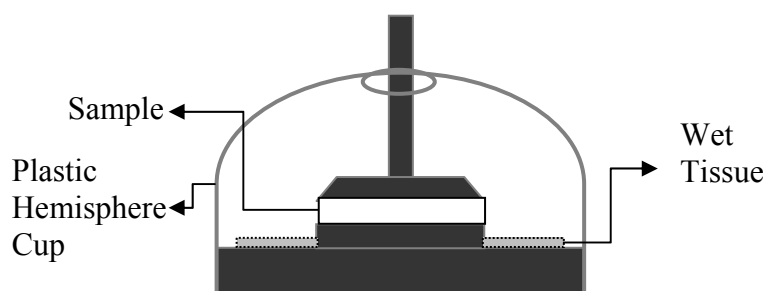


Figure 5.26. Schematic diagram of protection tool used for steady shear experiments.

The dynamic experiments prolonged much longer time than the steady shear experiments. The use of protection tool described in Figure 5.26 became inadequate. Figure 5.27 shows the stress sweep test results of polyacrylic acid stabilized submicron alumina dispersions. The successive stress sweep experiments showed that a significant change in the linear viscoelastic region. The magnitude and the shear stress range of G' shifted to much higher values. This may be caused by irreversible changes in structure of dispersion due to drying. This can be avoided by using fresh sample for each experiment. However, a frequency sweep test prolongs about 50 minutes and the sample is not stable in that time range. The use of non-volatile oil around sample became more appropriate way to make accurate measurements.

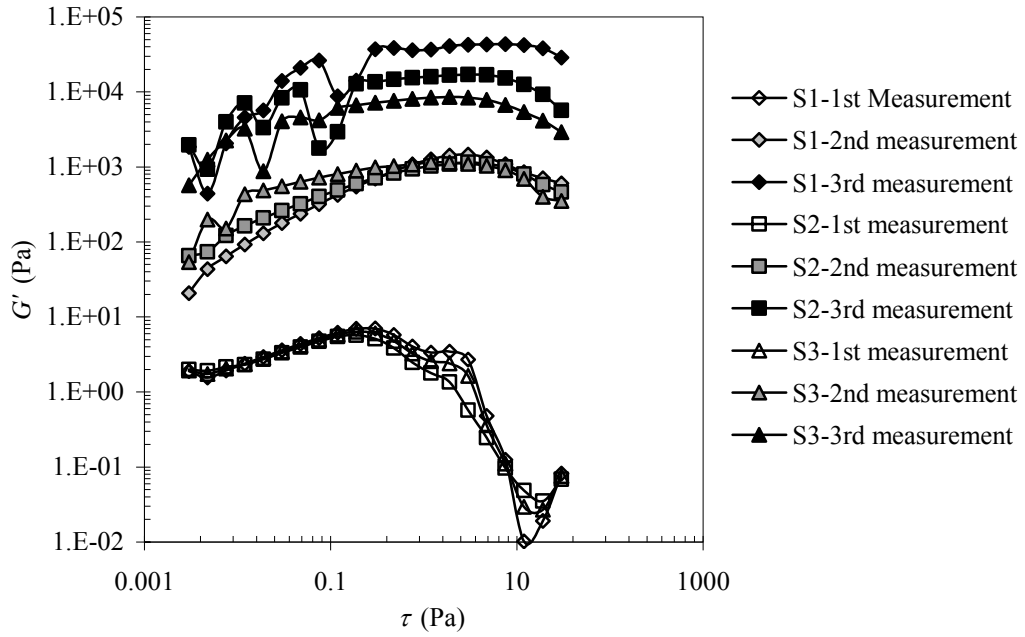


Figure 5.27. The results of stress sweep tests of 40 vol% α - Al_2O_3 dispersion with 3 wt% polyacrylic acid based on dry weight of submicron alumina.

The evaporation of water from sample can be eliminated by using the following protection tool. A hollow plastic cylinder which is 40 mm in diameter and 20 mm height was placed around the measurement space (see Figure 5.28). After the sample was loaded, annular volume between measurement space and the hollow cylinder was filled with non-volatile vegetable oil. The volume of vegetable oil filled was 3 mL. The enough amount of oil was filled in order to not to cover the upper part of measurement apparatus.

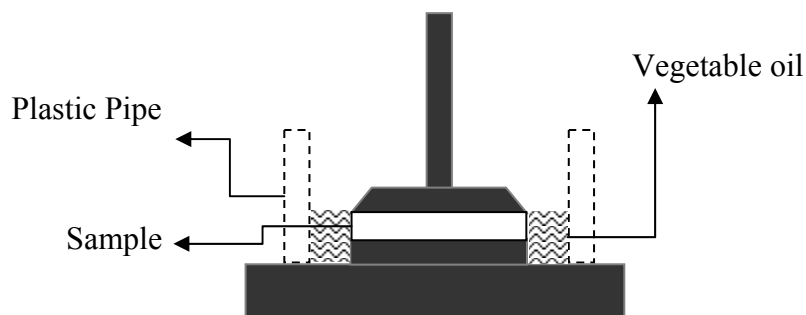


Figure 5.28. Schematic diagram of protection tool used for steady shear experiments.

The effect of drying and the performance of protection tool were observed by a time sweep dynamic experiment. In the time sweep experiment, the frequency and stress were kept constant and G' was monitored with respect to time. The variations in the G' of the dispersions having 35 and 45 vol% solids in fructose solutions which were determined from time sweep tests are given in Figure 5.29.

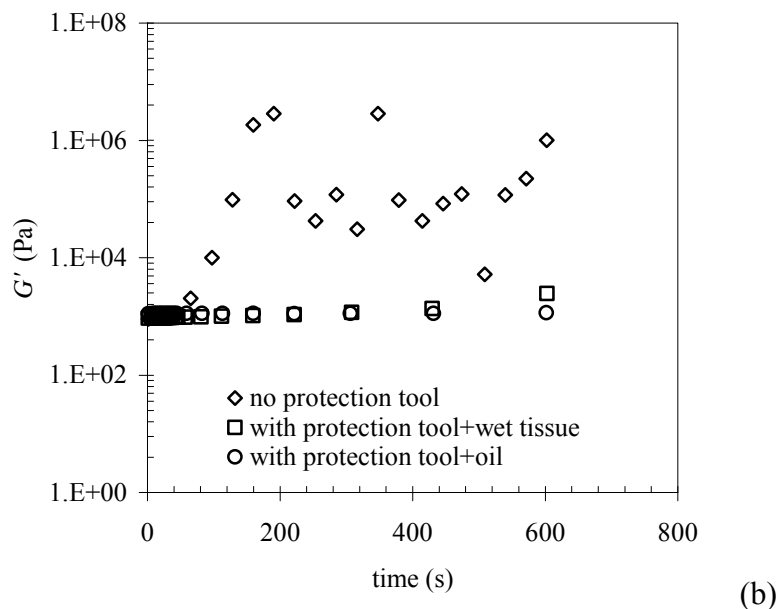
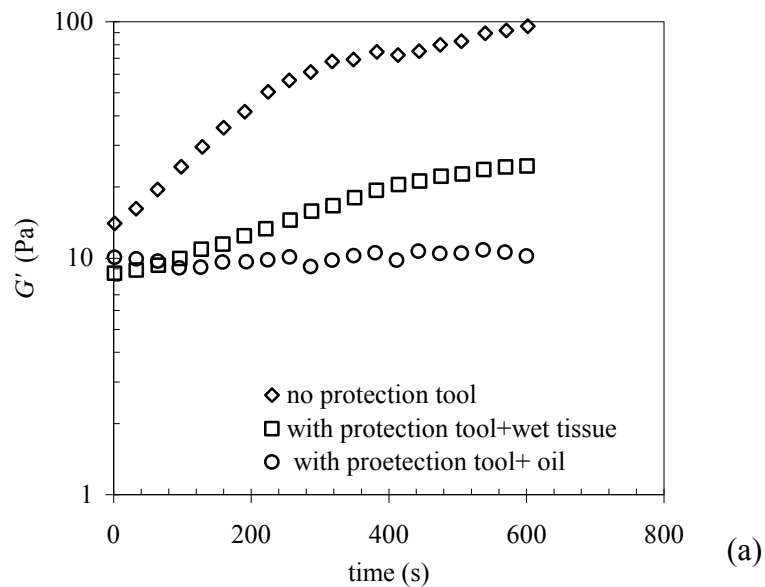


Figure 5.29. The variations in G' of the dispersions having (a) 35 vol% $\alpha\text{-Al}_2\text{O}_3$ and in 10wt% fructose solution and (b) 45 vol% $\alpha\text{-Al}_2\text{O}_3$ in 14 wt% fructose solution.

An increase in G' will show the beginning of the drying. It was noted that time passed for stress and frequency sweep tests were 15 and 50 minutes, respectively. As it is shown in the Figure 5.29, G' was monitored versus time for the samples without any protection tool, with cup and wet tissue and with oil. This experiment was performed to highly loaded dispersions (35 vol% α - Al_2O_3 and in 10wt% fructose solution and 45 vol% α - Al_2O_3 in 14 wt% fructose solution) because the drying became more serious when the dispersions have high solids content.

The G' significantly increased when no protection tool was used. The use of hemisphere and wet tissue did not provide enough time to complete one stress sweep test. When oil was used as a protection tool, the dispersion did not contact with air hence, evaporation was eliminated.

It was observed that the steady shear experiments were influenced by the presence of oil around the sample. Figure 5.30 showed the viscosity measurements on the dispersion having 40 vol% solids in 2.6 wt% fructose solution. The viscosity of the dispersion shifted above (0.938 to 1.133 Pa.s at 100 1/s) and the difference became more obvious when high shear rates reached. It was observed that oil mixed with the sample at shear rates higher than 200 1/s. The use of oil in the steady shear experiments was found to be inappropriate. This protection tool was used for only dynamic shear rheological experiments.

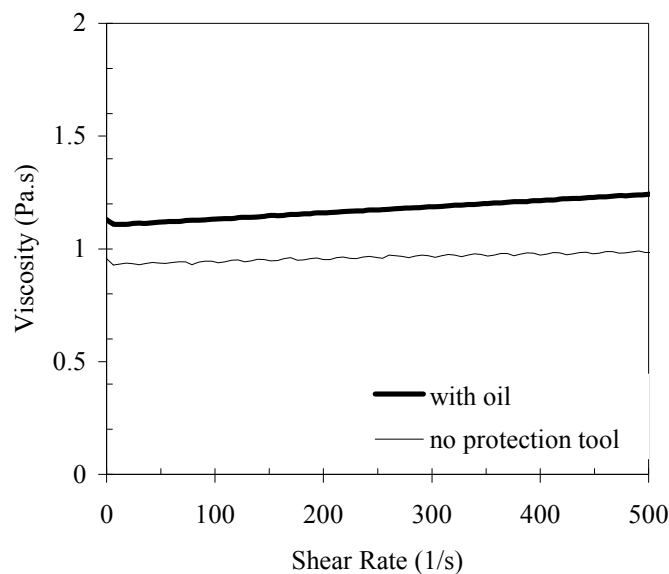


Figure 5.30. The influence of oil around sample on viscosity measurement of 40 vol% α - Al_2O_3 in 2.6 wt% fructose solution.

5.2.1. The Effect of Successive Experiments on Thixotropy of the Dispersions

Thixotropy is defined as decrease of viscosity (in time) under constant shear stress or shear rate, followed by a gradual recovery when the stress or shear rate is removed (Barnes, 1997). Thixotropic behavior is observed by shearing the material from zero to a certain shear rate (ramp up), holding at that shear rate for a certain time and taking back to zero (ramp down) in the same time interval of ramp up. The area of the thixotropic loop is a measure of time dependency of the dispersions under the state of motion.

All liquids with microstructure can show thixotropic behavior, because thixotropy reflects the change of the microstructure in flow by moving from one state to another and successively taking back. The driving force in microstructural change in flow is the competition between the breakdown of structure due to flow stresses and the structural built-up due to inflow collisions and Brownian motion. The particles move to a favorable position where they can attach themselves to other parts of microstructure by Brownian motion during structural built-up. Generally, thixotropic and any other time dependent behaviors are undesired because the rheological behavior of the liquid would be dependent on the pretreatment. Barnes (1997) stated that the measurement of thixotropy needs to be repeated until a constant loop is observed. Figure 5.32 shows typical thixotropic measurements which were done successively. The area of the thixotropy hysteresis is a measure of thixotropy. The thixotropy measurement was repeated for three times and the last measurement was taken into account based on the knowledge given by Barnes (1997).

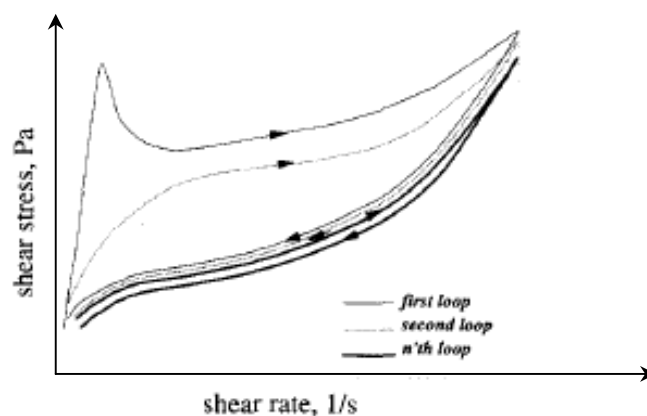


Figure 5.31. A typical thixotropic loop test (source: Barnes, 1997)

It was observed that when the thixotropic measurements were done successively on the same sample, the rheological behavior had changed. The thixotropic measurements of the 25 vol% α -Al₂O₃ dispersion in 1.3 wt% fructose solution showed that successive experiments on the same sample had an effect on the thixotropic areas (Figure 5.31). As the measurements were done successively, the thixotropic area decreased. The thixotropic areas are given in Table 5.2.

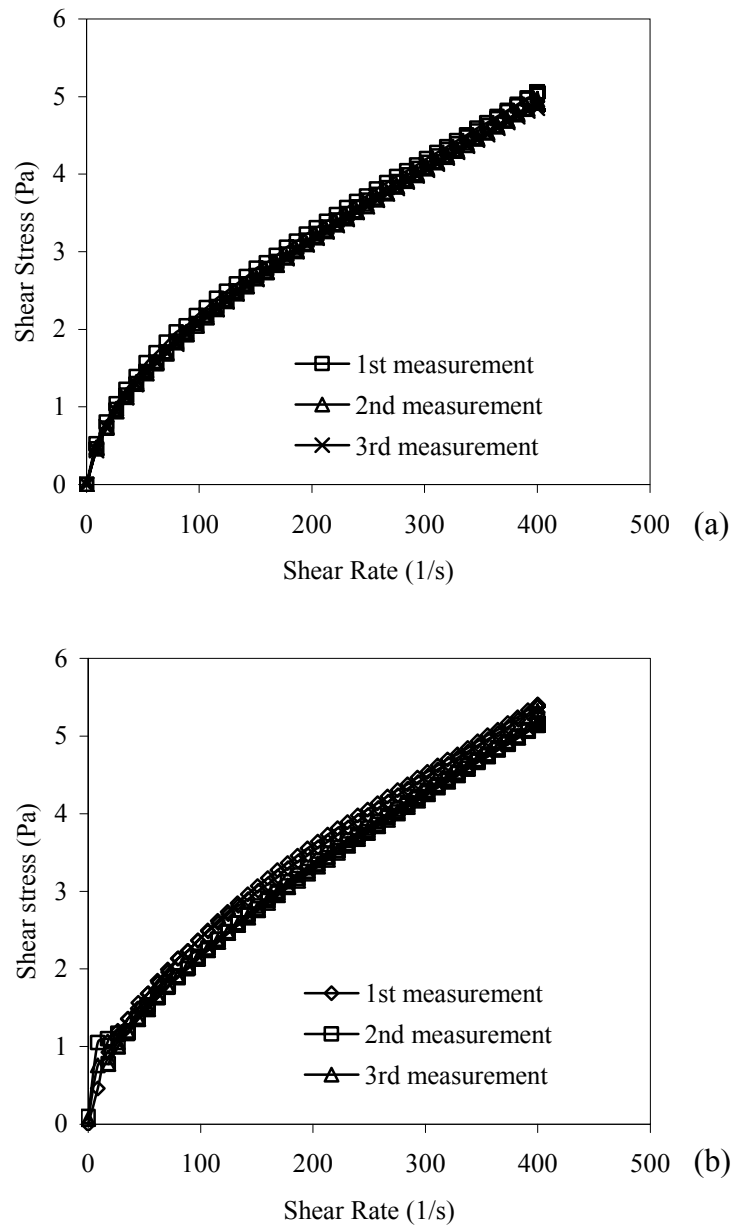


Figure 5.32. The effect of successive measurements on (a) the same sample and on (b) fresh samples on the thixotropic behavior of 25 vol% α -Al₂O₃ in 1.3 wt% fructose solution.

Table 5.2. The calculated thixotropic areas of 25 vol% α -Al₂O₃ in 1.3 wt% fructose solution.

# of measurement Sample	1 st Measurement (Pa.s)	2 nd Measurement (Pa.s)	3 rd Measurement (Pa.s)	Average (Pa.s)
Same Sample	31.35	12.58	8.24	17.39±12.28
Fresh Sample		22.24	24.76	26.28±4.50

5.3. Rheological Measurements of the Fructose Solutions

The rheological behavior of fructose solutions having different fructose concentrations was investigated. The fructose concentration was changed between 0.1 and 80 wt%. The viscosity and flow curves of the fructose solutions are given in Figure 5.33 and Figure 5.34. The flow curve of the fructose solutions showed Newtonian behavior. The viscosities of the fructose solutions were between 8×10^{-4} and 4.005 Pa.s and very similar to the values given in Telis et al. (2007). The viscosities and the consistency of the data to Newtonian model were tabulated in Table 5.3.

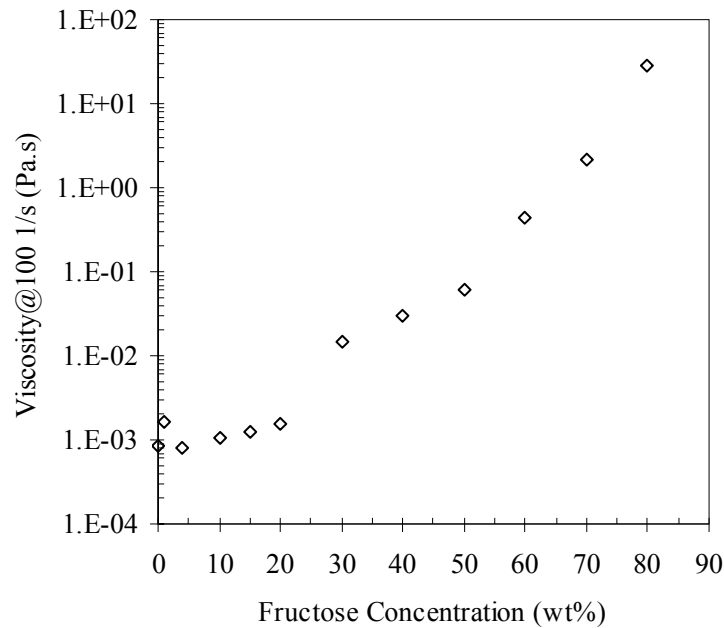


Figure 5.33. The viscosities of fructose solutions at 100 1/s.

Table 5.3. The viscosities, Reynolds Number at 100 and 200 1/s, and the data consistency of Newtonian model of Fructose Solutions.

Fructose Concentration (wt%)	Viscosity (Pa.s)	Reynolds No @100 1/s	Reynolds No @200 1/s	Consistency to Newtonian Model [$\tau = \eta\dot{\gamma}$] (R^2)
0.1	0.0008	43.50	98.75	0.95
1	0.0017	30.49	51.02	0.98
4	0.0008	43.50	76.28	0.98
10	0.0011	29.08	55.22	0.98
15	0.0013	22.96	47.32	0.98
20	0.0016	19.70	38.20	0.99
30	0.0145	11.03	21.57	0.99
40	0.0296	5.58	11.02	0.99
50	0.0597	2.24	4.48	0.99
60	0.4297	0.35	0.67	0.98
70	2.1593	0.12	0.26	0.98
80	28.12	0.01	0.01	0.99

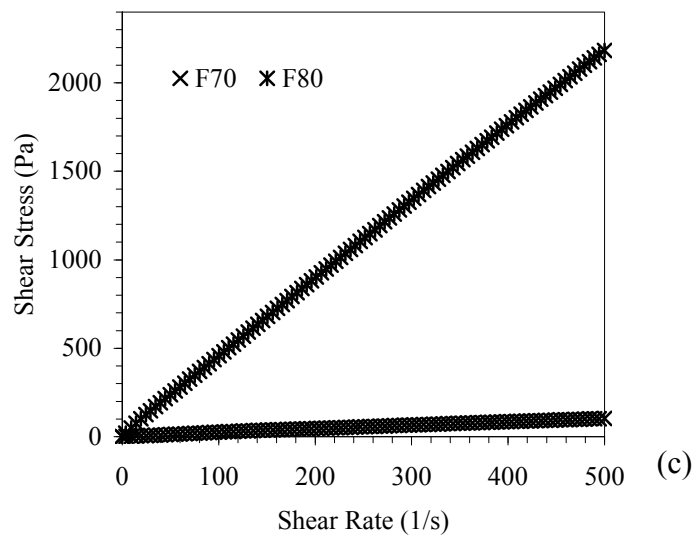
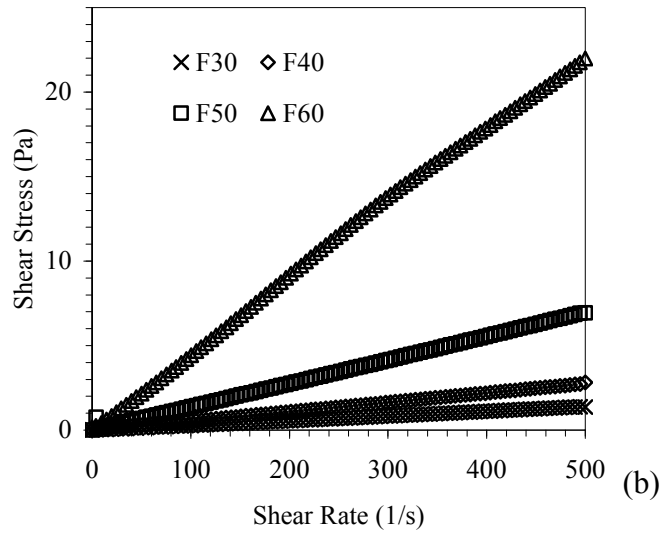
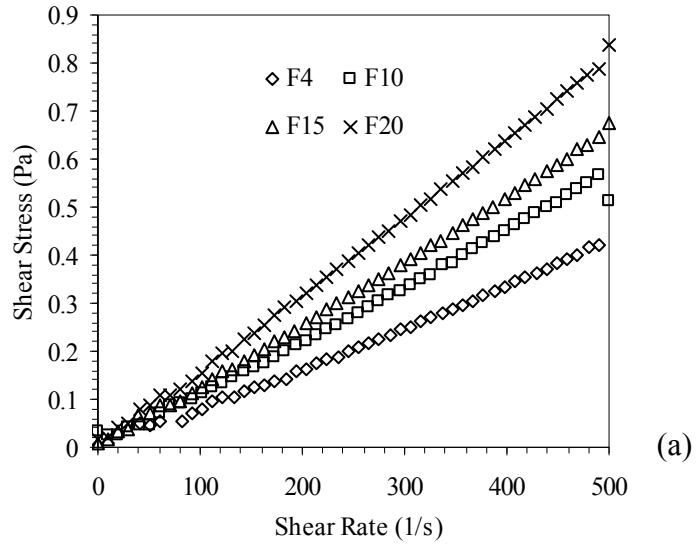


Figure 5.34. The flow curves of (a) 4, 10, 15 and 20 wt%, (b) 30, 40, 50 and 60 wt%, (c) 70, 80 wt% fructose solutions.

The fructose solutions having 0.1 and 1 wt% fructose had higher viscosity than 4 wt% fructose solution. The contribution of the flow inertia can produce shear thickening effect. It became more significant if the fluid showed non-Newtonian behavior. This inertia driven by secondary flow can be negligible if the $N_{RE} < 40$ for parallel plate measurement system (Collyer and Clegg, 1998). The calculated Reynolds Numbers of the solutions are given in the Table 5.3. The Reynolds Number of fructose solutions having 0.1 and 1 wt% fructose was beyond the critical value when the shear rate reached to 100 1/s. The measurements at high shear rate may increase the error contribution to the calculated viscosities. The edge effect is negligible if the distance of gap over diameter (h/R) is below 0.075. The error in measured torque becomes less than 2% for parallel plate measurement system. In this work, h/R was equal to 5.71×10^{-4} and the edge effect was negligible.

5.4. The Rheological Behavior of Submicron Alumina Dispersions

The rheological behavior of submicron alumina dispersions were determined by steady shear and dynamic shear rheology techniques. The rheological techniques for steady shear rheology used in this thesis involved the determination of flow curves, viscosity and thixotropy. The rheological techniques for the determination of dynamic shear rheology were stress sweep and frequency sweep tests. The more detailed information for the measurement techniques are given in Appendix-A.

5.4.1. The Effect of Solids Content and Fructose Concentration on the Steady Shear Rheology of the Submicron Alumina Dispersions

The effect of solids content and fructose concentration on the steady shear rheology of submicron alumina dispersions were investigated. The dispersions having 40 vol% solids content without fructose and in 1 wt% fructose solution had paste-like appearance and did not flow. The steady and dynamic shear measurements can not be done. The flow curves of the fructose solutions are given previously and all of them were Newtonian. The presence of submicron alumina particles and their concentration changed the flow characteristics significantly.

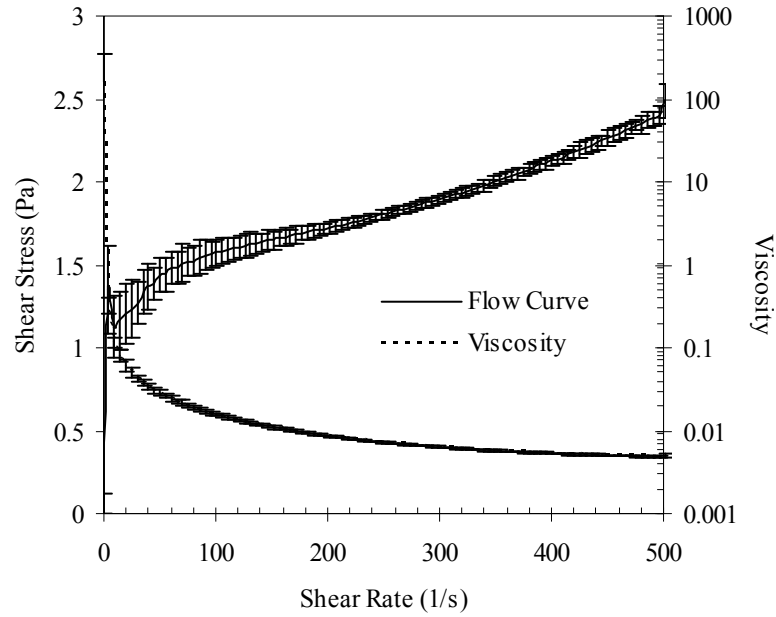


Figure 5.35. The flow and viscosity curves of 5 vol% submicron alumina dispersion in 1 wt% fructose solution.

The flow and viscosity curves of 5 vol% submicron alumina dispersion in 1 wt% fructose solution is given in Figure 5.35. The flow curves of the submicron alumina dispersions in different fructose concentrations (1-40 wt%) are given in Appendix B.1. The flow curves of all the submicron alumina dispersions in fructose solution were fitted to the Herschel-Bulkley (HB) model which is given as,

$$\tau = \tau_o + K\dot{\gamma}^n \quad (5.4)$$

where, τ_o is the Herschel-Bulkley yield stress (HB yield stress), K is a model parameter, consistency coefficient, and n is flow index. If $\tau_o=0$ and $n=1$, the model degenerate into the Newtonian model with a viscosity of K . The HB model describes the shear thinning behavior and the model parameters have dependence on solids concentration, particle size distribution and the properties of the interface between solids and liquid (Crowe, 2006). The parameter K represents the resistance to deformation. K is dependent on the magnitude of particle interactions under shear. As the magnitude of the attractive forces increases the consistency increases. The flow index, n , shows the easiness of the destruction of the microstructure. If n is greater than 1 the dispersion is described as shear thinning. If not, the dispersion is described as

shear thickening fluid (Peker and Helvacı, 2008). The response of a HB fluid to a stress is a slow shear flow provided a shear stress which is slightly greater than its actual yield stress. The model parameters of the HB model were tabulated in Table 5.4. The model parameters were determined by using the software of the rheometer (Haake, Rheowin, 3.61.00).

However, the flow behavior of the suspension having 5 vol% submicron alumina in 20 wt% fructose solution which is marked with superscripted star (*) was better explained by Newtonian behavior ($\tau = \eta\dot{\gamma}$) than HB ($\tau = \tau_o + K\dot{\gamma}^n$) and Bingham Plastic flow ($\tau = \tau_o + \eta\dot{\gamma}$) behaviors. The regression coefficient is 0.99 and the viscosity is 0.0024 Pa.s. This viscosity value was very similar to the viscosity values at 50 and 100 1/s which are 0.0025 and 0.0023 Pa.s.

The correlation coefficient was varied between 0.95 and 0.99. The model parameter, K , and flow index, n , were system dependent constants. The n value was varied between 0.23 and 1.88. The yield stresses of the dispersions were calculated by HB model. Yield stress of dispersion represents the shear stress threshold that breaks the connection between particles and initiates motion in the dispersion. The HB yield stress varied with the solids content and fructose concentration and it is given in Figure 5.36.

Table 5.4. The model parameters of Herschel-Bulkley Model ($\tau = \tau_o + K\dot{\gamma}^n$) calculated for the submicron alumina dispersions.

wt% of fructose solution	vol% solids content	τ_o (Pa)	K	n	R^2
1	5	0.33	0.36	0.26	0.96
	10	0.04	0.68	0.23	0.98
	20	0.27	0.11	0.59	0.99
	30	3.12	0.53	0.53	0.99
4	5	0.37	0.14	0.57	0.99
	10	0.61	0.0037	1.01	0.98
	20	0.37	0.15	0.56	0.99
	30	2.74	0.64	0.48	0.99
	40	12.81	3.53	0.48	0.99
10	5	0.45	0.01	0.86	0.99
	10	0.11	0.47	0.26	0.98
	20	0.13	0.45	0.28	0.98
	30	0.16	0.15	0.66	0.99
	40	1.40	1.56	0.47	0.99
20	5*	0.21	0.0001	1.88	0.95
	10	0.51	0.003	1.05	0.99
	20	0.21	0.04	0.79	0.99
	30	1.46	0.54	0.58	0.99
	40	11.08	3.83	0.45	0.99
30	5	0.77	0.06	0.63	0.99
	10	0.23	0.006	0.98	0.99
	20	1.03	0.30	0.67	0.99
	30	1.81	0.14	0.66	0.99
	40	16.03	0.42	0.84	0.99
40	5	0.04	0.05	0.75	0.99
	10	0.48	0.01	0.90	0.99
	20	1.21	0.04	0.86	0.99
	30	1.85	0.38	0.81	0.99
	40	2.18	10.98	0.28	0.99

(*) Newtonian behavior

The HB yield stress of the dispersion having 20 vol% solids decreased from 0.27 to 0.13 Pa when the fructose concentration was increased from 1 to 10 wt%. Further increase in fructose increased the HB yield stress. It increased approximately six times (0.21 to 1.20 Pa) for the dispersion having 20 vol% submicron alumina when the fructose concentration was increased two times (20 to 40 wt%). The reduction of the HB yield stress became more significant at higher solids content. Generally, the dispersions in 10 wt% fructose solution had the lowest HB yield stress.

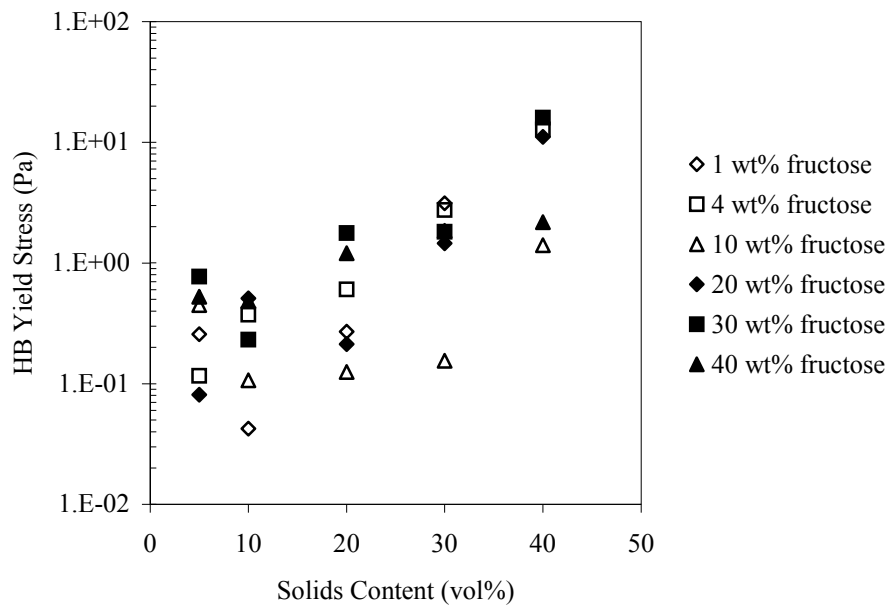


Figure 5.36. The variation of HB yield stress of the submicron alumina dispersions with solids content in semi-logarithmic distribution.

The variation of the consistency coefficient of the submicron alumina dispersions is given in Figure 5.37. The consistency coefficient was varied between 0.0001 and 10.97. It was more sensitive to the fructose concentration at low solids content than higher ones and had the lowest value for the dispersion having 5 vol % solids content in 20 wt% fructose concentration. The consistency coefficient of the dispersions having 10, 20 and 30 vol% solids in 20 and 30 wt% fructose solutions were comparable with each other. High solids content (40 vol%) and high fructose concentration (40 wt%) resulted in more resistance to flow under shear. The dispersion having 40 vol% solids had the lowest resistance to flow when it was prepared in 30 wt% fructose solution. Regarding the consistency coefficient, the dispersions in 20 wt%

fructose concentration can be considered as less resistant to flow due to particle interactions under shear.

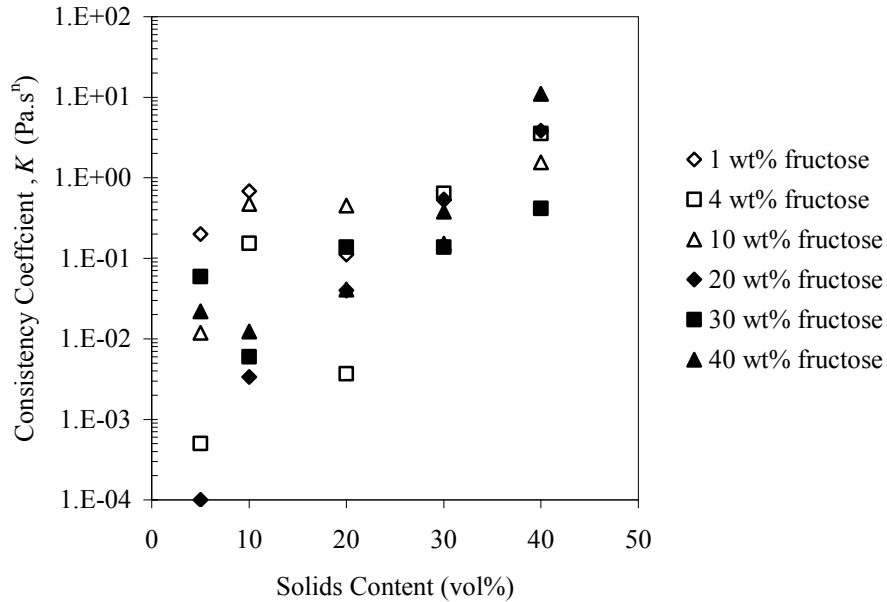


Figure 5.37. The variation of consistency coefficient, K , of submicron alumina dispersions with solids content in semi-logarithmic distribution.

The variation of flow index, n , of submicron alumina dispersions with solids content is given in Figure 5.38. The flow index of most of the dispersions was lower than 1 which described shear thinning behavior. Only the dispersions having 5 vol% solids in 4 and 20 wt% fructose solutions had flow index greater than 1. This may be caused due to instrumental or sample based errors. The Reynolds numbers were calculated for each suspension and all of them were lower than 40 which eliminated the possibility of error based on the secondary flow. The presence of air bubbles or inhomogeneity in the samples may caused the flow index to be higher than 1. Regarding the flow index of the dispersions, preparation of the submicron alumina dispersions in 10 wt% fructose solution made the suspensions more shear thinning. Increase in fructose concentration decreased the level of shear thinning behavior.

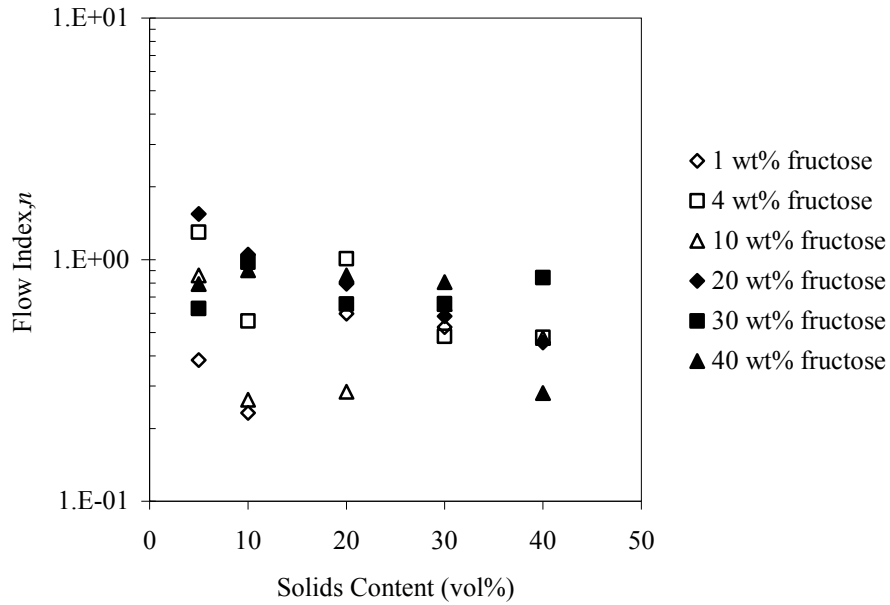


Figure 5.38. The variation of flow index, n , of submicron alumina dispersions with in semi-logarithmic distribution.

The viscosities of the dispersions at shear rates of 50 and 100 1/s are given in Figure 5.39. The viscosity increased at all shear rates with increasing solids content. The viscosity reduction was observed as the fructose concentration increased. As the shear rate was increased from 50 to 100 1/s, the viscosity of the dispersion having 20 vol% solids in 1 wt% fructose solution became approximately 1.5 times lower and decreased from 0.031 to 0.02 Pa.s. At 20 vol% solids content, the viscosity decreased from 0.031 to 0.0051 Pa.s at 50 1/s, as the fructose concentration was increased from 1 to 4 wt%. The viscosity of the dispersion having 40 vol% solids in 20 wt% fructose solution had its lowest value (0.034 Pa.s) at a shear rate of 50 1/s. The viscosities in concentrated fructose solutions were similar to each other.

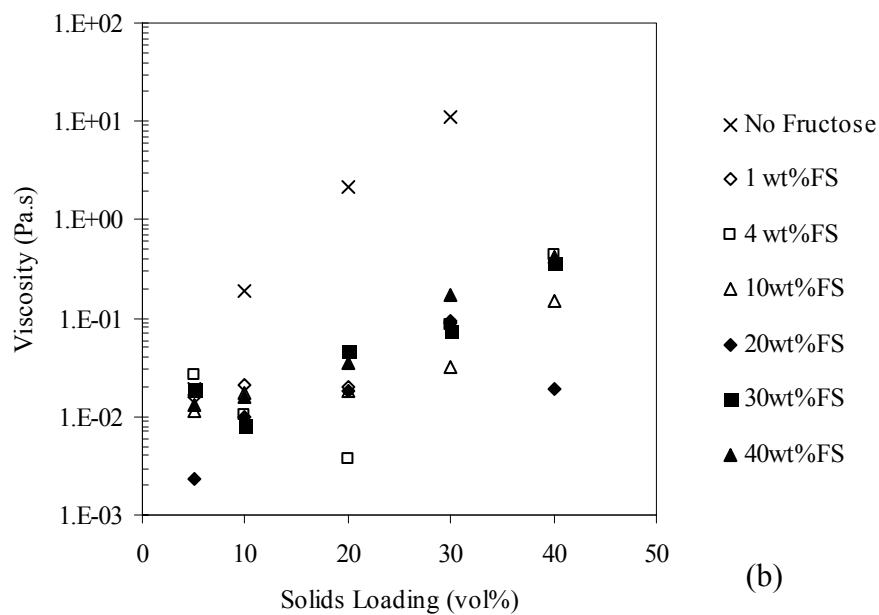
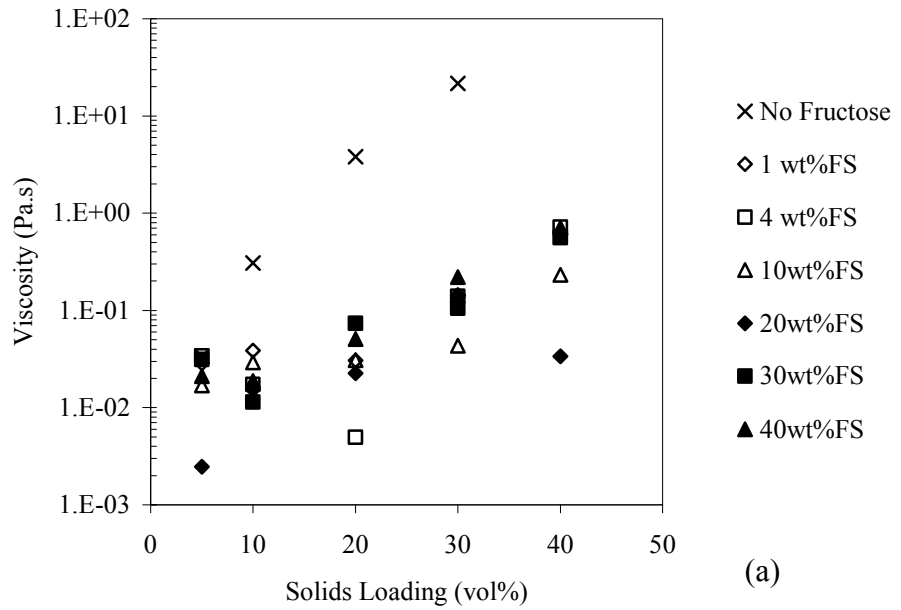


Figure 5.39. The viscosities of the submicron alumina dispersions at a shear rate of (a) 50 1/s and (b) 100 1/s.

However, the dispersion having 40 vol% submicron alumina particles has much lower viscosity when polyelectrolytes were used. Cesarano and Aksay (1988) reported that the dispersions having 40 vol% submicron alumina particles dispersed by Na^+ salt of polymethacrylic acid (PMMA) at pH about 6.8 was reported as 0.05 Pa.s at a shear rate of 9.3. The viscosity of the 40 vol% submicron alumina dispersion in 10 wt% fructose solution at a shear rate of 9.5 1/s was 0.75 Pa.s and 15 times higher than the

value which was reported by Cesarano and Aksay (1988). It was noted that the further pH adjustment was not done in our study as they did.

The preshearing and shearing conditions have a significant effect on the viscosity. The viscosity determination was done as follows in the study of Cesarano and Aksay (1988): The dispersions were presheared at 93 1/s to disperse particle clusters. The viscosity data was recorded while the shear rate was decreased stepwisely to 0.46 1/s. Then, the dispersion was hold undisturbed for 10 min for the nucleation and growth of particle clusters. The viscosity data was collected while the shear rate was increased to 93 1/s. There will be difference in viscosity when the measurements were done by increasing shear rate and by decreasing shear rate. The authors assumed that the dependence of viscosity on increasing and decreasing sweep was due to flocculation. Preshearing at high shear rates may cause particle migration especially for unstable dispersions. Generally, the viscosity determined by decreasing shear rate will be lower for dispersions having shear thinning behavior. A particle concentration gradient may occur in radial axis. Time required for the nucleation and growth of particle cluster maybe longer or shorter than 10 minutes. It can be determined by monitoring viscosity with respect to time after shearing and observing whether viscosity reaches its initial value or not.

The thixotropic behavior of the submicron alumina dispersions were observed by ramp up to 400 1/s, hold and ramp down and the thixotropic behavior of 5 vol% submicron alumina dispersion in 1 wt% fructose solution is given in Figure 5.40. The thixotropic behaviors of the dispersions are given in Appendix B.2. The thixotropic area of the dispersions was calculated by the software of the rheometer (Haake Rheowin 3.61.00). The variation of thixotropic area of the submicron alumina dispersions with solids content is given in Figure 5.41. The thixotropic loop area was decreased as the fructose concentration was increased. However, the fructose concentration maintaining the lowest or the highest thixotropic area was different for different solids content. The variation in thixotropic area became more significant as the solids content was increased.

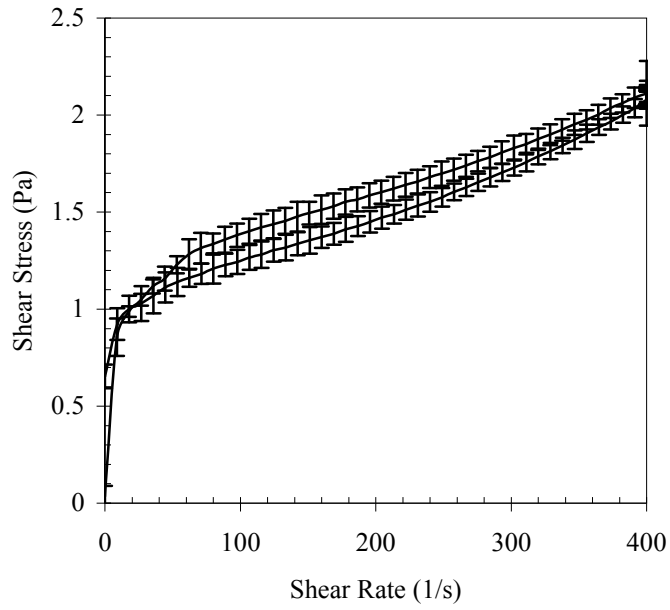


Figure 5.40. The thixotropic behavior of 5 vol% submicron alumina dispersion in 1 wt% fructose solution.

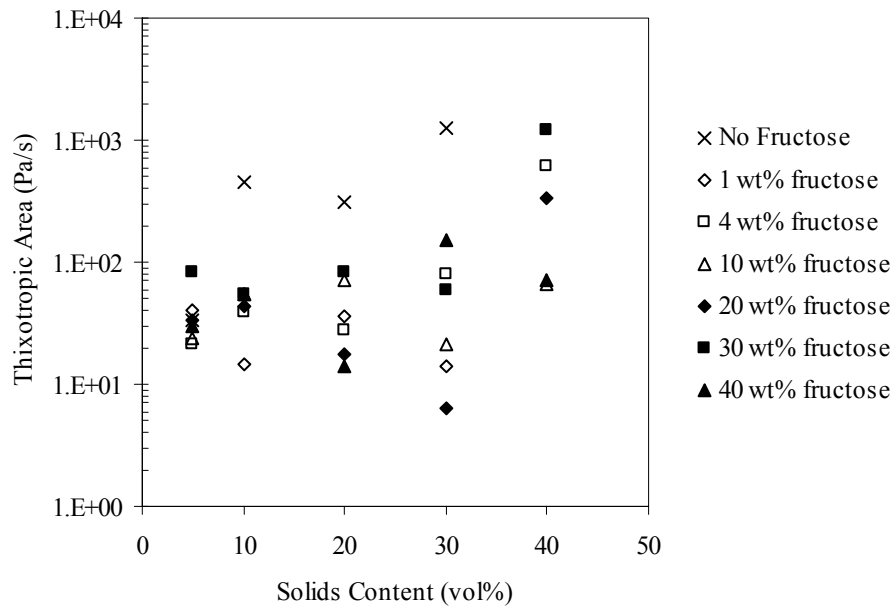


Figure 5.41. The variation of thixotropic loop areas of the submicron alumina dispersions with solids content.

5.4.2. The Effect of Solids Content and Fructose on the Dynamic Shear Rheology of the Submicron Alumina Dispersions

The dynamic shear rheology of the submicron alumina dispersions was investigated by stress and frequency sweep tests. The stress sweep tests were used for determination of the linear viscoelastic region (LVER) of the dispersion. Then, a stress value was picked in the LVER and used in frequency sweep test.

5.4.2.1. The Effect of Preshear on the Determination of LVER of the Submicron Alumina Dispersions

The shear history of the dispersions in the determination of dynamic shear rheology is very important because, a infinitesimal amount of stress naturally occurs even the preparation and the handling of the dispersions. The shear history dependency becomes more significant for highly concentrated dispersions because the particle network development and the interactions between the components of the system are remarkable (Wolthers et. al, 1996, Schmidt and Münstedt, 2002). Preshearing of the dispersions is used to eliminate shear history effect especially for highly concentrated dispersions.

The preshearing of the dispersions was done to eliminate the dependency of rheological behavior of dispersions on the shear history. First of all, 20 vol% α - Al_2O_3 dispersion in 1 wt% fructose solution without preshearing was subjected to stress sweep test. When three stress sweep tests were subsequently done, the elastic moduli (G') of dispersions were decreased significantly. The viscous moduli (G'') of the dispersions didn't change significantly. The linear viscoelastic region of the dispersion appeared in the same shear stress range as it is shown in Figure 5.42. The G' and the G'' moduli of the dispersion had a crossover at 1.5 Pa. After that point, the three dimensional network of the dispersion was broken down and the dispersion flowed at higher shear stress. This means that dispersion's structure has been changed. If there was not enough time to recover its three dimensional structure before the next experiment, the G' and G'' became smaller.

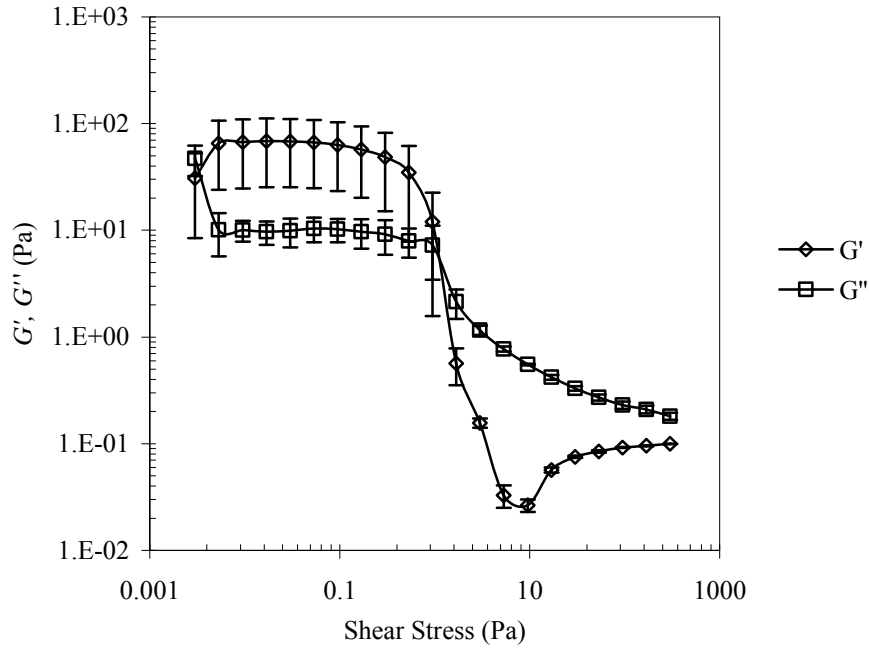


Figure 5.42. The results of stress sweep tests done for three times successively to 20 vol% submicron alumina with 1 wt% fructose solution without preshearing.

Different shear rates (50, 100, 200 1/s) were applied to eliminate shear history effect and hold undisturbed for different periods of time (300, 600, 900 s) for the dispersion having 20 vol% submicron alumina in 1 wt% fructose solution. The preshearing time was kept constant as 60 s.

The stress sweep tests of 20 vol% submicron alumina in 1 wt% fructose solution are shown in Figure 5.43. Since the G'' modulus of the dispersion was not significantly changed due to preshear and/or shear history, only the G' are given. It is seen that the range of shear stress where the LVER was observed was shifted to lower shear stresses and G' decreased as the holding time was increased.

The stress sweep test result of the dispersion which was presheared at 100 1/s is given in Figure 5.44. It was observed that the LVER of the dispersion was slightly related to preshear rate by increasing the holding time. The error of G' became smallest when the holding time equal to 600 s. However, increase of holding time to 900 s increased the error.

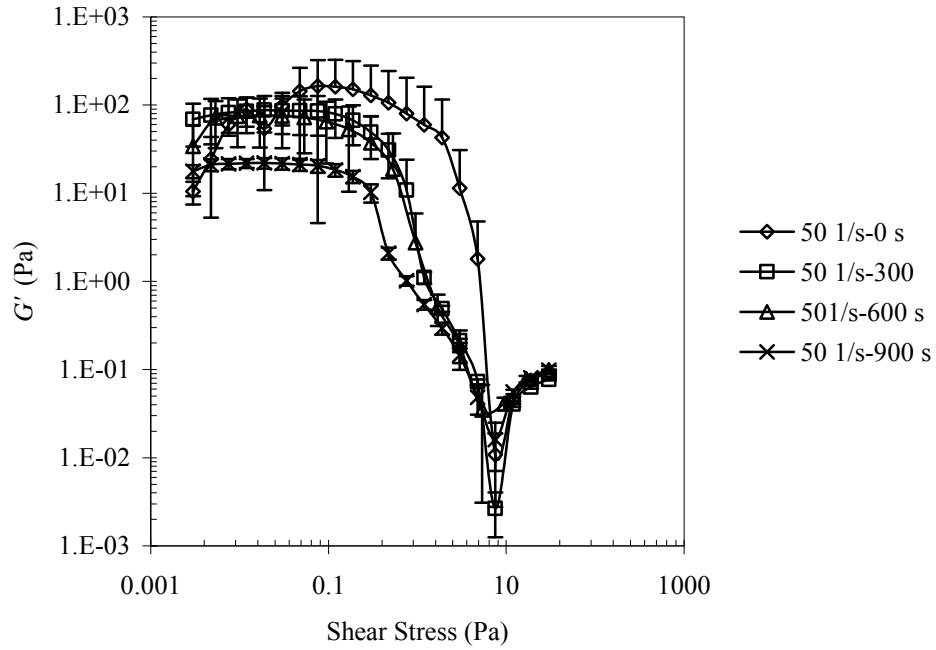


Figure 5.43. The results of stress sweep tests done for three times subsequently to 20 vol% submicron alumina in 1 wt% fructose solution which was presheared at 50 1/s and hold undisturbed for 0, 300, 600, and 900 s.

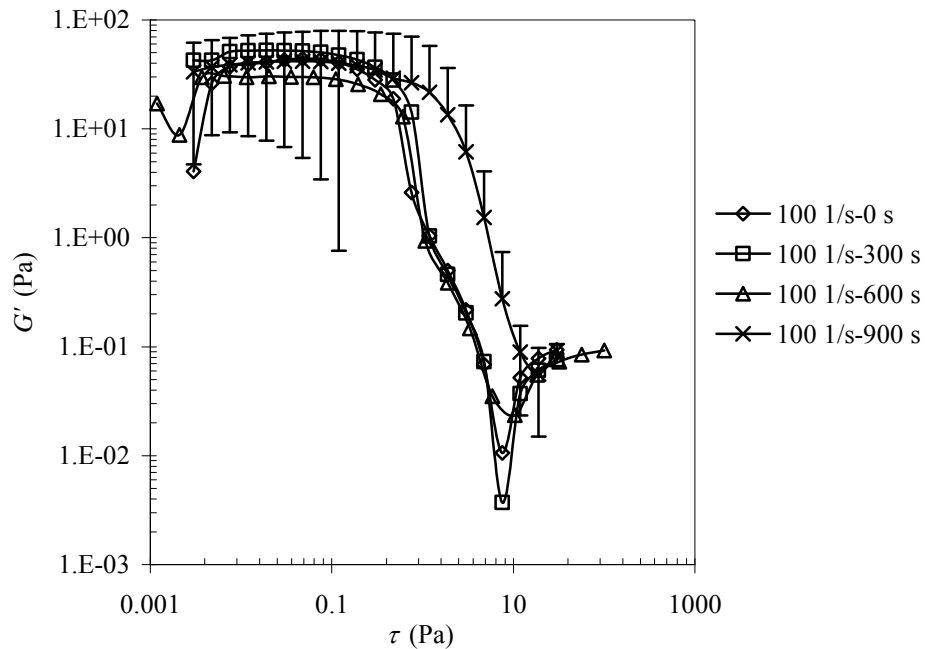


Figure 5.44. The results of stress sweep tests done for three times subsequently to 20 vol% submicron alumina in 1 wt% fructose solution which was presheared at 100 1/s and hold undisturbed for 0, 300, 600, and 900 s.

The stress sweep test results of presheared dispersions at a shear rate of 200 1/s are given in Figure 5.45. The G' and the LVER of the dispersion were independent of shear rate and holding time. The error in G' became very small for all measurements. The G' of dispersion (92.88 Pa at a shear stress of 0.03 Pa) was very close to the G' value of the first measurement without preshearing which was 93.06 Pa at shear stress of 0.03 Pa.

The stress sweep results of dispersion which was presheared at a shear rate of 300 1/s is given in Figure 5.46. The dispersion was mixed with the oil around the sample during preshearing and the G' values became inconsistent. It was decided that preshearing above 200 1/s was not suitable with this measurement apparatus. The use of cup and bob system may allow shearing at much higher shear rates. For example, the dispersions were subjected to preshearing at 200 Pa in the study of Kirby et. al. (2005). The highest possible shear rate was thought to be chosen, regarding Kirby's study. Since the G' value is much closer to the value without preshear and the error is smaller, preshearing at 200 1/s for 60 s followed by 600 s undisturbed hold were chosen for the dynamic measurements.

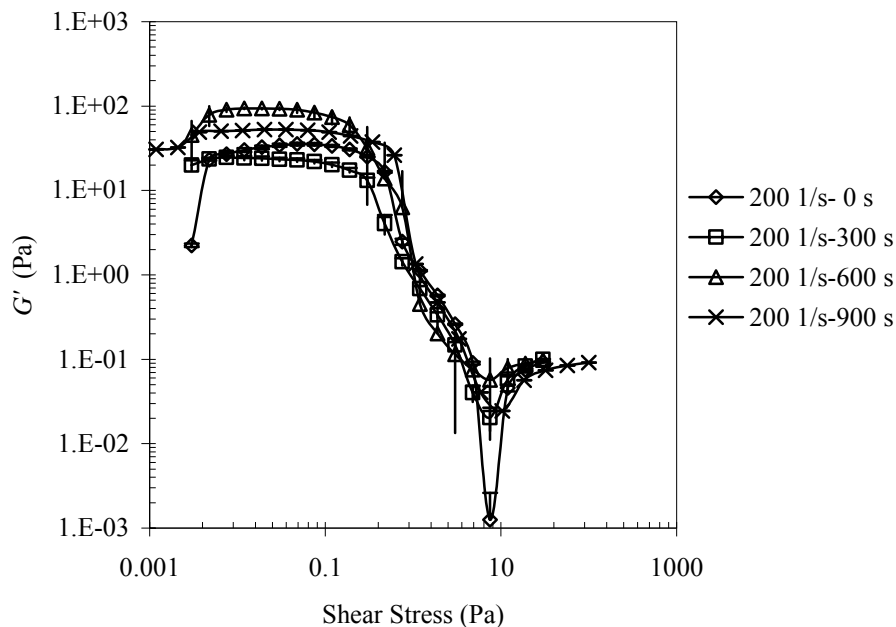


Figure 5.45. The results of stress sweep tests done for three times subsequently to 20 vol% submicron alumina in 1 wt% fructose solution which was presheared at 200 1/s and hold undisturbed for 0, 300, 600, and 900 s.

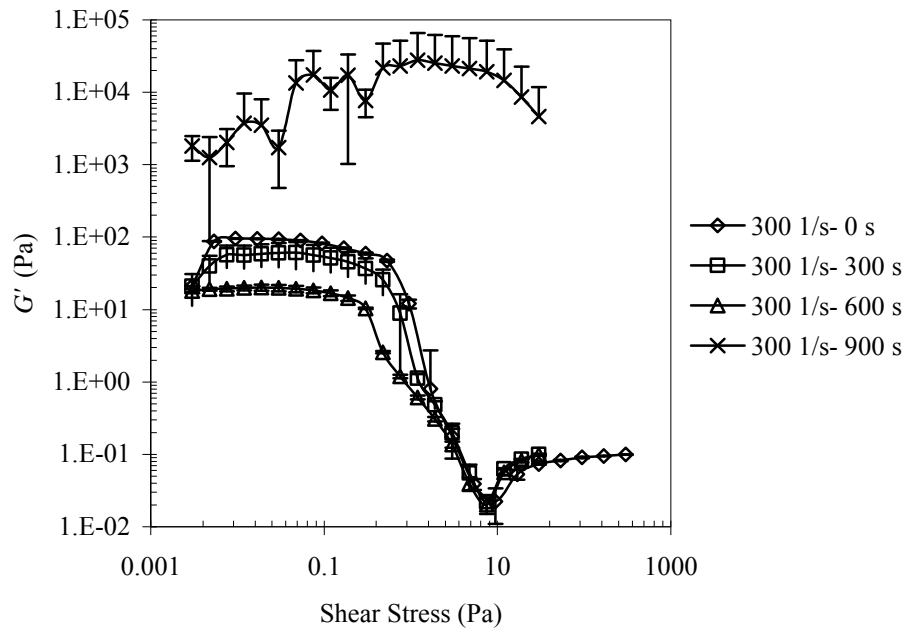


Figure 5.46. The results of stress sweep tests done for three times subsequently to 20 vol% submicron alumina in 1 wt% fructose solution which was presheared at 300 1/s and hold undisturbed for 0, 300, 600, and 900 s.

The studies on preshearing showed that it has more important influence on the viscoelastic properties of the dispersion as the solids content is increased (Wolthers et al, 1996, Schmidt and Münstedt, 2002). Preshearing at high shear rates may create high shear stress on the particles and result in diffusion of the particles. The diffusion of particles can lead to a collective migration of particles if gradients are present either in the particle volume fraction or in the shear rate distribution. High shear stresses on the particles made them to migrate to where the shear stress approaches to zero. Hence, there will be particle concentration gradient through the radian axes (Collyer and Clegg, 1998).

The particle migration was visually observed especially for the dispersions having low solids content in this study. When the preshearing were done at constant shear rate (200 1/s) the shear stresses were 2.33, 2.91, 20.93, 62.36 Pa for the dispersions having 10, 20, 30 and 40 vol% solids content in 1wt% fructose solution, respectively. This wide range of shear stress may cause particle migration and shear history in different extents. Keeping the shear stress constant to eliminate shear history may be more appropriate. In the study of Kirby et. al. (2005) the preshearing was done at 200 Pa without giving any reason. Lu (2006) and Schmidt and Münstedt (2002) did preshearing at low shear stresses at 0.6 Pa for 60 s and at 0.19 Pa for different periods of

time but they didn't give any information about keeping the shear stress constant and low. As a result, the dispersions need to be presheared at constant and low shear stress for longer period of time to eliminate particle migration due to high shear stresses.

The stress sweep tests give valuable information the stress amplitude dependence of the dispersion structure. The test was performed at constant temperature and frequency ($20^{\circ}\text{C}\pm 1$ and 6.28 rad/s, respectively in this work). The oscillating stress was increased in small steps. The response is G' and G'' and they are almost parallel in the lower stress range. This linear range is called as linear viscoelastic region (LVER). The further dynamic rheology measurements such as frequency, temperature and time sweeps are done in the LVER because; comparing two measurements can be accurate only if the boundary conditions are the same for both measurements and the relations between elastic and viscous moduli, frequency and shear stress etc. are well-defined.

The stress sweep test result of 5 vol% submicron alumina dispersion is given in Figure 5.47 and the stress sweep test results for the submicron alumina dispersions are given in Appendix B.3.

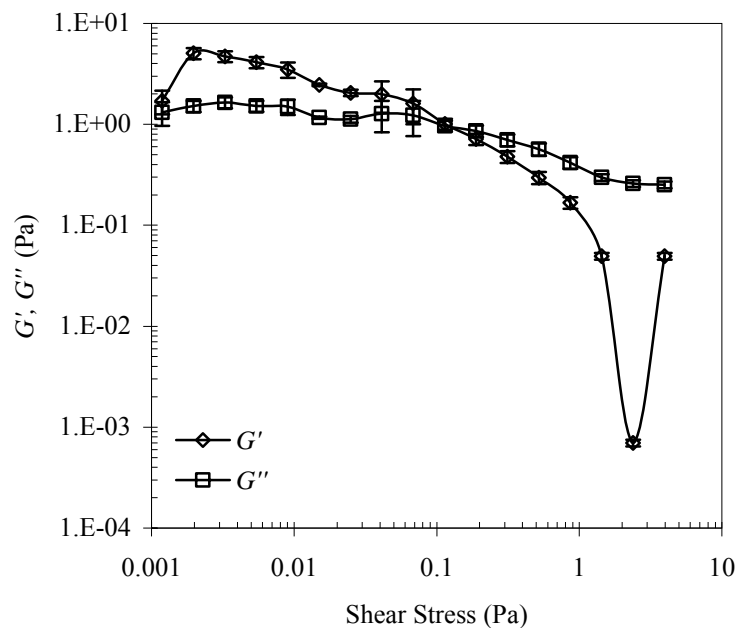


Figure 5.47. The stress sweep of 5 vol% submicron alumina dispersion in 1 wt% fructose solution.

The LVER of the dispersions at low solids content and fructose concentrations was relatively short. Generally, increase in the fructose concentration and solids content extended the LVER. As the solids content increased, the effect of the fructose content on the extension of LVER became more obvious.

The G' values at 0.01 Pa for the dispersions were collected and given in Figure 5.48. The LVER of the dispersions without fructose and having 40 vol% solids were located at much higher shear stress ranges. Hence, the G' and G'' values of these dispersions were not taken into account. The fructose addition to the dispersions having 5 vol% solids resulted in higher G' and G'' values. Both G' and G'' were ten times higher when the fructose concentration was increased from 1 to 30 wt%. The G' value for 20 vol% solids decreased from 9.5 to 7.4 at 0.01 Pa as the fructose concentration was increased from 1 to 4 wt%. Further increase in fructose concentration made G' to reach higher values. The G' was 25.7 Pa at 0.01 Pa when the dispersion having 20 vol% solids was prepared in 40 wt% fructose solution. It was observed that increasing fructose concentration lowers both G' and G'' in LVER. Both of them were reduced to lower values as the fructose concentration was increased to 4 wt%. However, further increase in fructose concentration showed an ascending G' and G'' . The reason behind this behavior may be non-adsorbed fructose molecules and their contribution to elastic part of the dispersion. The excess amount of fructose increased the G' more significantly than the G'' .

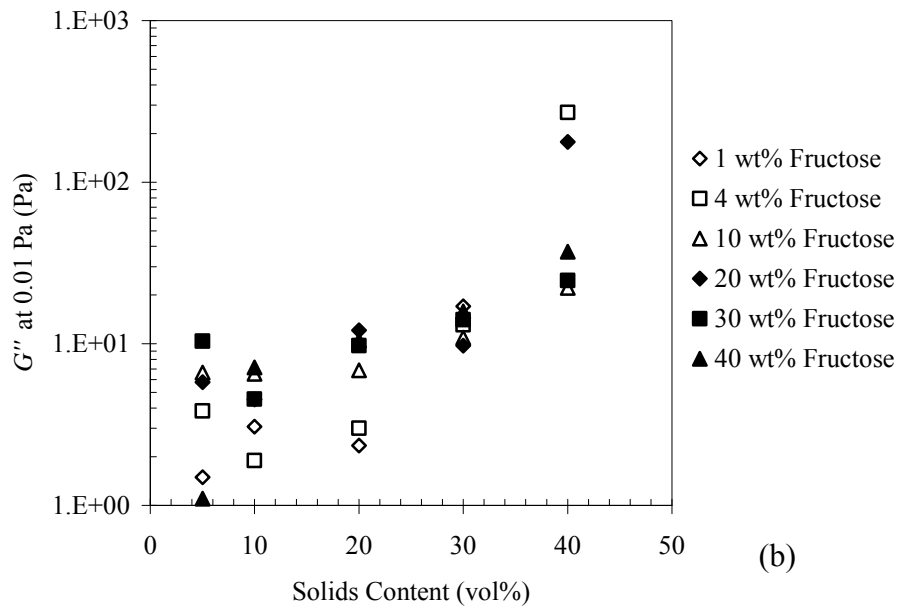
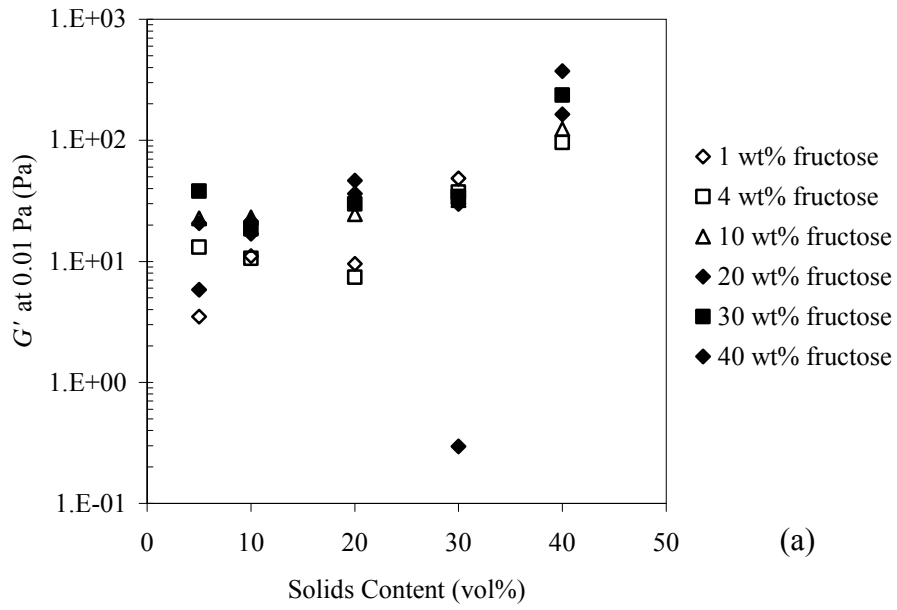


Figure 5.48. The variation of (a) G' and (b) G'' of the submicron alumina dispersions at a shear stress of 0.01 Pa.

In the frequency sweep, the material is subjected to a sinusoidal constant deformation while frequency is changing. The response is the complex modulus and can be separated in real and imaginary parts. This separation provides a measure of the stored (G') and lost energy (G''). The G' is defined as the stress in phase with the strain in sinusoidal shear deformation divided by strain. It is a measure of stored and recovered energy per cycle when different systems are compared at the same strain amplitude. The G'' is defined as the stress 90° out of phase with the strain divided by strain and it is a measure of the energy dissipated or lost as heat per cycle of sinusoidal deformation when different systems are compared at the same strain. The frequency sweep test is nearly a non-destructive test when it is done in the LVER (Ferry, 1980, Brummer, 2006).

The viscoelastic properties of the polymeric materials were extensively investigated (Ferry, 1980). The frequency dependence of G' for such materials has four regions when it is plotted against frequency. At high frequencies, the mobility of chain segments is highly restricted. The vibrational energy is stored by deformation of bond angle and distances. This region is called as glassy region. With decreasing frequencies, the mobility of the chain segments slowly increase. Hence, the G' value decreases with decreasing frequency. This region is rubbery-elastic region and called as transition region. The G' reaches to a plateau with decreasing frequency. The mobility of the polymer chains increases but still do not slip and past each other. This region is called as plateau region. At lower frequency, the G' decreases further because the deformation energy can no longer be stored. The material tends to dissipate more of the input energy through viscous flow and results in decreasing the G' and increasing the G'' . This region is called as flow region. The crosslinked polymers have no flow region and the G' exhibits a continuous plateau in the flow region. However, linear and branched polymers show a decreasing G' .

The frequency sweep test result of 5 vol% submicron alumina dispersion is given in Figure 5.49. The dependence of G' on angular frequency of the submicron alumina dispersions is given in Appendix-B.4. It was observed that there was no glassy region for the all dispersions in the frequency sweep tests regardless of solids content and fructose concentration. The G' of the dispersions rapidly decreased as the angular frequency was decreased from 628 rad/ (the upper limit of the angular frequency) to approximately 100 rad/s. Then, the G' and G'' continued to decrease or reached to

plateau region. The G' was dominant over the G'' at all frequencies. This behavior was attributed to a gel-like and more elastic structure.

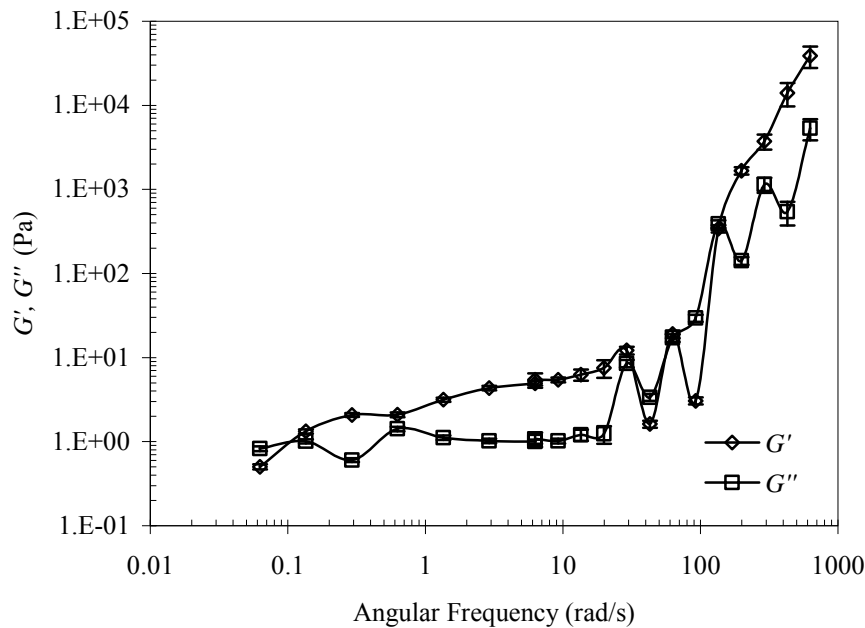


Figure 5.49. The frequency sweep of 5 vol% submicron alumina dispersion in 1 wt% fructose solution.

The G' and G'' of submicron alumina dispersions in fructose solutions at angular frequencies of 628, 6.28 and 0.0628 rad/s were collected to observe the variations at rubbery-elastic, plateau and flow regions. Figure 5.50 shows the variations of the G' and G'' with solids content in rubbery-elastic region. It was observed that the G' was dominant over the G'' and both G' and G'' of the dispersions without fructose had an ascending behavior as the solids content was increased. The G' of the dispersions without fructose varied between 7.4×10^3 and 5×10^6 Pa. When the dispersions were prepared in fructose solutions, the G' decreased and was almost constant regardless the solids content and the fructose concentration. The G' varied between 2.6×10^4 and 3.8×10^4 Pa. However, the G'' of the dispersions in fructose solutions slightly decreased with solids content and varied with fructose concentration. When the solids content was increased from 5 to 40 vol% in 40 wt% fructose solution the G'' decreased from 6.2×10^3 to 860 Pa. When the angular frequency was decreased to 6.28 rad/s, both G' and G'' reduced about a 100 times (Figure 5.51). The G' was more sensitive to solids content and fructose concentration. The variation of the G' was almost the same with the

behavior at 628 rad/s. The G' and G'' of the dispersions at 0.0628 rad/s is given with respect to solids content (Figure 5.52). The G' of the dispersion having 5 vol% solids decreased from 0.5 to 0.09 Pa when the fructose concentration was increased from 1 to 10 wt% and it was increased to 3.5 Pa when it was prepared in 40 wt% fructose solution. This indicated the reverse effect of fructose on the G' . The same behavior was observed regardless the solids content. Increasing the solids content had a significant effect on the G' at 0.0628 rad/s. As solids content was increased from 5 to 40 vol% in 10 wt% fructose solution, the G' increased from 0.095 to 67.34 Pa while the G'' were 0.32 and 18.85 Pa. The G' has a plateau starting from 100 rad/s at 40 vol% solids content. The G' became five times higher as the fructose concentration was increased from 10 to 40 wt%. The G'' values of the dispersions were reduced significantly by fructose addition but the concentration of fructose had the effect on G'' in the flow region as it was observed for G' . The G' values at 0.0628 rad/s was evaluated as the portion of energy stored in the dispersion (Lu, 2007). The amount of energy became higher as the solids content was increased but decreased with the presence of fructose.

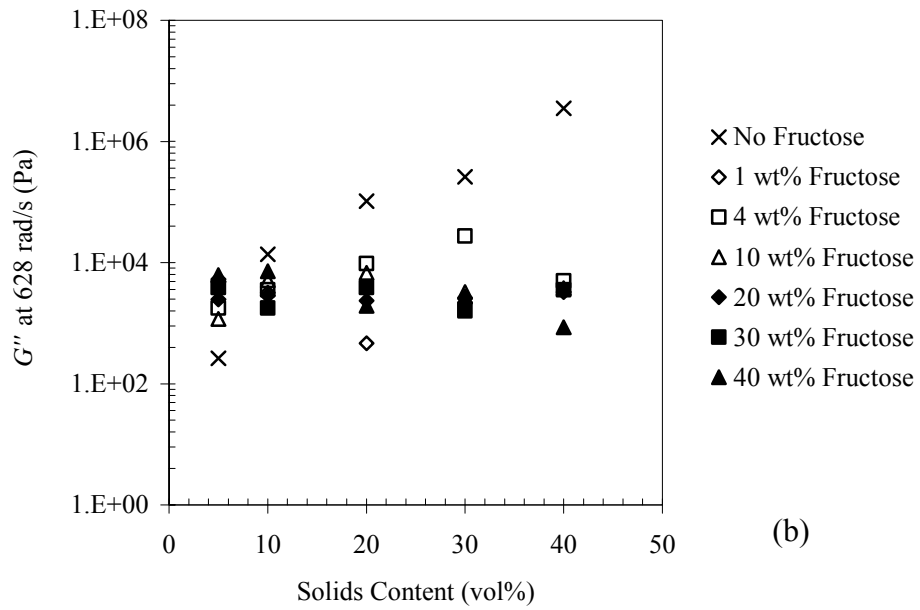
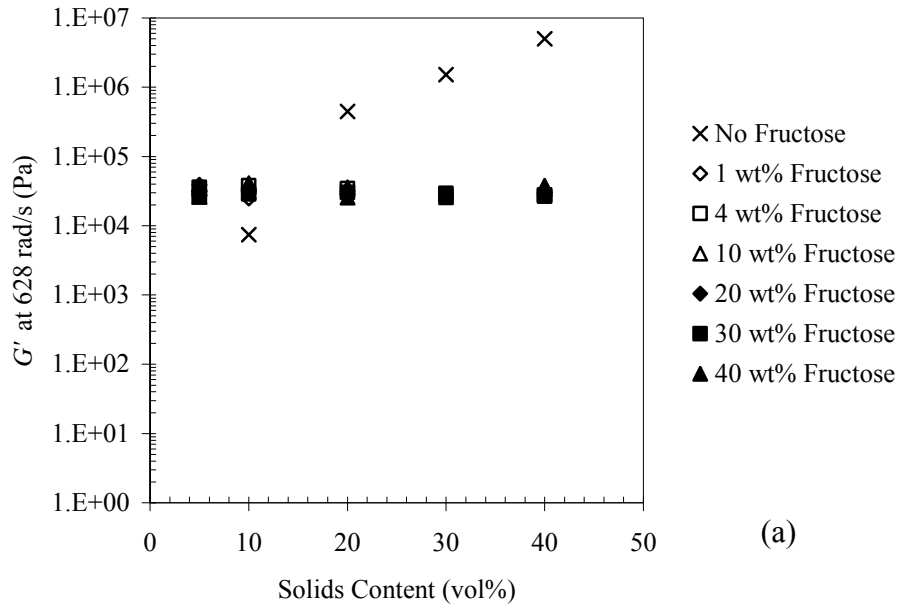


Figure 5.50. The variation of (a) G' and (b) G'' of the submicron alumina dispersions at an angular frequency of 628 rad/s.

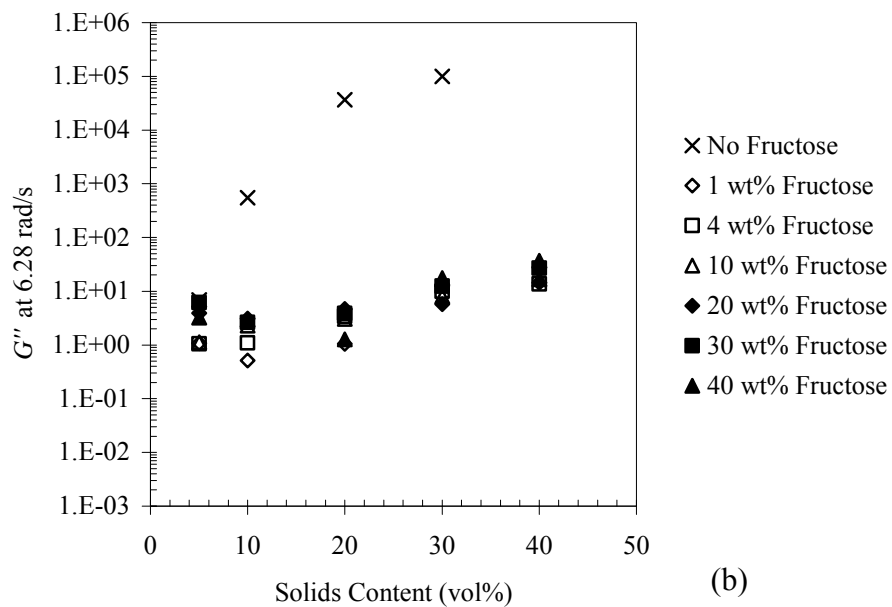
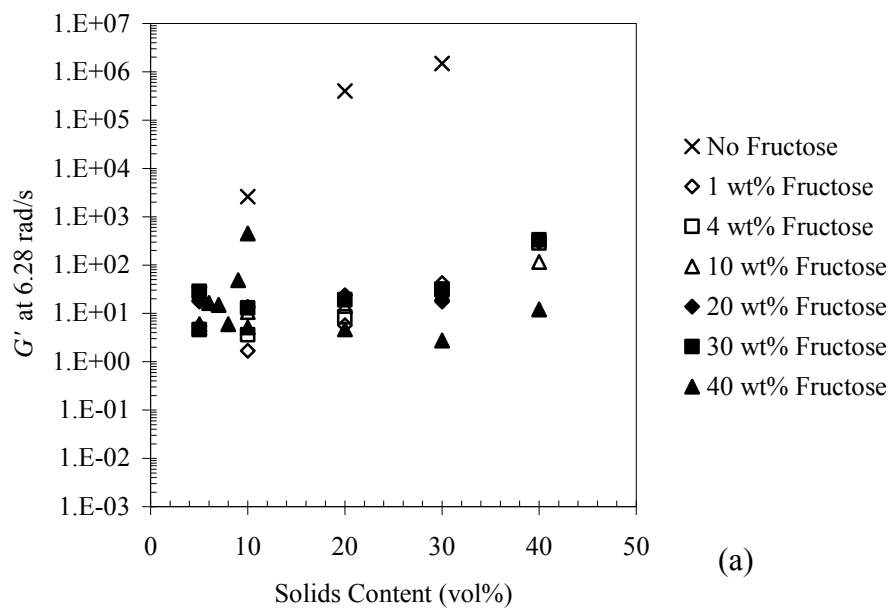


Figure 5.51. The variation of (a) G' and (b) G'' of the submicron alumina dispersions at an angular frequency of 6.28 rad/s.

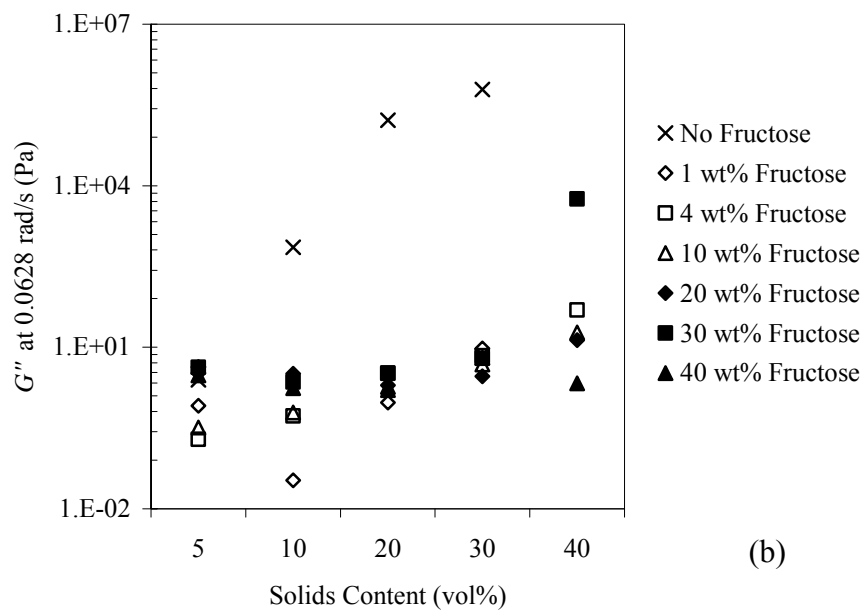
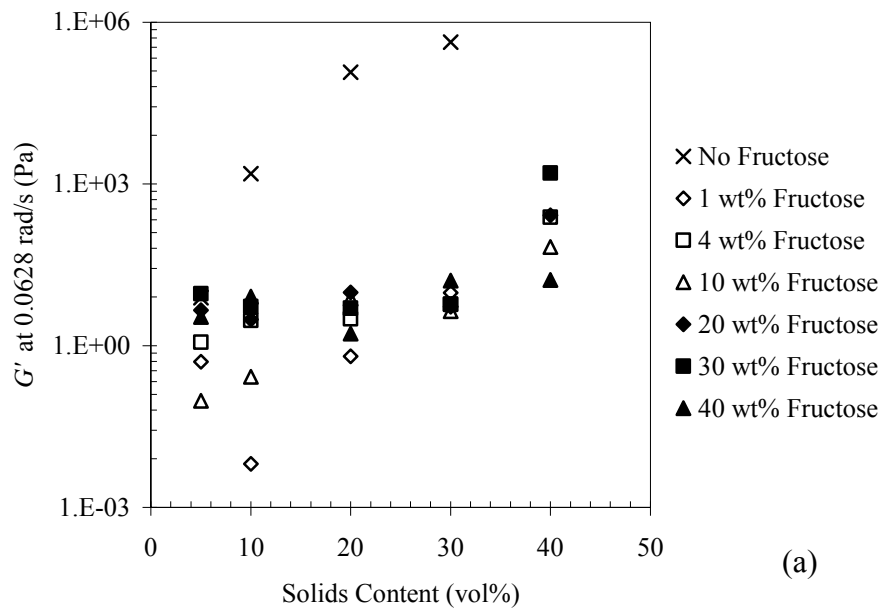


Figure 5.52. The variation of (a) G' and (b) G'' of the submicron alumina dispersions at an angular frequency of 0.0628 rad/s.

5.5. The Rheological Behavior of Nano Alumina Dispersions

5.5.1. The Effect of Solids Content and Fructose Concentration on the Steady Shear Rheology of the Nano Alumina Dispersions

The effect of solids content and fructose concentration on the steady shear rheology of nano alumina dispersions were investigated. The contribution of the nano particles to the flow was more significant than the submicron particles. The flow and viscosity curves of 5 vol% nano alumina dispersion in 1 wt% fructose solution are given in Figure 5.53. The flow curves of the nano alumina dispersions are given in Appendix C-1.

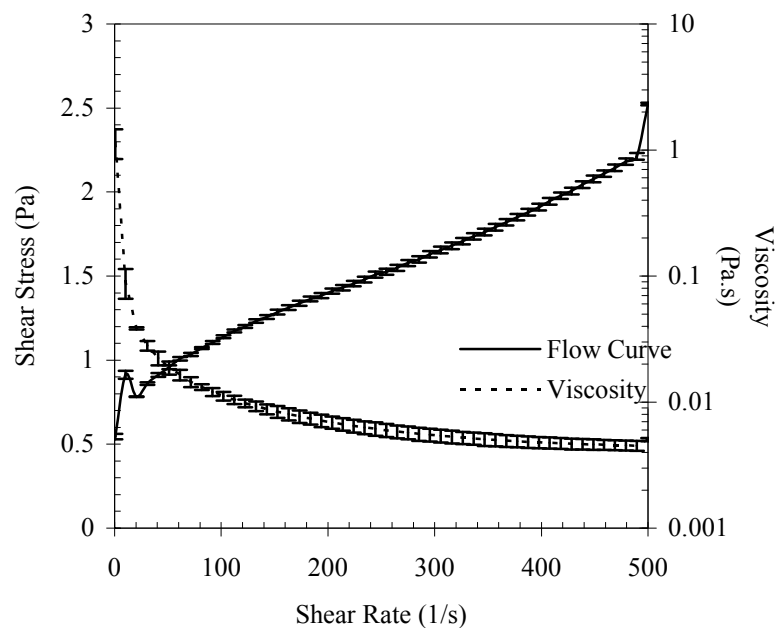


Figure 5.53. The flow and viscosity curves of 5 vol% nano alumina dispersion in 1 wt% fructose solution.

The flow curves of the nano alumina dispersions were fitted to the Herschel-Bulkley model. The model parameters of the Herschel-Bulkley model were tabulated in Table 5.5. The regression coefficients were varied between 0.95 and 0.99. Regarding the parameters of the HB model, the flow behavior of the dispersion having 20 vol% solids in 4 wt% fructose solution (marked superscripted *) was thought to be better explained by Newtonian or Bingham plastic models. The correlation coefficient was

0.998 for both models. The viscosities calculated from the models of Newtonian and Bingham plastic were 0.0065 and 0.0067 Pa.s. However, the actual viscosities at 50 and 100 1/s were 0.0913 and 0.0786 Pa.s, respectively. Since, the viscosity values calculated from the models were not comparable, it was concluded that the flow behavior was of the dispersion was better explained by the HB model.

The HB yield stresses of the dispersions varied between 0.002 and 35.24 Pa and its variation with solids content is further given in Figure 5.54. The presence of fructose decreased the HB yields stress, however, further increase in fructose made an ascending behavior of the HB yields stress. Generally, the dispersions prepared in 30 wt% fructose solution had the highest HB yields stress except the dispersions having 40 vol% solids. The dispersion having 40 vol% solids had the lowest HB yield stress in 30 wt% fructose solution.

The consistency index of the dispersions were varied between 0.0001 and 174.3 (Figure 5.55). It was either lower or higher than unity for the all nano alumina dispersions. The presence of fructose significantly lowered the particle interactions under shear which is indicated by low K values. The dispersions having 5, 10 and 20 vol% solids had smaller K values than the equivalent dispersions of submicron alumina. However, the K values of nano alumina dispersions with 30 and 40 vol% solids were much greater than the equivalent submicron K values which indicated that the particle-particle interactions under shear were much more dominant.

Table 5.5. The model parameters of Herschel-Bulkley Model ($\tau = \tau_o + K\dot{\gamma}^n$) calculated for the nano alumina dispersions.

wt% of fructose solution	vol% solids content	τ_o (Pa)	K	n	R^2
1	5	0.64	0.06	0.54	0.96
	10	0.22	0.009	0.87	0.98
	20	0.002	0.007	0.98	0.99
	30	0.32	0.56	0.63	0.99
4	5	0.33	0.29	0.31	0.95
	10	0.22	0.01	0.85	0.98
	20*	0.002	0.007	0.99	0.99
	30	0.20	0.32	0.70	0.99
	40	42.42	24.10	0.45	0.99
10	5	0.03	0.0001	1.58	0.99
	10	0.03	0.0002	1.45	0.99
	20	0.56	0.027	0.86	0.99
	30	1.07	4.95	0.41	0.99
	40	64.66	174.3	0.17	0.98
20	5	0.35	0.02	0.72	0.97
	10	0.02	0.087	0.58	0.97
	20	0.29	0.05	0.88	0.99
	30	1.95	2.757	0.5	0.99
	40	46.40	83.63	0.22	0.99
30	5	1.02	0.03	0.75	0.99
	10	1.06	0.02	0.86	0.99
	20	0.29	0.04	0.87	0.99
	30	2.18	3.90	0.47	0.99
	40	30.90	17.60	0.35	0.99
40	5	0.24	0.001	1.22	0.99
	10	0.13	0.02	0.89	0.99
	20	0.48	0.21	0.76	0.99
	30	0.40	1.43	0.61	0.99
	40	35.24	21.98	0.47	0.99

(*) Newtonian behavior

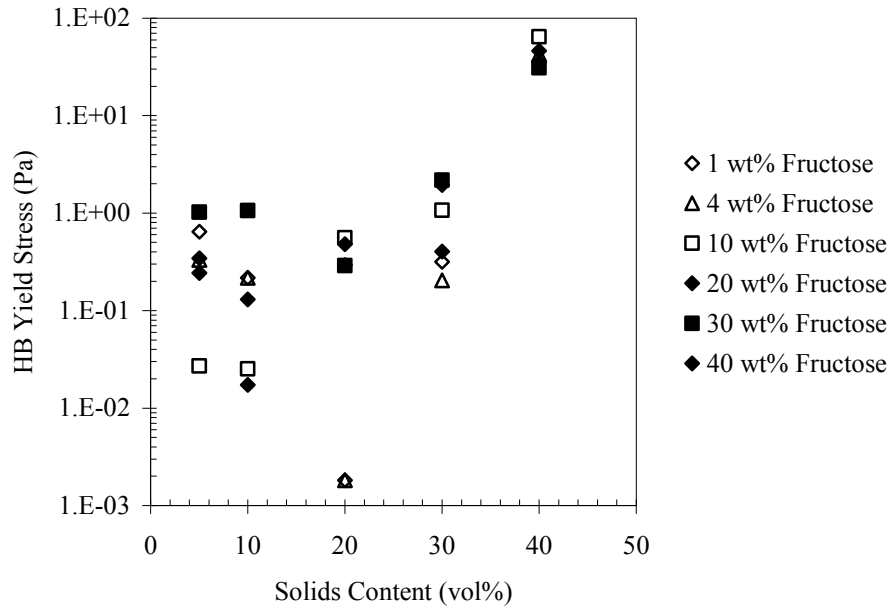


Figure 5.54. The variation of HB yield stress of the nano alumina dispersions with solids content in semi-logarithmic distribution.

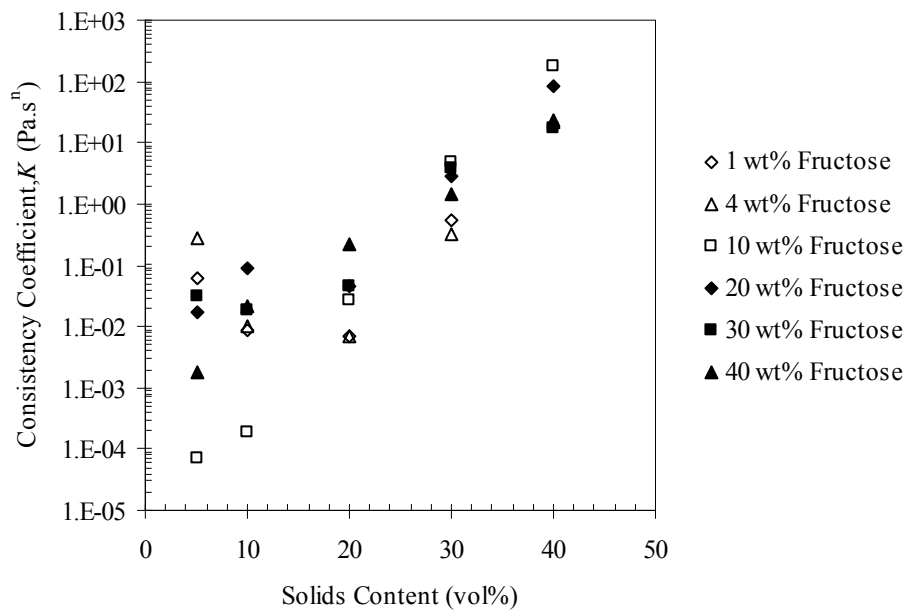


Figure 5.55. The variation of consistency coefficient, K , of nano alumina dispersions with solids content in semi-logarithmic distribution.

The flow index of the nano alumina dispersions varied between 0.17 and 1.58. The range of flow index was shifted to lower values when it was compared to the flow index values (0.23-1.88) for the dispersion having submicron alumina particles. The

variation of the flow index of the nano alumina dispersions is given in Figure 5.56. The more solids and fructose, the lower the flow index was. The dispersions became more shear thinning. The flow index of several dispersions (5 and 10 vol% nano alumina dispersions in 10 wt% fructose solution and 5 vol% nano alumina dispersion in 40 wt% fructose solution) were greater than 1. The consistency coefficients of these dispersions were very low. These dispersions were checked whether the flow behaviors were fitted to any model rather than HB model. The viscosities of the dispersions having 5 and 10 vol% in 10 wt% fructose solution which was calculated from Newtonian model were the same (0.0022 Pa.s) and comparable with the actual viscosities (0.0017 and 0.0022 Pa.s, respectively). When Bingham plastic model was applied to the dispersions, the Bingham plastic yield stress was 0.021 and 0.02 Pa and viscosities were 0.0022 and 0.0027 Pa.s, respectively. The correlation coefficients for Bingham plastic model were bigger than those for Newtonian model, but lower than the values for HB model. The HB model explained the flow behavior of these dispersions more accurately. The flow behavior of the dispersion having 5 vol% nano alumina in 40 wt% fructose solution was also checked and it was found that the viscosities calculated from Newtonian (0.0077 Pa.s) and Bingham plastic (0.0076 Pa.s) models were much lower than the actual (3.56 Pa.s at a shear rate of 50 1/s and 2.28 Pa.s at a shear rate of 100 1/s). Even though the correlation coefficients for these models were 0.99, the HB model was fitted to the data of flow behavior better regarding the viscosity of the dispersion. The Reynolds numbers of these dispersions were calculated and were not bigger than 40. There was no inertial contribution due to secondary flow. The use of a measuring apparatus with a bigger diameter may eliminate this problem.

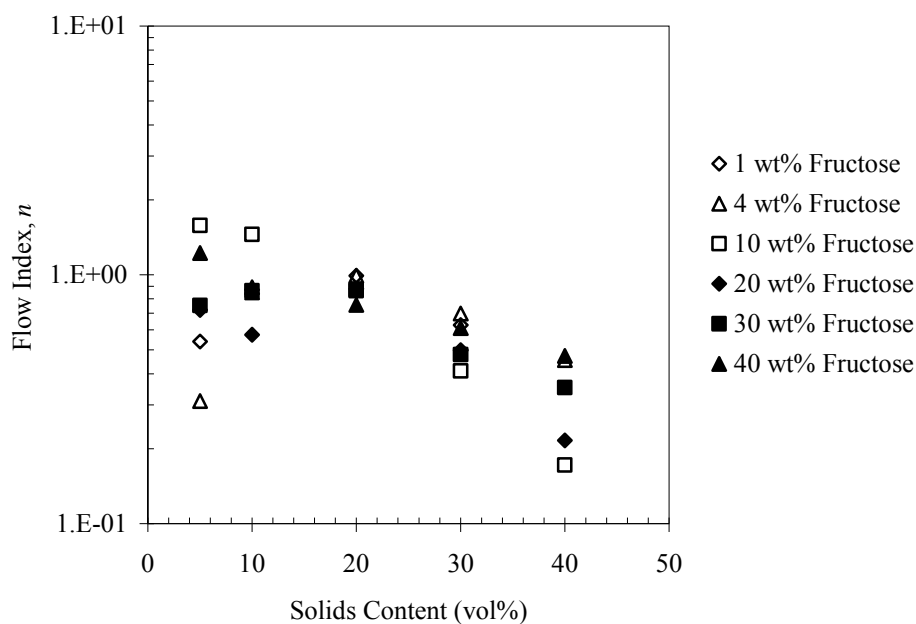


Figure 5.56. The variation of flow index, n , of nano alumina dispersions with in semi-logarithmic distribution.

The viscosity of the nano alumina dispersions at shear rates of 50 and 100 1/s are given in Figure 5.57. The viscosity increased at all shear rates with increasing solids content. Increasing fructose concentration for the dispersions having low solids content had a reverse effect on viscosity. Increasing fructose concentration at high solids content decreased the viscosity. The effect of fructose on the viscosity was more obviously seen for the dispersion having 40 vol% solids content. The viscosity at 50 1/s was decreased from 4.77 to 2.09 Pa.s. The viscosity of the dispersion with 40 vol% submicron alumina in 40 wt% fructose solution was 0.71 Pa.s.

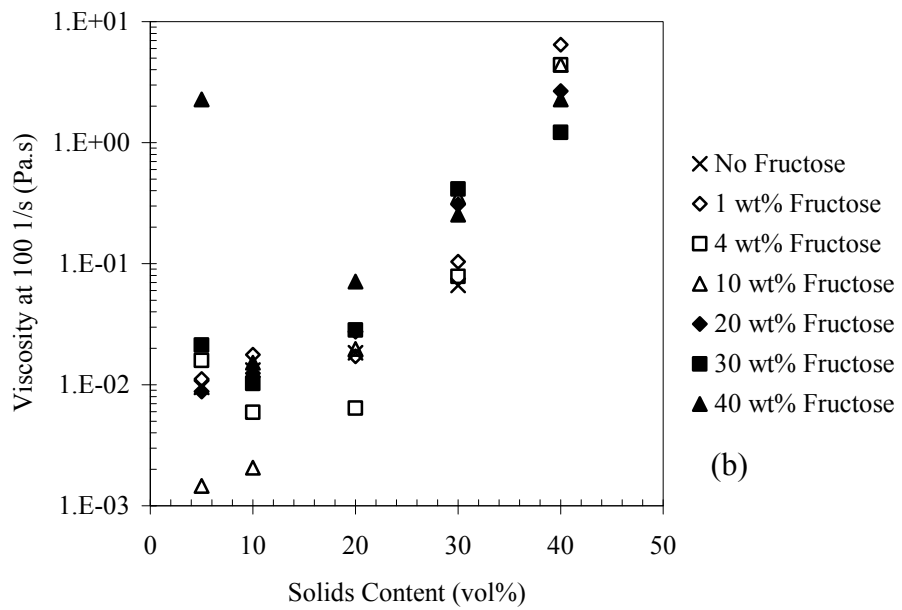
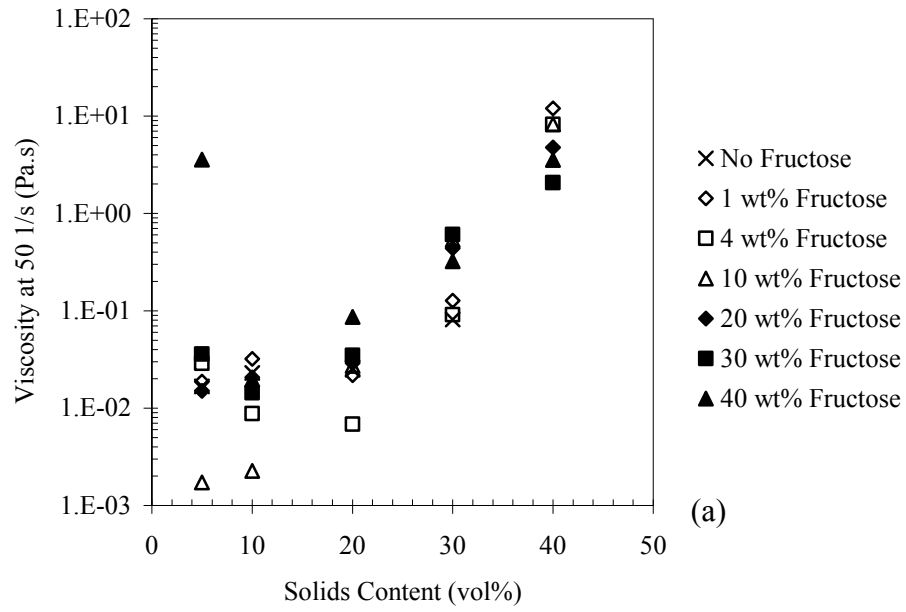


Figure 5.57. The viscosities of the nano alumina dispersions at a shear rate of (a) 50 1/s and (b) 100 1/s.

The thixotropic behavior of 5 vol% nano alumina dispersion in 1 wt% fructose solution is given in Figure 5.58. The thixotropic behavior the nano alumina dispersions are given in Appendix C-2. The variation of thixotropic area of the nano alumina dispersions versus solids content is given in Figure 5.59. The thixotropic area gives the idea on the time dependency of the dispersions. The thixotropic area increased with increasing solids content. The thixotropic area generally was at its lowest value when the dispersion was prepared in 20 wt% fructose. However, the relation of thixotropic area and fructose concentration was complicated. The fructose concentration necessary to maintain for the lowest and/or the highest thixotropic area of the nano alumina dispersions was different as the solids content was changed.

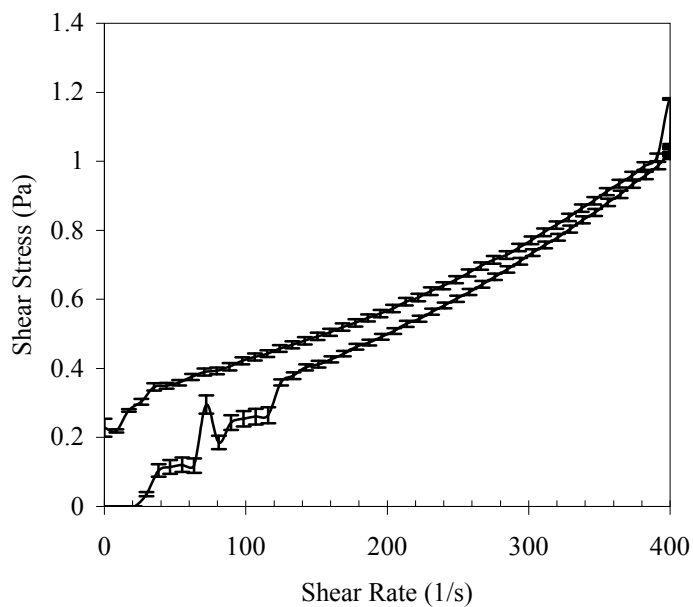


Figure 5.58. The thixotropic behavior of 5 vol% nano alumina dispersion in 1 wt% fructose solution

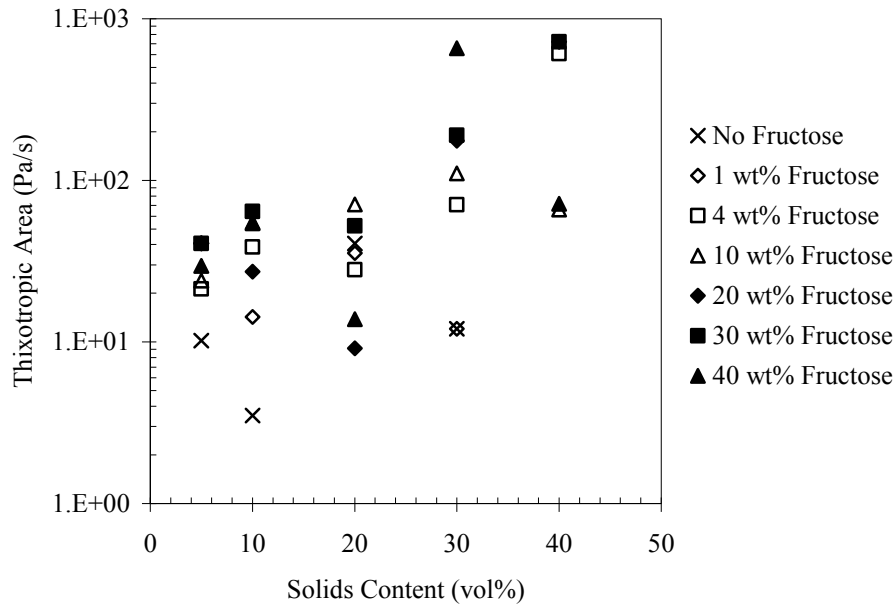


Figure 5.59. The variation of thixotropic loop areas of the nano alumina dispersions with solids content.

5.5.2. The Effect of Solids Content and Fructose on the Dynamic Shear Rheology of the Nano Alumina Dispersions

The stress amplitude dependence of nano alumina dispersions was investigated by applying stress sweep test and the stress sweep of 5 vol% nano alumina dispersion in 1 wt% fructose solution is given in Figure 5.60. The LVER of the dispersions with low solids content most likely located at smaller stresses than our instrument can measure. The LVER of the 5 and 10 vol% nano alumina dispersions in 20, 30, and 40 wt% fructose solution was probably ended before 0.001 Pa. Since the beginning and the end of the LVER can not be determined the stress value for frequency sweep test was chosen as 0.001 Pa. The LVER was more clearly seen when the solids content was increased to 20 vol% in 20 wt% fructose solution. When the fructose concentration was increased to 30 wt% the LVER shifted to lower shear stress range. However, further addition of fructose extended the LVER. The higher solids content extended the range of the LVER and increased the G' and G'' values. For most of the dispersions, the LVER ended before or after 0.01 Pa. Hence, the variation of the G' and G'' with solids content at 0.01 Pa is not given. The stress sweeps of the nano alumina dispersions are given in Appendix C-3.

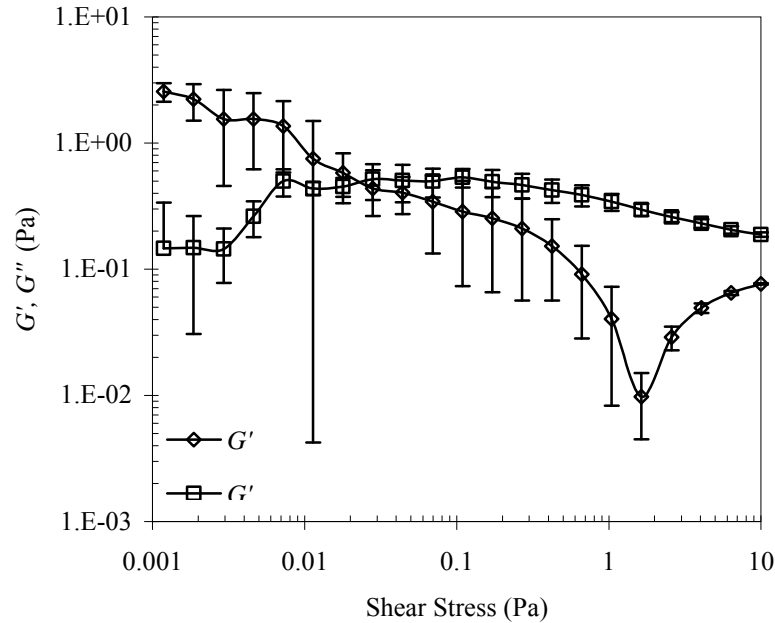


Figure 5.60. The stress sweep of 5 vol% nano alumina dispersion in 1 wt% fructose solution.

The frequency sweep of 5 vol% nano alumina dispersion is given in Figure 5.61. Similar to the behavior of submicron alumina dispersions, the nano alumina dispersions did not show glassy region which is observed at high frequencies regardless of solids content and fructose concentration. The G' rapidly decreased with decreasing angular frequency up to about 50 rad/s. While the G' and G'' continued to decrease after 50 rad/s for the dispersions with low solids content (5 and 10 vol%), the G' and G'' reached to a plateau for the dispersions with higher solids content. This means that a portion of the given energy was stored in the dispersion. The G' of the nano alumina dispersions with 40 vol% solids content without fructose and in fructose solutions of 1-20 wt% was not a function of angular frequency. This kind of behavior was attributed to a solid like behavior. The viscoelastic behavior became more angular frequency dependent as fructose content was increased. The frequency sweeps of the nano alumina dispersions are given in Appendix C-4.

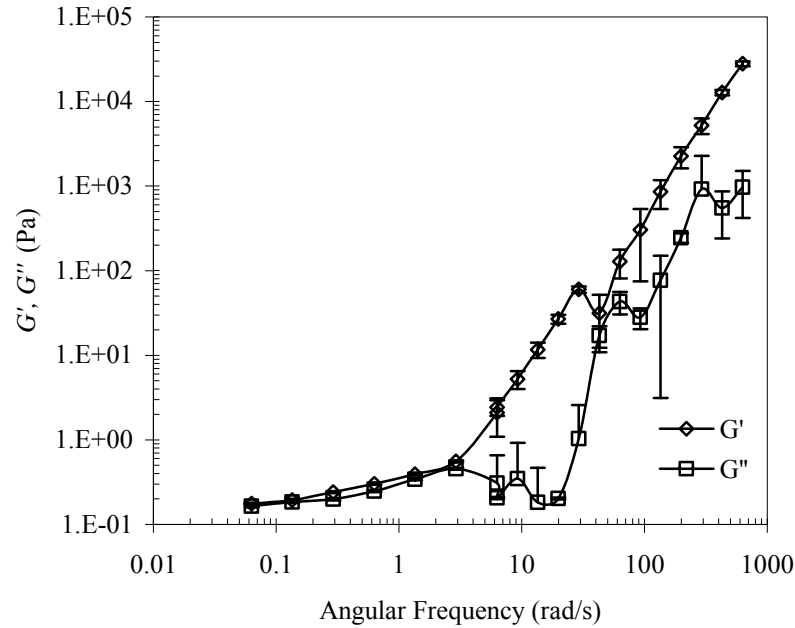


Figure 5.61. The frequency sweep of 5 vol% nano alumina dispersion in 1 wt% fructose solution.

The G' and G'' of nano alumina dispersions in fructose solutions at angular frequencies of 628, 6.28 and 0.0628 rad/s were collected to investigate the variations at rubbery-elastic, plateau and flow regions. The variations of the G' and G'' of the nano alumina dispersions in rubbery-elastic region with solids content is given in Figure 5.62. It was observed that the G' did not change with respect to solids content regardless of fructose concentration. The dispersions without fructose showed the same behavior and in the same order of magnitude. The G' of the dispersion having 5 vol% solids varied between 3.1×10^3 and 2.9×10^3 . The G'' of the dispersions was slightly increased with both solids content and fructose concentration. As the angular frequency was decreased to 6.28 rad/s, the G' became more sensitive to solids content and fructose concentration as seen in Figure 5.63. Both G' and G'' decreased about 10^4 times. The G' of the dispersion with 10 vol% nano alumina at an angular frequency of 628 rad/s was 2.9×10^4 which was decreased to 2.9 at 6.28 rad/s. The G' at 6.28 rad/s increased with solids content and fructose concentration. At high solids content, the G'' became higher with increasing fructose concentration. The variations of the G' and G'' values at an angular frequency of 0.0628 rad/s with solids content are given in Figure 5.64. The G' and G'' were exponentially increased as the solids content was increased. The effect of fructose

on both G' and G'' was significant. About a ten fold decrease in G' was observed by increasing the fructose concentration from 10 to 20 wt% for the dispersion having 20 vol% solids. The more significant decrease was observed when the fructose concentration was increased to 40 wt% and the G' was decreased from 3.9 to 0.013 Pa. Despite the decrease in the G' for the dispersions with 10, 20 30 vol% solids in 40 wt% fructose solutions, the G' was the lowest when the dispersion having 40 vol% solids was prepared in 10 wt% fructose solution. The same behavior was observed for the G'' values. This indicated that the 40 vol% dispersion did not store the given energy as much as it did in dispersions with higher fructose concentrations.

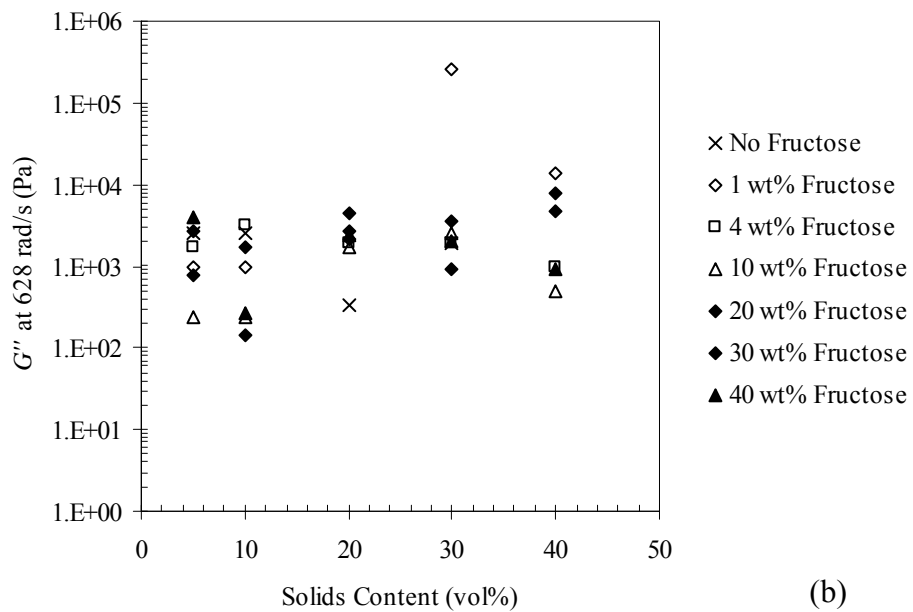
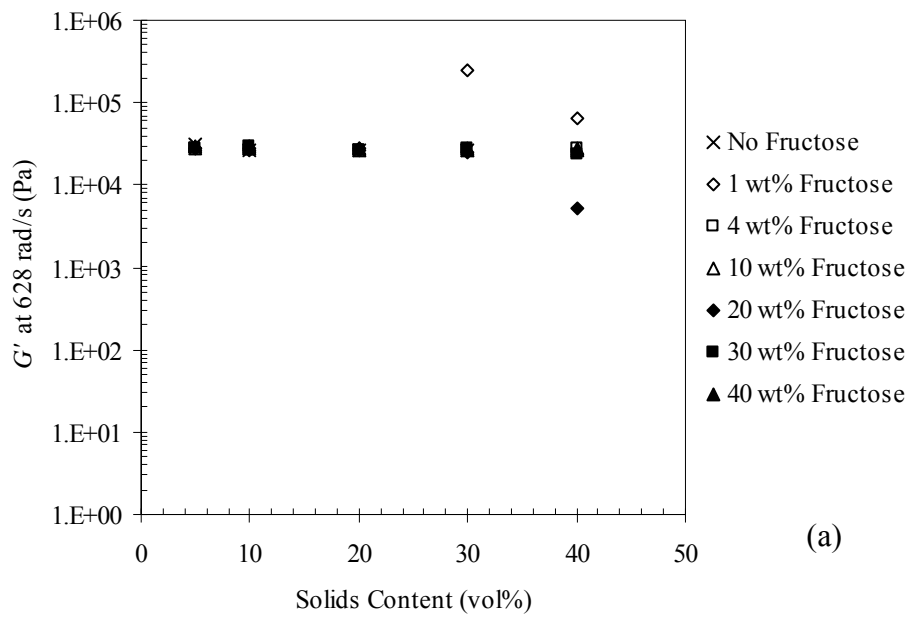


Figure 5.62. The variation of (a) G' and (b) G'' of the nano alumina dispersions at an angular frequency of 628 rad/s.

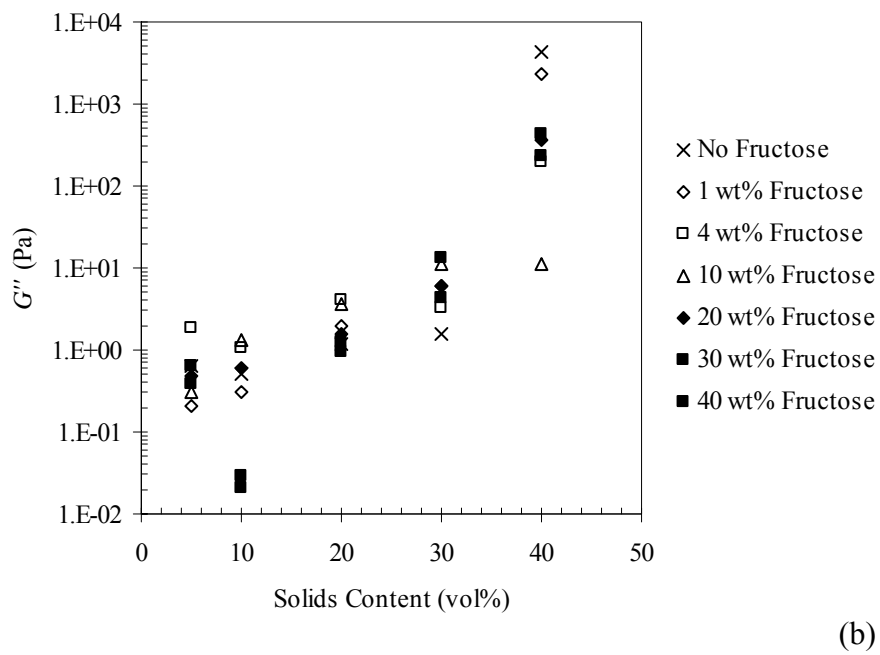
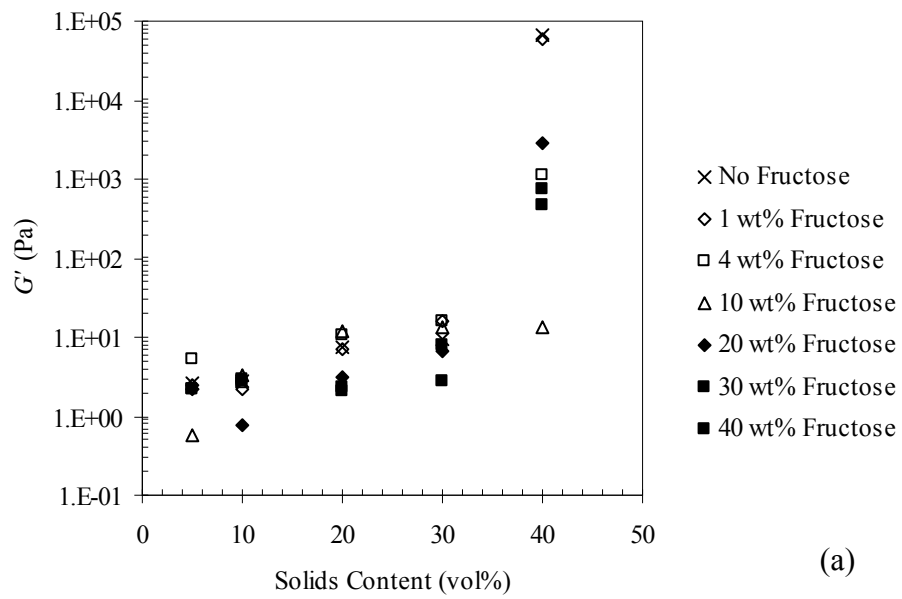


Figure 5.63. The variation of (a) G' and (b) G'' of the nano alumina dispersions at an angular frequency of 6.28 rad/s.

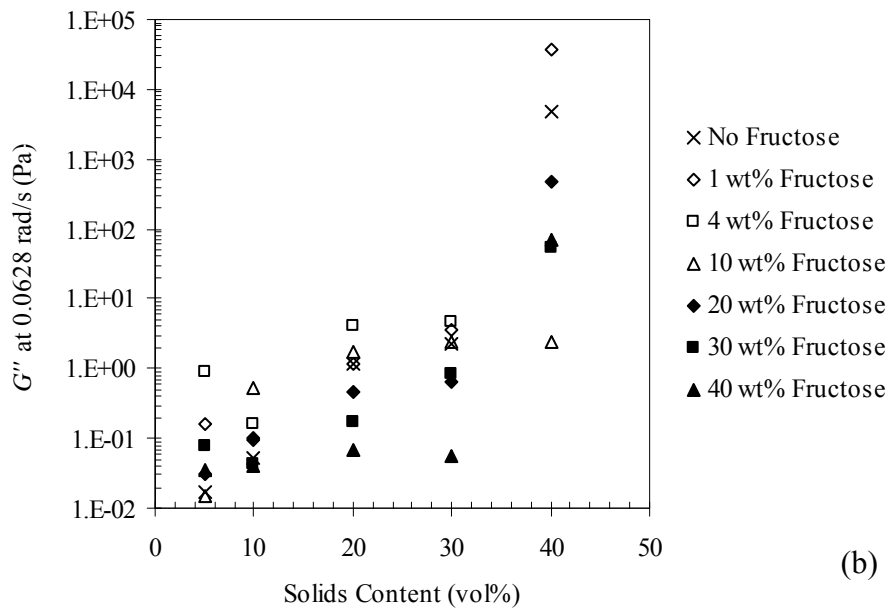
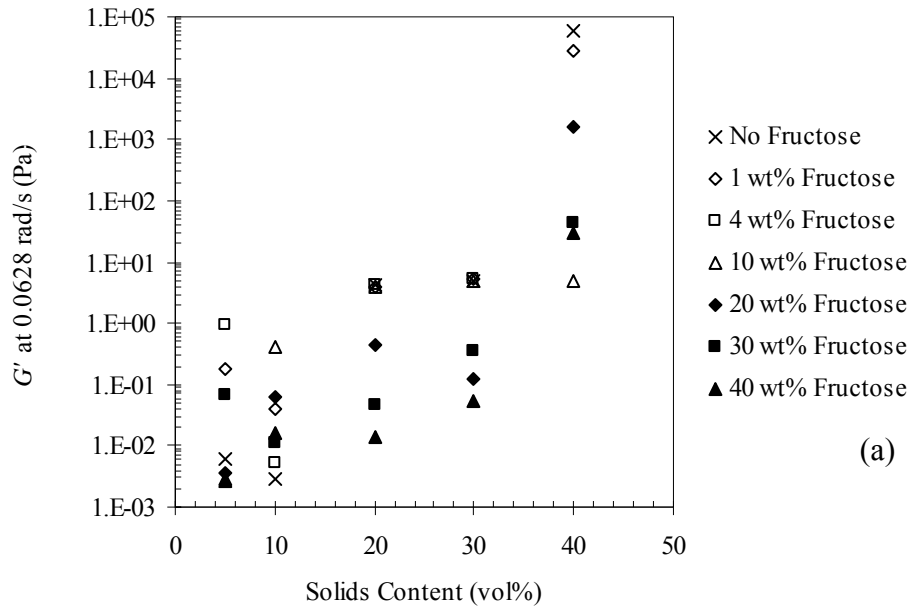


Figure 5.64. The variation of (a) G' and (b) G'' of the nano alumina dispersions at an angular frequency of 0.0628 rad/s.

5.6. The Rheological Behavior of Nano Titania Dispersions

The titania dispersions were prepared in two different ways: the first one is the same with the preparation of submicron and nano alumina dispersions. However, the same effect of fructose on nano titania powder was not observed. The time of mixing and repetition of ultrasonic treatment did not make any difference on the fluidity of the samples. It was thought that one reasonable way to enhance the flow properties of the nano titania dispersions was the adjustment of pH. The interactions of D-fructose and D- glucose with acids and bases were reviewed in a study on the chromatographic separation of fructose and glucose (Kuptsevich et al., 1987). It mentioned that monosaccharides (D-fructose and D-glucose) undergo isomeric interconversions under influence of bases. It was noted that sugar forms a complex with the aqueous alkaline solutions at high pH ($\text{pH} \geq 9$) which is followed by alkaline transformation and decomposition. The color of the fructose solution at pH of about 9 turned into yellow when the solution was kept at 80°C . The further increase in pH increased the intensity of color. The change in color was evaluated as decomposition of fructose. A fructose solution (10 wt%) was prepared by adjusting the pH at about 3 to observe any changes of color. The color of the solution was clear and same as the fructose solution without pH adjustment. The pH adjustment of the nano titania dispersions was done in acidic medium in order to keep the stability of fructose. The stability of the nano titania dispersion with respect to pH was evaluated by regarding the zeta potential curve of nano titania. The zeta potential of titania was highest at pH of 3 and IEP of titania was at a pH of 5. As a result, the pH of the nano titania dispersions was adjusted about to $\text{pH} = 3$.

It was observed that the color of the nano titania dispersions without pH adjustment turned into yellowish brown during mixing. When the sample was avoided from exposure to light, the change in color was postponed. The dispersions with pH adjustment were also avoided from exposure of light and the color of the dispersions were light yellow and remained the same for at least one week. Then, the color turned into yellow but not brown.

5.6.1. The Effect of Solids Content and Fructose Concentration on the Steady Shear Rheology of the Nano Titania Dispersions

The steady shear rheology of nano titania dispersions in fructose solutions were observed. The flow curve of 5 vol% nano titania dispersion in 10 wt% fructose solution without pH adjustment is given in Figure 5.65. The dispersion with high solids contents (higher than 20 vol%) were paste like and did not have enough fluidity to observe steady shear rheological measurements. The flow curves of the dispersions are given in Appendix D.1.

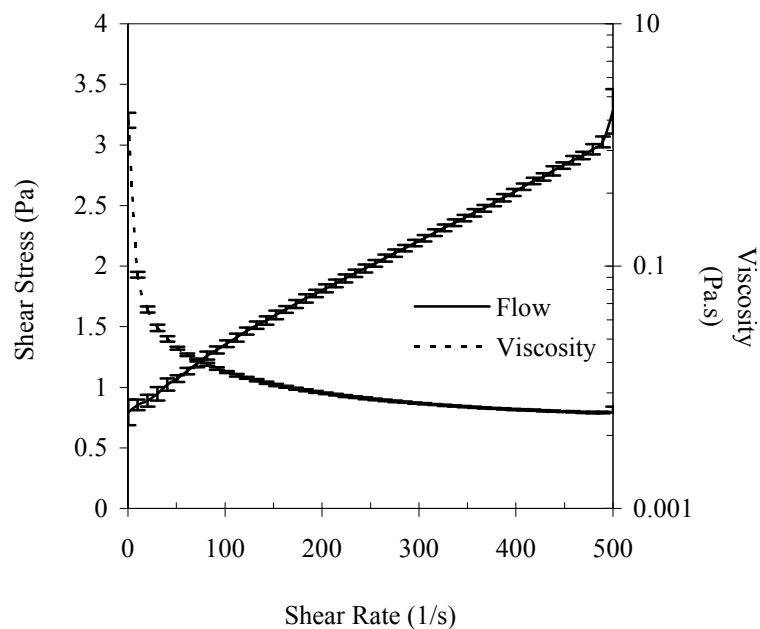


Figure 5.65. The flow curve of 5 vol% nano titania dispersion in 10 wt% fructose solution without pH adjustment.

The flow curves of nano titania dispersions were fitted to the HB model. The parameters of the model for the dispersions without and with pH adjustment were tabulated in Table 5.6 and Table 5.7, respectively. The correlation coefficients of the flow curves varied between 0.97 and 0.99 for the dispersions without pH regulation and between 0.81 and 0.99 for pH regulated dispersions. The flow index of the dispersion having 10 vol% nano titania in 10 wt% fructose was higher than 1. This indicated shear thickening behavior. However, the flow curve of the dispersion did not show a shear thickening behavior. Therefore, Newtonian and Bingham plastic models were applied. It

was determined that the flow behavior of the dispersion also fitted to Newtonian model (η was 0.0165 Pa.s) and Bingham plastic model (τ_o and η were 0.0042 Pa and 0.01652 Pa.s, respectively). The correlation coefficients of the models were both 0.999. The viscosities of the dispersion at 50 1/s and 100 1/s were 0.0202 and 0.0185 Pa.s. The viscosities of the dispersion determined from the models were comparable. The flow behavior of the dispersion can be also explained by these models.

The flow indexes of the pH adjusted dispersions with 5 vol% solids without fructose and in 4 wt% fructose solution were bigger than 1. The flow curve of pH adjusted dispersion with 5 vol% solids was also explained by Bingham plastic model. The correlation coefficient and the yield stress of the model were 0.99 and 0.28 Pa. The values were very similar when they were determined from HB model. The viscosity determined from Bingham plastic model was 0.0034 Pa.s which was much lower than viscosity determined at shear rates of 50 1/s and 100 1/s. The flow curve of the dispersion with 5 vol% solids in 4 wt% fructose solution were checked for its fit to both Newtonian and Bingham plastic models. The correlation coefficient of both Newtonian and Bingham plastic models was 0.98. The viscosity determined from Newtonian model was 0.0028 Pa.s. The yield stress and the viscosity determined from Bingham plastic model was 0.023 Pa and 0.0027 Pa.s, respectively. The viscosities determined from the models were very close to the viscosity value at a shear rate of 100 1/s but the viscosity at a shear rate of 50 1/s was 0.0032 Pa.s. Newtonian and Bingham plastic models did not explain the flow curve of the dispersion better than HB model.

Table 5.6. The model parameters of Herschel-Bulkley Model ($\tau = \tau_o + K\dot{\gamma}^n$) calculated for the nano titania dispersions without pH adjustment.

wt% of fructose solution	vol% solids content	τ_o (Pa)	K	n	R^2
No Fructose	5	5.33	0.34	0.52	0.99
	10	0.73	0.13	0.62	0.99
	20	3.83	0.74	0.56	0.98
10	5	0.69	0.01	0.86	0.99
	10	10.21	0.78	0.45	0.99
	20	71.02	83.93	0.25	0.98
20	5	0.62	0.07	0.65	0.99
	10	9.96	0.51	0.53	0.99
	20	27.16	150	0.19	0.95
30	5	0.56	0.02	0.84	0.99
	10	7.15	0.12	0.73	0.99
	20	25.41	86.48	0.19	0.97
40	5	0.47	0.05	0.78	0.99
	10	0.09	0.13	1.04	0.99
	20	39.15	50.98	0.35	0.99

Table 5.7. The model parameters of Herschel-Bulkley Model ($\tau = \tau_o + K\dot{\gamma}^n$) calculated for the nano titania dispersions with pH adjustment.

wt% of fructose solution	vol% solids content	τ_o (Pa)	K	n	R^2
~pH3	5	0.29	0.003	1.02	0.99
	10	18.83	96.39	0.22	0.81
	20	0.14	0.34	0.60	0.99
1 and ~pH3	5	1.43	0.01	0.88	0.99
	20	30.04	77.88	0.25	0.96
4 and ~pH3	5	0.08	0.0002	1.48	0.99
	10	25.24	0.09	0.38	0.98
	20	26.12	121.9	0.23	0.98
10 and ~pH3	5	0.28	0.08	0.57	0.99
	10	3.17	3.72	0.23	0.98
	20	34.48	235.8	0.19	0.94
20 and ~pH3	5	0.365	0.063	0.63	0.99
	10	45.06	158.6	0.26	0.94
	20	36.37	67.95	0.20	0.99
30 and ~pH3	5	0.45	0.02	0.84	0.99
	10	4.57	0.38	0.53	0.99
	20	28.03	0.84	0.59	0.99
40 and ~pH3	5	2.33	0.07	0.76	0.99
	10	1.85	0.05	0.79	0.99

The variations of the HB yield stress of the dispersions without and with pH adjustment are given in Figure 5.66. The HB yield stresses were decreased by pH adjustment. The addition of fructose to the dispersions without pH adjustments increased the HB yield stresses. However, the preparation of the dispersions in 40 wt% fructose solution resulted in comparable yield stresses without fructose and with pH adjustment. The addition of fructose to the pH adjusted nano titania dispersions increased the HB yield stress of the dispersions. The variation of the HB yield stress with fructose concentration was more significant.

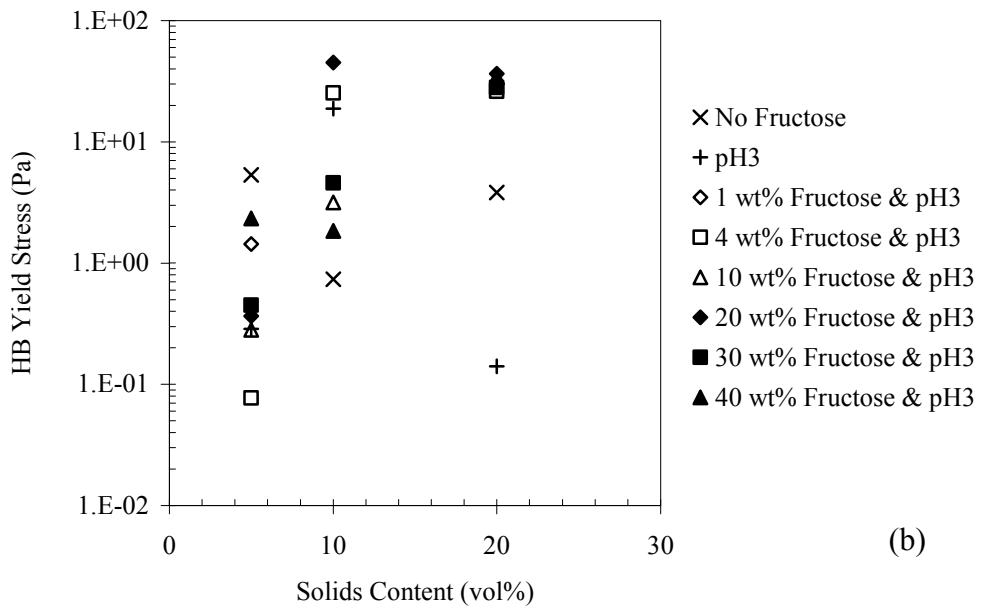
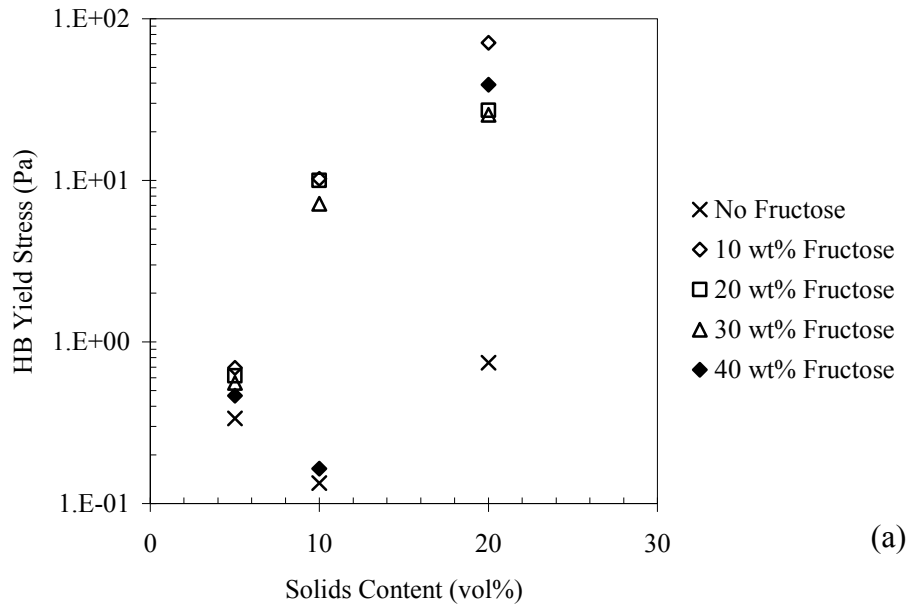


Figure 5.66. The variation of HB yield stress of the nano titania dispersions with solids content in semi-logarithmic distribution (a) without pH adjustment and (b) with pH adjustment.

The effect of the presence of fructose on the consistency coefficient of the dispersions with and without pH adjustment however was not similar to its effect on the

HB yield stress. While the K values increased with solids content, the addition of fructose decreased the consistency coefficient of the dispersions. The K values were smallest for the dispersions without pH adjustment which were prepared in 40 wt% fructose solution except for the dispersion with 5 vol% solids (Figure 5.67.a). After pH adjustment, the relation of the K values with solids content and fructose concentration became complicated (Figure 5.67.b). The pH adjustment itself decreased the K . This indicated that the particle interactions under shear were very sensitive to pH of the nano titania dispersions. The addition of fructose led to smaller K values. High fructose concentrations (30 and 40 wt%) resulted in smallest K values except the dispersions with 5 vol% solids. The fructose concentrations higher than 10 wt% fructose increased the particle interactions under shear.

The variation of the flow index of the nano titania dispersions is given in Figure 5.68. The flow index became smaller at higher solids content. This showed the increasing tendency of shear thinning. The addition of fructose without pH adjustment decreased the n , but when the fructose concentration was 40 wt%, the flow index became higher. The pH adjustment of the dispersions resulted in smaller n values. The dispersions in 30 and 40 wt% fructose concentrations had much higher n values than the dispersions with only pH adjustment.

The effect of solids content on the viscosity of nano titania dispersions were significant. The presence of the fructose decreased the viscosity of the dispersion regardless of the pH adjustment (Figure 5.69). The dispersion with 5 vol% solids had a viscosity of 0.16 Pa.s at a shear rate of 50 1/s which was 10 times higher than the equivalent nano alumina dispersion. The viscosities of the dispersion in 10 wt% and 40 wt% fructose solution without pH adjustment were 0.021 and 0.034 Pa.s, respectively. The variation in the viscosity of the dispersions with pH adjustment with respect to solids content is given in Figure 5.70. The adjustment of pH itself decreased the viscosity to 0.01 Pa.s. Further increase in fructose concentration resulted in higher viscosities for the pH adjusted dispersions. Similar results were observed for higher solids contents.

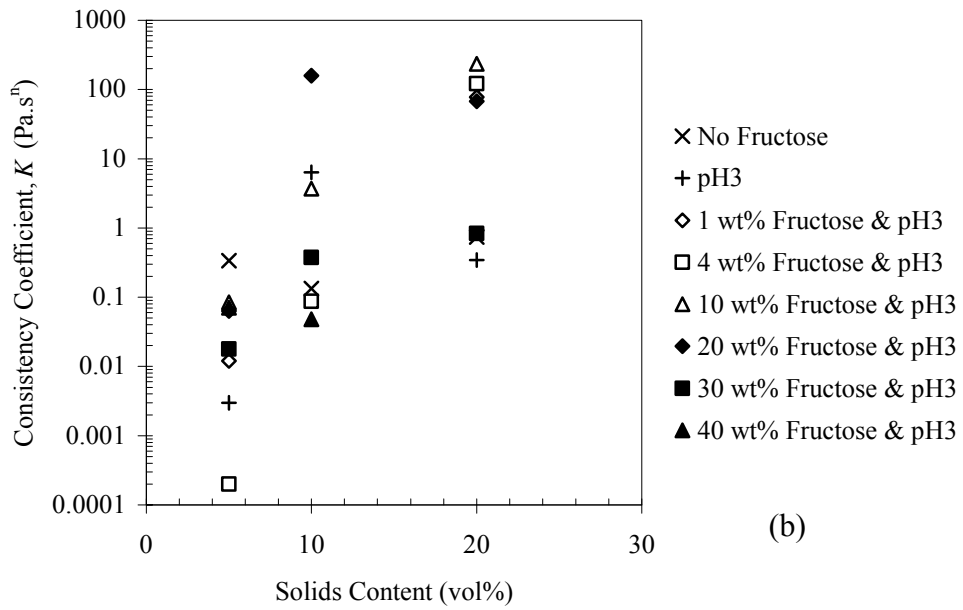
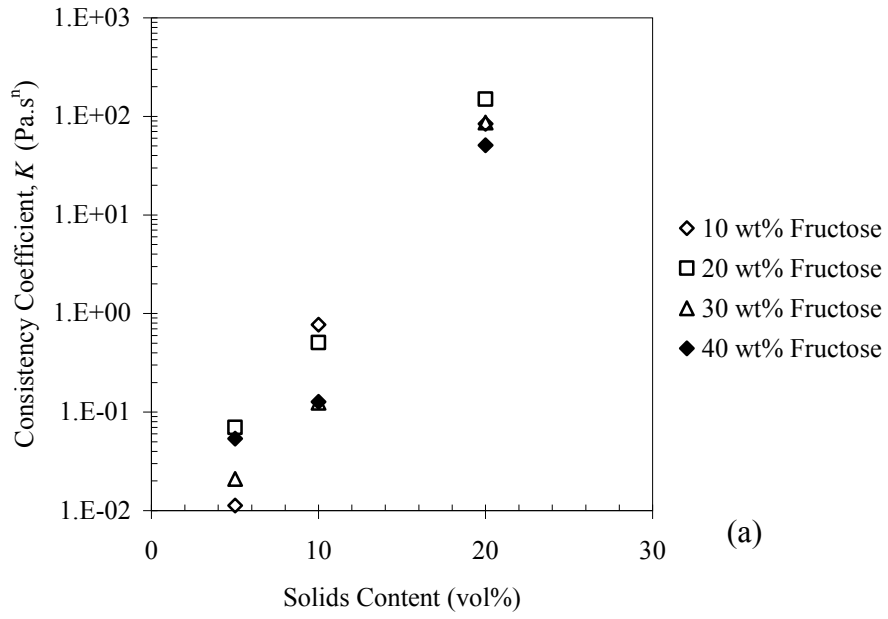


Figure 5.67. The variation of consistency coefficient, K , of the nano titania dispersions with solids content in semi-logarithmic distribution (a) without pH adjustment and (b) with pH adjustment.

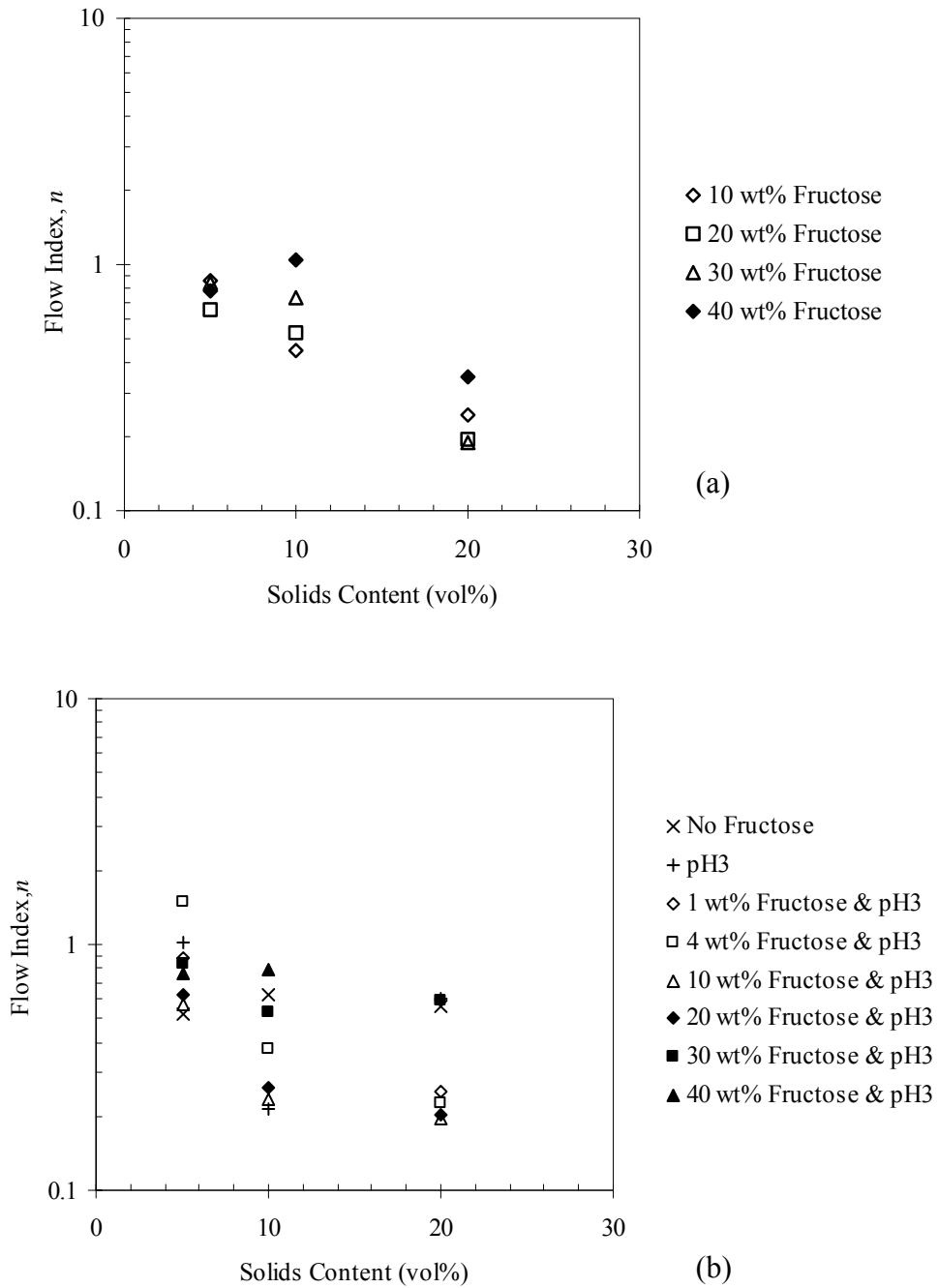


Figure 5.68. The variation of flow index, n , of the nano titania dispersions with solids content in semi-logarithmic distribution (a) without pH adjustment and (b) with pH adjustment.

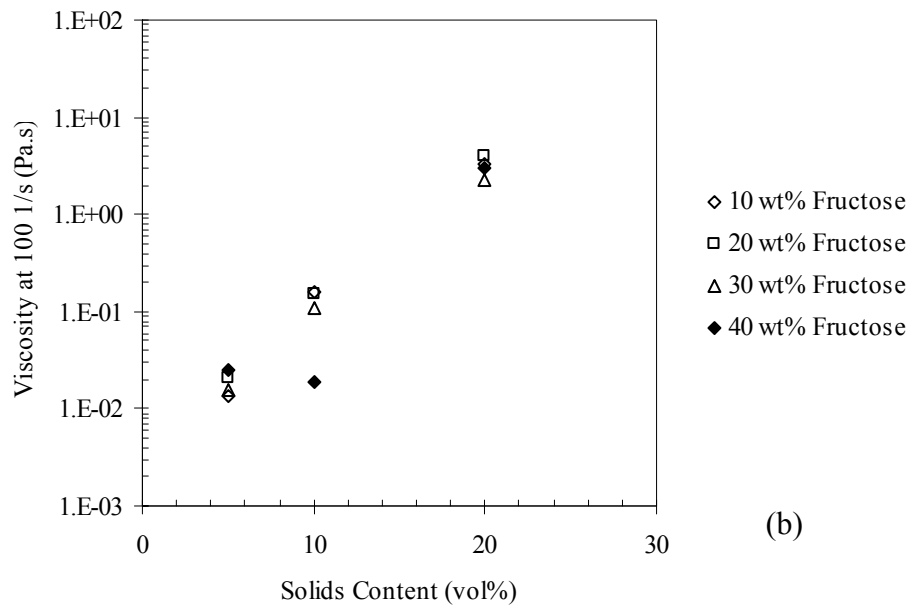
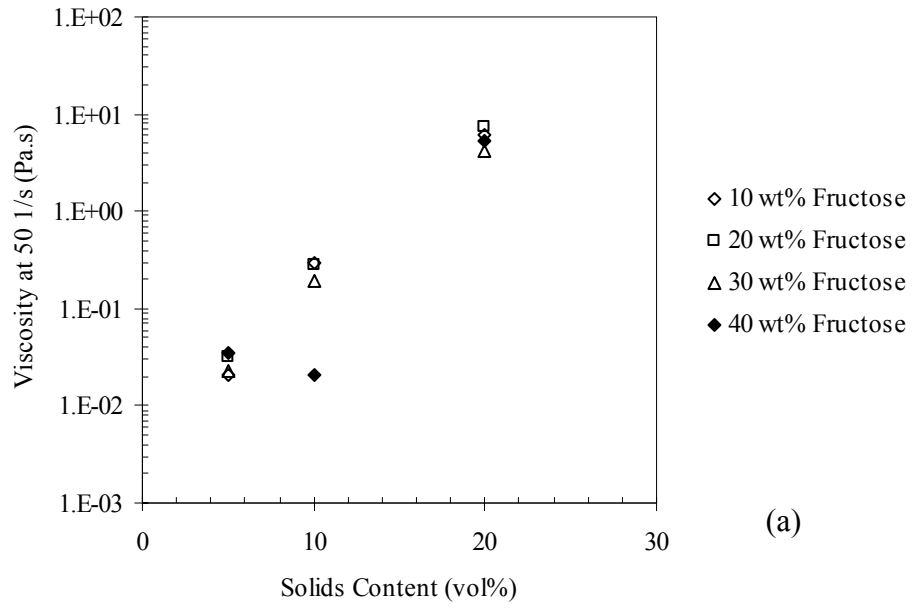


Figure 5.69. The viscosities of the nano titania dispersions at a shear rate of (a) 50 1/s and (b) 100 1/s.

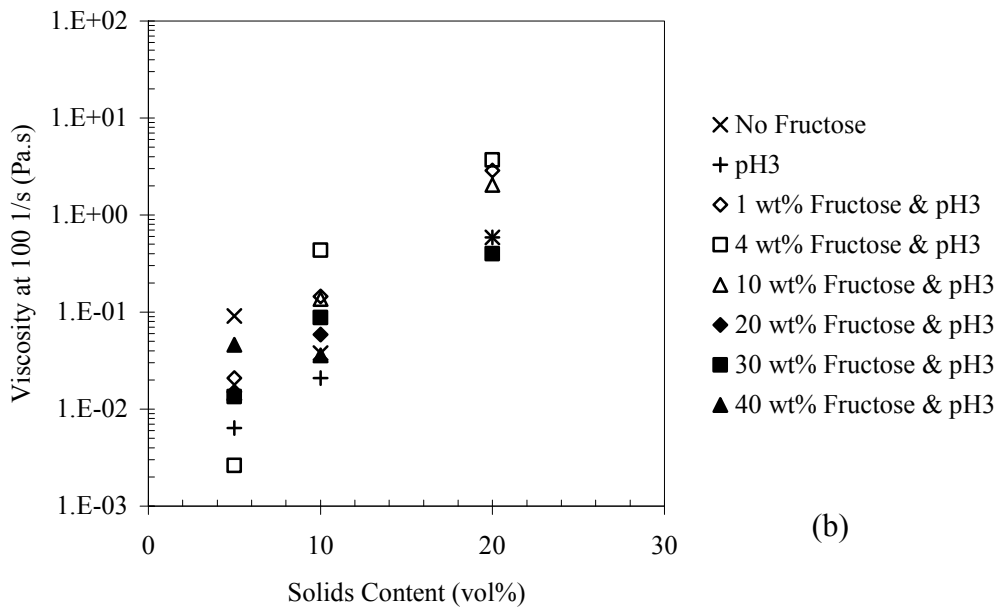
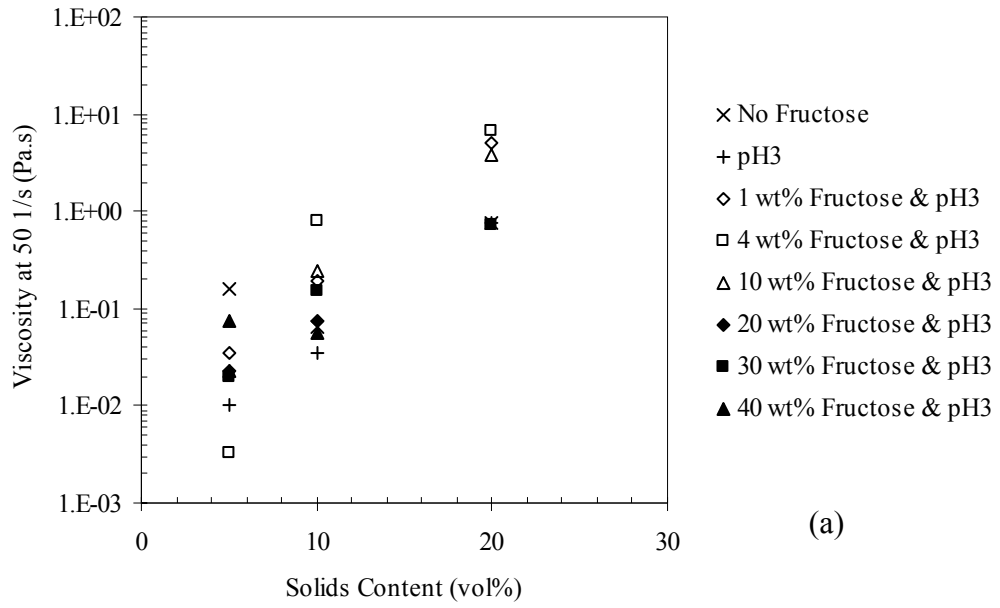


Figure 5.70. The viscosities of the nano titania dispersions at a shear rate of (a) 50 1/s and (b) 100 1/s with pH adjustment.

The thixotropic behavior of 5 vol% nano titania in 10 wt% fructose solution without pH adjustment is given in Figure 5.71. The thixotropic behavior of the nano

titania dispersions are given in Appendix D-2. The variations in thixotropic area of the dispersions with and without pH adjustment with respect to solids content are given in Figure 5.72. The thixotropic area increased with increasing solids content. The fructose concentration necessary to maintain the lowest and/or the highest thixotropic area of the nano titania dispersions was different as the solids content was changed. This fact was also observed for the pH adjusted nano titania dispersions. The thixotropic areas without fructose and pH adjustment of the dispersions with different solids content were almost the same. The addition of fructose to the dispersions with 5 vol% solids decreased the thixotropic area. However, the thixotropic area became higher at higher solids contents with increasing fructose concentrations. The variation of thixotropic area with fructose concentration was more significant. Time dependency of the dispersions increased with the presence of relatively low levels of fructose at high solids contents, but decreased as the fructose concentration was increased. The opposite behavior was observed for the dispersions having 5 vol% solids.

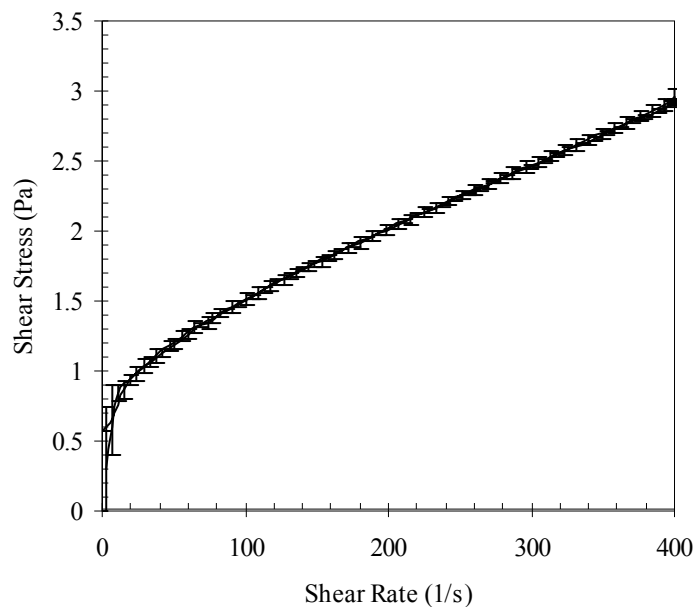


Figure 5.71. The thixotropic behavior of 5 vol% nano titania in 10 wt% fructose solution without pH adjustment.

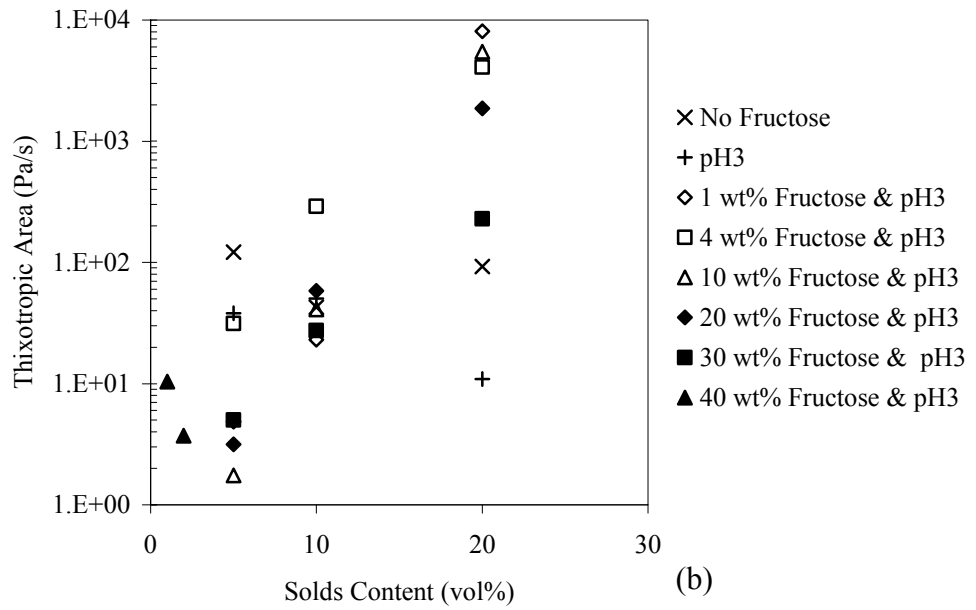
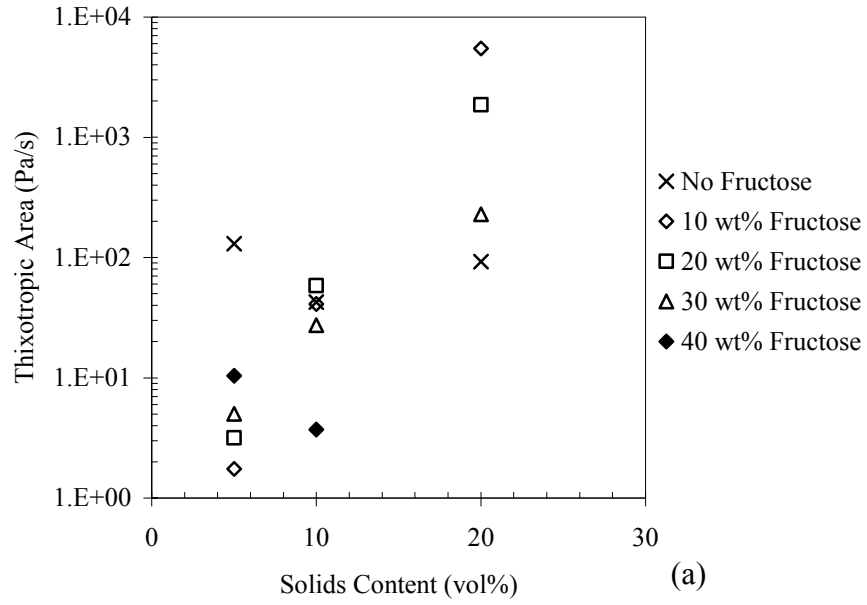


Figure 5.72. The variation of thixotropic loop areas of the nano titania dispersions with solids content (a) without pH adjustment and (b) with pH adjustment.

5.6.2. The Effect of Solids Content and Fructose on the Dynamic Shear Rheology of the Nano Titania Dispersions

The stress sweeps of pH adjusted nano titania dispersions in 1 wt% fructose solution is given in Figure 5.73. Similar to the nano alumina dispersions, the LVER of the dispersions with low solids content most likely located at smaller stresses than our instrument can measure. Generally, the LVER of the dispersions with 5 vol% solids with or without pH adjustment in fructose solutions ended at 0.001 Pa. Since the beginning and the end of the LVER can not be determined, the stress value for frequency sweep test was chosen as 0.001 Pa. The pH adjustment and the presence of fructose had significant effect on the extent of the LVER of the nano titania dispersions. The addition of fructose to the dispersions without pH adjustment made the LVER shorter and lower the shear stress where the LVER is located. The adjustment of the pH did not change the extent of LVER. The addition of fructose to the pH adjusted nano titania dispersions decreased both G' and G'' in LVER. Most of the nano titania dispersions did not have the LVER at 0.01 Pa. Hence the variation of the G' and G'' with solids content at 0.01 Pa was not given. The stress sweeps of the nano titania dispersions with and without pH adjustment and fructose content are given in Appendix D-3.

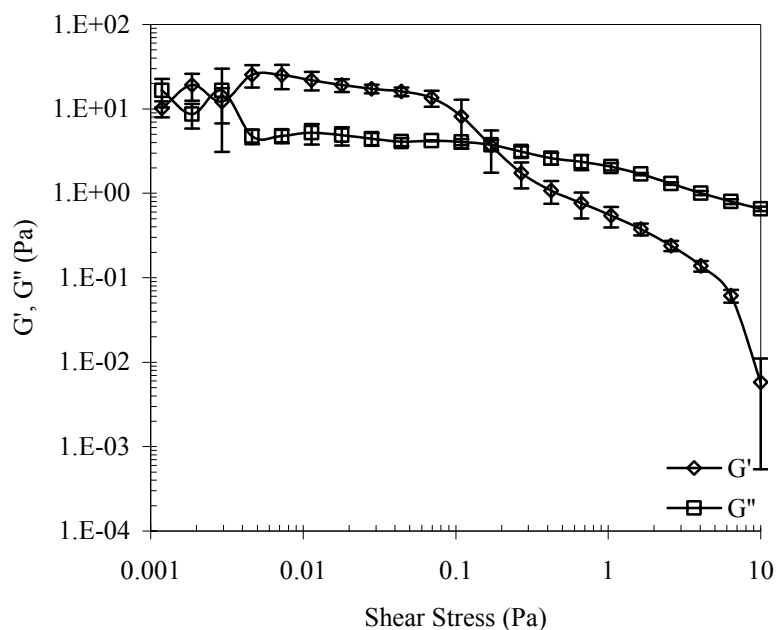


Figure 5.73. The stress sweeps of pH adjusted nano titania dispersions in 1 wt% fructose solution.

The frequency sweep of pH adjusted nano titania dispersion in 1 wt% fructose solution is given in Figure 5.74. Similar to the behavior of submicron and nano alumina dispersions, the nano titania dispersions did not show glassy region which is observed at high frequencies regardless of solids content and fructose concentration. Both G' and G'' decreased rapidly upto 100 rad/s and then reached to plateau region for the dispersion without pH adjustment and fructose. The addition of fructose affected the frequency dependency of the dispersions. The G' and G'' of the dispersions in 10 and 20 wt% fructose solutions decreased continuously in applied range of frequency. Further increase in fructose made the plateau region appear again but the G' and G'' values were at least ten times lower. The pH adjustment of the nano titania dispersions decreased the G' and G'' but the behavior were similar to the dispersions without fructose. The addition of fructose to the pH adjusted dispersions decreased initially the G' and G'' but the dispersions became frequency independent later which indicated solid like behavior. This effect was observed for fructose concentrations higher than 20 wt% for the dispersions with 10 and 20 vol% solids. The frequency sweeps of the nano titania dispersions are given in Appendix D-4.

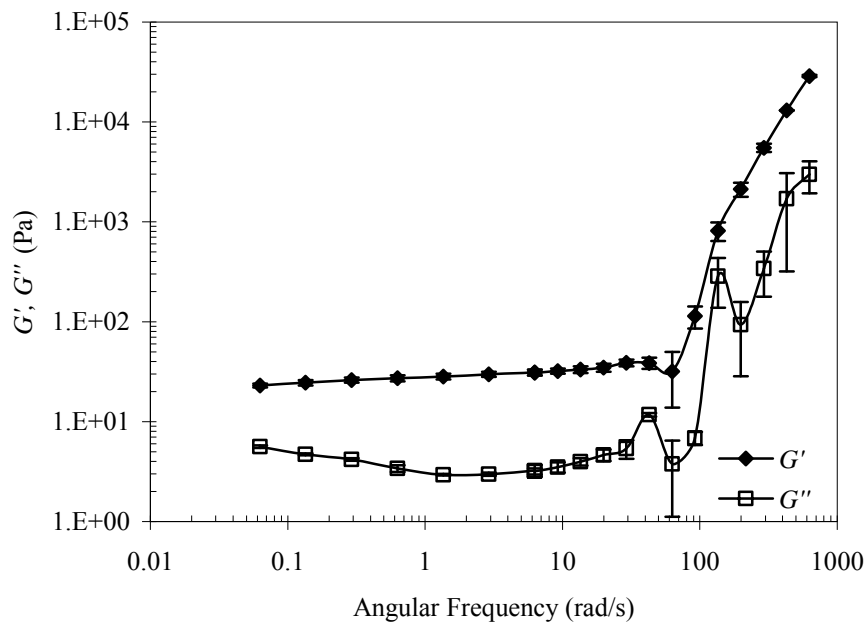


Figure 5.74. The frequency sweep of pH adjusted nano titania dispersion in 1 wt% fructose solution.

The G' and G'' of nano titania dispersions in fructose solutions with and without pH adjustment at angular frequencies of 628, 6.28 and 0.0628 rad/s were collected to observe the variations at rubbery-elastic, plateau and flow regions. The variations of G' and G'' of the dispersions in fructose solutions at an angular frequency of 628 rad/s are given in Figure 5.75. The G' was slightly decreased from 2.8×10^4 to 1.4×10^3 Pa by increasing solids content. Similar to the behavior of G' and G'' of submicron alumina and nano alumina, the G' was not significantly effected by the increasing fructose concentration. When the angular frequency was lowered to 6.28 rad/s, the G' was lowered by increasing fructose concentration (from 31 to 6.28 Pa) and increased by increasing solids content (from 31 to 450 Pa). The viscous part of the dispersions was not a function of fructose concentration. The variations of G' and G'' with solids content in plateau region are given in Figure 5.76. Further decrease in angular frequency to 0.0628 rad/s made the G' and G'' lower in magnitude. Both G' and G'' varied with solids content and fructose concentration in flow region and the fructose concentration for the lowest or highest G' and G'' were different for different solids contents. The variations of G' and G'' of the nano titania dispersions with fructose at 0.0628 rad/s are given in Figure 5.77. The dependency of G' and G'' on frequency was different from the equivalent dispersions of submicron alumina and nano alumina.

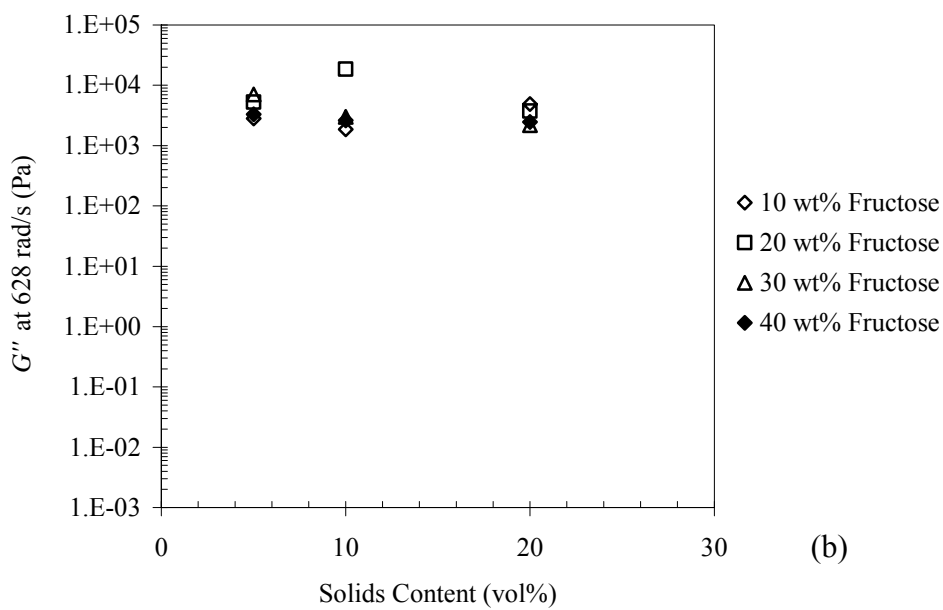
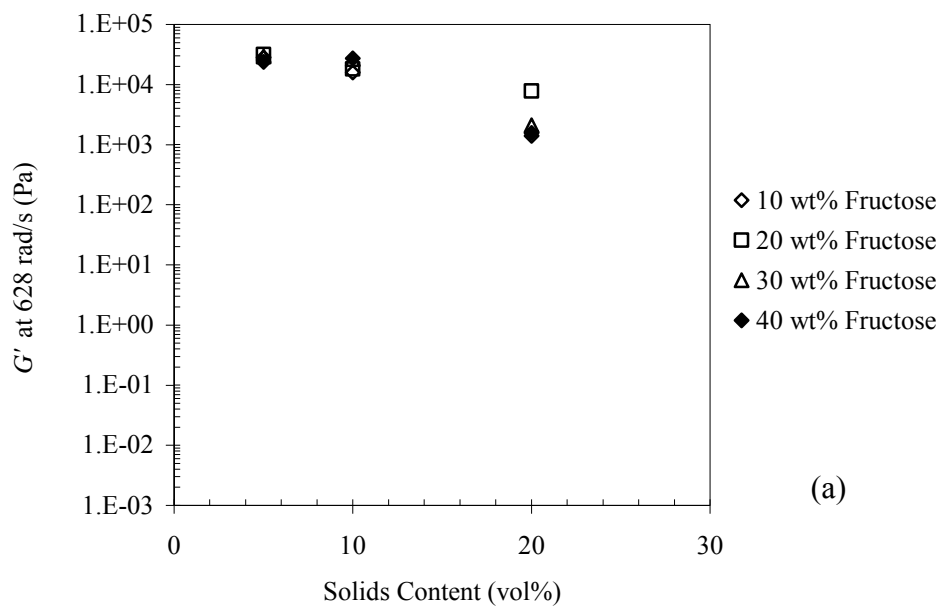


Figure 5.75. The variation of (a) G' and (b) G'' of the nano titania dispersions without pH adjustment at a angular frequency of 628 rad/s.

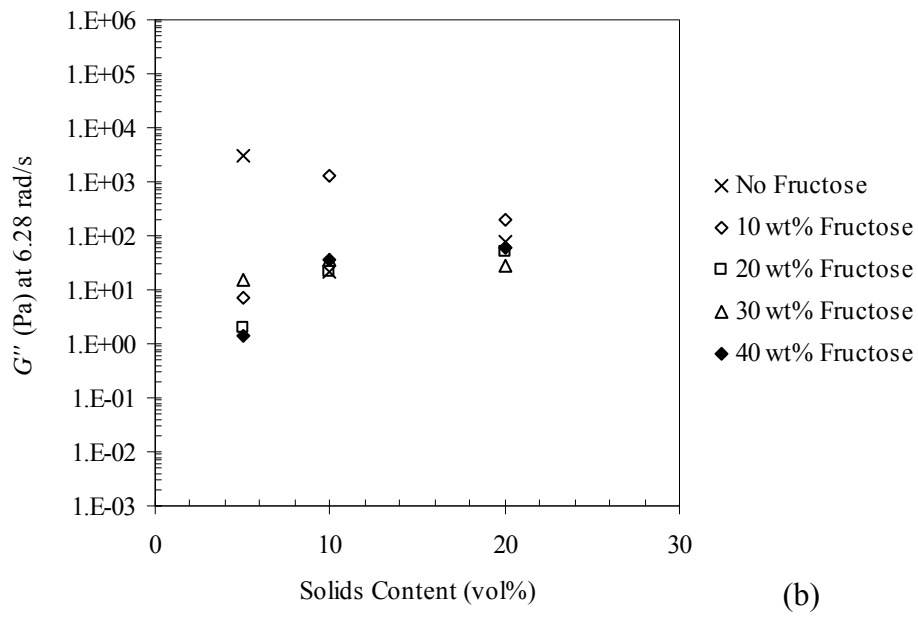
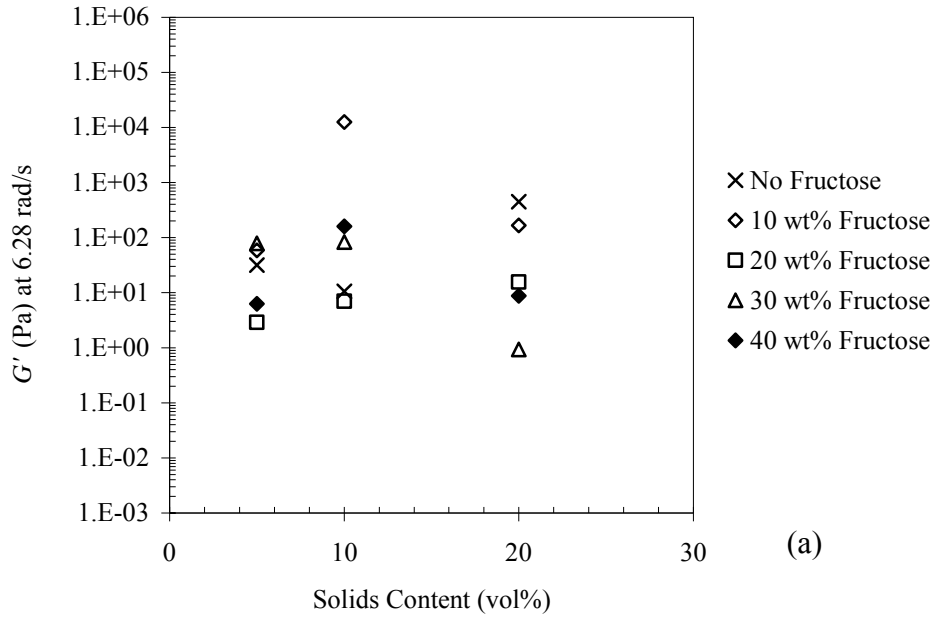


Figure 5.76. The variation of (a) G' and (b) G'' of the nano titania dispersions without pH adjustment at a angular frequency of 6.28 rad/s.

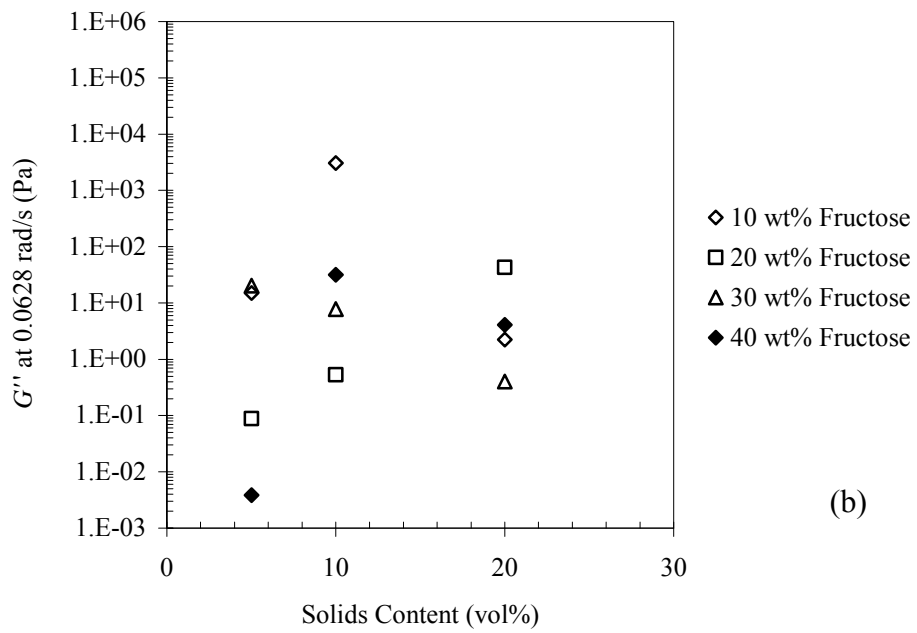
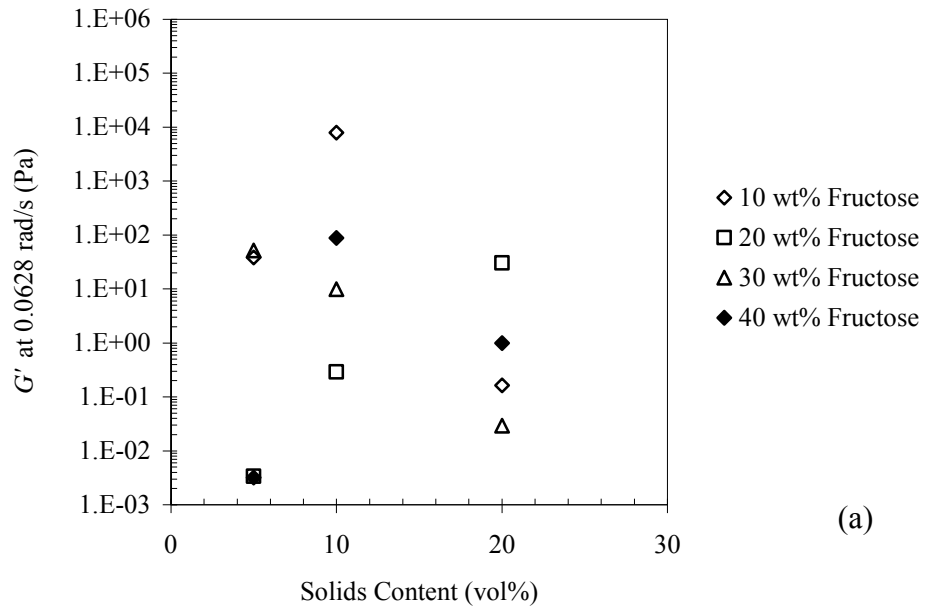


Figure 5.77. The variation of (a) G' and (b) G'' of the nano titania dispersions without pH adjustment at a angular frequency of 0.0628 rad/s.

The frequency dependency of the pH adjusted nano titania dispersions with solids content and fructose concentration were determined by observing the variations of the G' and G'' at rubbery-elastic, plateau and flow regions. The G' in rubbery-elastic region was almost the same order of magnitude with the dispersion without pH adjustment. The G'' was more sensitive to fructose concentration. However, the fructose concentration for the highest G'' differed with solids content. The variations of the G' and G'' with solids content at an angular frequency of 628 rad/s are given in Figure 5.78. The contribution of pH adjustment was more significant at lower angular frequencies. When the angular frequency was reduced to 6.28 rad/s, the G' decreased from 2.6×10^4 to 1.41 Pa. Both G' and G'' varied with solids content and fructose concentration but the relation between them can not be established (Figure 5.79). The G'' of the dispersions in 10 wt% fructose solution increased with solids content. For other dispersions, the G'' was first increased and then decreased as the solids content was increased. Lowering the angular frequency to 0.0628 rad/s made the G' and G'' smaller (Figure 5.80). Similar to the behavior at 6.28 rad/s, the G' and G'' were varied with solids content and fructose concentration but the relations of G' and G'' with solids content and fructose concentration was not understood.

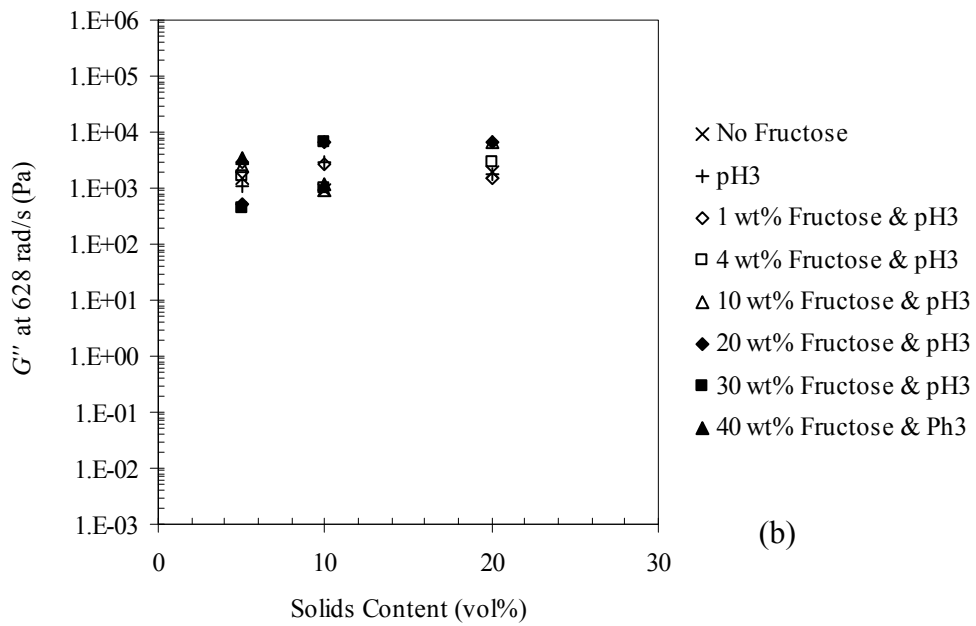
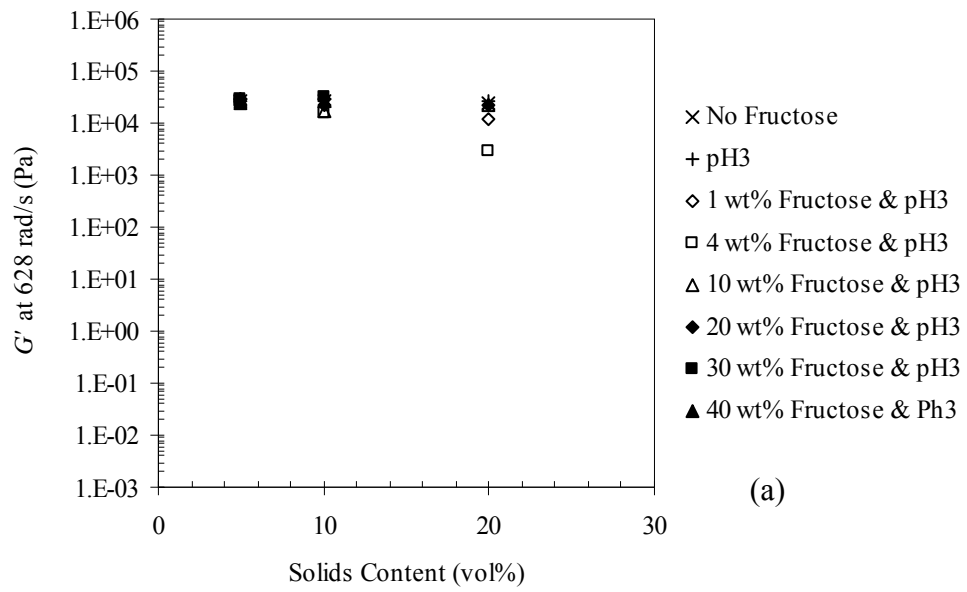


Figure 5.78. The variation of (a) G' and (b) G'' of the nano titania dispersions with pH adjustment at a angular frequency of 628 rad/s.

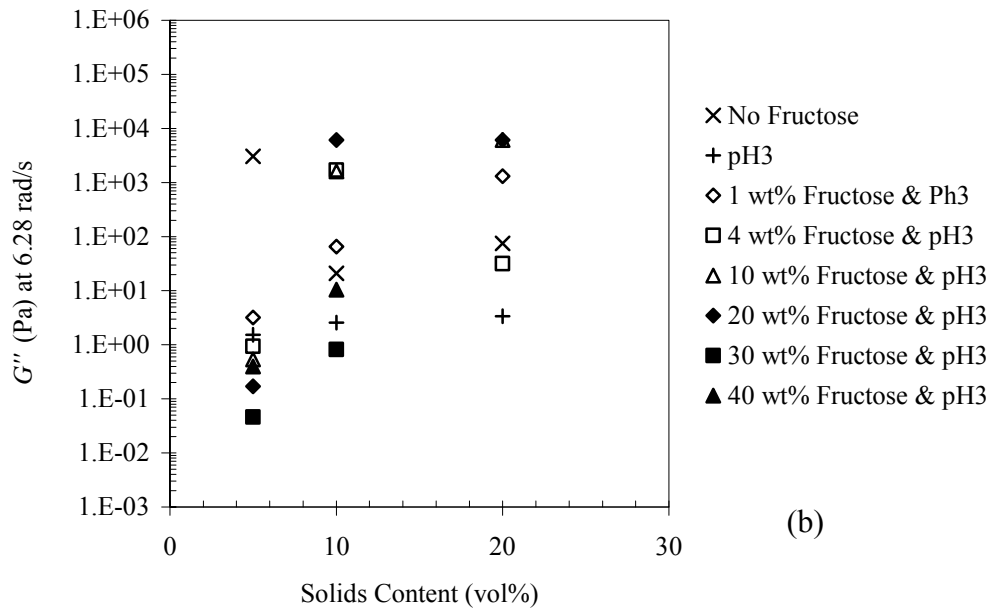
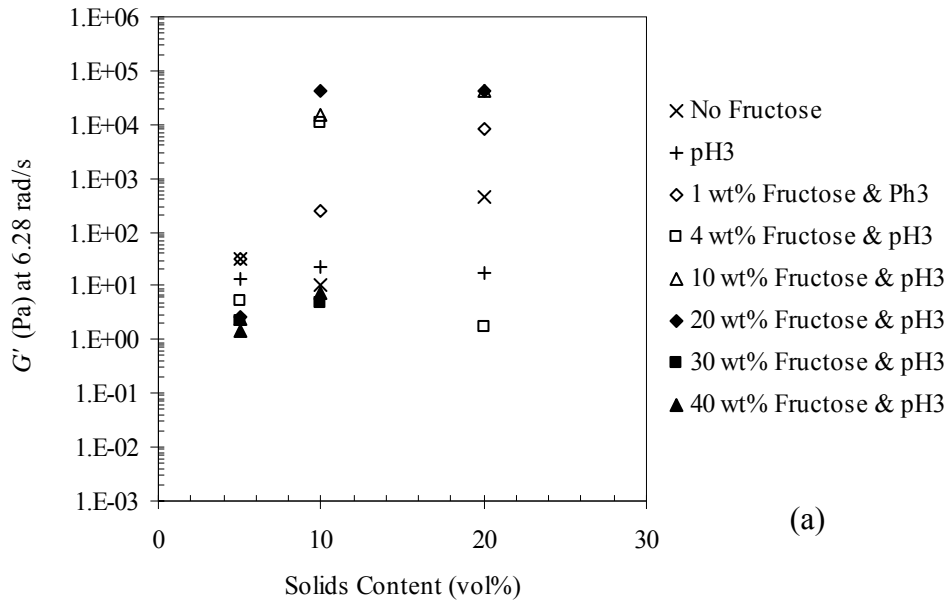


Figure 5.79. The variation of (a) G' and (b) G'' of the nano titania dispersions with pH adjustment at a angular frequency of 6.28 rad/s.

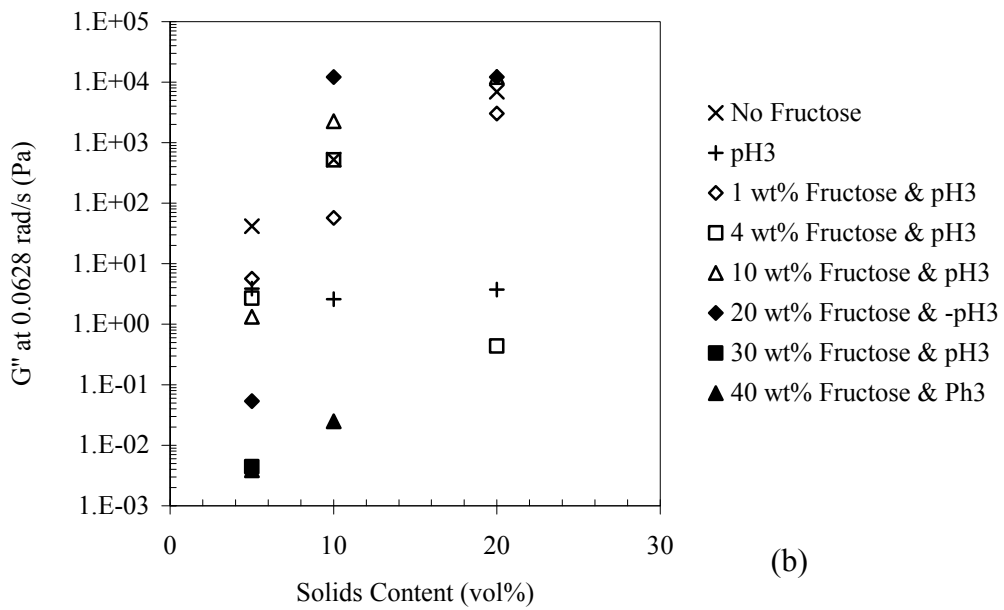
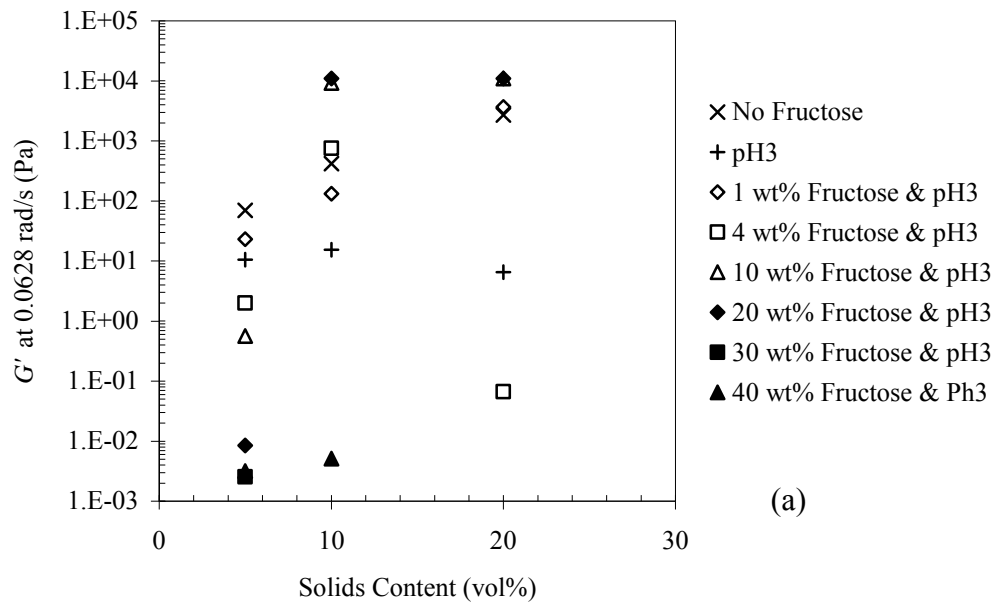


Figure 5.80. The variation of (a) G' and (b) G'' of the nano titania dispersions with pH adjustment at a angular frequency of 0.0628 rad/s.

5.7. The Comparison of Dynamic Shear Rheological Behavior of Submicron Alumina, Nano Alumina and Nano Titania Dispersions

The dependency of angular frequency of the submicron alumina, nano alumina, and nano titania dispersions were compared considering the available surface in 1 mL dispersion. The comparison was done at constant solids content of 20 vol%. The variation of the G'/G'' ratio was done for higher solids content, because higher solids content of nano titania dispersions can not be prepared. The available surface area was calculated by multiplying the required amount of powder and its surface area. The available surface area of submicron alumina, nano alumina and nano titania for 20 vol% dispersions were 9.8, 25.7 and 105.8 m² in 1 mL dispersion. It was noted that the nano titania dispersions without pH adjustment were taken into account in this part. The G' and G'' values at 628, 6.28 and 0.0628 rad/s were collected and the ratio of G' over G'' was plotted with respect to the available surface area. The ratio of G'/G'' gives the idea about how dominant the elastic part of the dispersion over the viscous part is. Lewis (2000) was stated that if the $G'/G'' \gg 1$ the dispersion has solid like behavior. If the ratio was about 1, the dispersion has gel like structure. The liquid like behavior is observed when the ratio is below 1.

Figure 5.81 shows the variation of G'/G'' ratio of the dispersions having 20 vol% solids in rubbery–elastic region. It was observed that the G'/G'' ratio was in order of 10 in magnitude for submicron alumina and nano alumina dispersions and dependent on the fructose concentration. It was expected that the G'/G'' ratio will be much greater than 10 for nano titania dispersions. However, the ratio varied between 13.09 to 0.25. This indicated that the dispersions had gel like behavior in 20 and 30 wt% fructose solutions and liquid like behavior in 10 and 40 wt% fructose solutions. It was believed that the nano titania particles was not dispersed as it was supposed to be and were agglomerated. Despite of high surface area, the particles in the dispersions were much higher than 11 nm which is the particle/crystal size determined from surface area and XRD data.

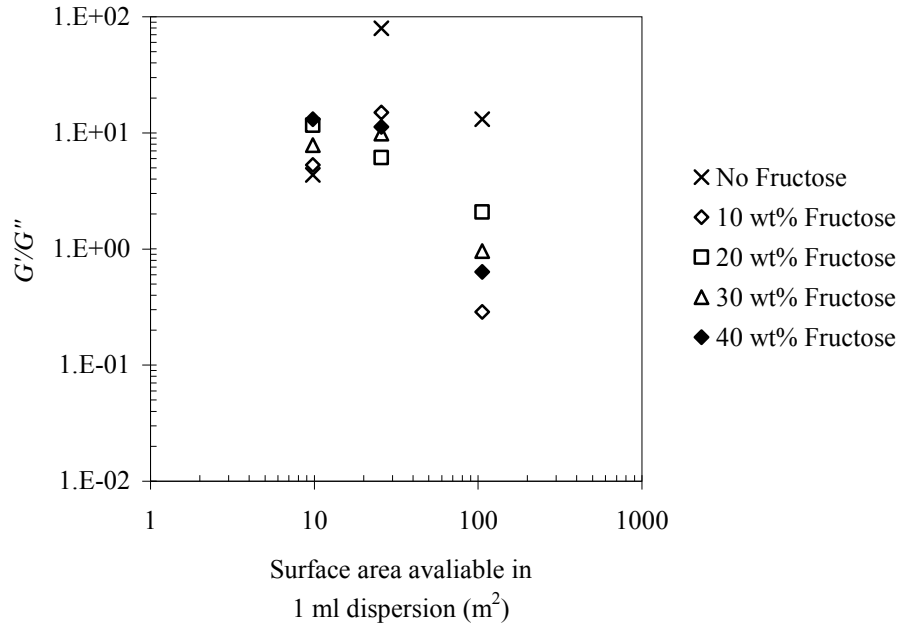


Figure 5.81. The variation of the G'/G'' of the dispersions at 628 rad/s with surface area available in 1 mL dispersion.

The variation of G'/G'' ratio of the dispersions at 6.28 rad/s with surface area is given in Figure 5.82. The G'/G'' ratio was lower in plateau region than it was in rubbery elastic region as it was supposed to be. The ratio of submicron alumina dispersions were almost constant regardless the fructose concentration and was below 10. The variation of G'/G'' ratio lowered and became fructose concentration dependent as the surface area was higher.

Figure 5.83 shows the variation of G'/G'' ratio in flow region. The G'/G'' ratio of the submicron alumina, nano alumina and nano titania in flow region was lower than as it was in plateau region and dependent on fructose concentration. The higher the surface area available in 1 mL dispersion, the lower the G'/G'' ratio was. However, the reverse was expected. The G'/G'' ratio was lower than 1 for nano titania dispersion which means that the G'' was dominant over G' in flow region. Both submicron alumina and nano alumina dispersions had the lowest G'/G'' ratio in 40w wt% fructose solution. However, the fructose concentration was needed to be 10 or 30 wt% fructose solutions to obtain the lowest G'/G'' ratio.

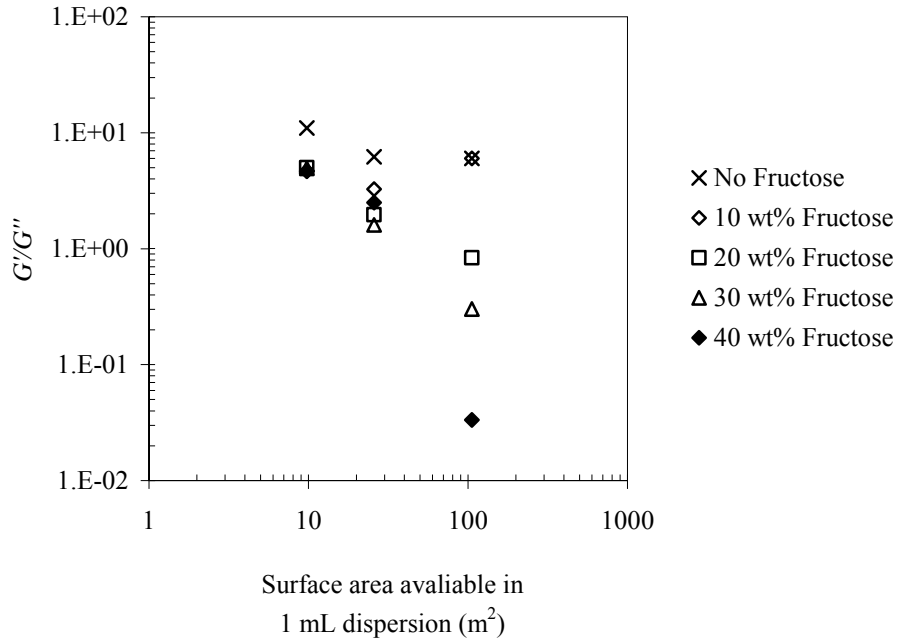


Figure 5.82. The variation of the G'/G'' of the dispersions at 6.28 rad/s with surface area available in 1 mL dispersion.

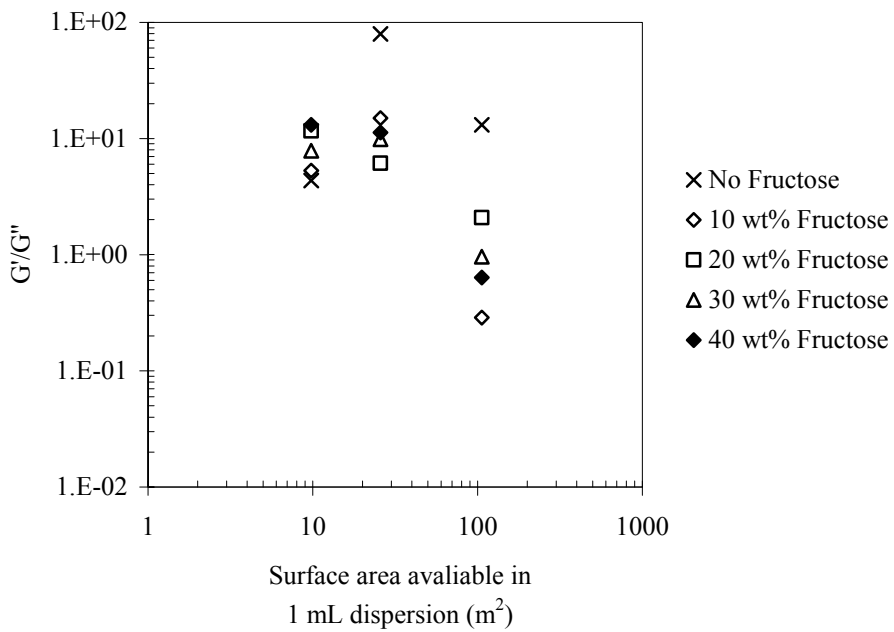


Figure 5.83. The variation of the G'/G'' of the dispersions at 0.0628 rad/s with surface area available in 1 mL dispersion.

5.8. The Densification Behavior of Freeze Dried Submicron Alumina and Nano Alumina Dispersions

The submicron and nano alumina dispersions were consolidated by freeze drying. The details of the consolidation are given in experimental section. The densities of the green and sintered bodies are tabulated in Table 5.8. DP defines the dry pressed bodies and AC and NA represent freeze dried submicron alumina and nano alumina in the related Table. For example, AC40-4 defines the freeze dried sample prepared from a dispersion having 40 vol% solids in 4 wt% fructose solution.

Table 5.8. The green body and sintered body densities of submicron and nano alumina.

Submicron Alumina	Before Sintering	After Sintering (1400°C)	Nano Alumina	Before Sintering	After Sintering (1200°C)
DP1	1.59	2.85	DP1	1.4	2.38
DP2	1.97	3.64	DP2	1.53	2.04
DP3	1.87	3.56	DP3	1.53	2.05
AC40-4	1.07	2.55	NA30-4	0.98	1.29
AC40-10	1.12	2.64	NA30-4	1.08	1.3
AC40-10	1.09	2.62	NA30-10	1.11	1.48

The nano titania dispersions were not freeze dried because the dispersions with high solids content can not be prepared. The nano alumina dispersions at high solids content did not have enough fluidity. The densities of the freeze dried bodies were much lower than the dry pressed bodies. Having insufficient solids content and expansion of water during freezing may lead to porous structure. The bodies prepared from nano alumina were much more porous than the bodies of submicron alumina.

The shrinkage curves of submicron alumina, nano alumina and nano titania are given in Figure 5.74. The powders were dry pressed at 37.5 MPa using a stainless steel die having a diameter of 10 mm. The alumina pellets start sintering at about 1100°C and the rate of densification of the nano alumina pellet is higher than submicron pellet at 1200°C which may be attributed both to phase transformation and particle size

difference. The nano titania densification occurs in two stages. The first stage in the 500-850°C range may most likely be controlled by the 7-10 nm crystallites in the structure and account for the 18% of the total 26% shrinkage at 1200°C. The second stage is due to the sintering of densified submicron original agglomerates of the powder primary crystallites.

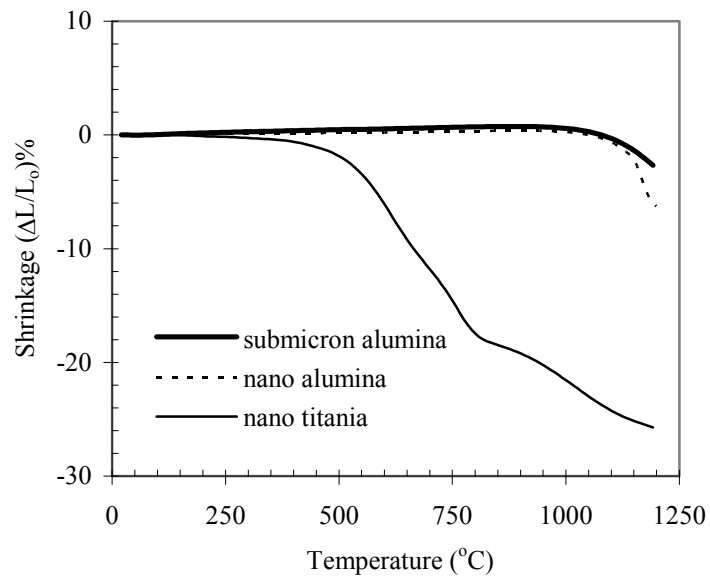


Figure 5.84. The shrinkage curves of submicron alumina, nano alumina and nano titania powders.

CHAPTER 6

CONCLUSIONS

This thesis focused on the determination of the effect of particle size and a non-electrolyte dispersant on the rheological behavior of the nano and submicron ceramic powder dispersions. The effects of the volume fraction, the particle size and the concentration of D-fructose, a monosaccharide, on steady and dynamic shear rheology of ceramic powder dispersions were investigated.

It was experienced that drying of samples during rheological measurements and the shear history of the dispersions led to inaccurate rheological measurements. The drying problem of the dispersions was eliminated by using two different protection tools. The steady shear experiments were done by placing a hemispherical cup on top of the measurement space and a wet tissue to provide a saturated environment. The dynamic measurements were conducted by using a non-volatile oil around the sample to prevent its contact with the atmosphere. The samples were presheared before rheological measurements to eliminate the dependency of the rheological behavior on shear history. The dispersions were presheared at different shear rates and hold undisturbed for different periods of time before dynamic measurements. After preshearing the storage modulus (G') was observed with respect to shear stress. The G' value was much closer to the value without preshear and the variation of the G' became smaller. However, preshearing at high shear rates resulted in particle migration in the dispersions and the particle migration can be visually observed especially for the dispersions with low solids content. The preshearing was applied at low and constant shear stress instead of shear rate for longer times to eliminate shear history dependency. Preshearing at a shear stress of 0.1 Pa for 30 s and holding undisturbed for 300 s was chosen based on the measurements on stress sweep tests.

The rheological behavior of the fructose solutions were determined by steady shear rheological techniques. The flow behaviors of the fructose solutions were Newtonian and the viscosity of the solution was between 8×10^{-4} and 28.12 Pa.s. The effect of fructose on the rheology of the dispersions was significantly affected by the surface characteristics. The point of zero charge of nano titania was much lower than

the submicron and nano alumina powders. The pH adjustment of the dispersions regulated the rheological behavior. The steady shear rheological experiments showed that the solids content and fructose concentration have significant effects on the rheological behavior of the dispersions.

The HB yield stress, the consistency coefficient, and thixotropic area increased with solids content and decreased by fructose addition regardless of the particle size. Increasing solids content and fructose concentration made the dispersion more shear thinning. The particle-particle interactions under shear were lower with respect to the dispersions without fructose. When the particle size approaches to nano, the viscosity increased significantly and became time dependent for dispersions with solid contents higher than 20 vol%.

The HB yield stress of submicron alumina suspensions with 40 vol% solids decreased approximately 10 times (12.81 to 1.40 Pa) by increasing the fructose concentration from 4 to 10 wt%. The HB yield stress of nano alumina dispersion with 40 vol% solids decreased from 46.40 to 30.90 Pa by increasing the fructose concentration from 20 to 40 wt%. The HB yield stress of nano titania dispersions without pH adjustment decreased from 72.02 to 25.41 by increasing the fructose concentration from 10 to 30 wt%. The HB yield stress became lower with pH adjustment. The excess amount of fructose increased the HB yield stress and viscosity. The viscosity of the dispersions increased at all shear rates with the increasing solids content which was more pronounced in nano powder dispersions. Viscosity reduction was observed as the fructose concentration was increased. The submicron alumina dispersions had their lowest viscosity in the 10 wt% fructose solution. It was observed that the higher the fructose concentration at low solids content the higher the viscosity was. The higher the fructose concentration at high solids contents, the lower the viscosity became.

The dynamic shear rheological experiments showed that the LVER of the dispersions at low solids content was relatively short. The LVER extended with increasing the solids content and fructose concentration. For all dispersions, the G' was dominant over G'' in the LVER. Similarly, G' was dominant over the G'' in frequency sweep tests regardless of the solids content, particle size and fructose concentration. This indicated that the dispersions had gel-like properties. There was no glassy region in the frequency sweep tests for all dispersions. It was observed that the G' of the

dispersions rapidly decreased from 628 rad/s to 100 rad/s for submicron alumina dispersions. However, the decrease of G' continued up to 50 rad/s for nano alumina dispersions. Both G' and G'' decreased rapidly as the angular frequency decreased to 100 rad/s and then, reached to the plateau region for the nano titania dispersion without pH adjustment and fructose addition. Further increase in fructose concentration made the dispersions frequency dependent. However, the pH adjustment for the nano titania dispersions caused the dispersions to be frequency independent again.

The energy stored by the solid part of the dispersions was observed by evaluating the G' values at 0.0628 rad/s. The energy stored in the dispersion was increased with increasing fructose concentration indicating the contribution of free fructose to G' . At 40 vol% solids content, the G' was independent of angular frequency. This behavior was attributed to a solid like and more elastic structure for both submicron and nano alumina dispersions. The G' and G'' of nano titania dispersions without and with pH adjustment varied with solids content and fructose concentration but their relation was not clearly established yet.

The ratio of G'/G'' decreased as the angular frequency was decreased regardless of the surface area available in 1 mL dispersion and fructose concentration. The G'/G'' ratio of nano titania dispersions was lower than those of submicron alumina and nano alumina dispersions. This is an indication of the fact that nano titania powder was not well dispersed and were partially agglomerated.

As a conclusion, nonionic small molecules like fructose can be used to regulate rheological behavior of ceramic powder dispersions. These environmentally friendly molecules may become new dispersants for the ceramic powder dispersions.

This research demonstrated that particle size, solids content and dispersant concentration have important influence on the rheological behavior. The relations between the valuable rheological information reported in this work and the dispersion microstructure (particle-particle/liquid medium) have not been elucidated yet. The determination of rheological behavior of these and other ceramic powders with different surface characteristics may help on the development of a better understanding of the dispersion microstructure.

The determination of the relation between the dispersion structure and green/fired body microstructure may help to improve the colloidal processing of the

ceramics. Freeze drying can be used for the consolidation of ceramic powder dispersions.

Recent studies on the rheological behavior of the dispersions showed that shear thickening dispersions can be evaluated as new emerging applications such as dampers, armors, brakes in vehicles, sensors, micro-fluidic materials, vibration and/or noise reduction in vehicles, prosthetic limbs. Understanding the mechanism of the transition in this rheological behavior of the dispersions is the key for these applications of powder dispersions. The determination of the rheological behavior of the dispersions in organic media needs to be investigated for understanding of particle-particle and particle/medium interactions.

REFERENCES

- Amari, T. (1997). Non-linear Viscoelastic Properties of concentrated Suspensions. *Progress in Organic Coatings*, 31, 11-19.
- Aoki, Y., Hatano, A., and Watanabe, H. (2003). Rheology of carbon black dispersions. I. Three types of viscoelastic behavior. *Rheologica Acta*, 42, 209-216.
- Bae, H. S., Lee, M. K., Kim, W. W., and Rhee, C. K., (2003). Dispersion properties of TiO₂ nano-powder synthesized by homogeneous precipitation process at low temperatures. *Colloids and Surfaces A: Physicochemical Engineering Aspects* 220, 169-177
- Barnes, H. A. (1997). Thixotropy-A review. *Journal of Non-Newtonian Fluid Mechanics*, 70, 1-33.
- Barnes, H. A. (1989). *An introduction to rheology*. Amsterdam:Elsevier Publishing.
- Boger, D. V., and Murthy, A.V.R. (1969). Normal stress measurements and evaporation effects on the weissenberg rheogoniometer. *Transaction of the Society of Rheology*, 13(3), 405-408.
- Bowen, P., and Carry, C., Luxembourg, D., Hofmann, H. (2005). Colloidal processing and sintering of nano-sized transition aluminas. *Powder Technology*, 157, 100-107.
- Bowen, P., Carrys, C. (2002). From powders to sintered pieces: forming, transformations and sintering of nanostructured ceramic oxides. *Powder Technology*, 128, 248-255.
- Brummer, R. (2006). *Rheology essentials of cosmetic and food emulsions*. Berlin: Springer Laboratory.
- Cesarano, J. III, and Aksay, I. (1988). Processing of highly concentrated aqueous α -alumina dispersions stabilized with polyelectrolytes. *Journal of American Ceramic Society*, 71(12), 1062-1067.
- Colins, P. M., and Ferrier, R. J. (1995). *Monosaccharides, their chemistry and their roles in natural products*. Chichester: John Wiley and Sons.
- Collyer, A. A., and Clegg, D. W. (1998). *Rheological measurement* (2nd ed.). London: Chapman and Hall.
- Crowe C. T. (Ed.). (2006). *Multiphase Flow Handbook*. Florida: Taylor and Francis Groups LLC.

- Cousset, P. (2005). *Rheometry of pastes, suspensions and granular materials, applications in industry and environment*. New York: Wiley-InterScience.
- Desset, S., Spalla, O., Lixon, P., and Cabane, B. (2001). From powders to dispersions in water: effect of adsorbed molecules on the re-dispersion of alumina particles. *Langmuir*, 17, 6408-6418.
- Evanko, C. R., Delisio, R. F., Dzombak, D. A., and Novak Jr., J. W. (1997). *Colloids and surfaces A: physicochemical and engineering aspects*, 125, 95-107.
- Ferry, J. D. (1980). *Viscoelastic properties of polymers*.(3rd ed.). New York: John Wiley and Sons.
- Franks, G. V., and Lange, F. F. (1999). Mechanical behavior of saturated, consolidated, alumina powder compacts: effect of particle size and morphology on the plastic-to-brittle transition. *Colloids and Surfaces A: Physicochemical and Engineering Aspects*, 146, 5-17.
- Goodwin, J. W., and Hughes, R. W. (2000). *Rheology for chemists, an introduction*. Royal Society of Chemistry.
- Hunter, R. J. (2001). *Foundations of colloid science*.(2nd ed.). London: Oxford Press.
- Ibrahim, M., Alam, M., El-Haes, H., Jalbout, A. F., and de Leon, A. (2006). Analysis of the structure and vibrational spectra of glucose and fructose. *Ecl. Quím.*, São Paulo, 31(3), 15-21.
- Kim, J. C., Auh, K. H., and Schilling, C., H. (2000). Effects of polysaccharides on the rheology of alumina slurries. *Journal of European Ceramic Society*, 20, 256-266.
- Kirby, G. H., Cooley, K. M., and Armstrong, B. L. (2005). Tailored rheological behavior of mullite and BSAS dispersions using a cationic electrolyte: *Proceedings of GT2005 ASME Turbo Expo: Power for Land, Sea and Air*. Reno-Tahoe, Nevada, USA.
- Kuptsevich, Y. E., Larinov, O. G., Stal'naya, I. D., Nakhapetyan, L. A., and Pronin, A. Y. (1987). Chromatographic separation of glucose and fructose. *Russian Chemical Reviews*, 56 (3), 299-306.
- Lange, F. F. (1998). Colloidal processing of powder for reliable ceramics. *Current Opinion in Solid State and Materials Science*, 3, 496-500.
- Lebrette, S., Pagnoux, C., and Abelard, P. (2004). Stability of aqueous TiO₂ suspensions: influence of ethanol, *Journal of Colloid and Interface Science*, 280, 400-408.
- Lewis, J. A. (2000). Colloidal processing of ceramics. *Journal of American Ceramic Society*. 83, 2341-2359.

- Li, C., and Akinç, M. (2005). Role of bound water on the viscosity of nanometric alumina dispersions. *Journal of American Ceramic Society*, 88, 1448-1454.
- Lim, L. C., Wong, P. M., and Ma, J. (1997). Colloidal processing of sub-micron alumina powder compacts. *Journal of Materials Processing Technology*, 67, 137-141.
- Liu, Q., and Laskowski, J. S. (2002). Adsorption of Polysaccharides on Mineral Surfaces from Aqueous Solutions. In *Encyclopedia of Surface and Colloid Science*. Marcel Dekker Inc.
- Liu, D-M. (1998a). Rheology of aqueous dispersions containing highly concentrated nano-sized zirconia powders. *Journal of Materials Science Letters*, 17, 1883-1885.
- Liu, D-M. (1998b). Dispersion Characteristics of nano-sized ceramic powder in an aqueous medium. *Journal of Materials Science Letters*, 17, 207-210.
- Liu, D-M. (1998c). Rheology of aqueous suspensions containing highly concentrated nano-sized zirconia powders, *Journal of Materials Science Letters*, 17, 1883-1885.
- Liu, D-M. (1999). Adsorption, rheology, packing and sintering of nano-sized ceramic powders. *Ceramics, International*, 25, 107-113.
- Liu, S., Xiao, H., and Li, Y. (2005). Adsorption of poly(acrylic acid) onto the surface of titanium dioxide and the colloidal stability of aqueous suspension. *Journal of Colloid and Interface Science*, 281, 155-163.
- Lu, K., and Kessler, C. (2006). Colloidal dispersion and rheology study of nanoparticles. *Journal of Material Science*, 41, 5613-5618.
- Lu K. (2007). Rheological behavior of carbon nanotube-alumina nanoparticle dispersion systems. *Powder Technology*, 177, 154-161.
- Lyklema, J. (2005). *Fundamentals of Interface and Colloid Science: Vol. 4*. (1st ed.) San Diego: Particulate Colloids, Academic Press.
- Macosko, C. W. (1994). *Rheology: principles, measurements, and applications*. New York: Wiley-VCH.
- Morrison, F. A. (2000). *Understanding rheology*. New York: Oxford University Press.
- Olhero, S. M., and Ferrira, J. M. (2004). Influence of particle size distribution on rheology and particle packing silica based dispersions. *Powder Technology*, 139, 69-75.
- Pettersson, A., Marino, G., Pursihemo, A., and Rosenholm, J. B. (2000). Electrosteric stabilization of Al₂O₃, ZrO₂, and 3Y-ZrO₂ suspensions: effect of dissociation and type of electrolyte. *Journal of Colloids and Interface Science*, 228, 73-81.

- Peker, S. M., and Helvacı, Ş. Ş. (2008). *Solid-liquid two phase flow*. Amsterdam: Elsevier.
- Rouquerol, F., Rouquerol, J., and Sing, K. (1999). *Adsorption by powders and porous solids, principles, methodology and applications*. San Diego: Academic Press.
- Schilling, C. H., Li, C., Tomasik, P., and Kim, J-C. (2002a). The rheology of alumina dispersions: influence of polysaccharides. *Journal of the European Ceramic Society*, 22, 923.
- Schilling, C. H., Sikora, M., Tomasik, P., Li, C., and Garcia, V. (2002b). Rheology of alumina nanoparticle dispersions: effects of lower saccharides and sugar alcohol. *Journal European Ceramic Society*, 22 (9), 917-921.
- Schmidt, M., and Münstedt, H. (2002). Rheological behavior of concentrated monodisperse dispersions as a function of preshear conditions and temperature. *Rheologica Acta*, 41, 193-204.
- Schramm, G. (1994). *A practical approach to rheology and rheometry*. Berlin: HAAKE Rheometers.
- Shanefield, D. J. (1996). *Organic additives and ceramic processing*. Boston: Kluwer Academic Publishig.
- Sigmund, W. M., Bell, N. J., and Bergström, L. (2000). Novel power-processing methods for advanced ceramics. *Journal of American Ceramic Processing*, 83 (7), 1557-1574.
- Sikora, M., Garcia, V. J., Schilling, C. H., Li C., Tomasik, P., and Li, C. (2004). Blends of maltodextrin and other polysaccharides as binders of aqueous α -alumina dispersions for ceramic processing”, *Starch/Starke*, 56, 424.
- Singh, B. P., Bhattacharjee, S., Besra, L., and Segupta, D. K. (2005). Electrokinetic and adsorption studies of alumina suspensions using Darvan C as a dispersant. *Journal Colloid and Interface Science*, 289, 592-596.
- Snoswell, D. R. E., Duan, J., Fornasiero, D., and Ralston, J. (2005). Colloid stability of synthetic titania and influence of surface roughness. *Journal of Colloid and Interface Science*, 286 (2), 526-535.
- Spurr, R. A., and Myers, H. (1957). Quantitative analysis of anatase-rutile mixtures with an x-ray diffractometer. *Analytical Chemistry*, 29 (5), 760-762.
- Stanek, J., Cerny, M., Kocourek, J., and Pacak, J. (1963). *The Monosaccharides*. New York: Academic Press.

- Tari, G., Ferreira, J. M. F., Fonseca, A. T., and Lyckfeldt, O. (1998). Influence of particle size distribution on colloidal processing of and alumina. *Journal of European Ceramic Society*, 18, 249-253.
- Telis, V. R. N., Telis-Romero, J., Mazzotti, H. B., and Gabas, A. L. (2007). Viscosity of aqueous carbohydrate solutions at different temperatures and concentrations. *International Journal of Food Properties*, 10, 185-195.
- Tohver, V., Smay, J. E., Braem, A., Vraun, P. V., and Lewis, J. A. (2001). Nanoparticle halos: a new colloid stabilization mechanism: *Proceedings of the National Academy of Science*, 98, 8950-8954.
- Tseng, W. J., and Wu, C. H. (2003). Sedimentation, rheology and particle-packing structure of aqueous Al₂O₃ dispersions, *Ceramics International*, 29, 821-828.
- Wolthers, W., Duits, M. H. G., van de Ende, D., and Mellema, J. (1996). Shear history dependence of the viscosity of aggregated colloidal dispersions. *Journal of Rheology*, 40 (5), 799-811.
- Zaman, A. A. and Dutcher, C. S. (2006). Viscosity of electrostatically stabilized dispersions of monodispersed, bimodal, and trimodal silica particles. *Journal of American Ceramic Society*, 89 (2), 422-429.
- Zhou, Z., Scales, P. J., and Boger, D. V. (2001). Chemical and physical control of the rheology of concentrated metal oxide dispersions. *Chemical Engineering Science*, 56, 2901-2920.

APPENDICES

APPENDIX A. IMPORTANT PARAMETERS IN RHEOLOGICAL MEASUREMENTS OF CERAMIC POWDER DISPERSIONS

If a material has Newtonian behavior, measuring its viscosity would be sufficient to characterize its properties. However, if the material is non-Newtonian it may have both viscous and elastic properties. The characterization of such fluids require both steady and dynamic shear rheological methods. Steady shear rheological methods include the determination of flow curves and viscosity curves, thixotropy and, yield point. Dynamic shear rheological methods include the determination of creep and recovery and stress/strain, frequency, time and, temperature sweeps (Schramm, 1994; Haake Rheometer Manual).

A.1. The Determination of Flow/Viscosity Curves

Flow curves and/or viscosity curves are taken into consideration to examine the flow properties under changing shear and stress conditions. A flow curve actually represents the shear stress (τ) as a function of shear rate ($\dot{\gamma}$) while a viscosity curve shows the viscosity (η) as a function of shear rate. There are four different ways to obtain flow curve or viscosity curve. The experiment can be done in controlled rate mode (reflects shear rate) or controlled stress mode (reflects shear stress). For both modes, there are two choices; ramping or stepwise controlling (known as steady shear) the changing parameter. In ramping, shear stress or shear rate is increased continuously depending on the defined time (t). If time is too short a noisy data will be collected. In stepwise controlling, shear stress or shear rate is increases in step wise way. The number of steps and time spent for each step are defined by user. If each data point is measured at equilibrium, there will be no time effect. Controlled rate is the most commonly used mode in which the start and the end shear rate are defined considering instrumental limitations. One must consider when a low viscous material is tested at low shear rates the corresponding shear stress can be out of the instrument limits. Likewise, very high viscous materials at low shear stresses may be resulted in very high shear rates which are out of specs. The time required for the observing a flow or a viscosity curve is directly affected by the materials time dependent behavior. These parameters should be well-defined and might not be changed from one test to other to make comparisons. The most common representation of a viscosity curve is a log-log distribution (viscosity as a function of shear rate) while flow curves represented in linear distribution (shear stress as a function of shear rate) (Schramm, 1994; Haake Rheometer Manual).

A.2. The Determination of Thixotropy

The determination of time related flow properties of materials, a thixotropy test is considered. This test can be performed either controlled rate or controlled stress mode. The most common way to determine thixotropic loop is using controlled rate mode. It is very similar to a flow curve. Basically, this test involves two steps: a ramp up and a ramp down. In the controlled rate mode, the start and the end shear rates are defined. Sometimes at the maximum shear rate it is held for a certain time before ramping down. One of the important issue is to observe the maximum shear rate that the material stays stable. This maximum shear rate value may be material dependent but it should be set to a certain value for comparison. The measured data is represented in a linear diagram of shear stress as a function of shear rate. Due to destruction of interior structure of material, a shear thinning behavior usually observed during ramping up. The downward ramp usually shows lower shear stress values because the material can't rebuild its structure fast enough. If the test is conducted too fast a noisy thixotropy curve is observed. Likewise, if the test is too slow, there will be much more time to rebuild interior structure during ramp down period and a smaller hysteresis area will be observed (Schramm, 1994; Haake Rheometer Manual).

A.3. The Determination of Creep and Recovery

The creep and recovery test is an alternative way for obtaining the relaxation and viscoelastic properties of a material. A constant stress below yield stress is applied to the material and deformation monitored with time. Compliance (J) is defined as the reciprocal of modulus ($J=1/G=\gamma/\tau$) where G is modulus and γ is strain. The value and shape of creep compliance curve are fundamentally important. Subject to a constant stress, the strain of an ideally elastic material would be constant and the material would return its original shape when the stress removed. In contrast, an ideal viscous material would show a steady flow, producing a linear response to stress with the inability to recover any of the imposed deformation. Viscoelastic materials will exhibit a non linear response to strain and, due to their ability to partially recover structure by storing energy, will show a deformation less than initial deformation (Schramm, 1994; Haake Rheometer Manual).

A.5. The Determination of Stress Sweep Curves

This test is applied in order to determine the range of LVER of a material. The practical way to determine the range of LVER is to observe the region where G' and G'' are independent of stress or strain value. However, LVER is frequency dependent. Therefore, several frequencies may need to be applied in order to figure out the frequency range. The relation between torque and shear stress must be considered. The minimum torque value should be checked and the starting shear stress should correspond to a torque value which is five or ten times of the minimum torque. The final shear stress value might be three decades greater than the starting one. However, high shear stress value might cause a shear like motion. A break criterion may be helpful. When deformation of material exceeds a certain value the measurement stops and proceeds with the next element in job procedure. The stress sweep test may give useful information to determine yield stress. Since this test is very sensitive to applied frequency value, one need to consider at which conditions yield stress is measured. The measured data presented in the material's functions (G' , G'' , and δ) versus shear stress graph (Schramm, 1994; Haake Rheometer Manual).

A.7. The Determination of Frequency Sweep Curves

The frequency sweep results indicate the structural conditions of the material. After a stress sweep test is applied to material in order to observe stress range of LVER of the material, a stress value is picked up in this region. This stress value correlates with a torque, which is at least 5 times higher than the specified minimum torque. The material is subjected to higher to lower frequencies and its structure is considered not changed during the test. It might be necessary to split the frequency sweep into a few steps. This is a simple way to prevent unacceptable test time by arranging different waiting period and repetitions. The test involves definition of a starting and an ending frequency values. Each data point requires at least two cycles. The estimated time required for each point is reciprocal of the actual frequency which is multiplied by the number of cycles that assigned. The number of data points is a number of logarithmically equidistant frequencies per decade depending on user. The measured data is presented in the material's functions (G' , G'' , $|\eta^*|$ and δ) versus frequency graph (Schramm, 1994; Haake Rheometer Manual).

APPENDIX B. THE RHEOLOGICAL BEHAVIOR OF SUBMICRON ALUMINA DISPERSIONS

B.1. The flow and viscosity curves

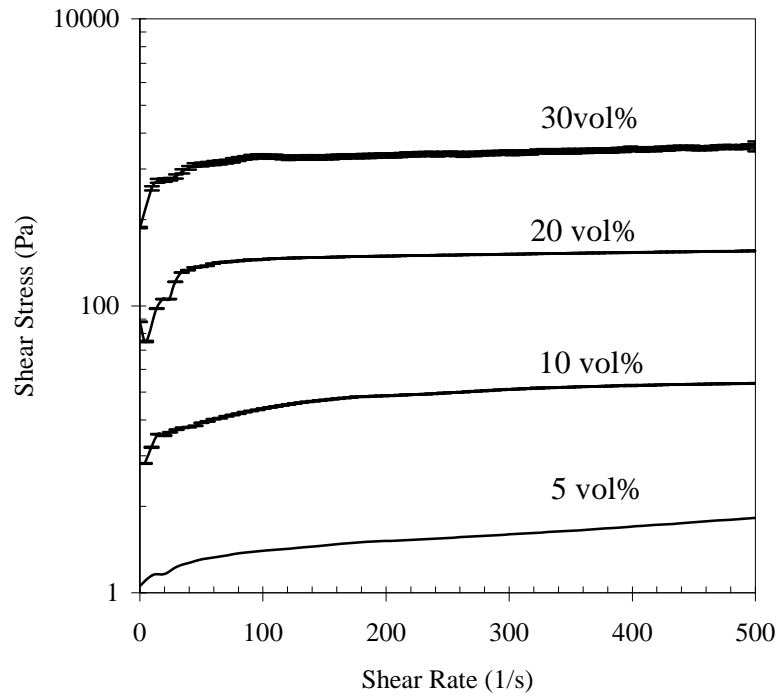


Figure 1. The flow curves of submicron alumina dispersions without fructose.

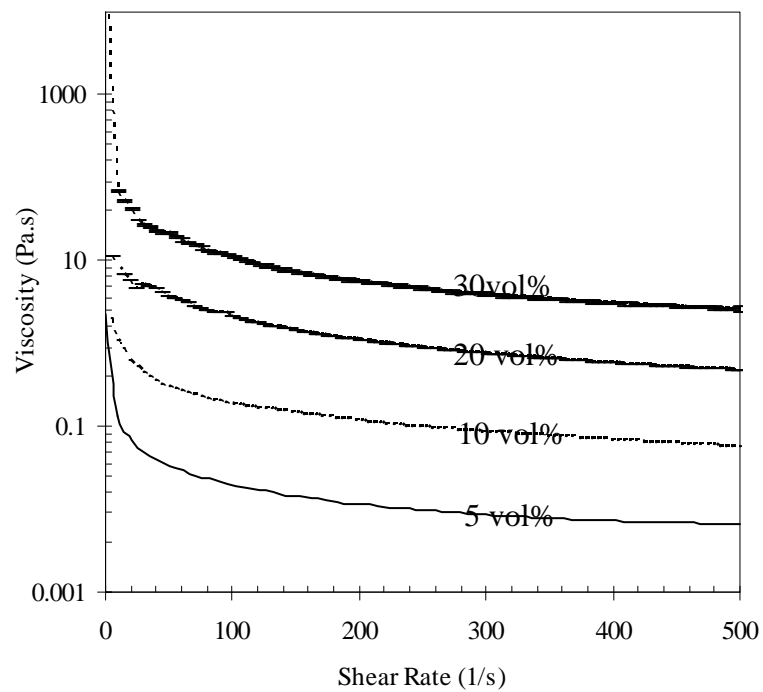


Figure 2. The viscosity curves of submicron alumina dispersions without fructose.

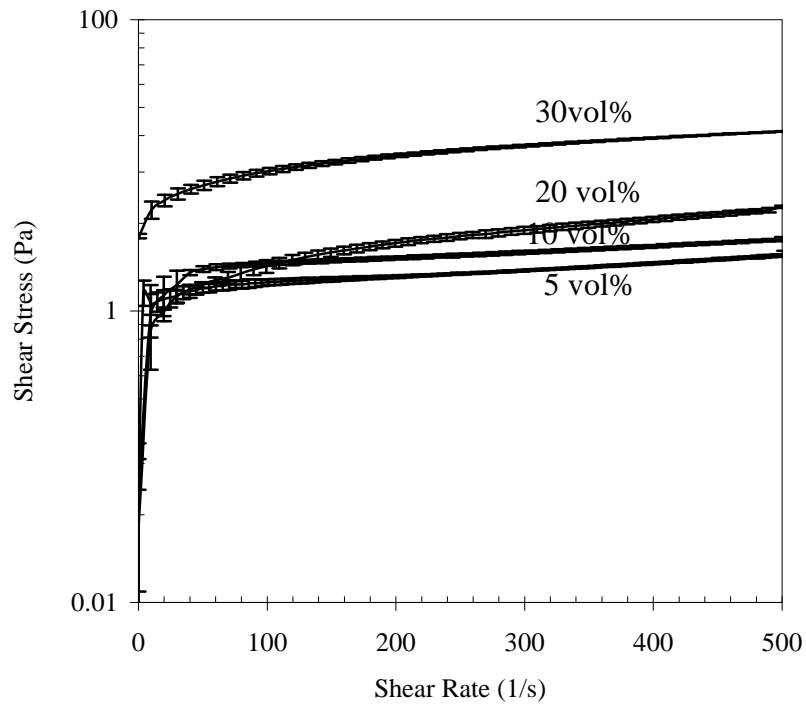


Figure 3. The flow curves of submicron alumina dispersions in 1 wt% fructose solution.

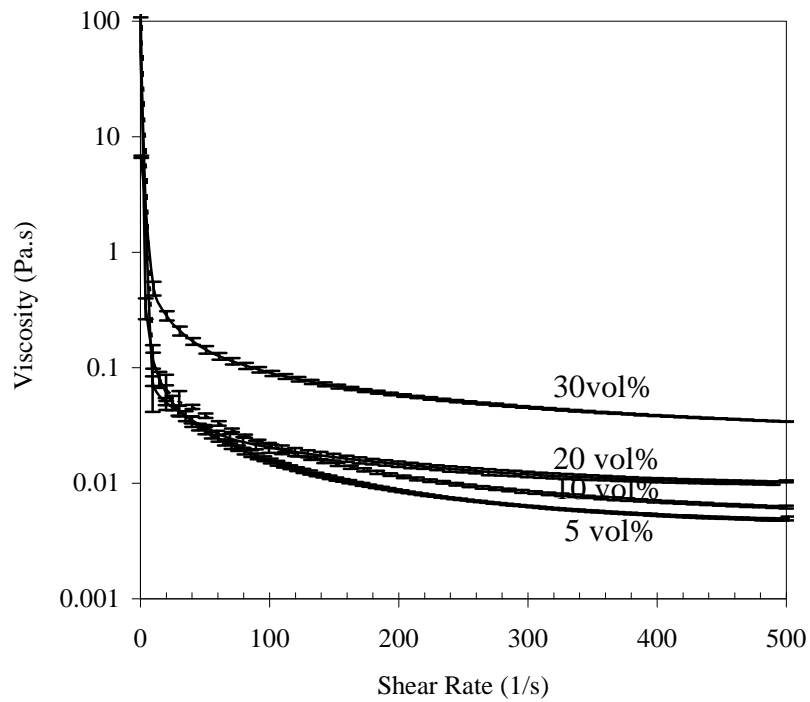


Figure 4. The viscosity curves of submicron alumina dispersions in 1 wt% fructose solution.

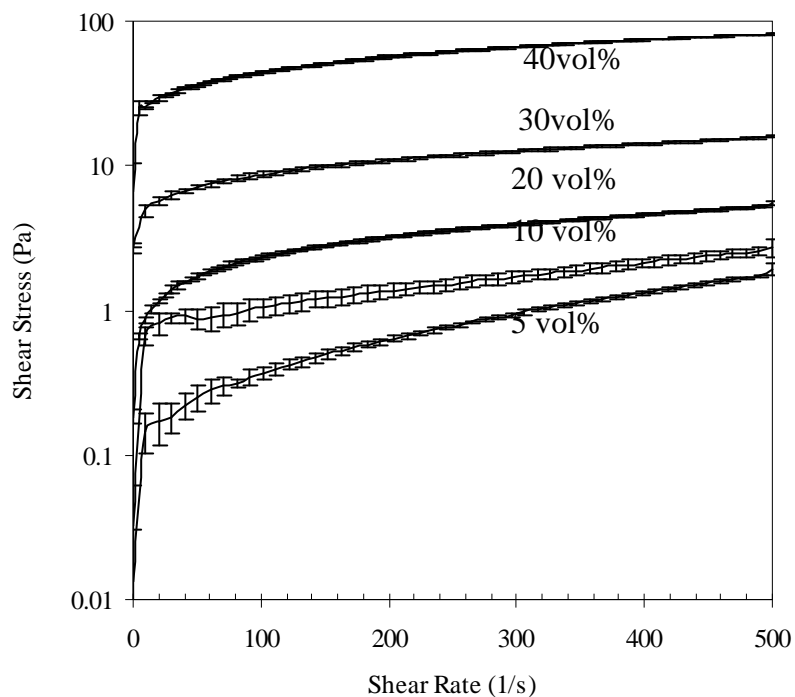


Figure 5. The flow curves of submicron alumina dispersions in 4 wt% fructose solution.

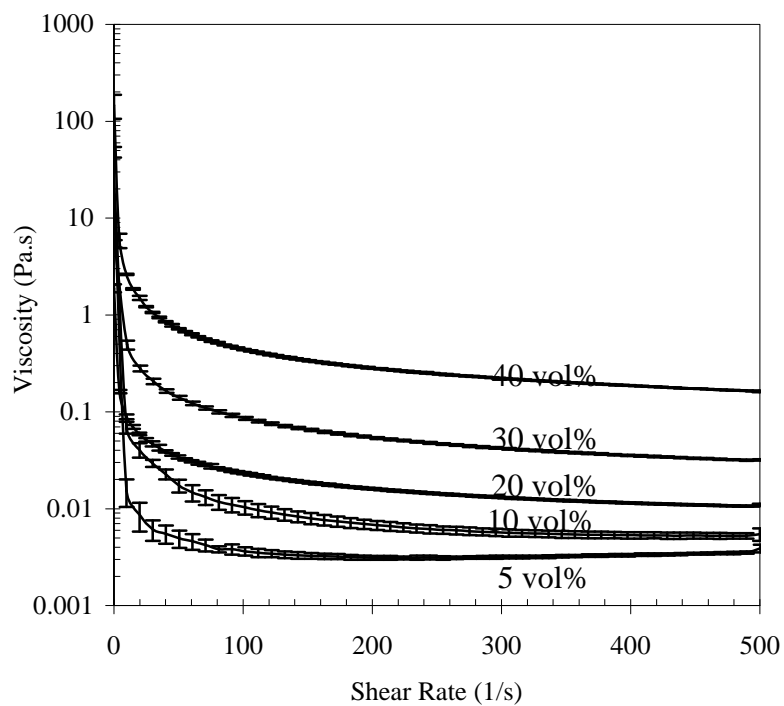


Figure 6. The viscosity curves of submicron alumina dispersions in 4 wt% fructose solution.

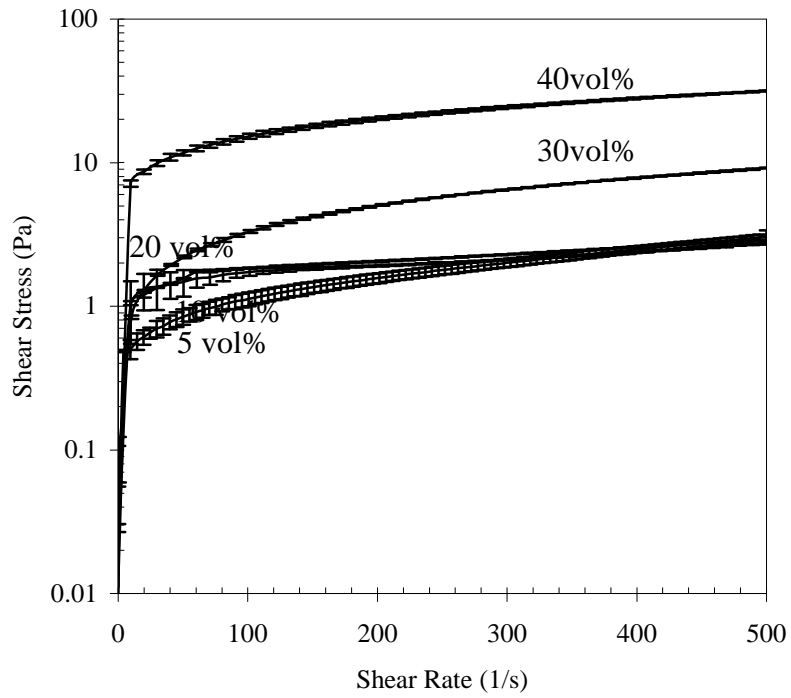


Figure 7. The flow curves of submicron alumina dispersions in 10 wt% fructose solution.

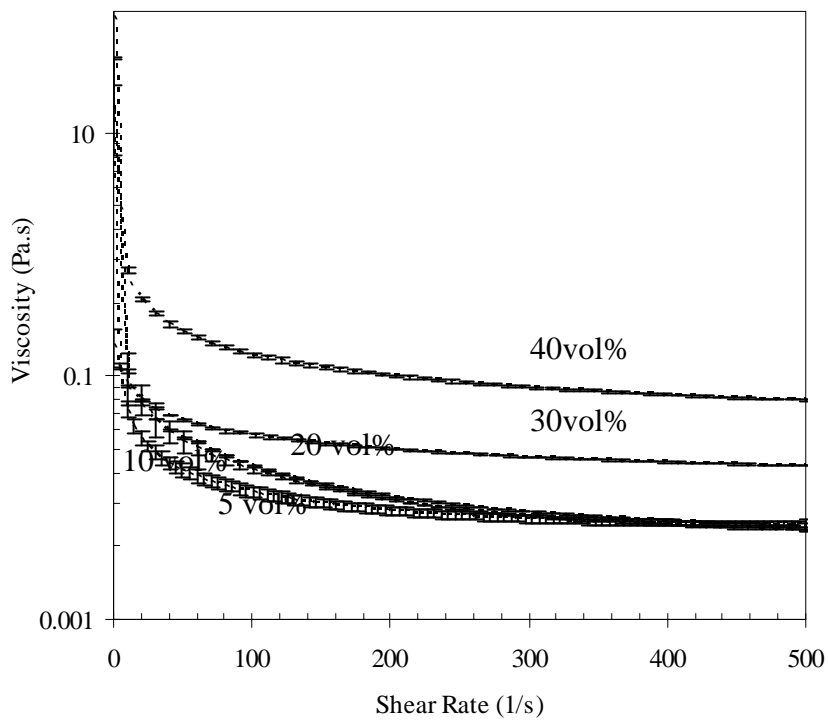


Figure 8. The viscosity curves of submicron alumina dispersions in 10 wt% fructose solution.

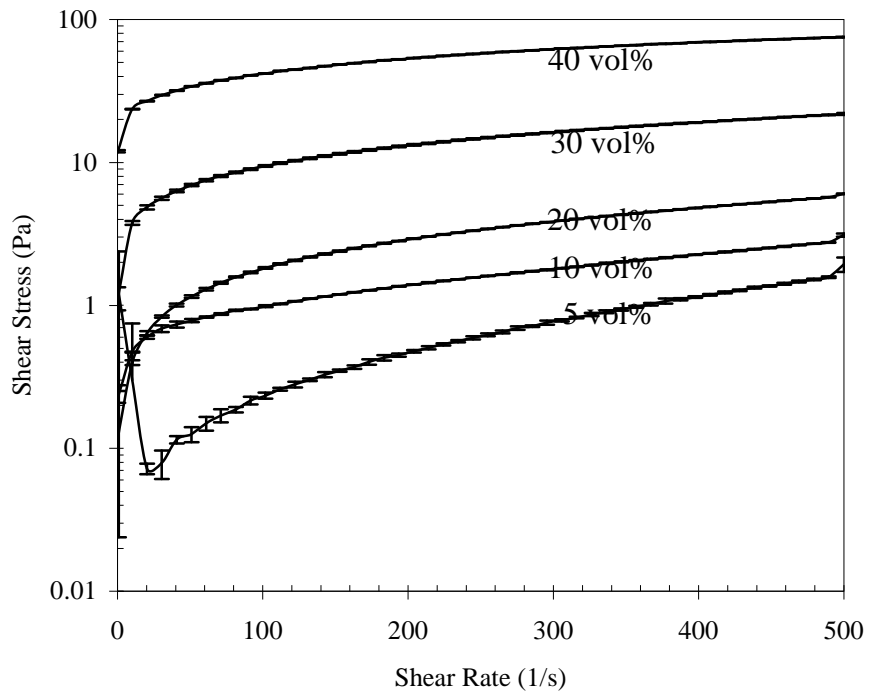


Figure 9. The flow curves of submicron alumina dispersions in 20 wt% fructose solution.

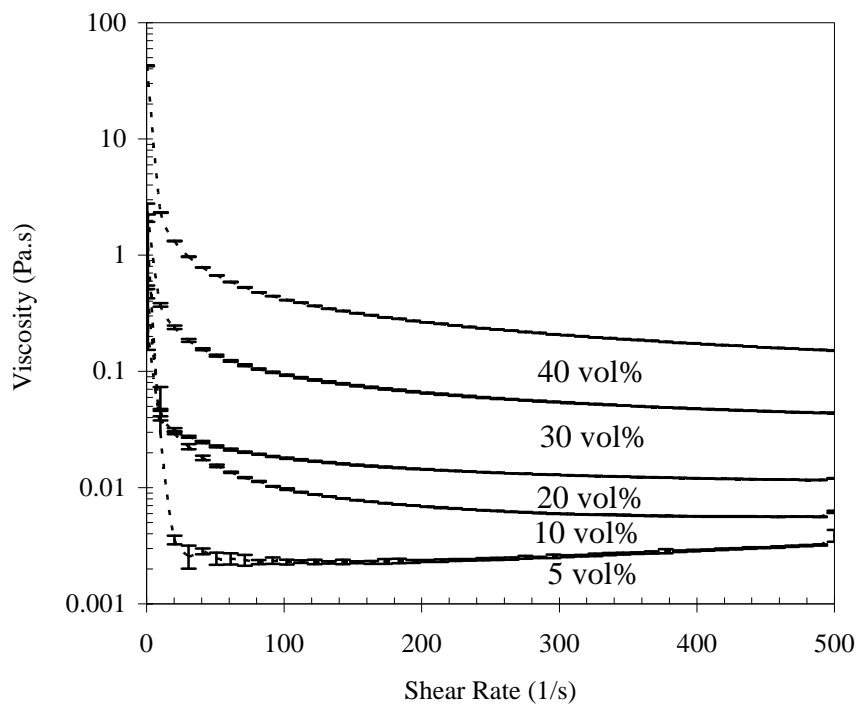


Figure 10. The viscosity curves of submicron alumina dispersions in 20 wt% fructose solution.

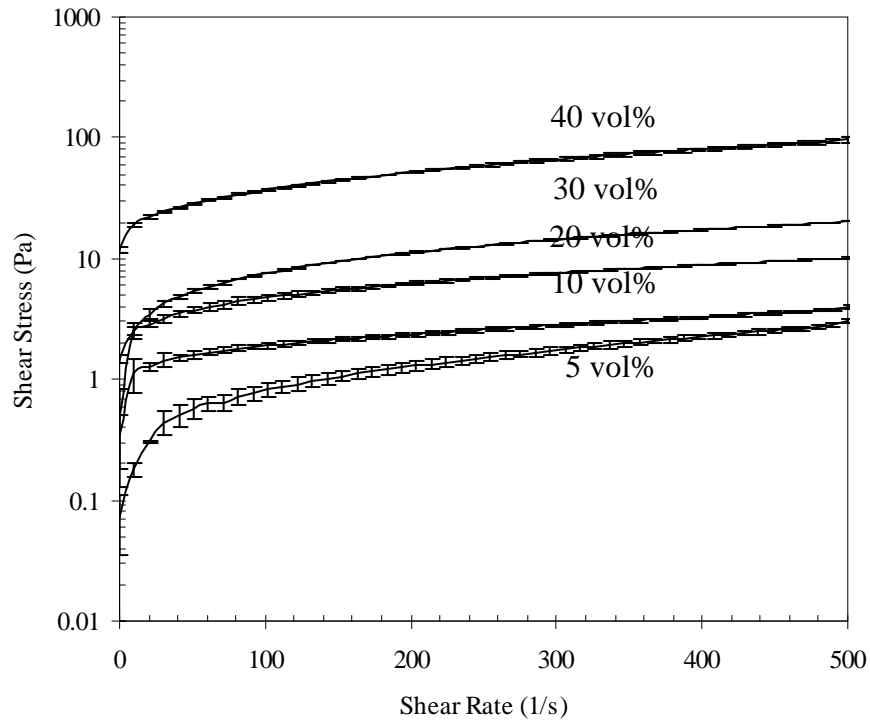


Figure 11. The flow curves of submicron alumina dispersions in 30 wt% fructose solution.

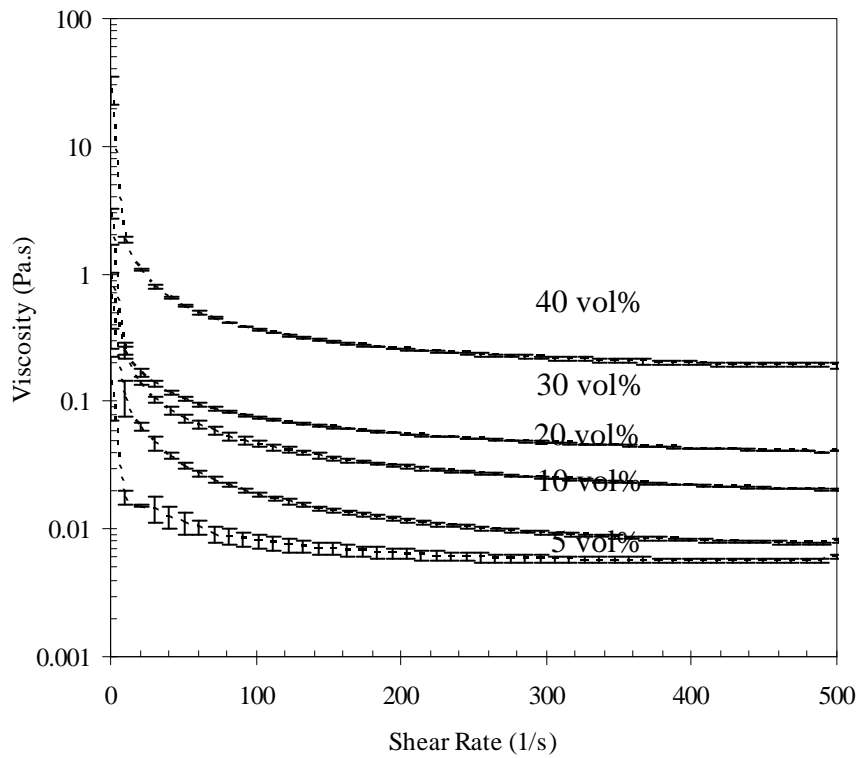


Figure 12. The viscosity curves of submicron alumina dispersions in 30 wt% fructose solution.

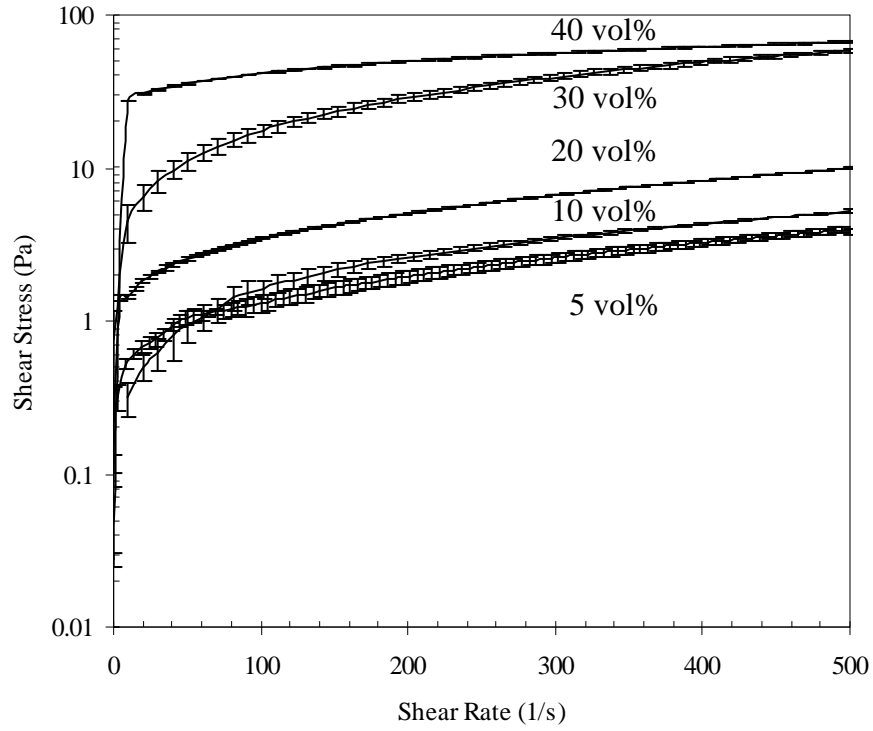


Figure 13. The flow curves of submicron alumina dispersions in 40 wt% fructose solution.

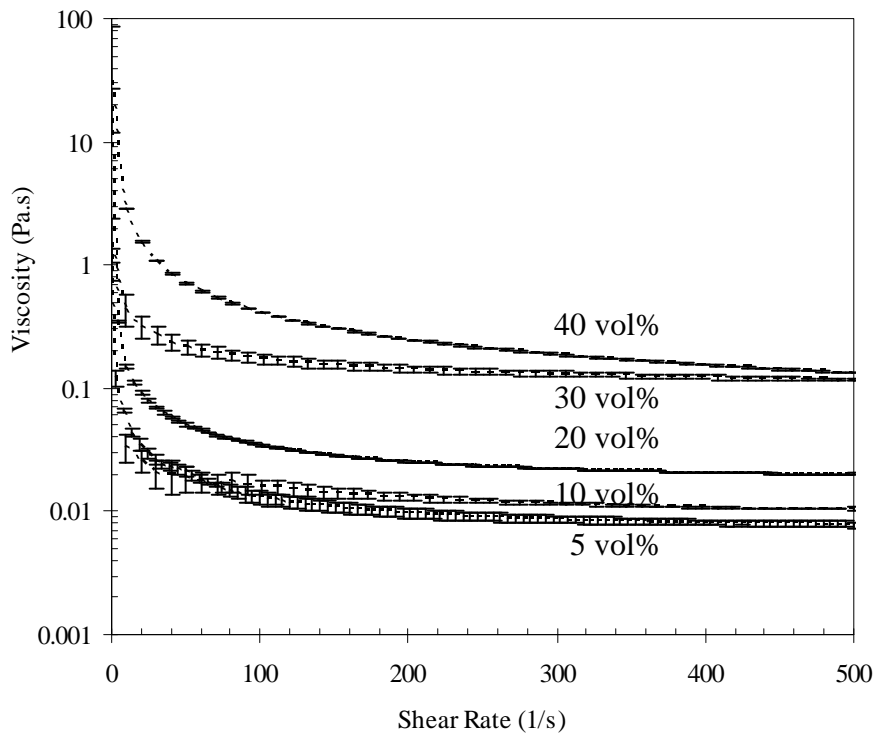


Figure 14. The viscosity curves of submicron alumina dispersions in 40 wt% fructose solution.

B.2. The thixotropy curves

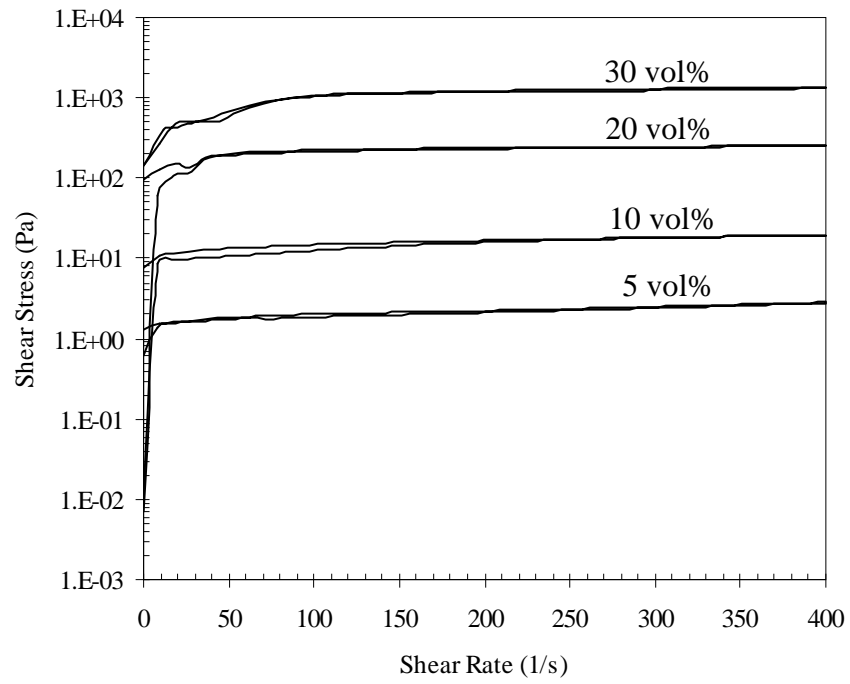


Figure 1. The thixotropy curves of submicron alumina in water.

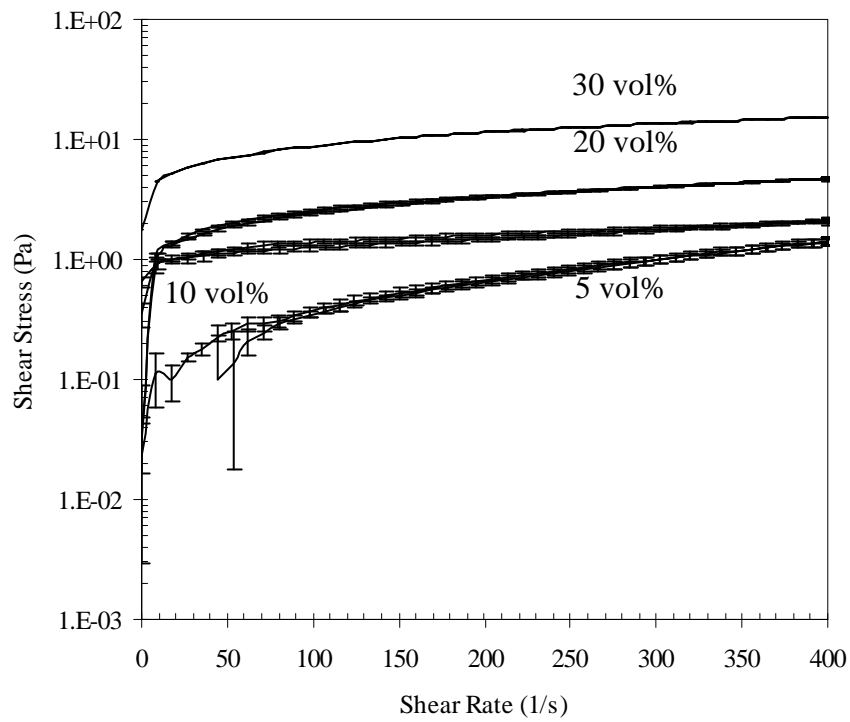


Figure 2. The thixotropy curves of submicron alumina in 1 wt% fructose solution.

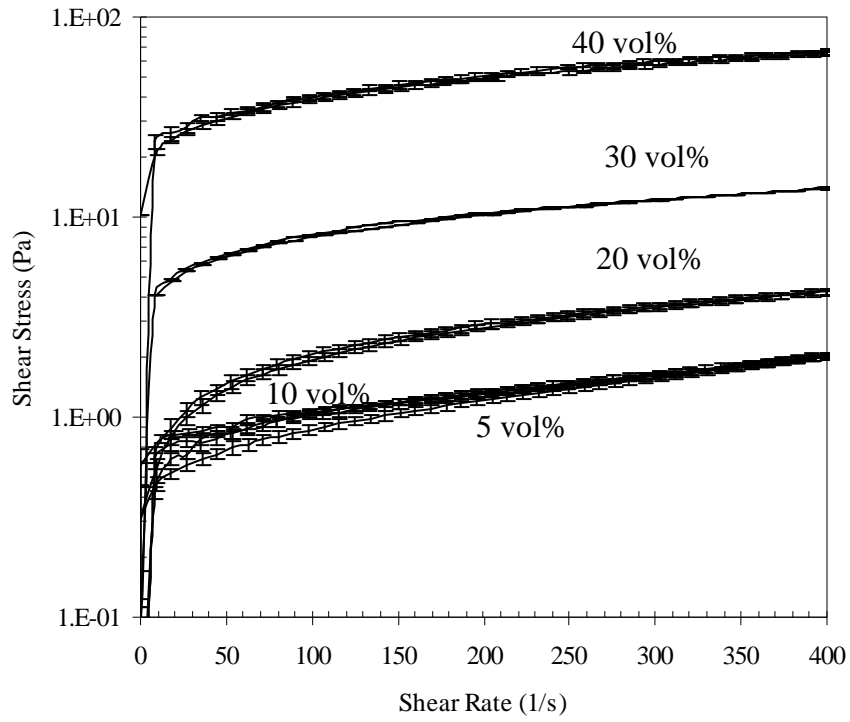


Figure 3. The thixotropy curves of submicron alumina in 4 wt% fructose solution.

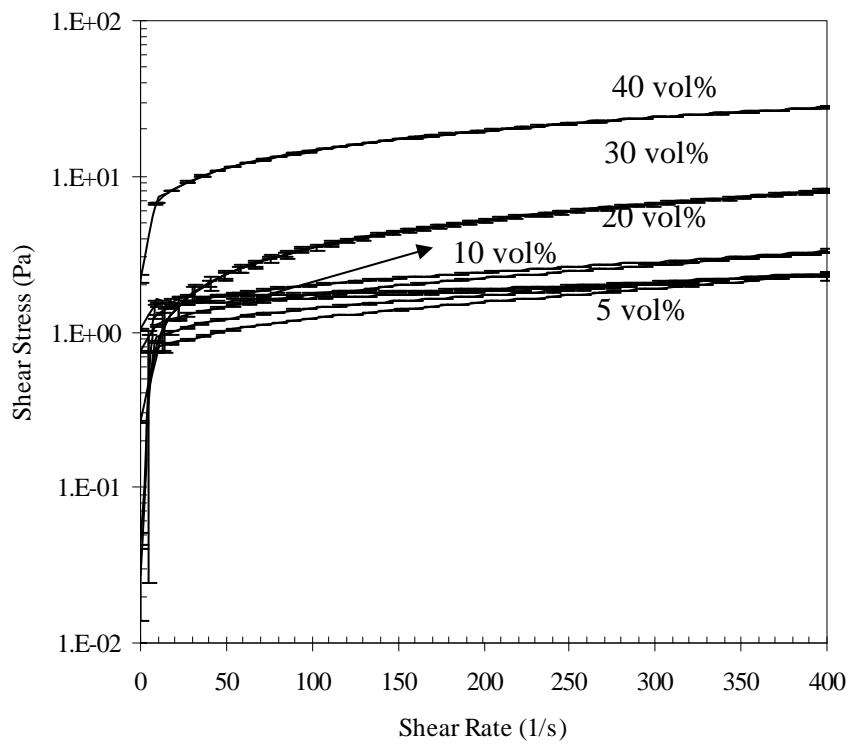


Figure 4. The thixotropy curves of submicron alumina in 10 wt% fructose solution.

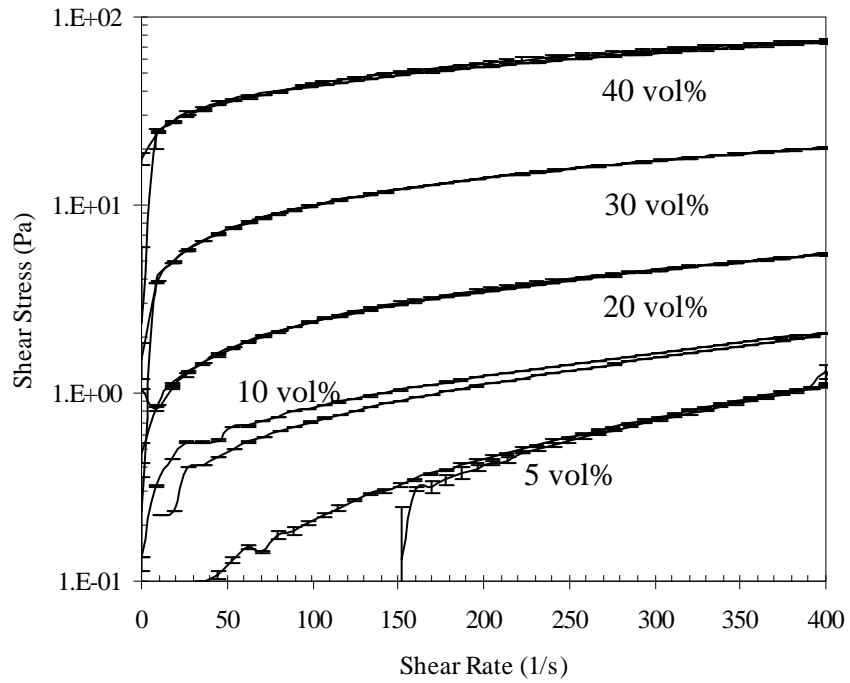


Figure 5. The thixotropy curves of submicron alumina in 20 wt% fructose solution.

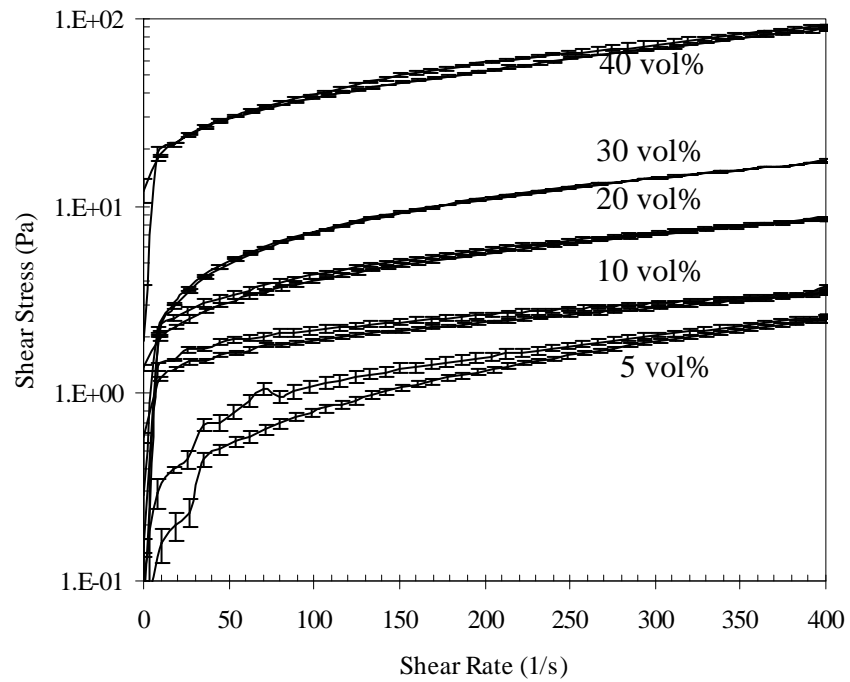


Figure 6. The thixotropy curves of submicron alumina in 30 wt% fructose solution.

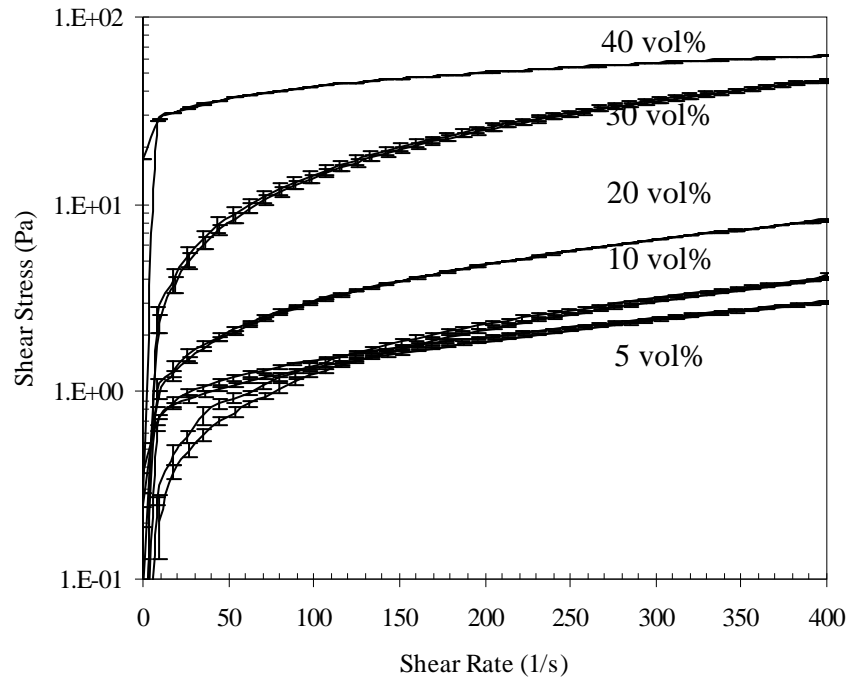


Figure 7. The thixotropy curves of submicron alumina in 40 wt% fructose solution.

B.3. The stress sweeps

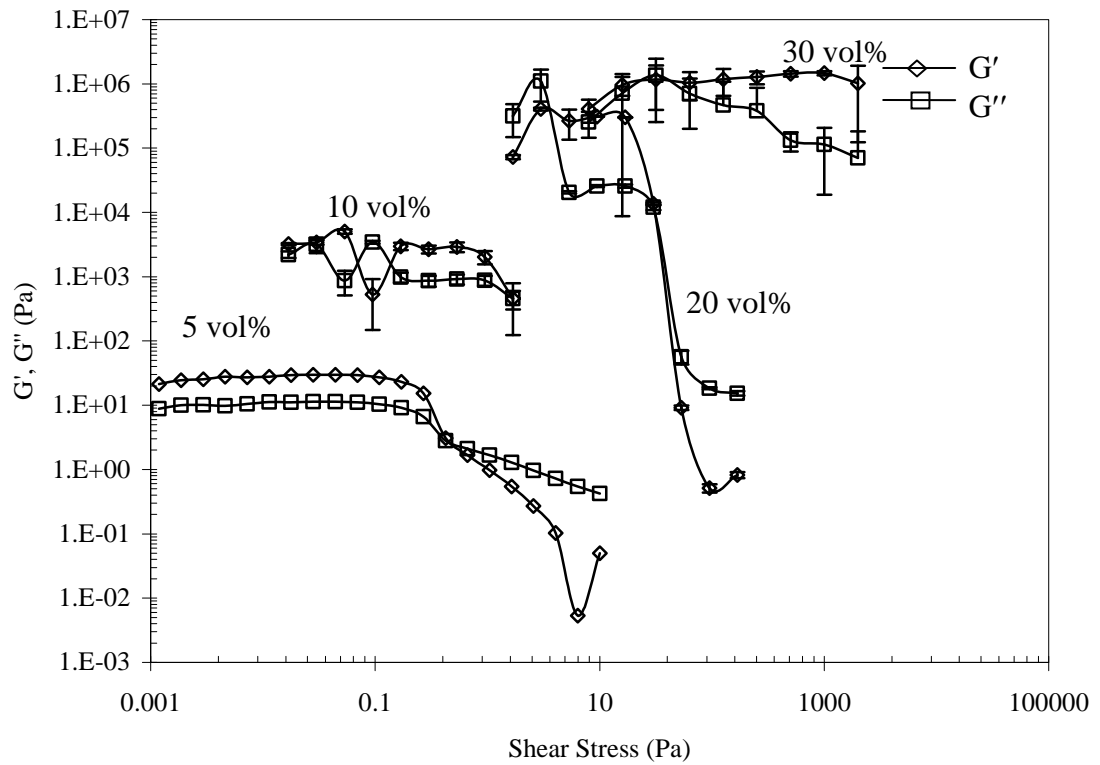


Figure 1. The stress sweeps of submicron alumina dispersions in water.

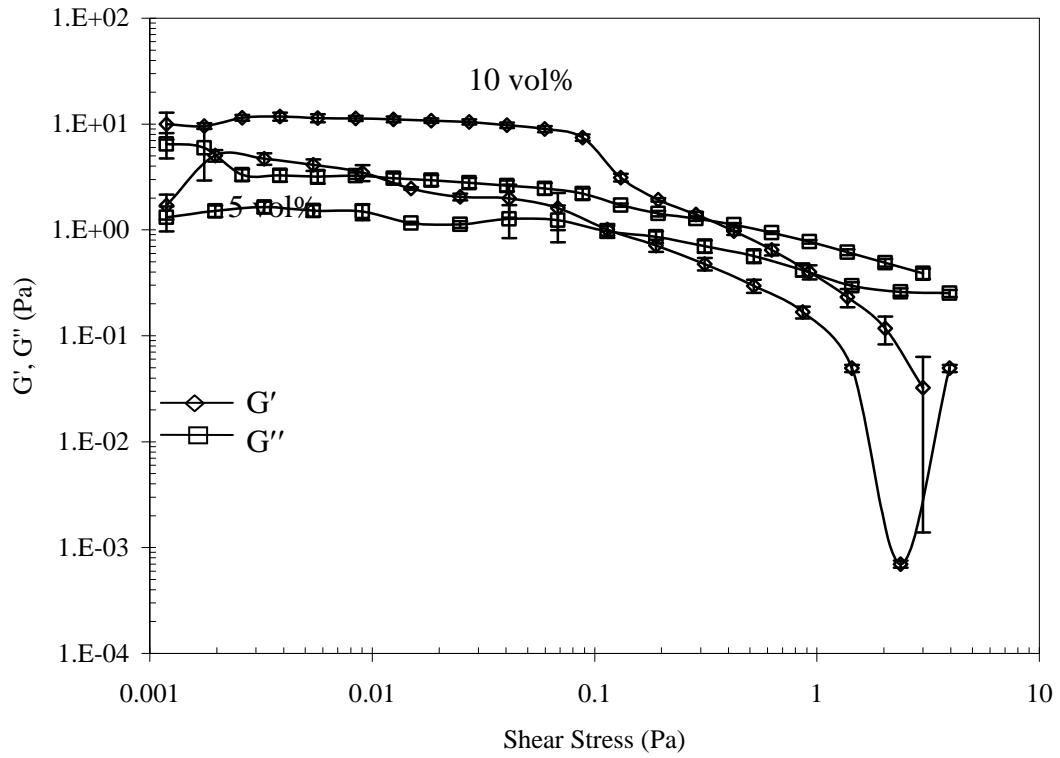


Figure 2. The stress sweeps of submicron alumina dilute dispersions in 1 wt% fructose solution.

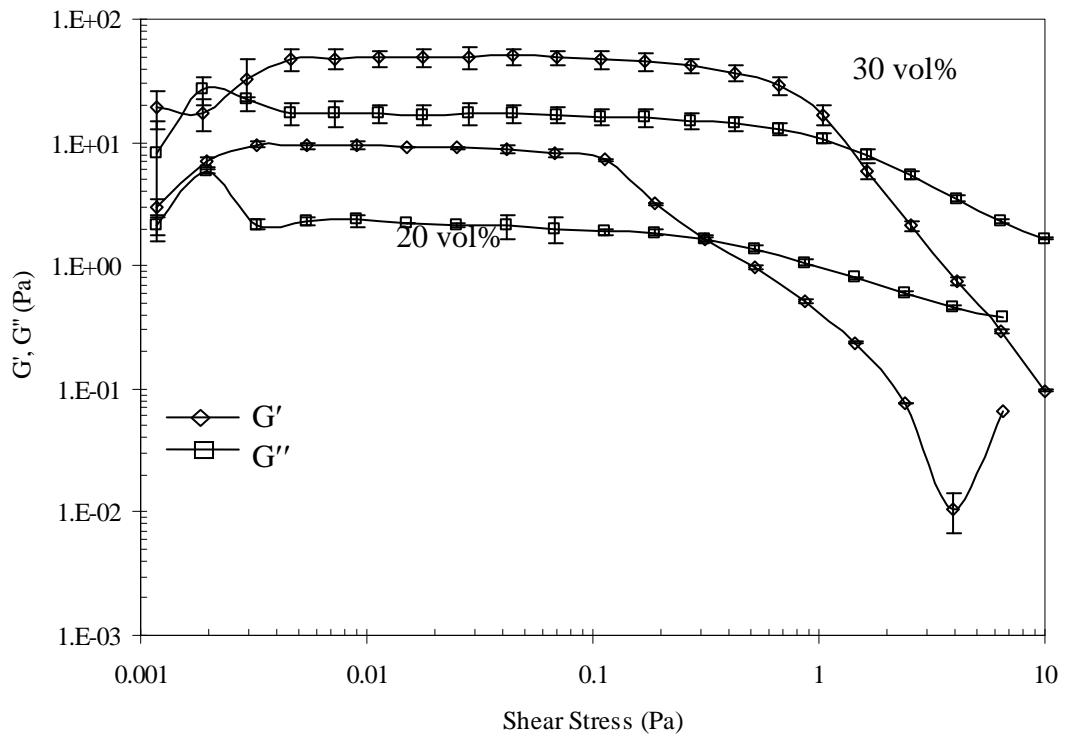


Figure 3. The stress sweeps of submicron alumina concentrated dispersions in 1 wt% fructose solution.

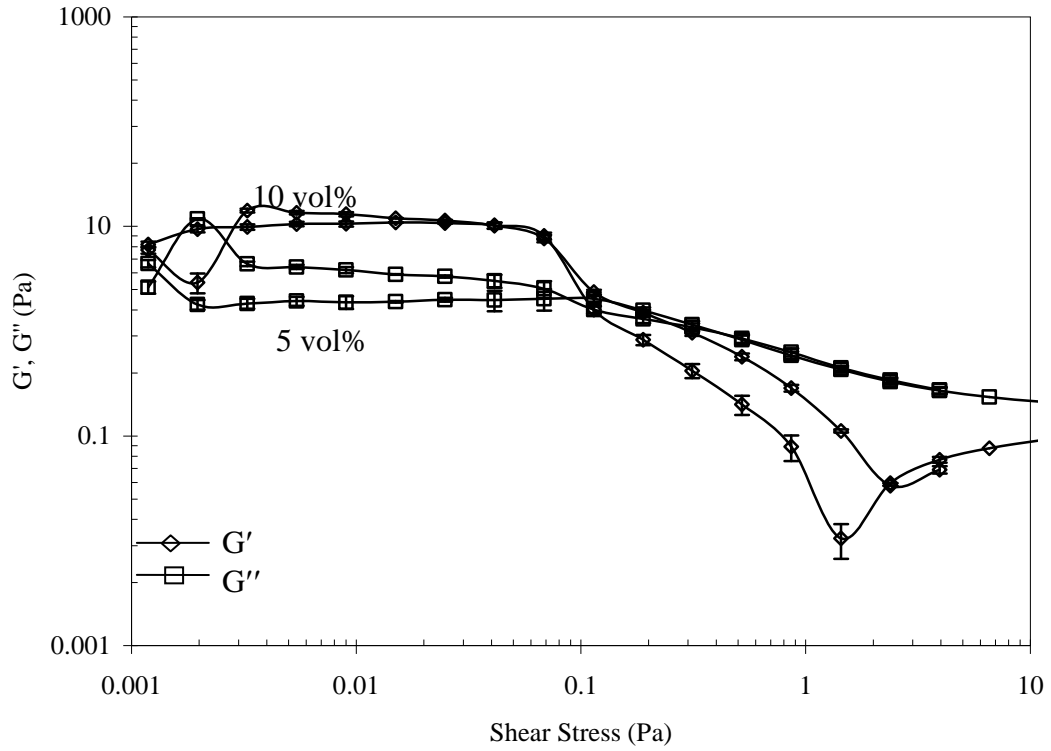


Figure 4. The stress sweeps of submicron alumina dilute dispersions in 4 wt% fructose solution.

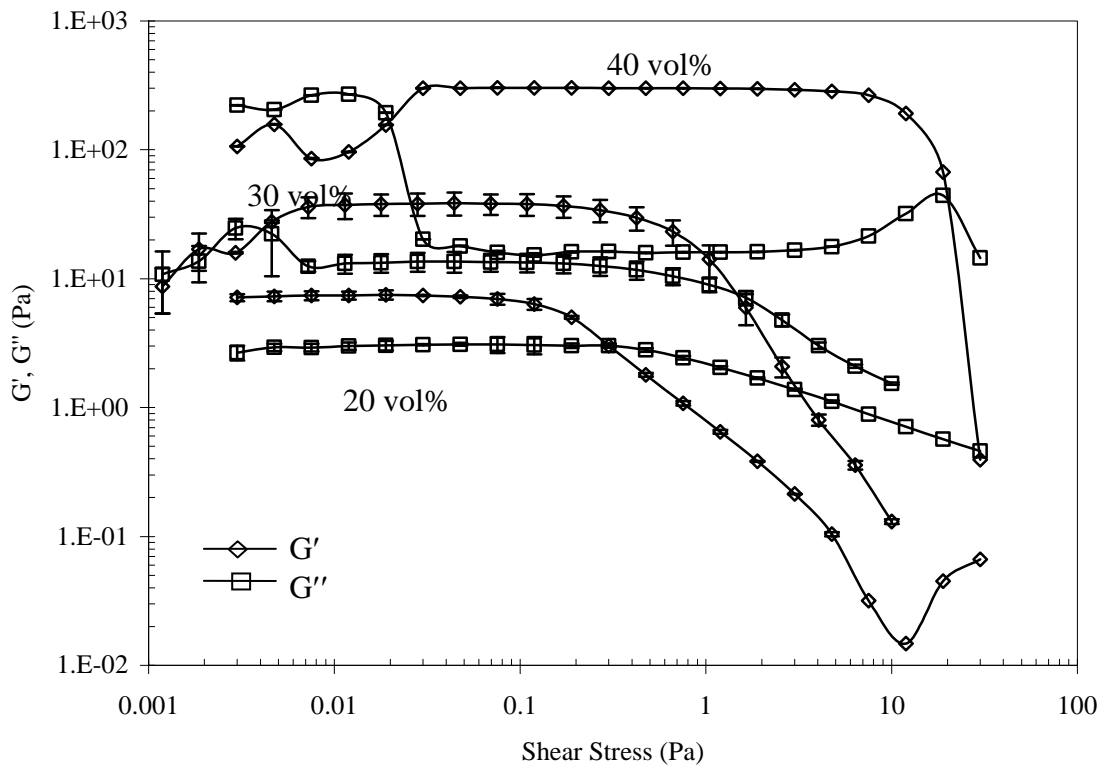


Figure 5. The stress sweeps of submicron alumina concentrated dispersions in 4 wt% fructose solution.

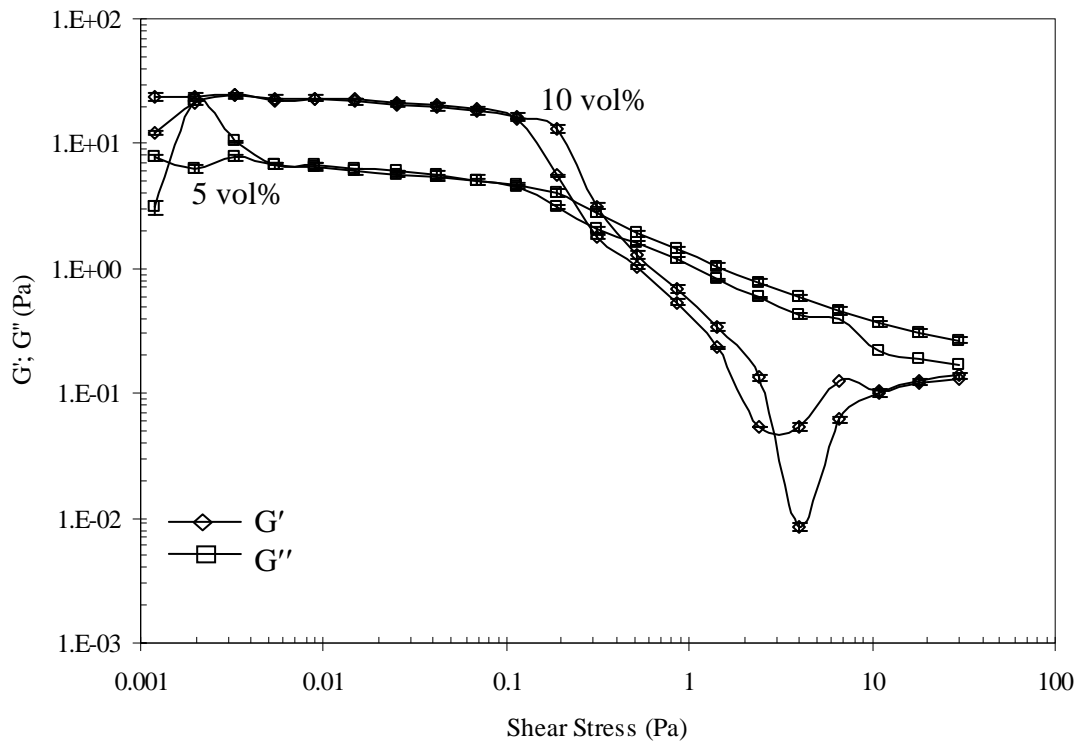


Figure 6. The stress sweeps of submicron alumina dilute dispersions in 10 wt% fructose solution.

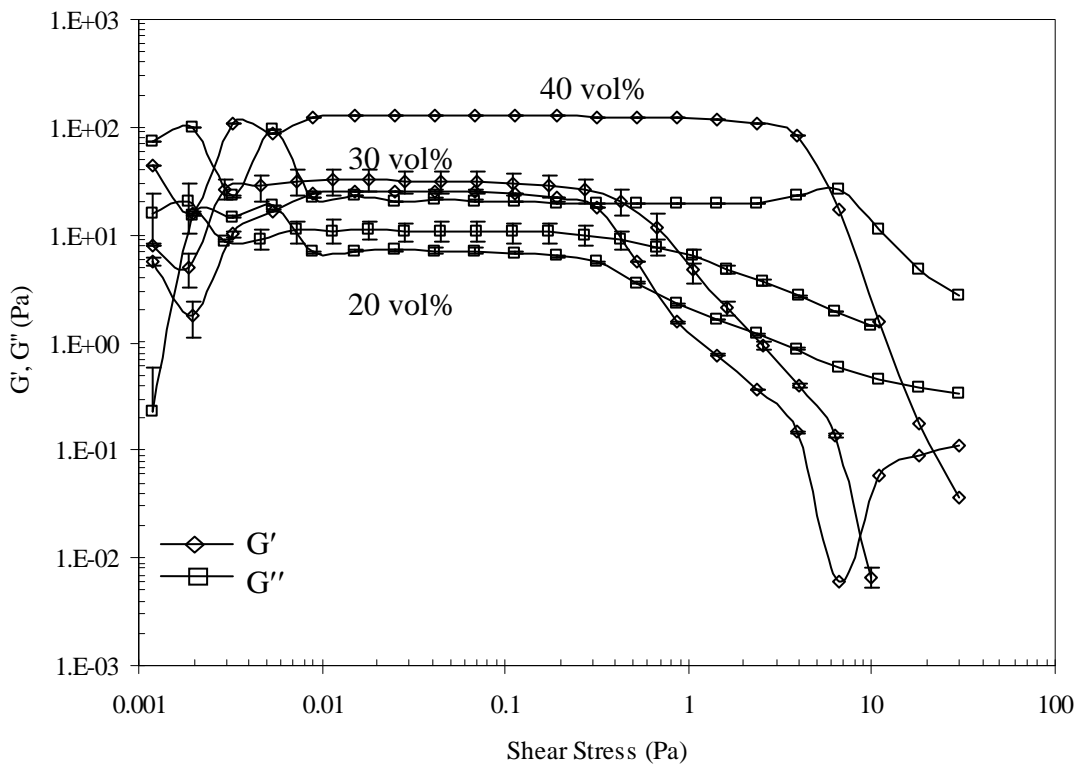


Figure 7. The stress sweeps of submicron alumina concentrated dispersions in 10 wt% fructose solution.

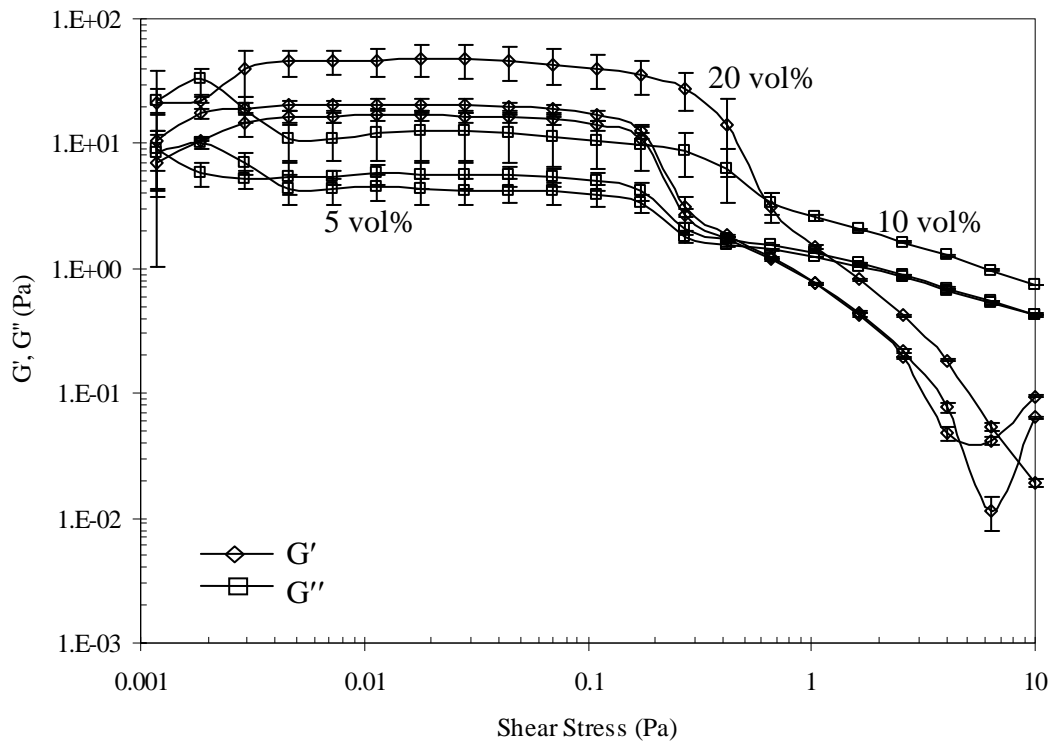


Figure 8. The stress sweeps of submicron alumina dilute dispersions in 20 wt% fructose solution.

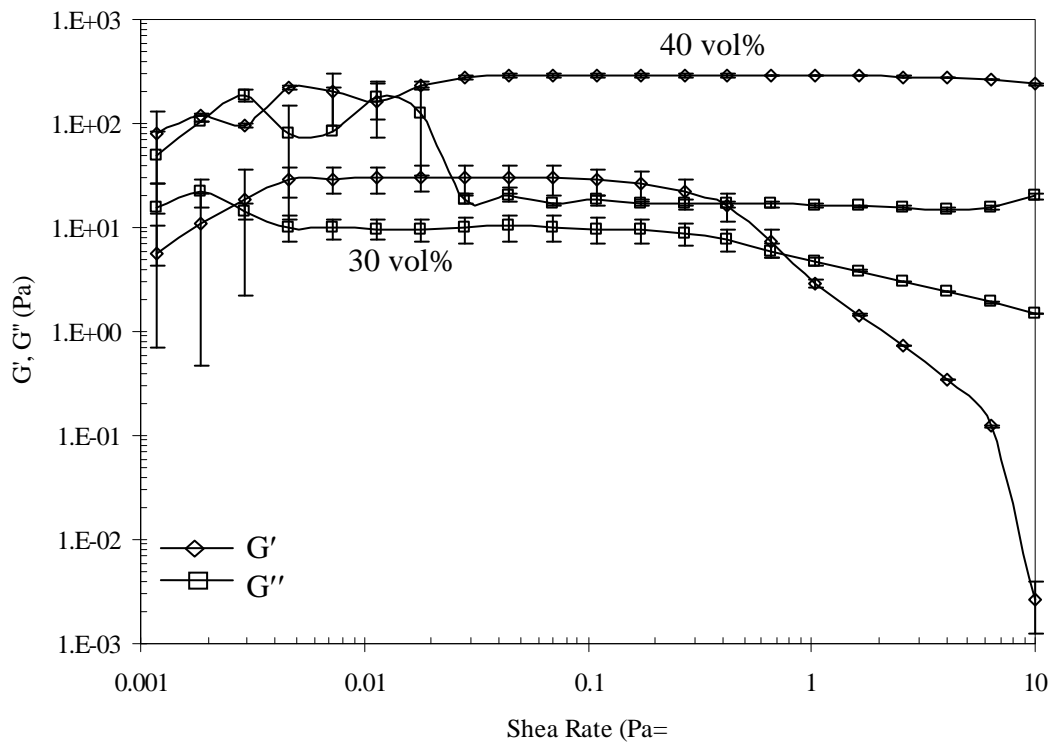


Figure 9. The stress sweeps of submicron alumina concentrated dispersions in 20 wt% fructose solution.

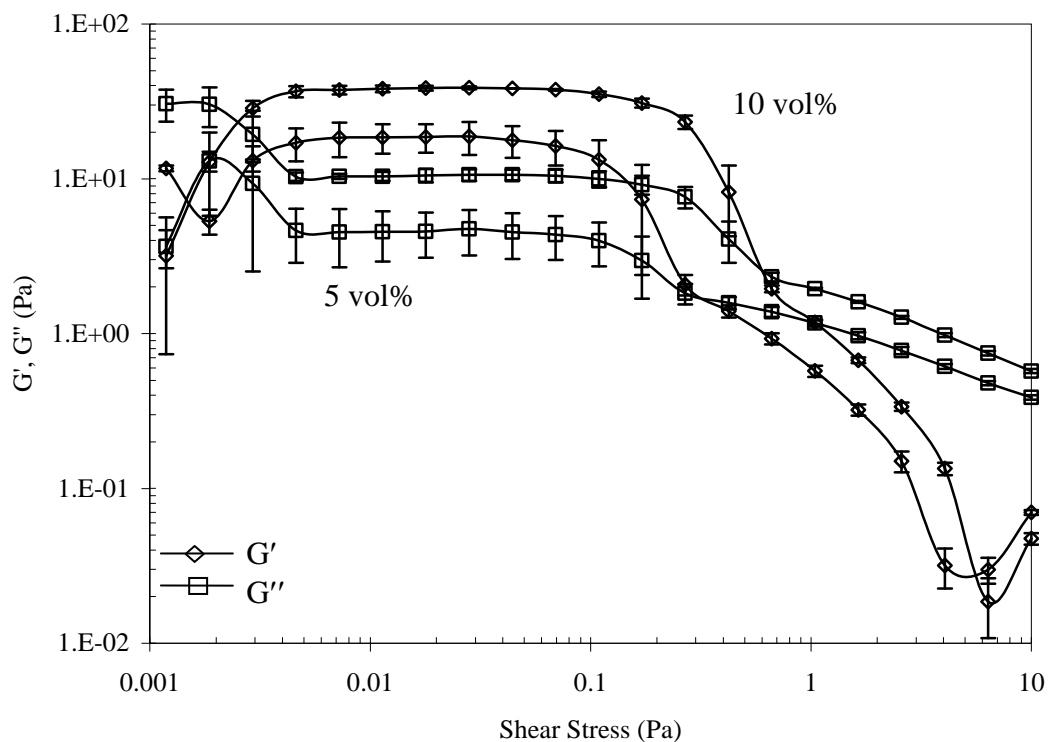


Figure 10. The stress sweeps of submicron alumina dilute dispersions in 30 wt% fructose solution.

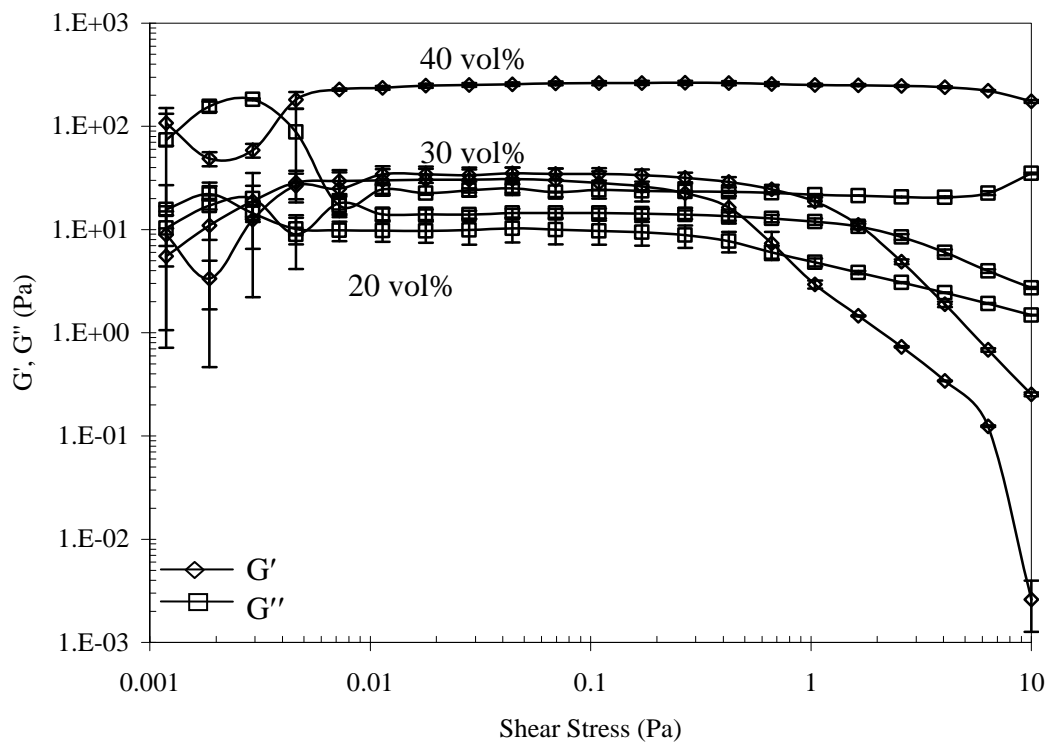


Figure 11. The stress sweeps of submicron alumina concentrated dispersions in 30 wt% fructose solution.

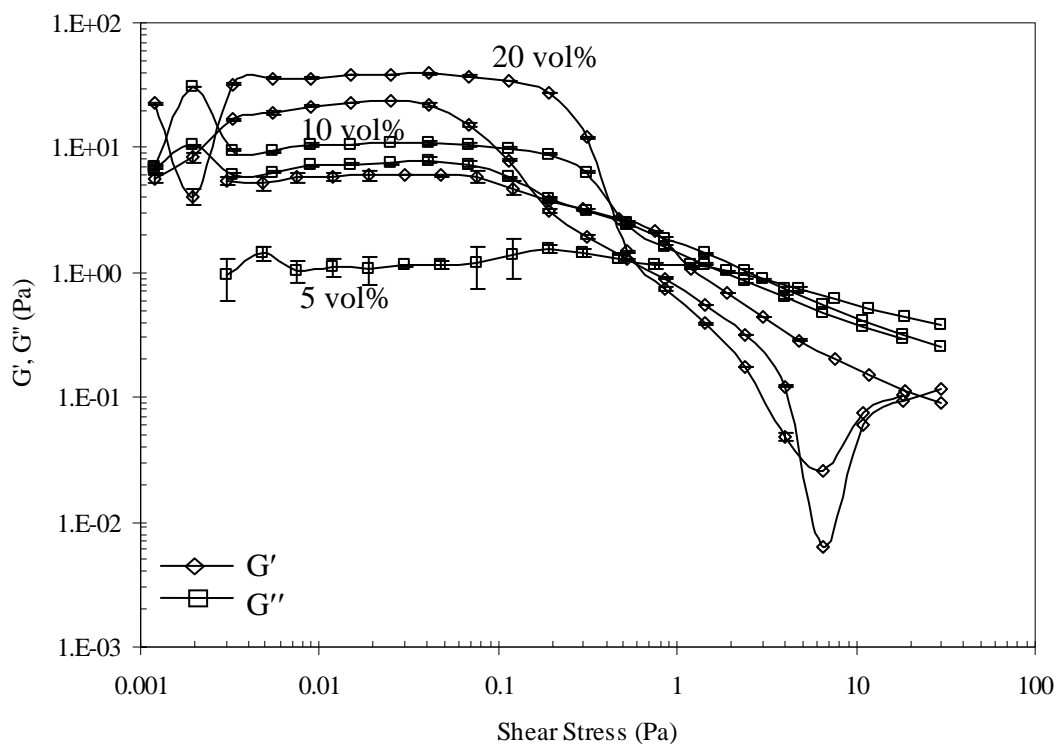
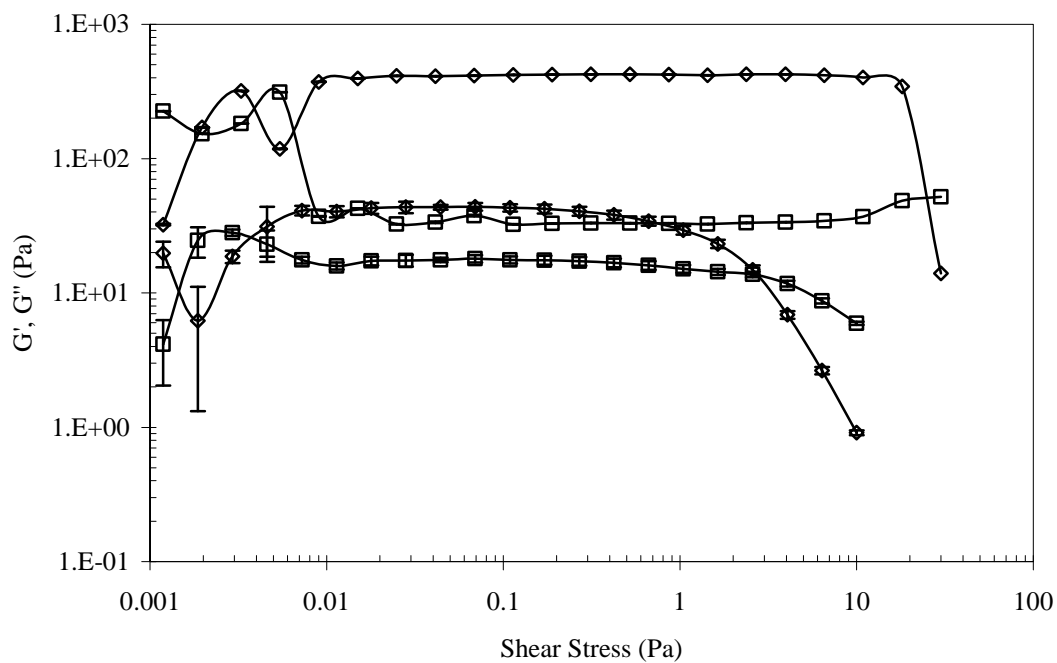


Figure 12. The stress sweeps of submicron alumina dilute dispersions in 40 wt%



fructose solution.
Figure 13. The stress sweeps of submicron alumina concentrated dispersions in 40 wt% fructose solution.

B.4. The frequency sweeps

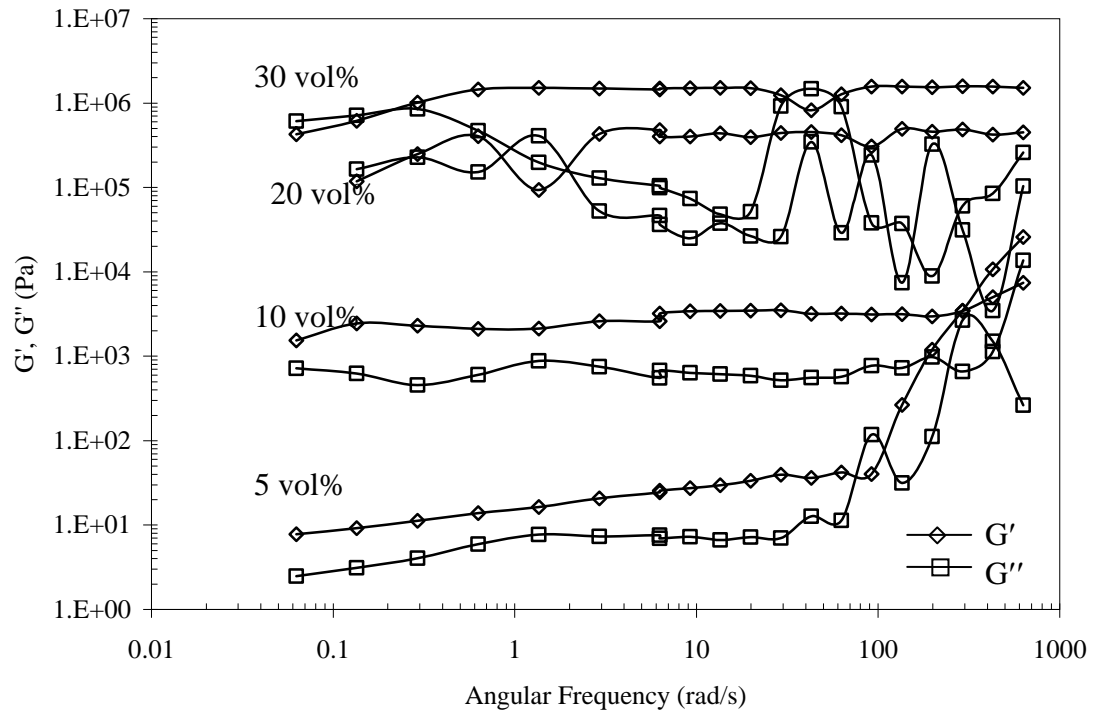


Figure 1. The frequency sweeps of submicron alumina dispersions water.

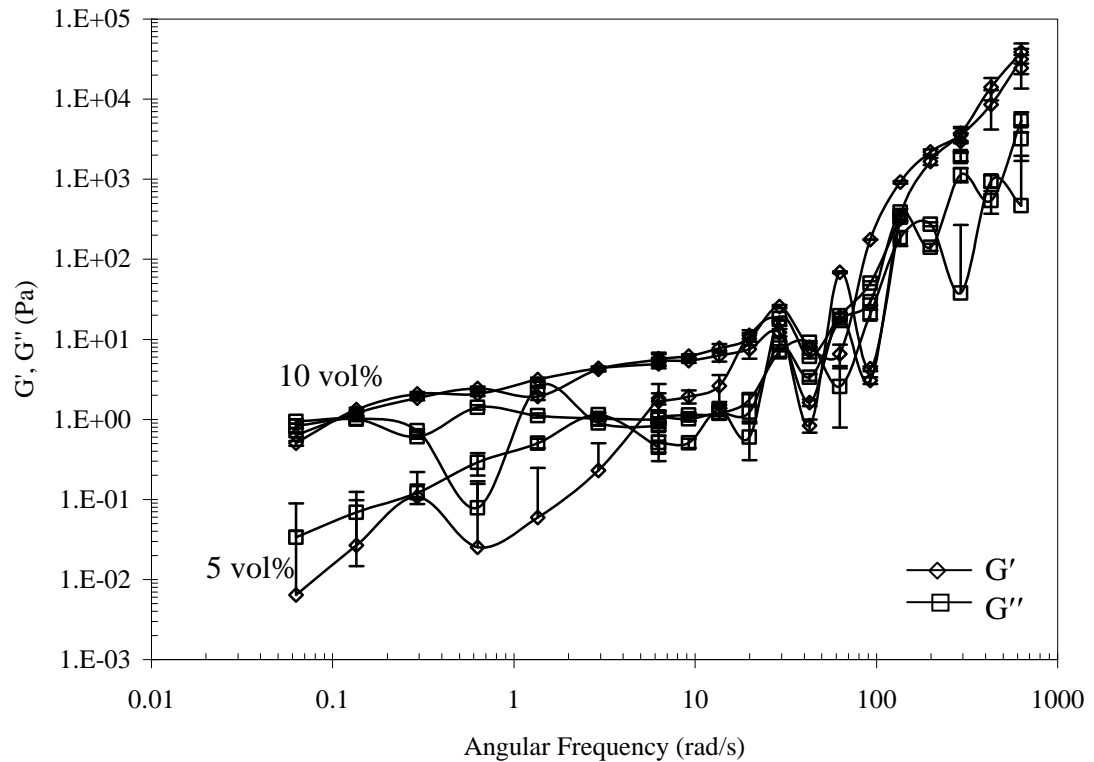


Figure 2. The frequency sweeps of submicron alumina dilute dispersions 1 wt% fructose solution.

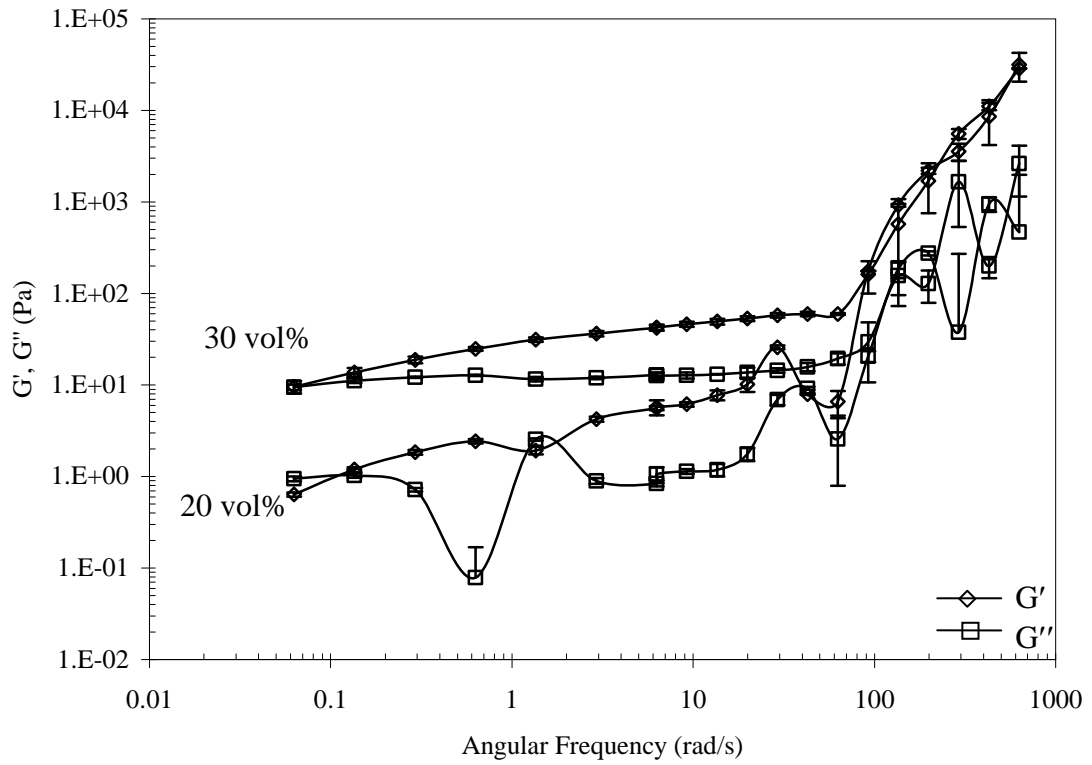


Figure 3. The frequency sweeps of submicron alumina concentrated dispersions 1 wt% fructose solution.

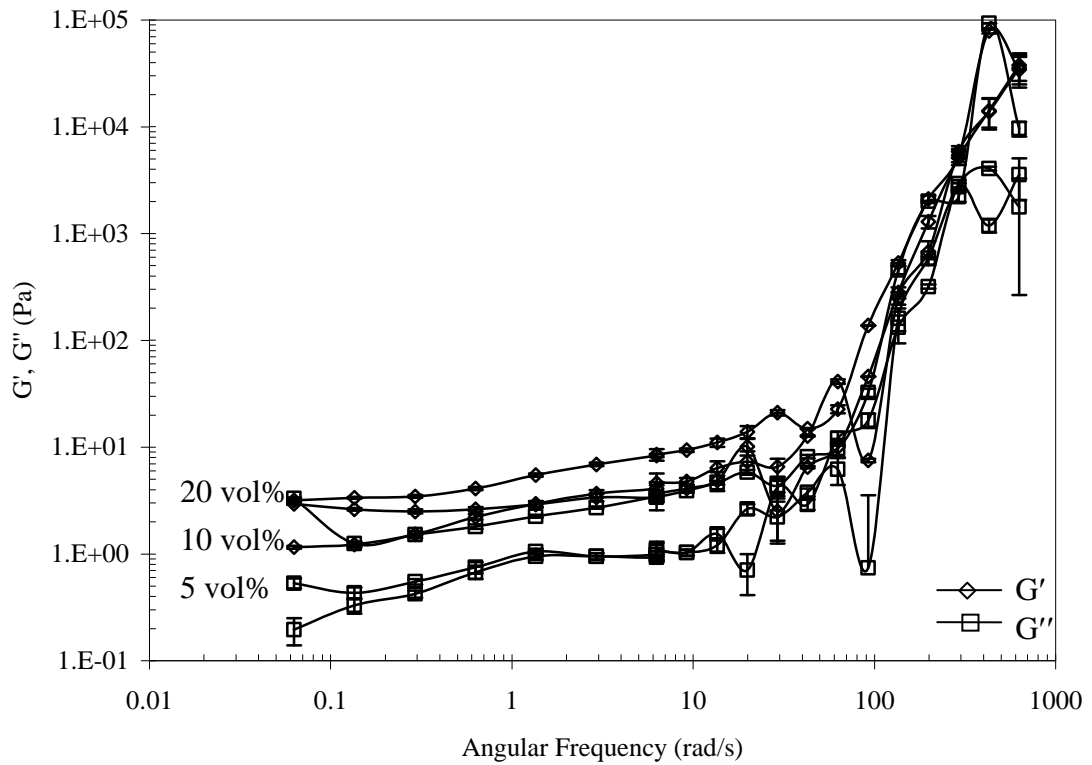


Figure 4. The frequency sweeps of submicron alumina dilute dispersions 4 wt% fructose solution.

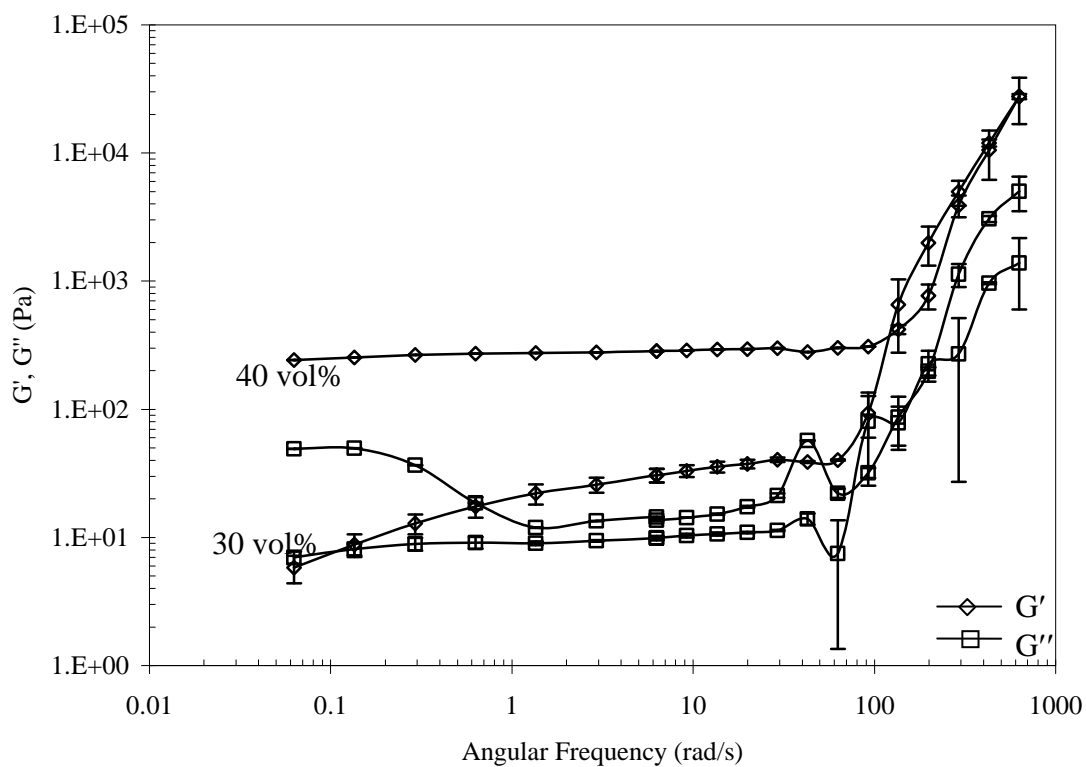


Figure 5. The frequency sweeps of submicron alumina concentrated dispersions 4 wt% fructose solution.

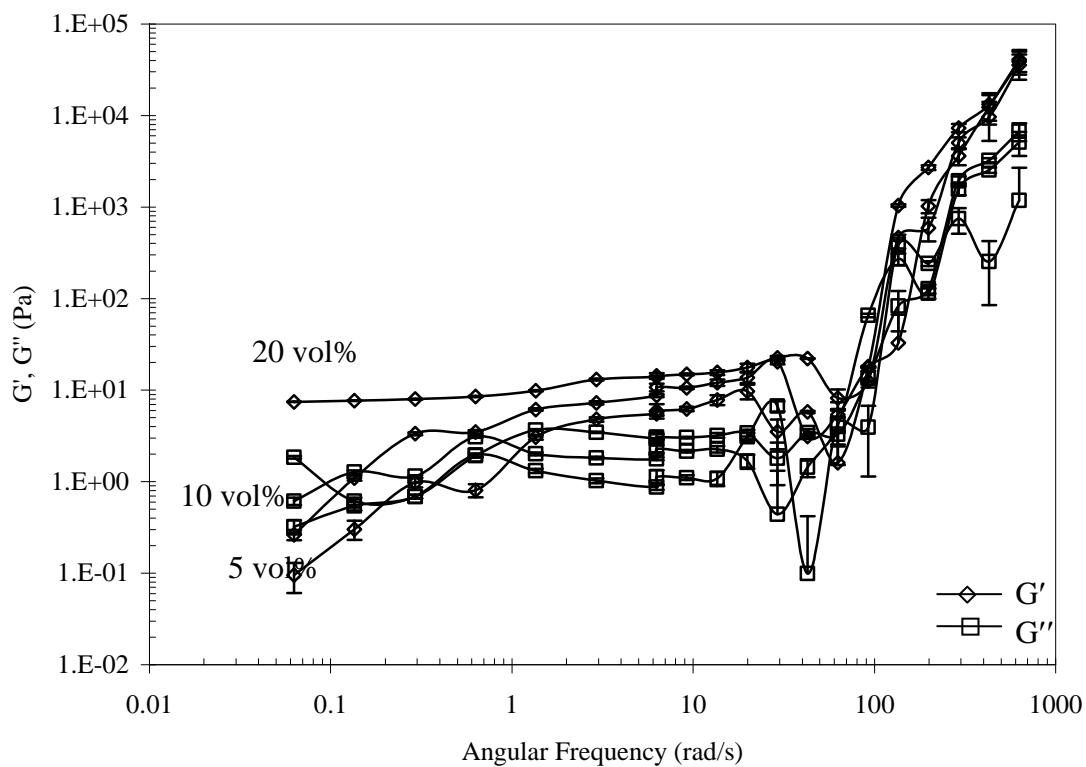


Figure 6. The frequency sweeps of submicron alumina dilute dispersions 10 wt% fructose solution.

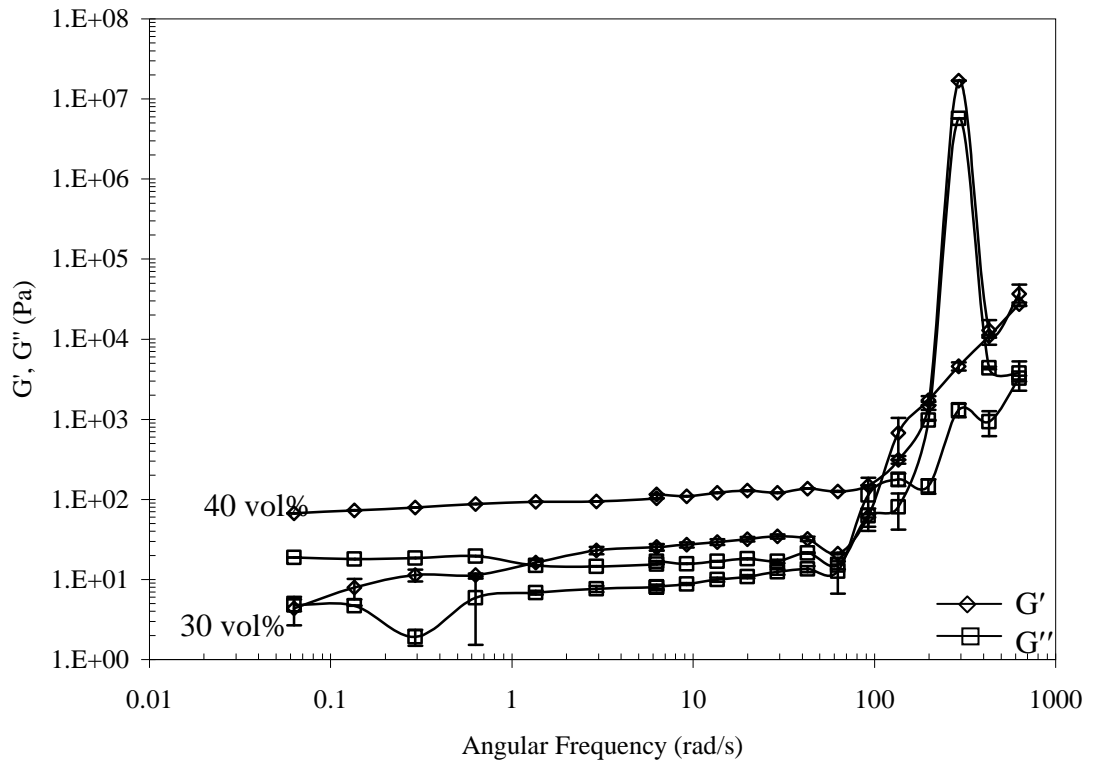


Figure 7. The frequency sweeps of submicron alumina concentrated dispersions 10 wt% fructose solution.

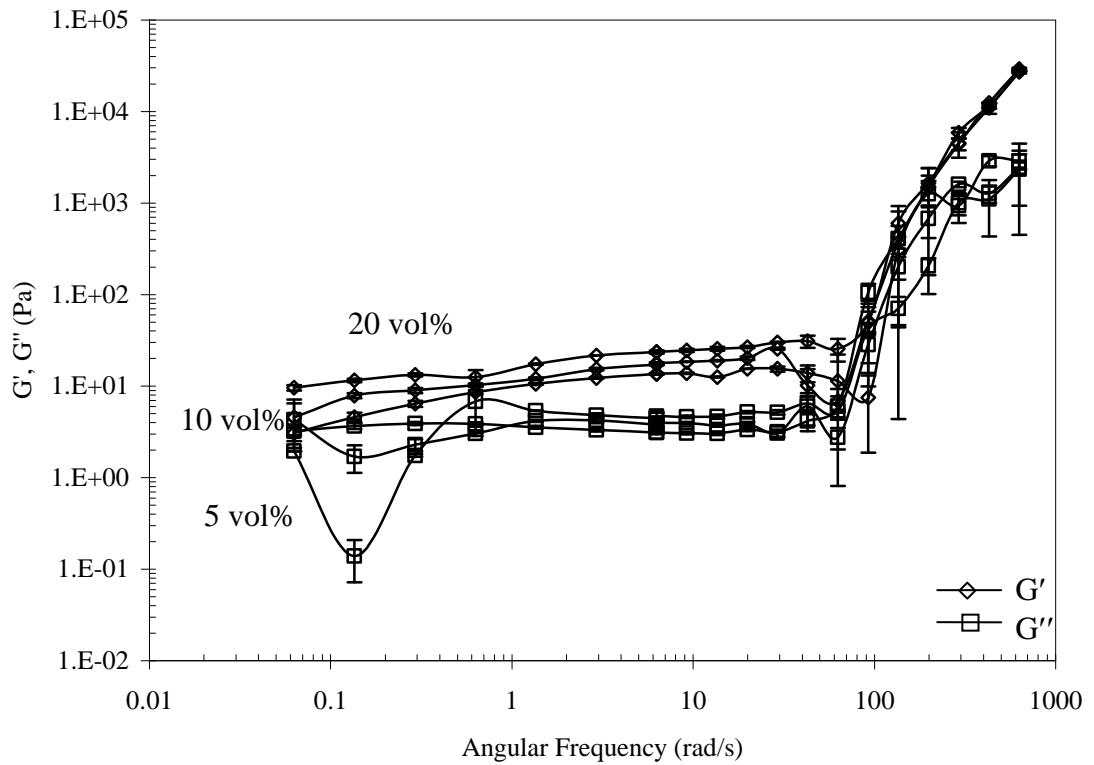


Figure 8. The frequency sweeps of submicron alumina dilute dispersions 20 wt% fructose solution.

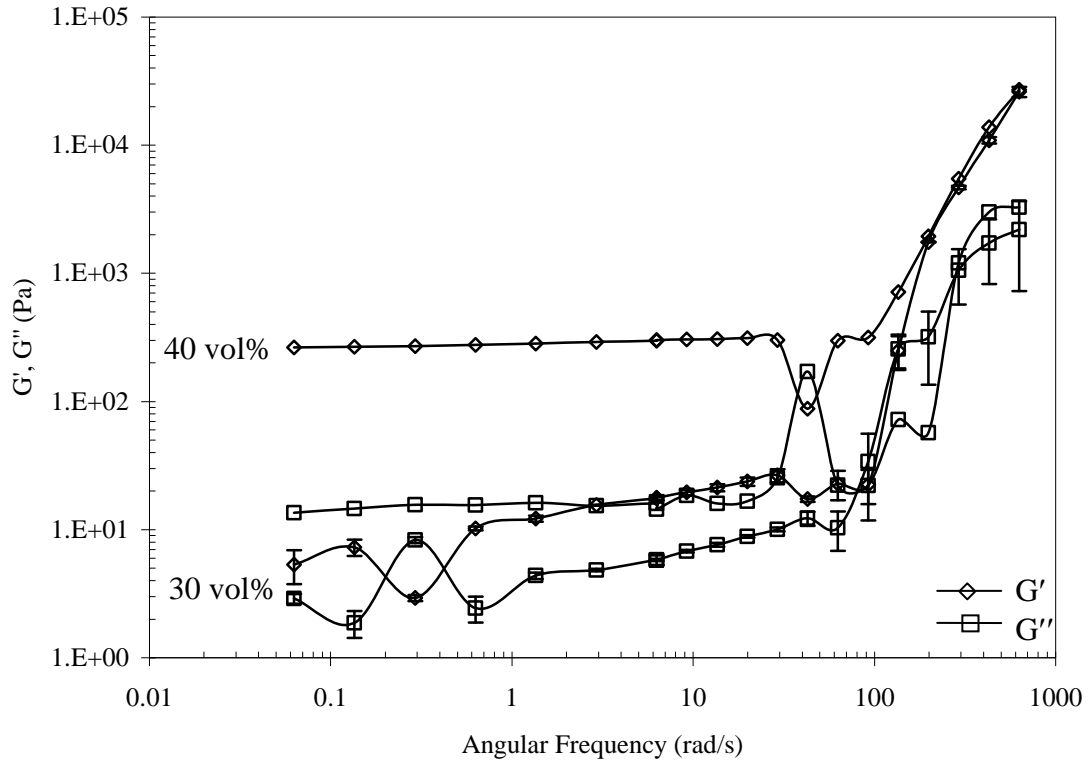


Figure 9. The frequency sweeps of submicron alumina concentrated dispersions 20 wt% fructose solution.

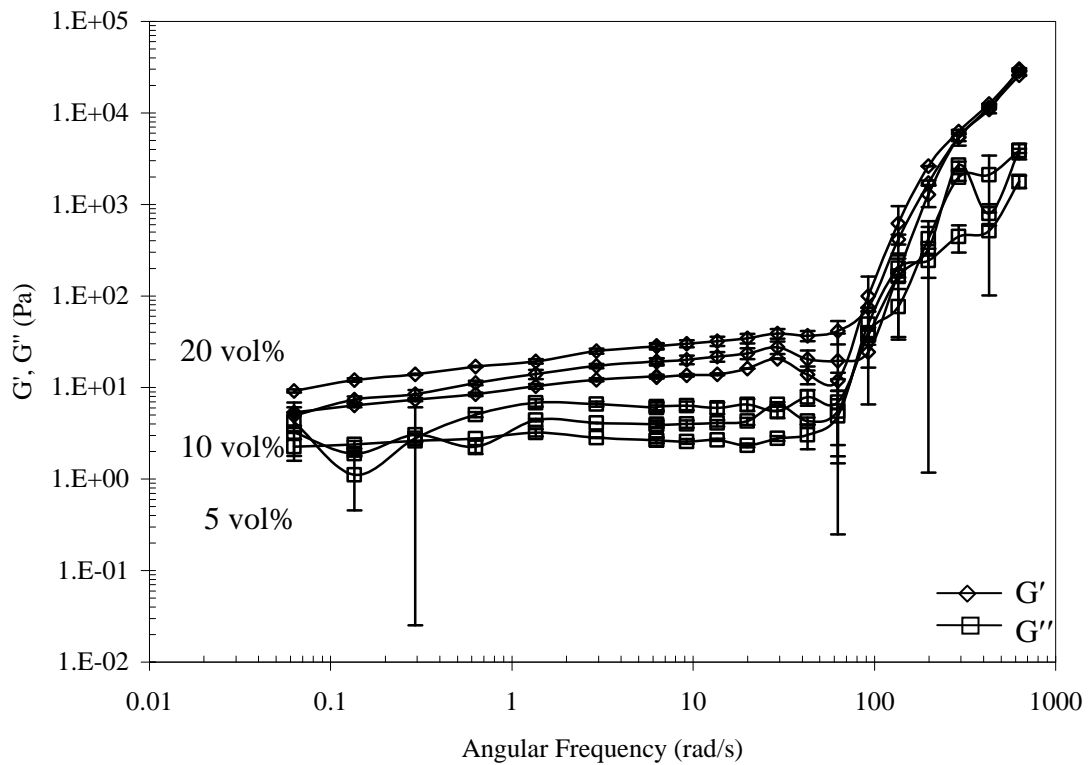


Figure 10. The frequency sweeps of submicron alumina dilute dispersions 30 wt% fructose solution.

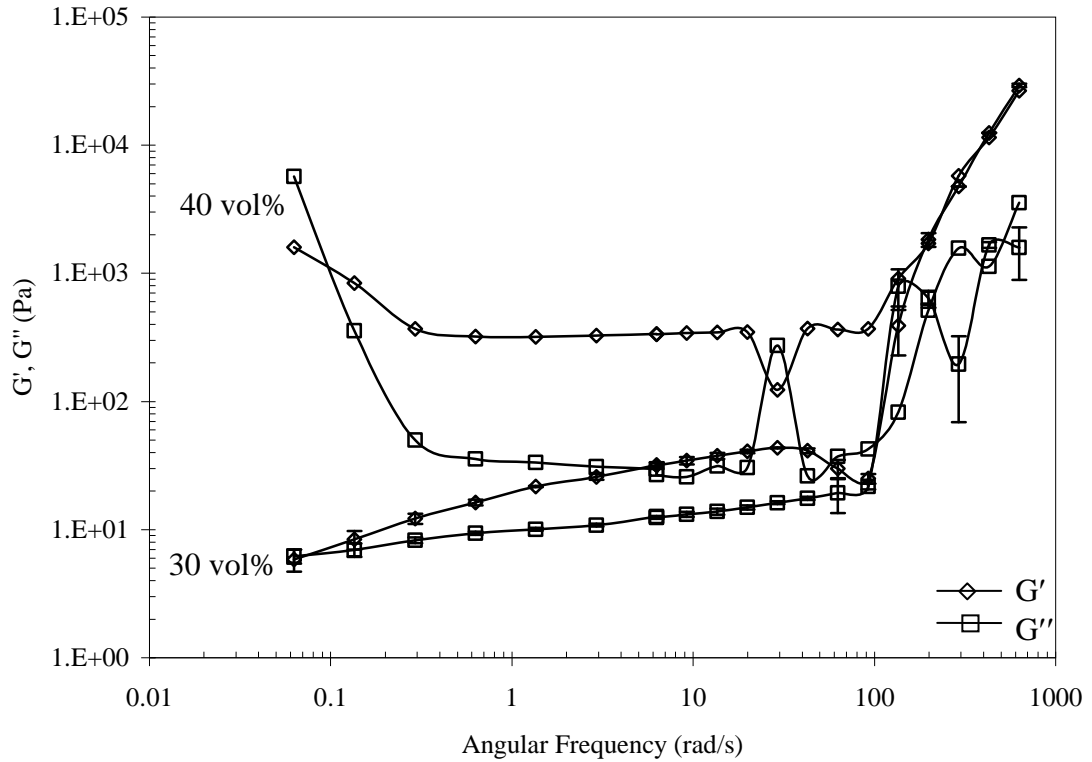


Figure 11. The frequency sweeps of submicron alumina concentrated dispersions 30 wt% fructose solution.

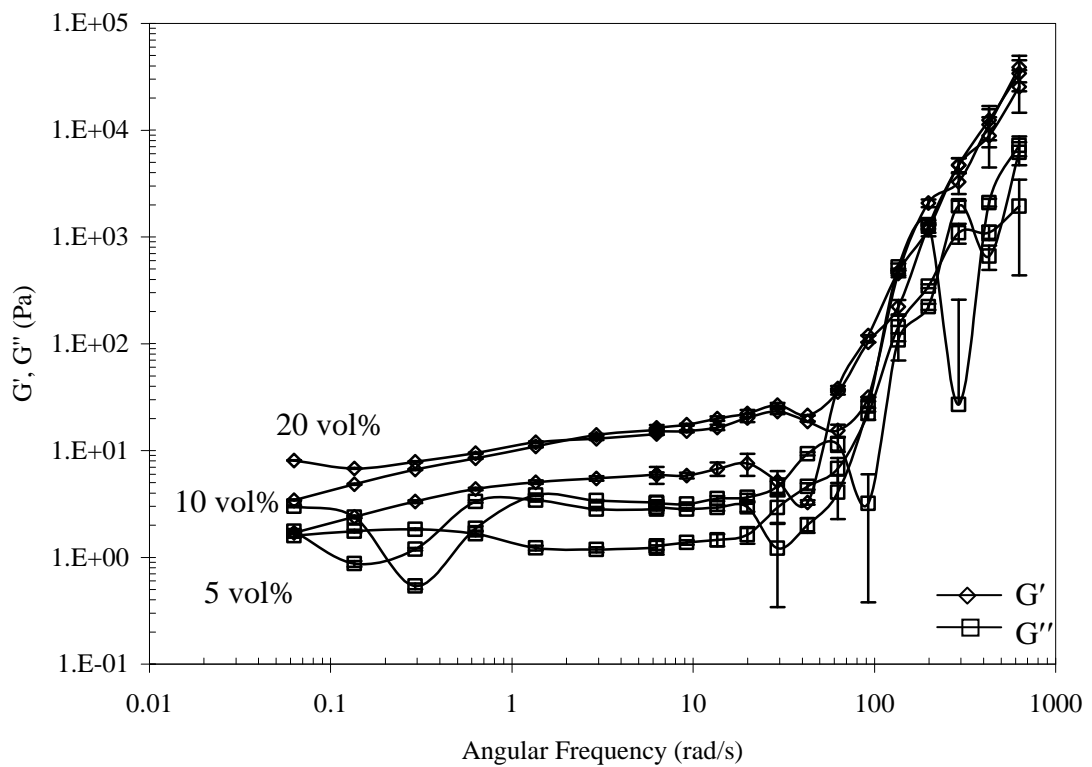


Figure 12. The frequency sweeps of submicron alumina dilute dispersions 40 wt% fructose solution.

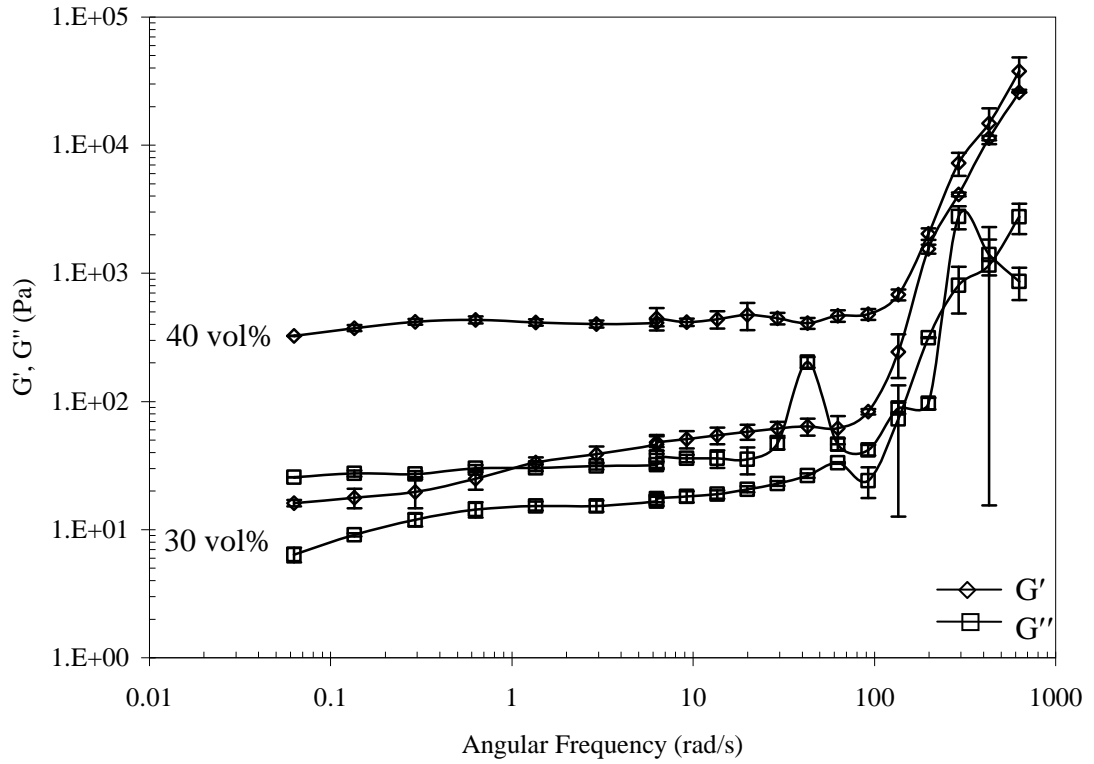


Figure 13. The frequency sweeps of submicron alumina concentrated dispersions 40 wt% fructose solution.

APPENDIX C. THE RHEOLOGICAL BEHAVIOR OF NANO ALUMINA DISPERSIONS

C.1. The flow and viscosity curves

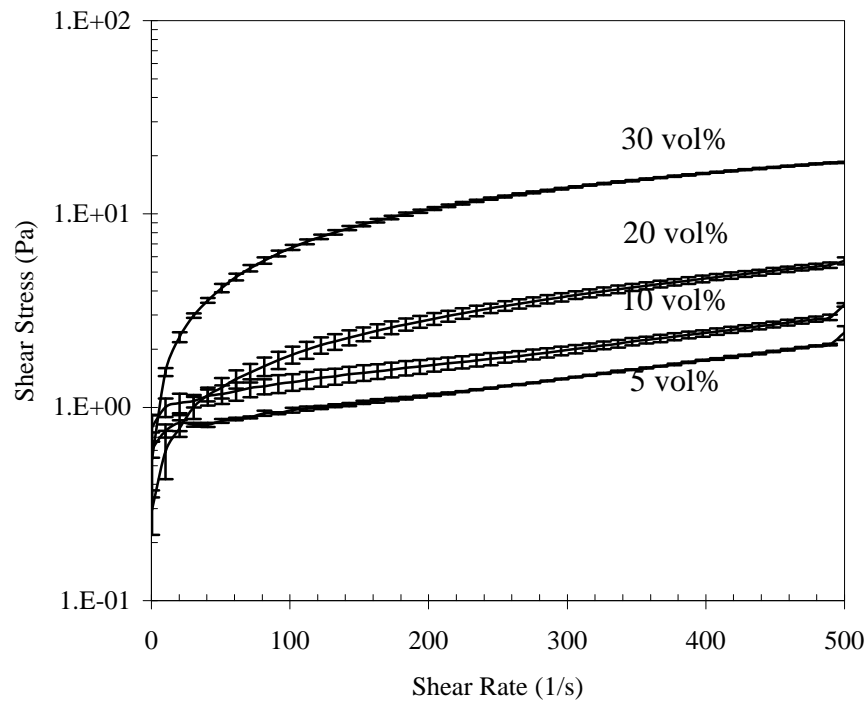


Figure 1. The flow curves of nano alumina dispersions without fructose.

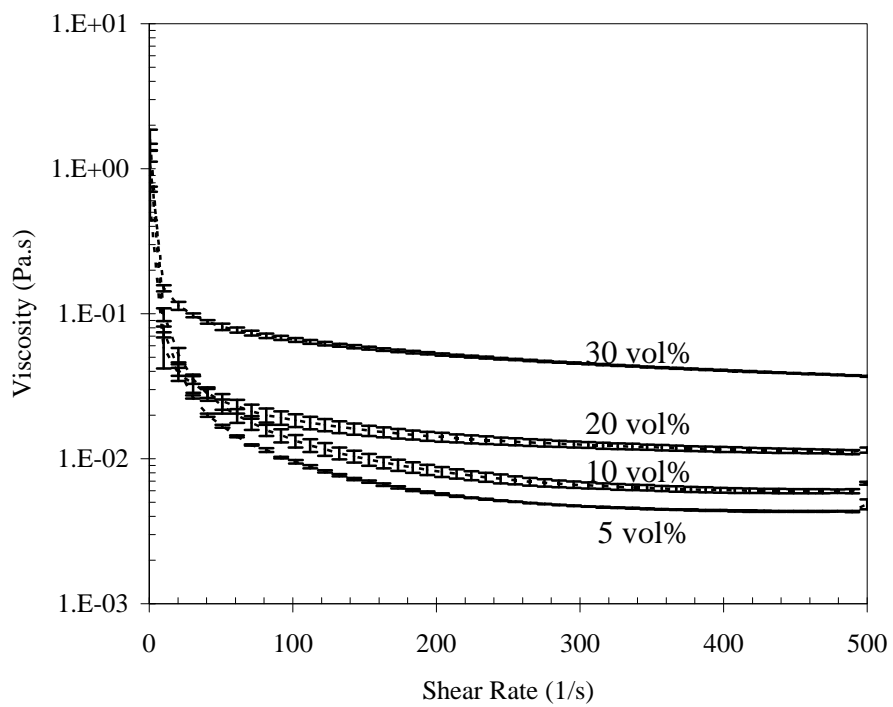


Figure 2. The viscosity curves of nano alumina dispersions without fructose.

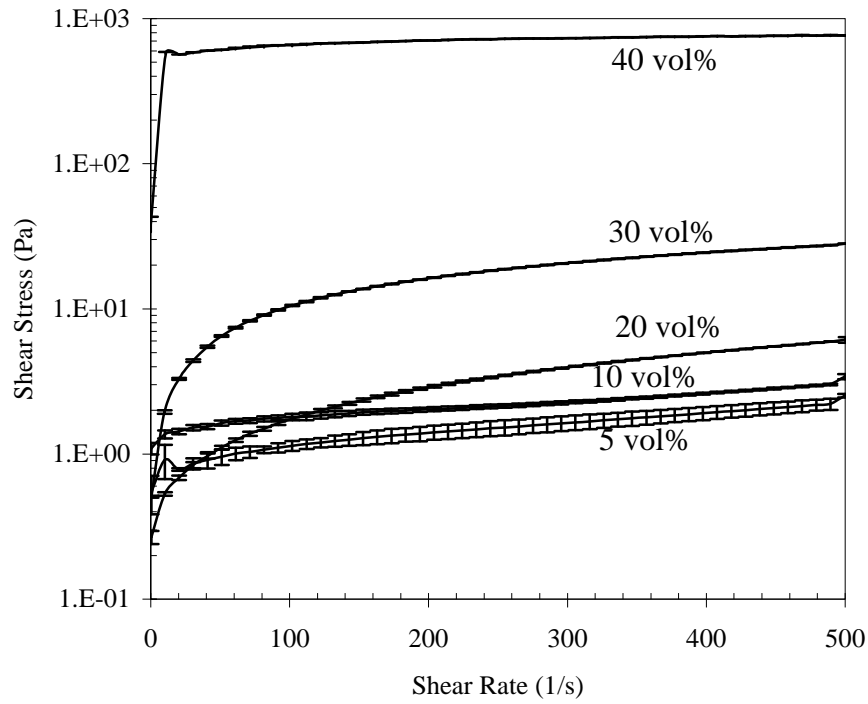


Figure 3. The flow curves of nano alumina dispersions in 1 wt% fructose solution.

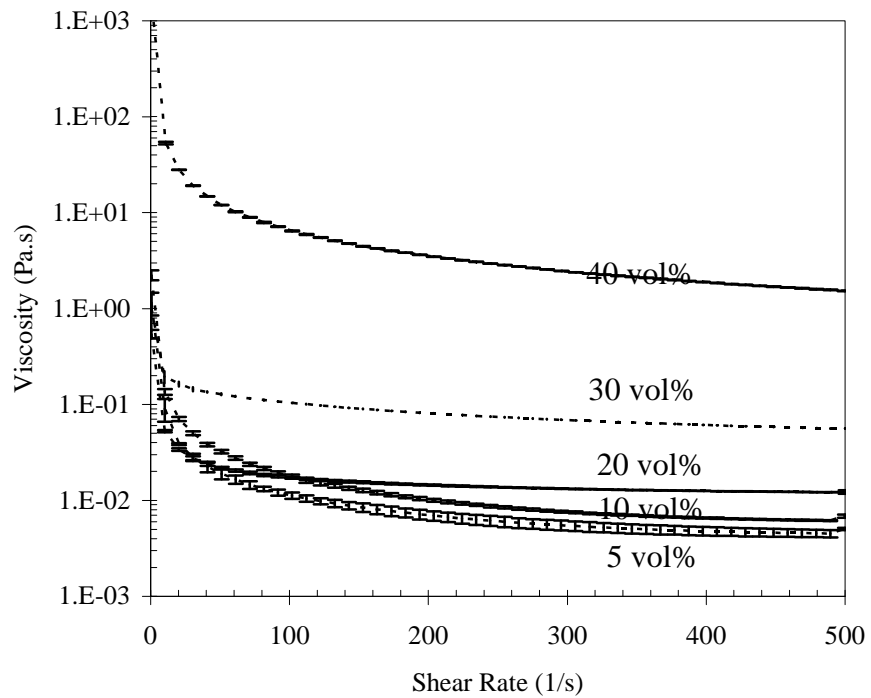


Figure 4. The viscosity curves of nano alumina dispersions in 1 wt% fructose solution.

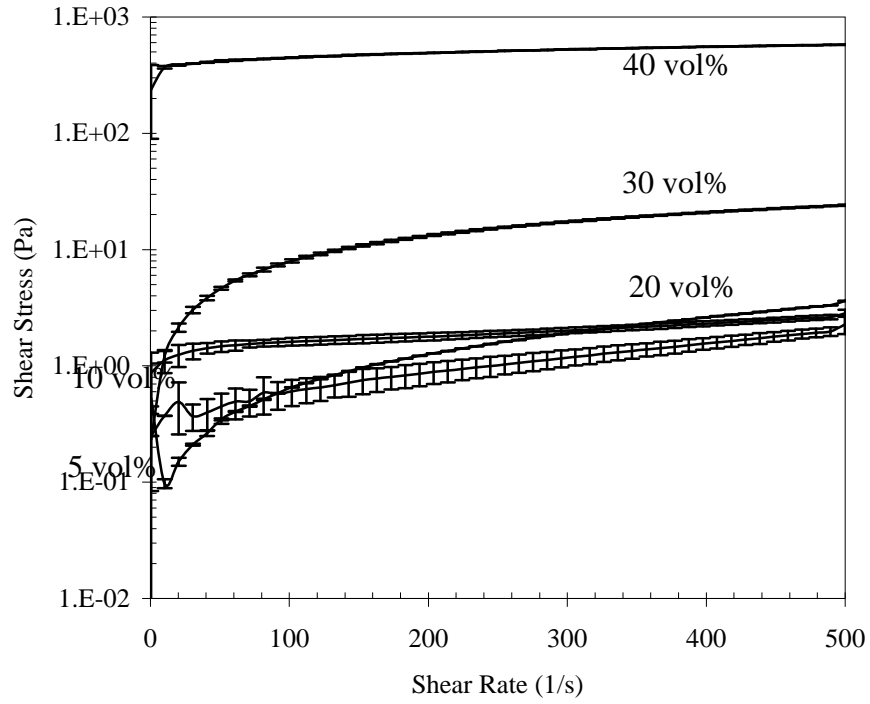


Figure 5. The flow curves of nano alumina dispersions in 4wt% fructose solution.

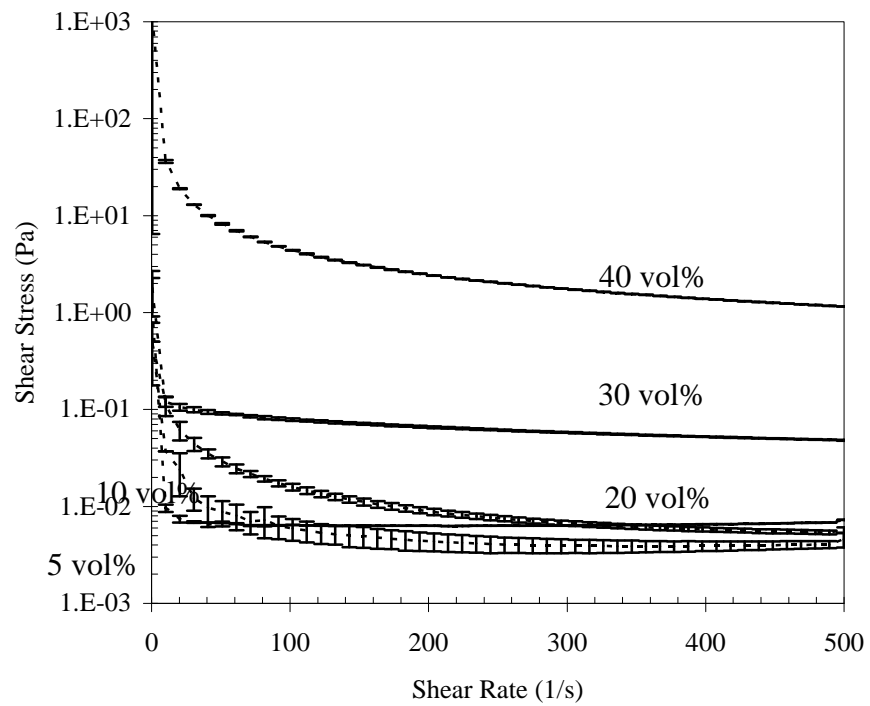


Figure 6. The viscosity curves of nano alumina dispersions in 4 wt% fructose solution.

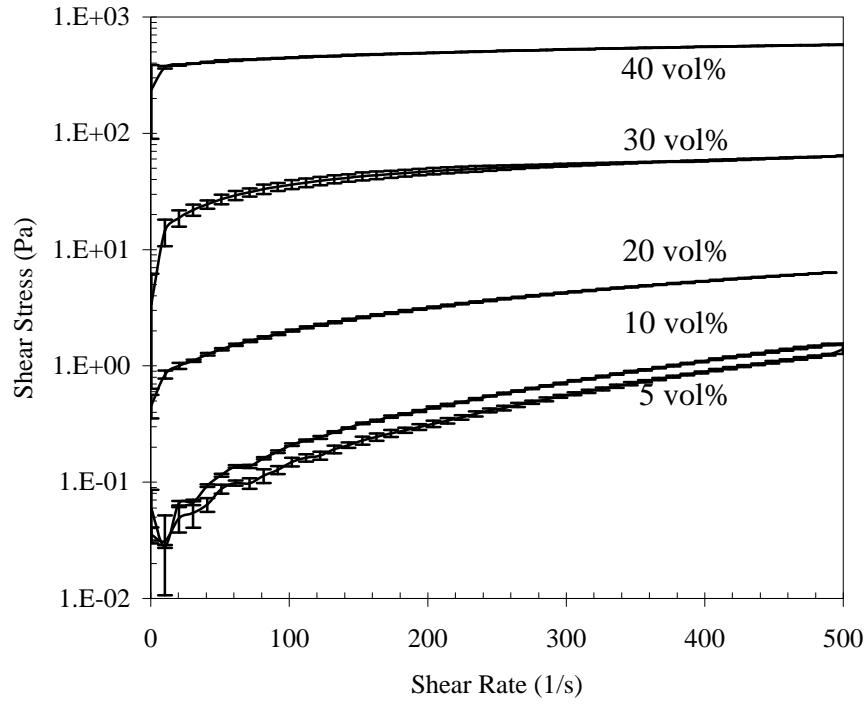


Figure 7. The flow curves of nano alumina dispersions in 10wt% fructose solution.

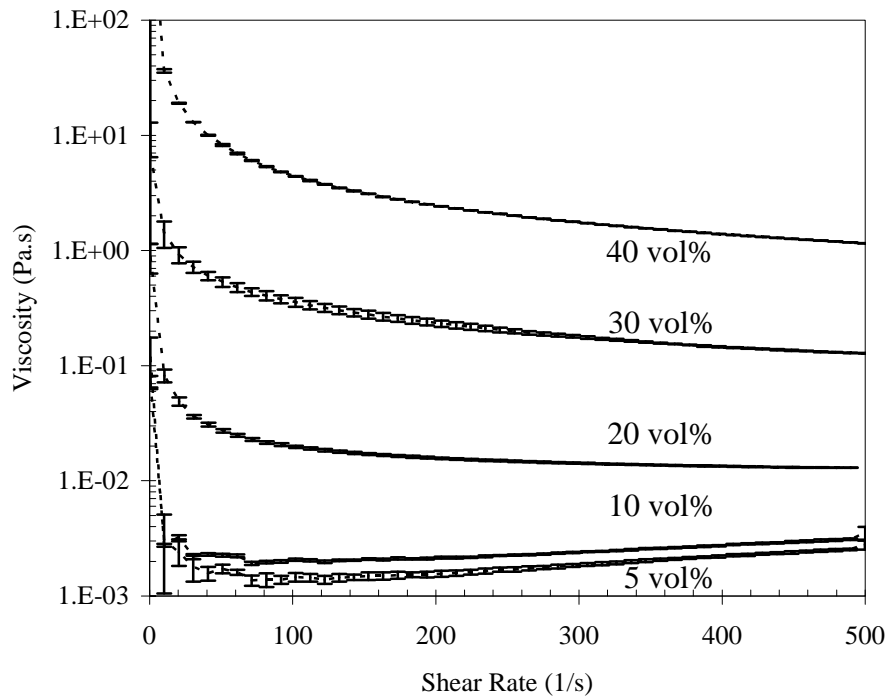


Figure 8. The viscosity curves of nano alumina dispersions in 10 wt% fructose solution.

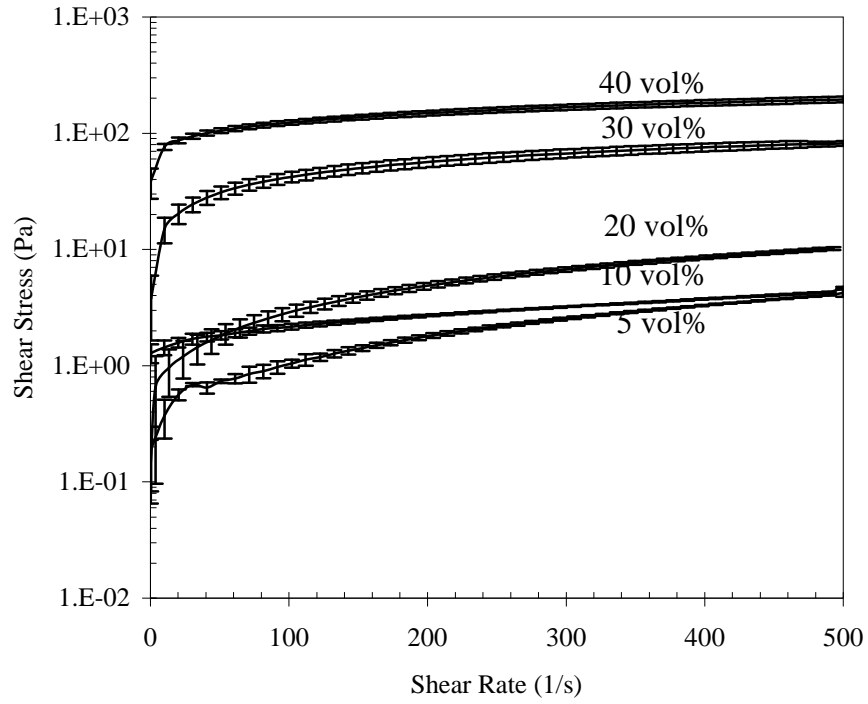


Figure 9. The flow curves of nano alumina dispersions in 20wt% fructose solution.

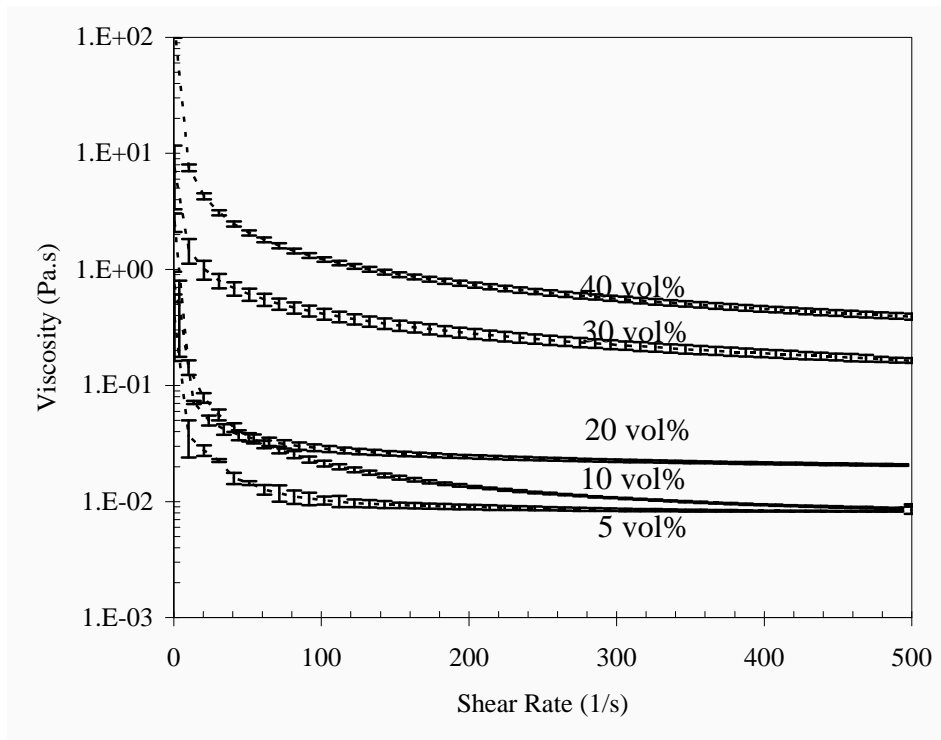


Figure 10. The viscosity curves of nano alumina dispersions in 20 wt% fructose solution.

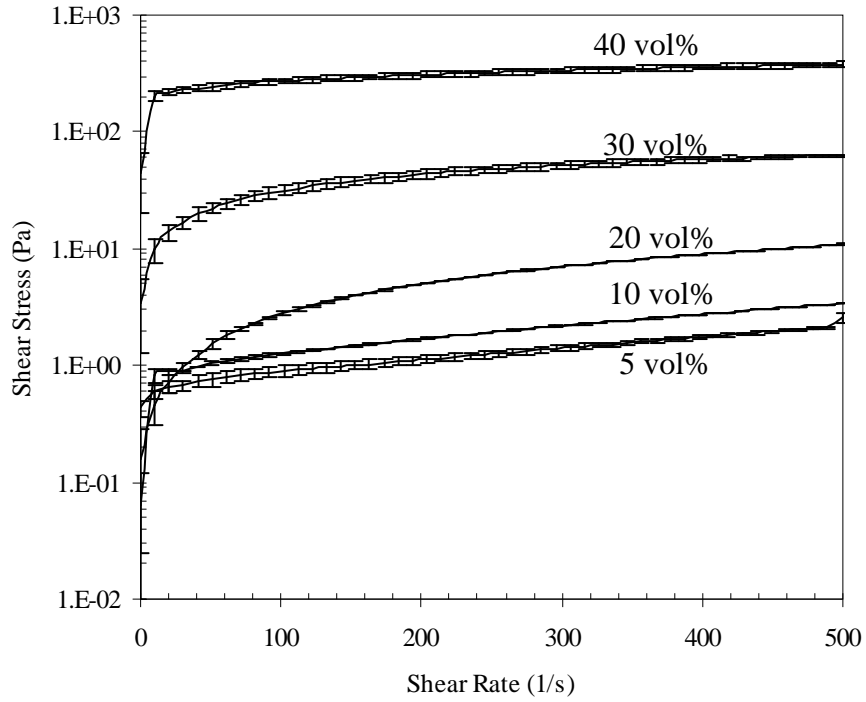


Figure 11. The flow curves of nano alumina dispersions in 30wt% fructose solution.

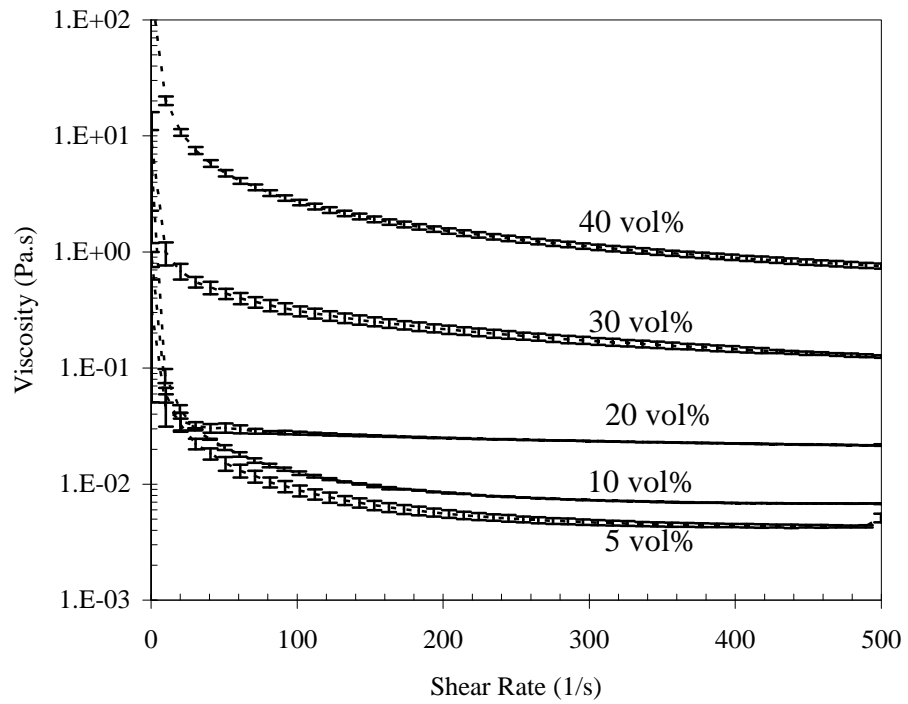


Figure 12. The viscosity curves of nano alumina dispersions in 30 wt% fructose solution.

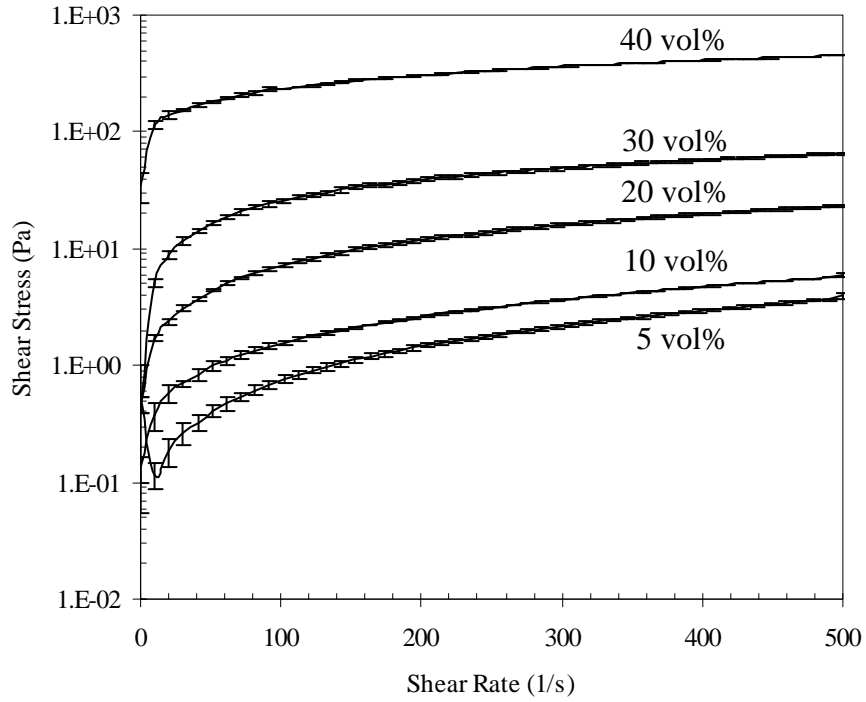


Figure 13. The flow curves of nano alumina dispersions in 40wt% fructose solution.

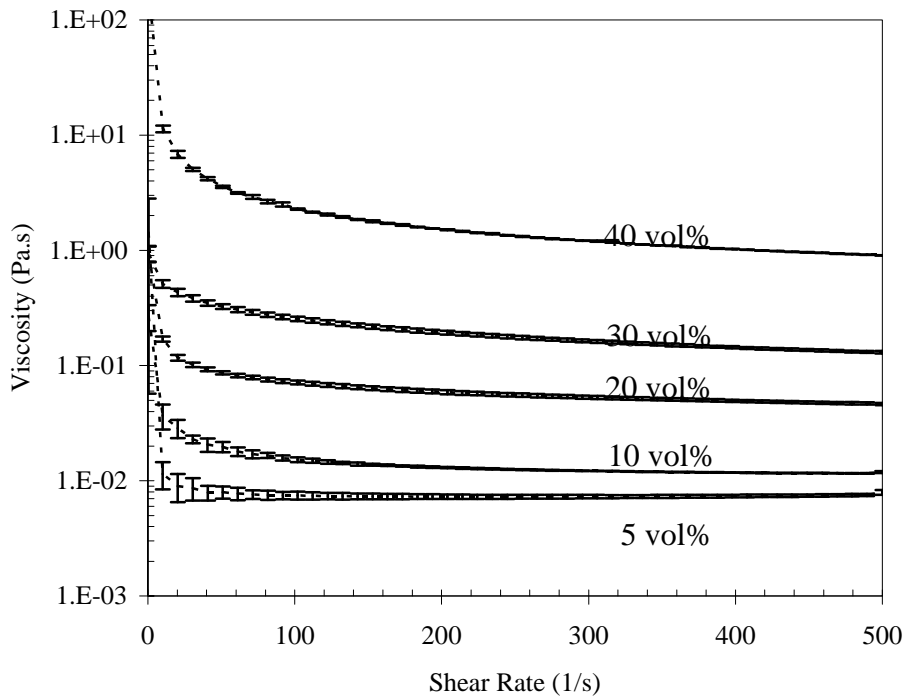


Figure 14. The viscosity curves of nano alumina dispersions in 40 wt% fructose solution.

C.2. The thixotropy curves

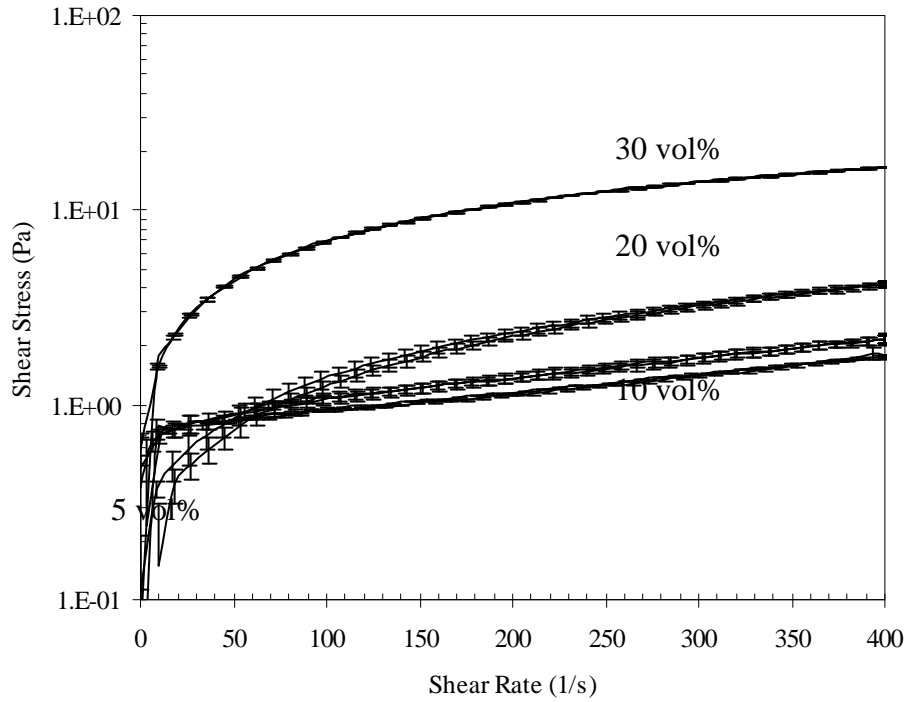


Figure 1. The thixotropy curves of nano alumina in water.

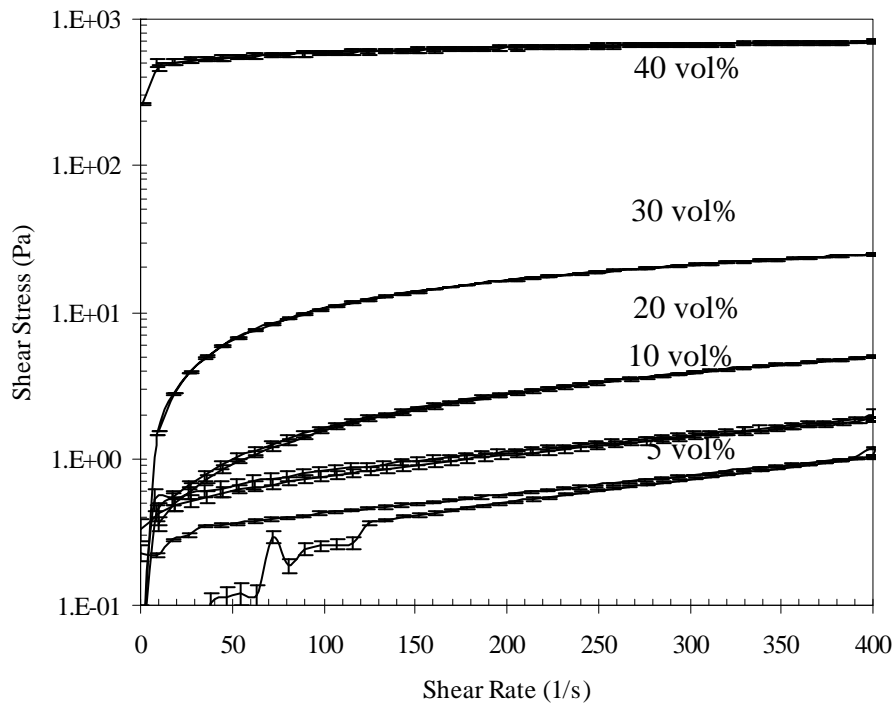


Figure 2. The thixotropy curves of nano alumina in 1 wt% fructose solution.

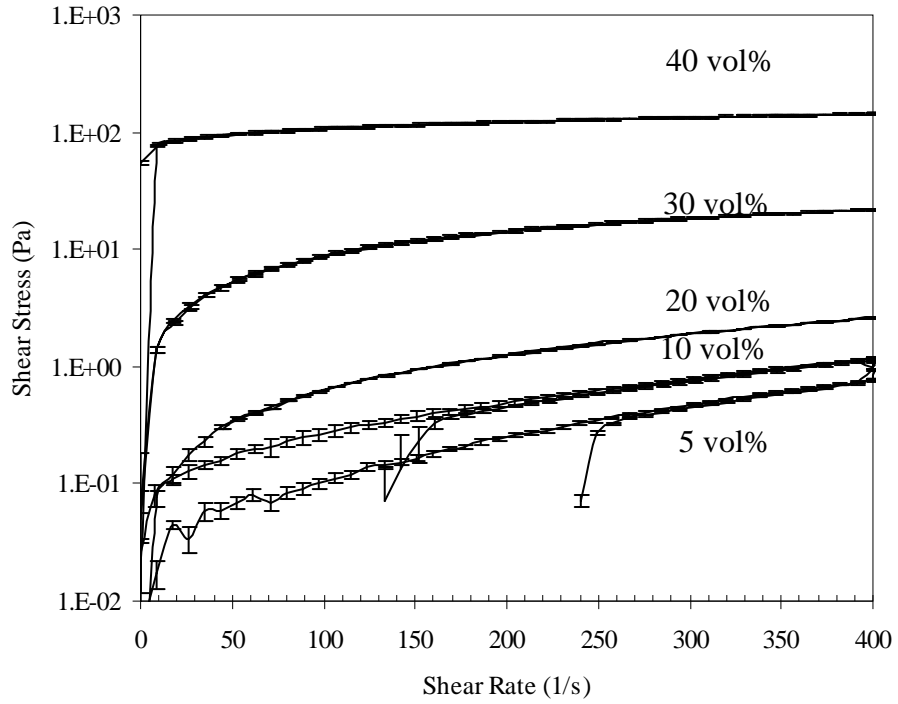


Figure 3. The thixotropy curves of nano alumina in 4 wt% fructose solution.

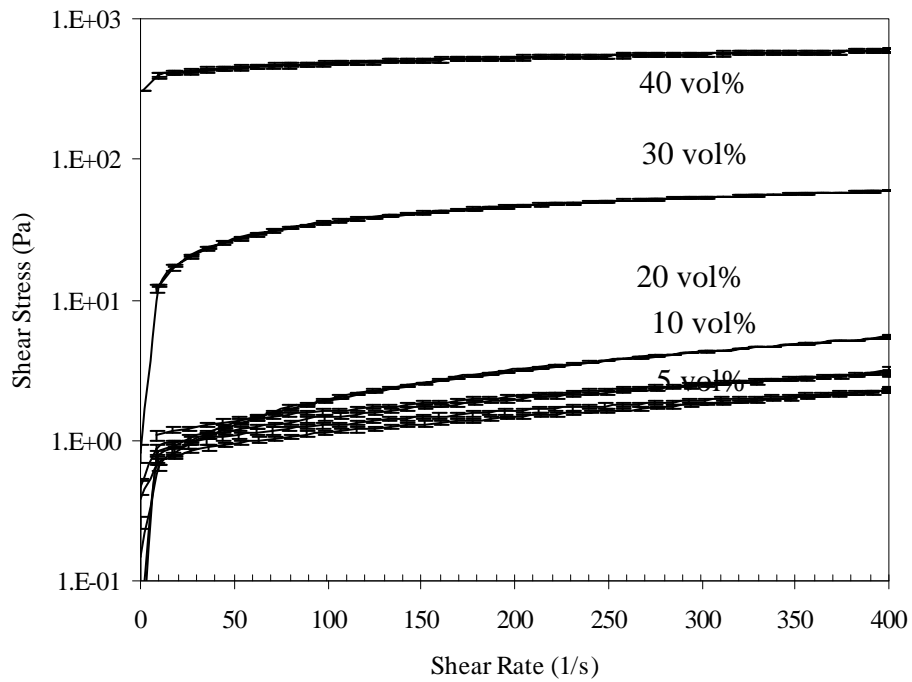


Figure 4. The thixotropy curves of nano alumina in 10 wt% fructose solution.

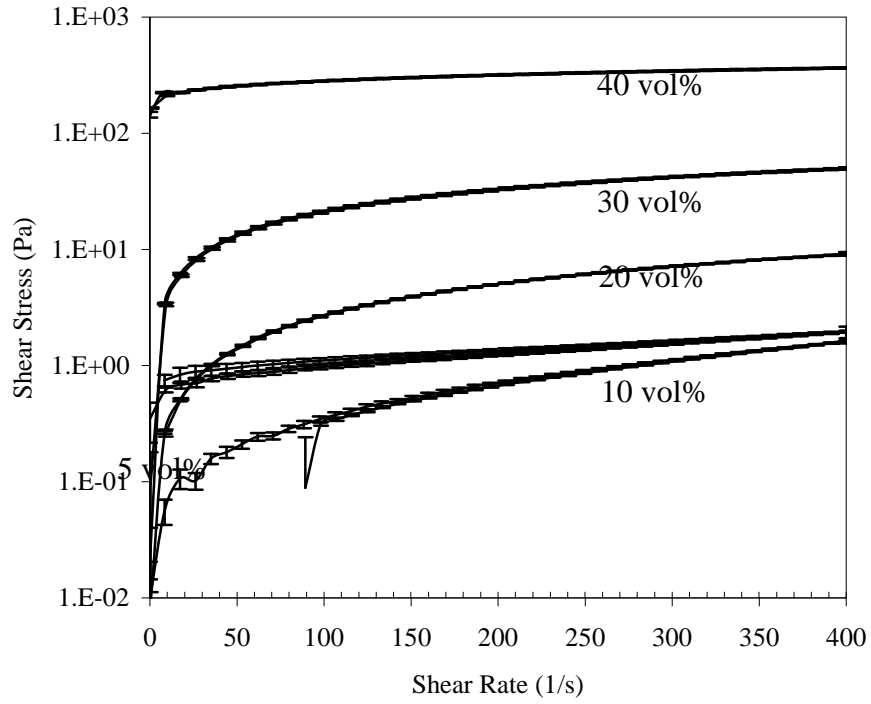


Figure 5. The thixotropy curves of nano alumina in 20 wt% fructose solution.

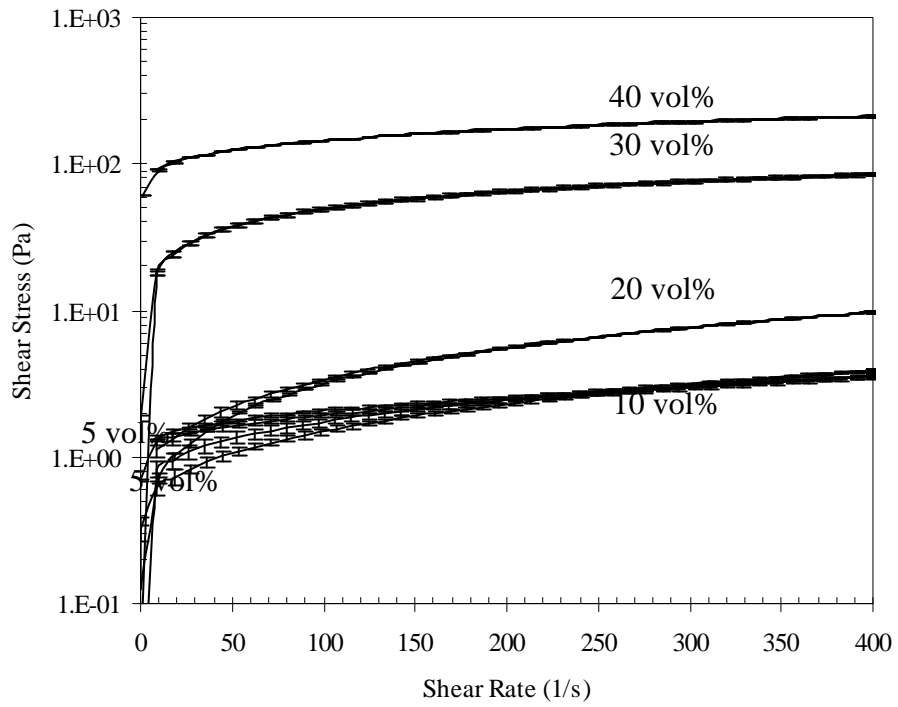


Figure 6. The thixotropy curves of nano alumina in 30 wt% fructose solution.

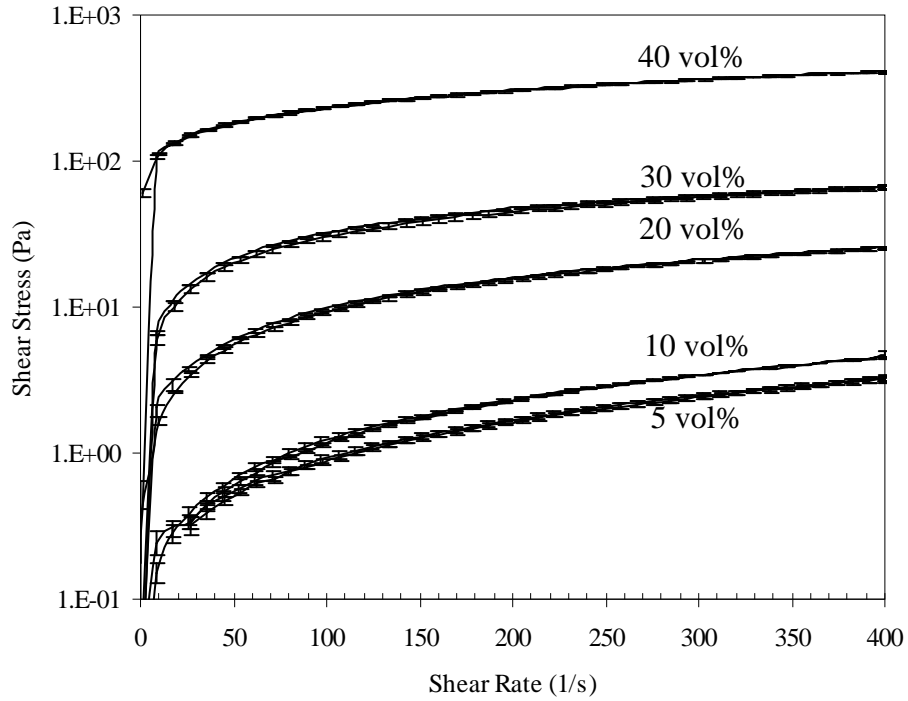


Figure 7. The thixotropy curves of nano alumina in 40 wt% fructose solution.

C.3. The stress sweeps

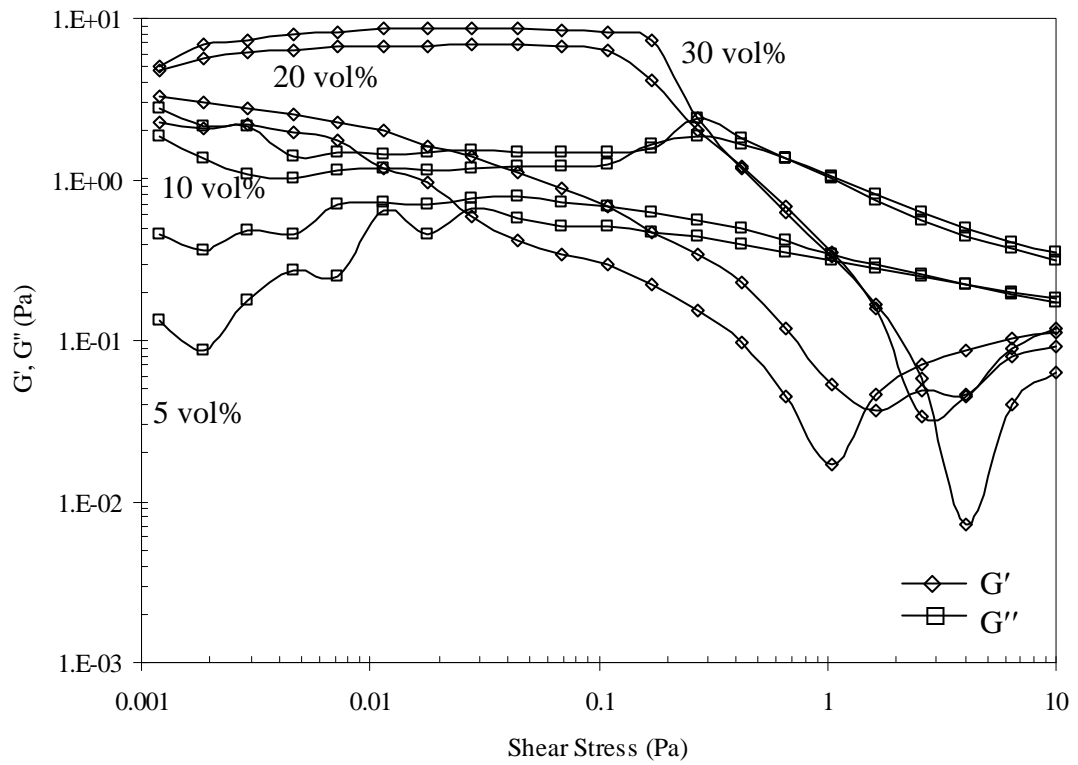


Figure 1. The stress sweeps of nano alumina dispersions in water.

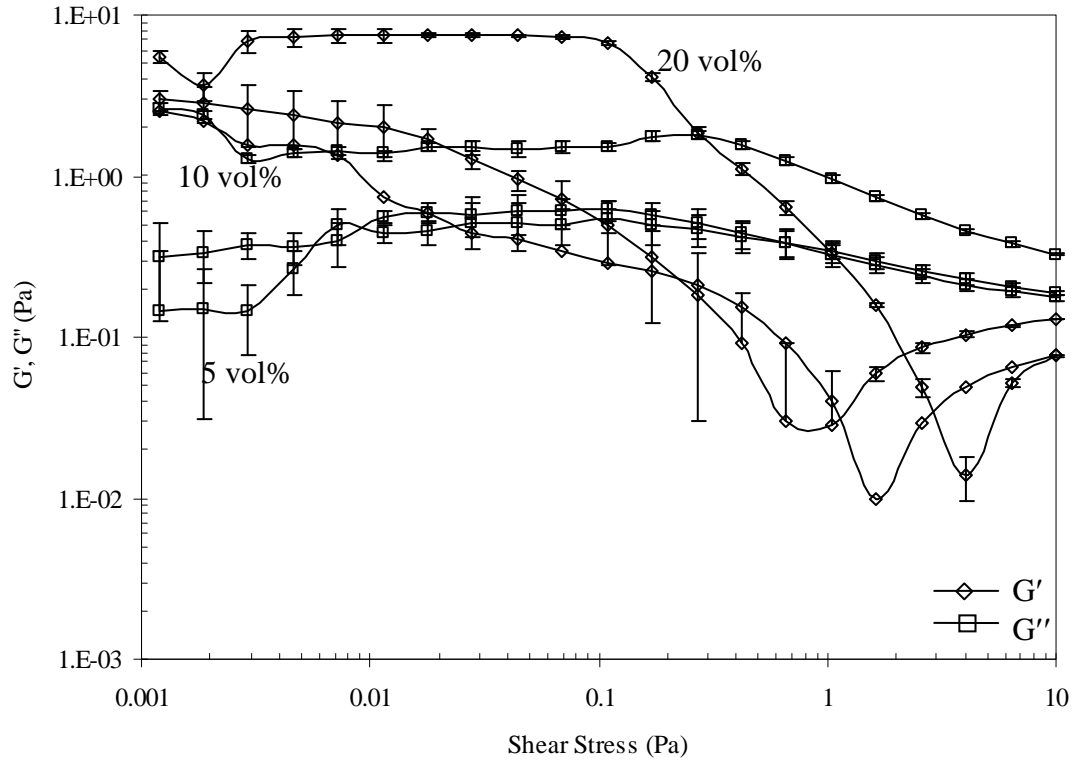


Figure 2. The stress sweeps of nano alumina dilute dispersions in 1 wt% fructose solution.

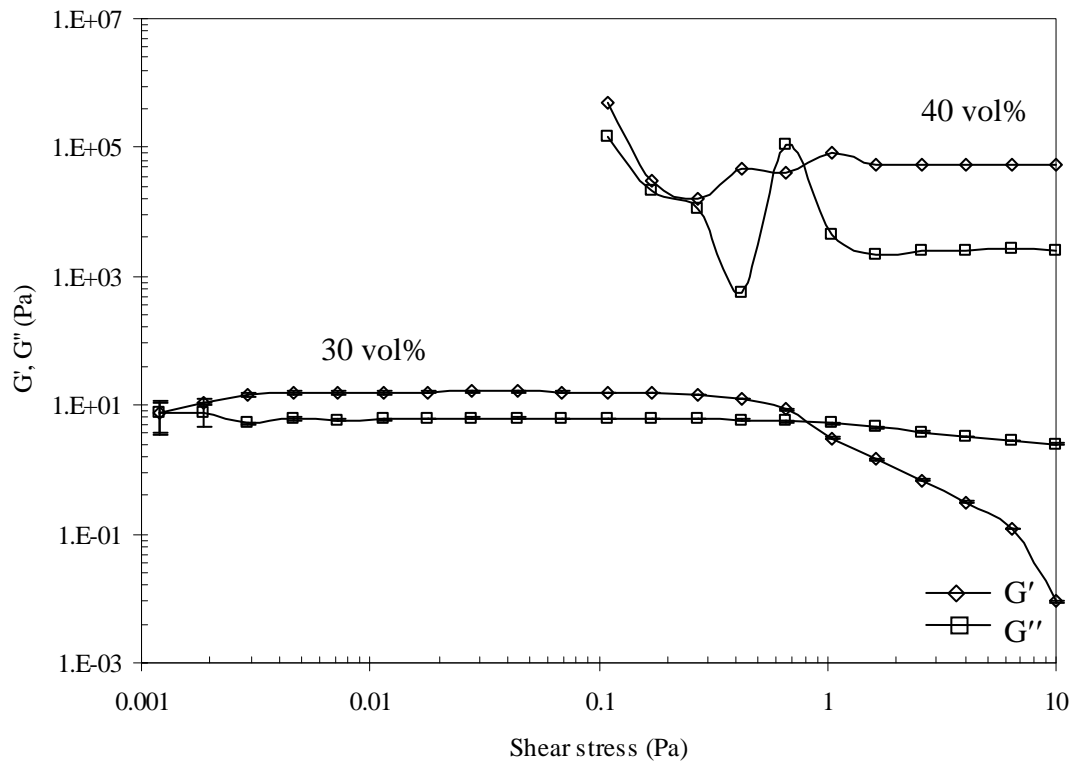


Figure 3. The stress sweeps of nano alumina concentrated dispersions in 1 wt% fructose solution.

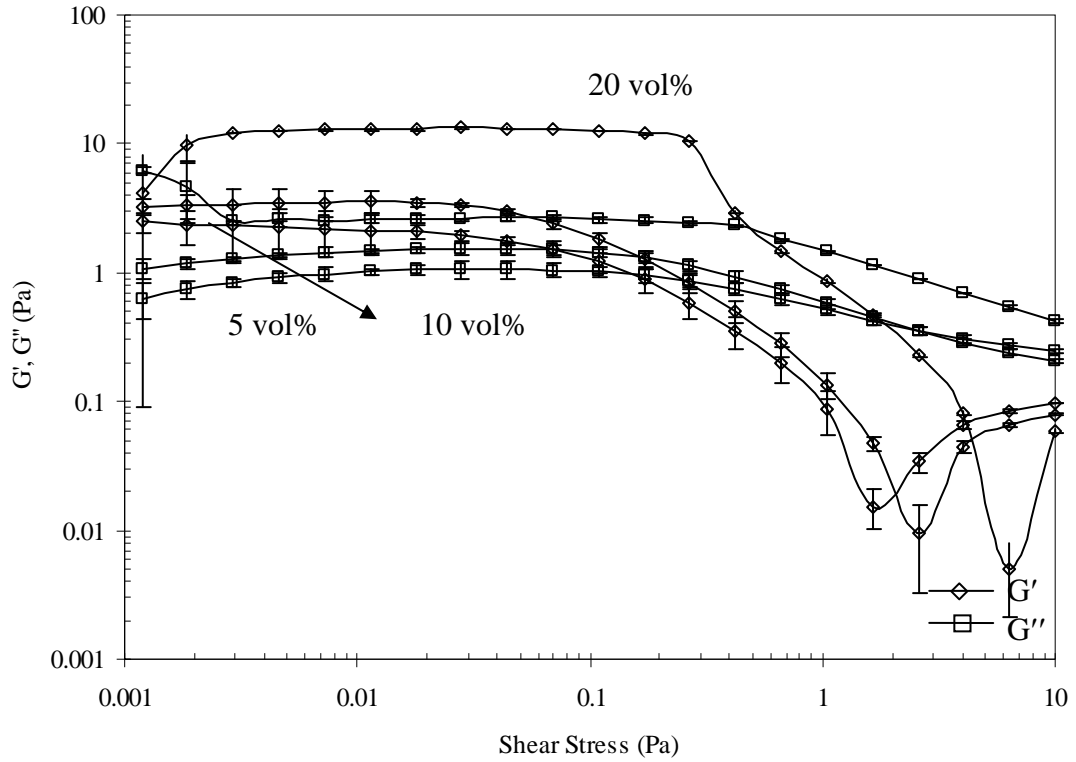


Figure 4. The stress sweeps of nano alumina dilute dispersions in 4 wt% fructose solution.

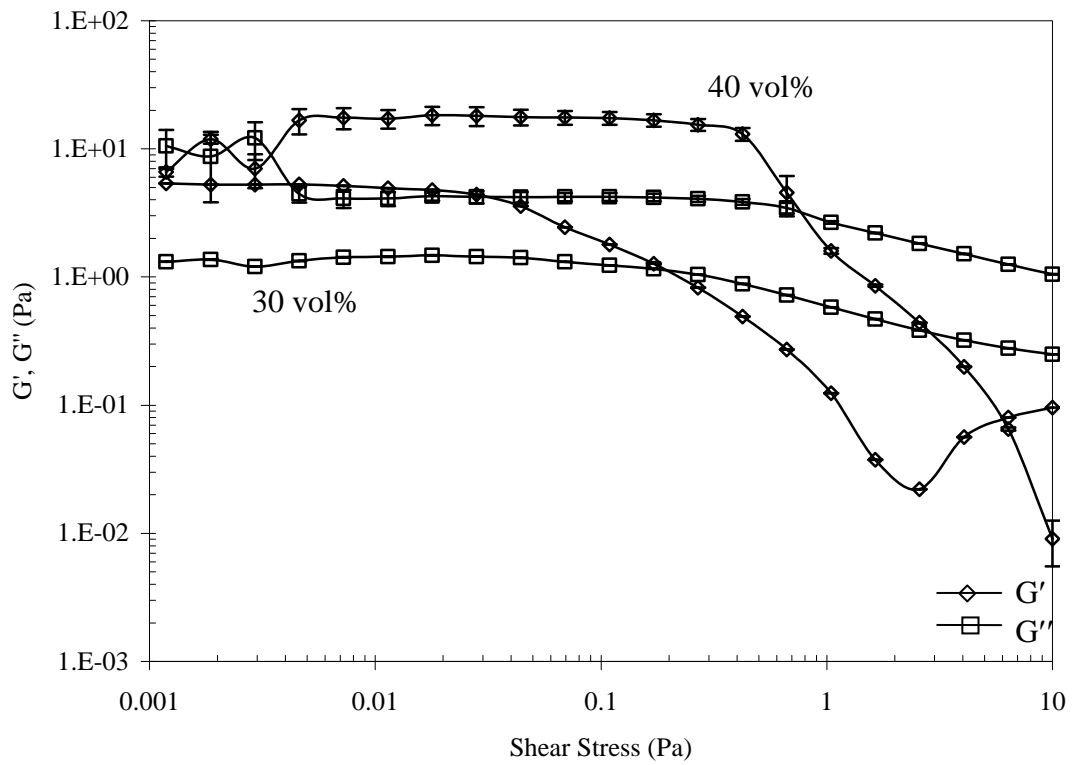


Figure 5. The stress sweeps of nano alumina concentrated dispersions in 4 wt% fructose solution.

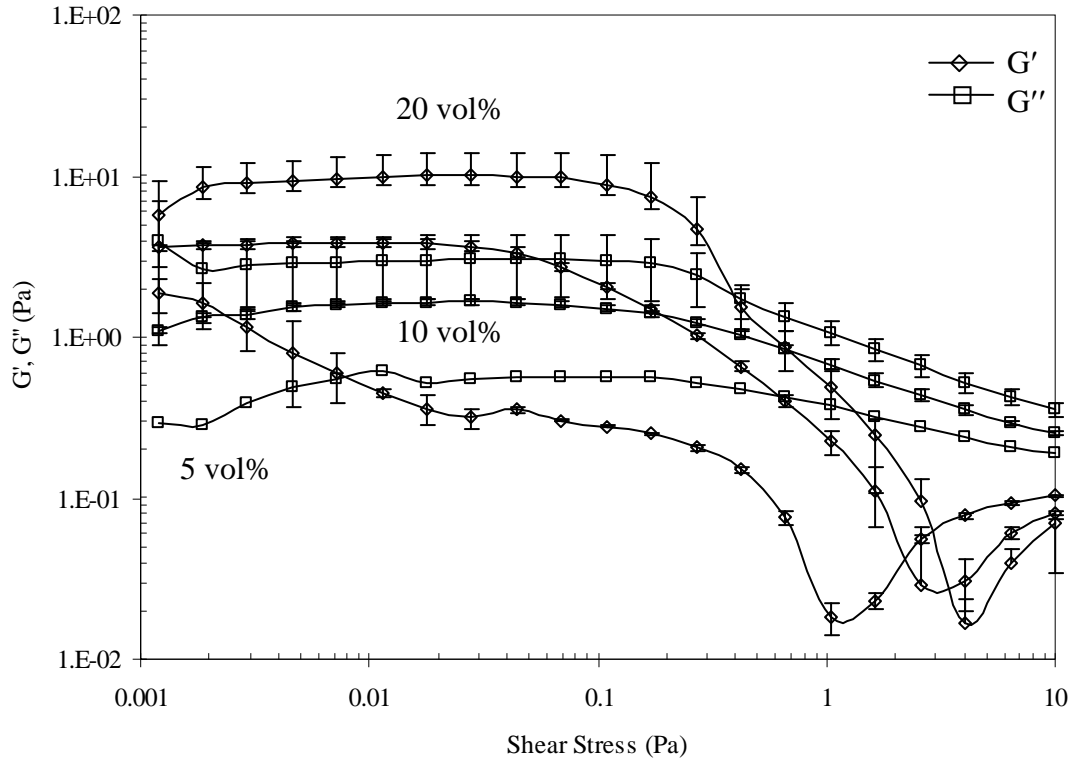


Figure 6. The stress sweeps of nano alumina dilute dispersions in 10 wt% fructose solution.

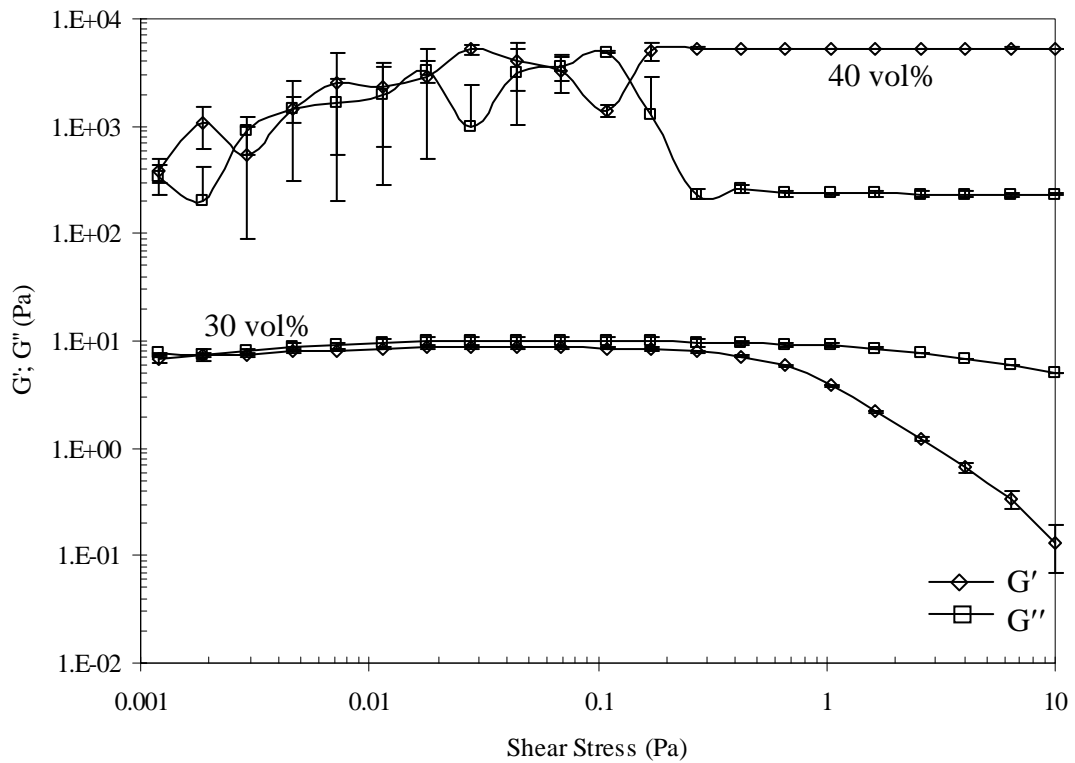


Figure 7. The stress sweeps of nano alumina concentrated dispersions in 10 wt% fructose solution.

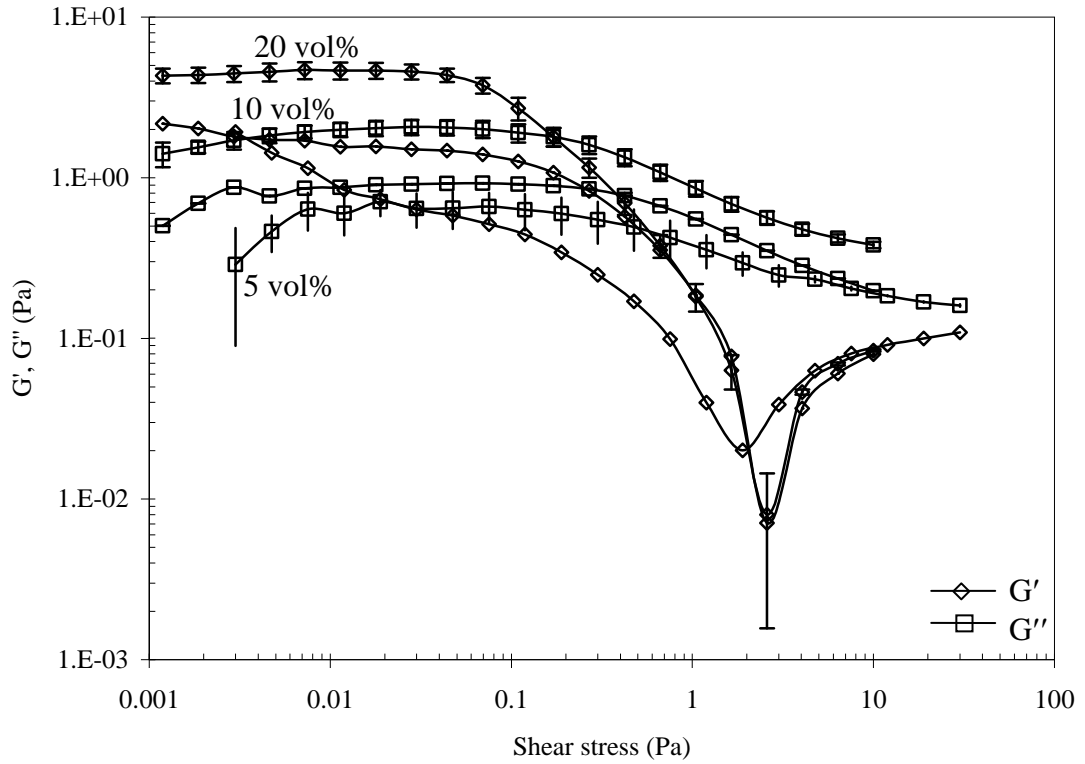


Figure 8. The stress sweeps of nano alumina dilute dispersions in 20 wt% fructose solution.

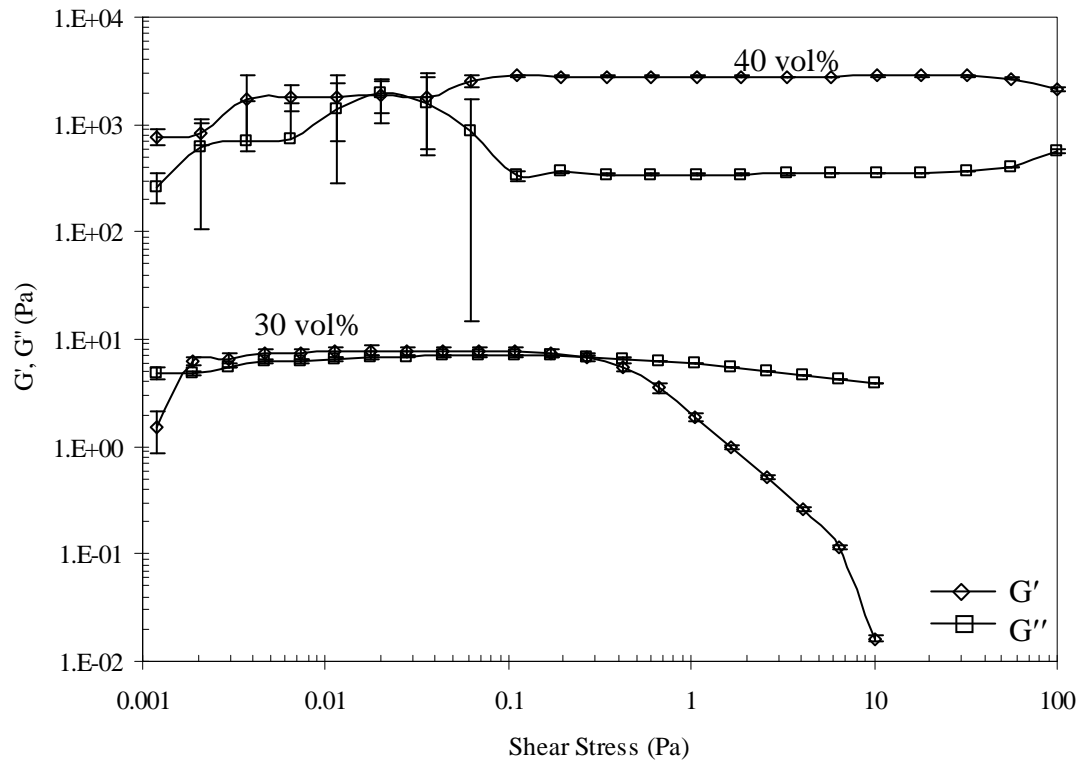


Figure 9. The stress sweeps of nano alumina concentrated dispersions in 20 wt% fructose solution.

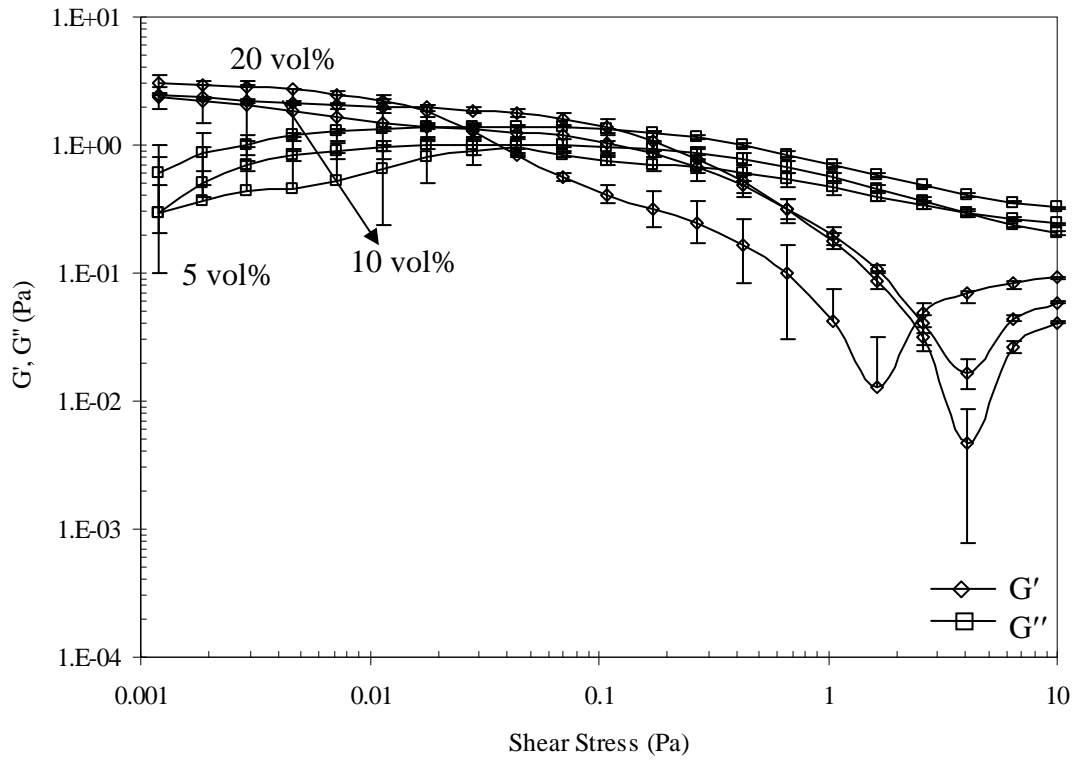


Figure 10. The stress sweeps of nano alumina dilute dispersions in 30 wt% fructose solution.

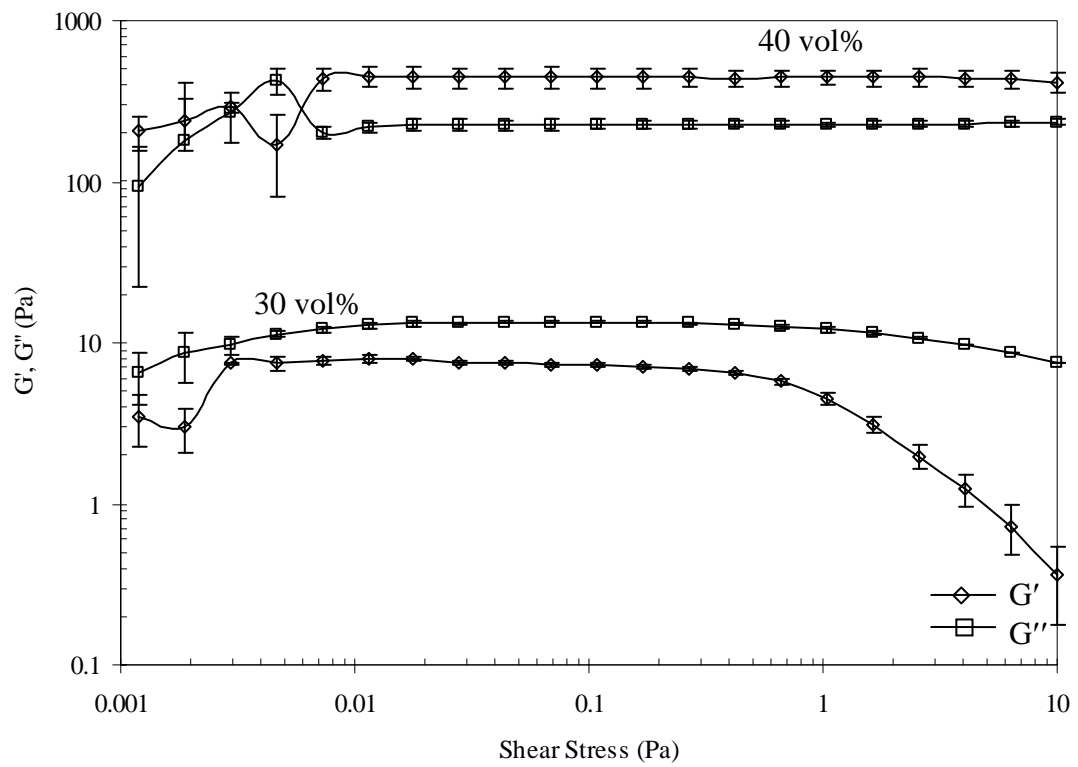


Figure 11. The stress sweeps of nano alumina concentrated dispersions in 30 wt% fructose solution.

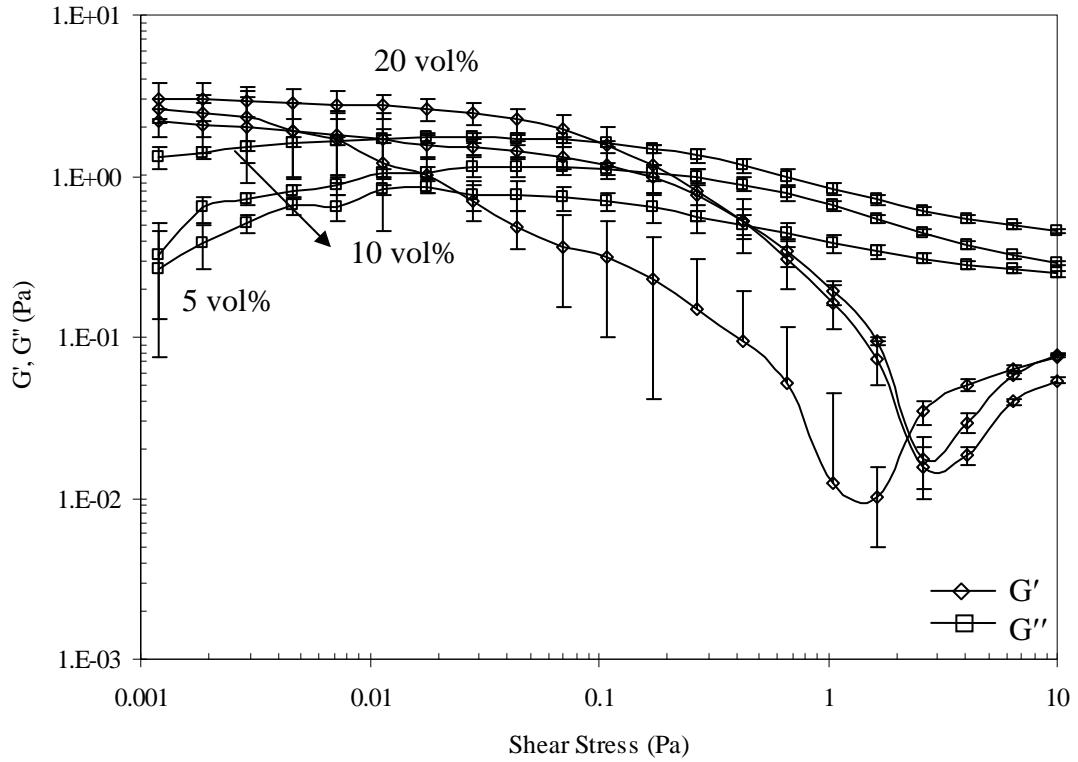


Figure 12. The stress sweeps of nano alumina dilute dispersions in 40 wt% fructose solution.

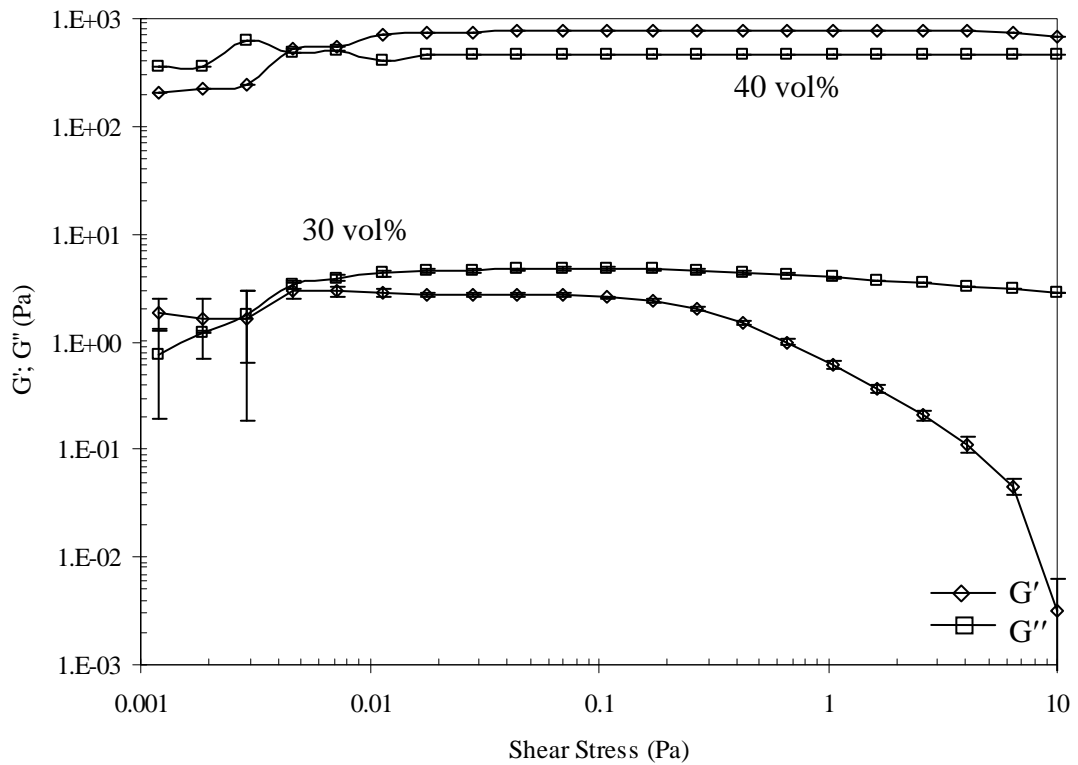


Figure 13. The stress sweeps of nano alumina concentrated dispersions in 40 wt% fructose solution.

C.4. The frequency sweeps

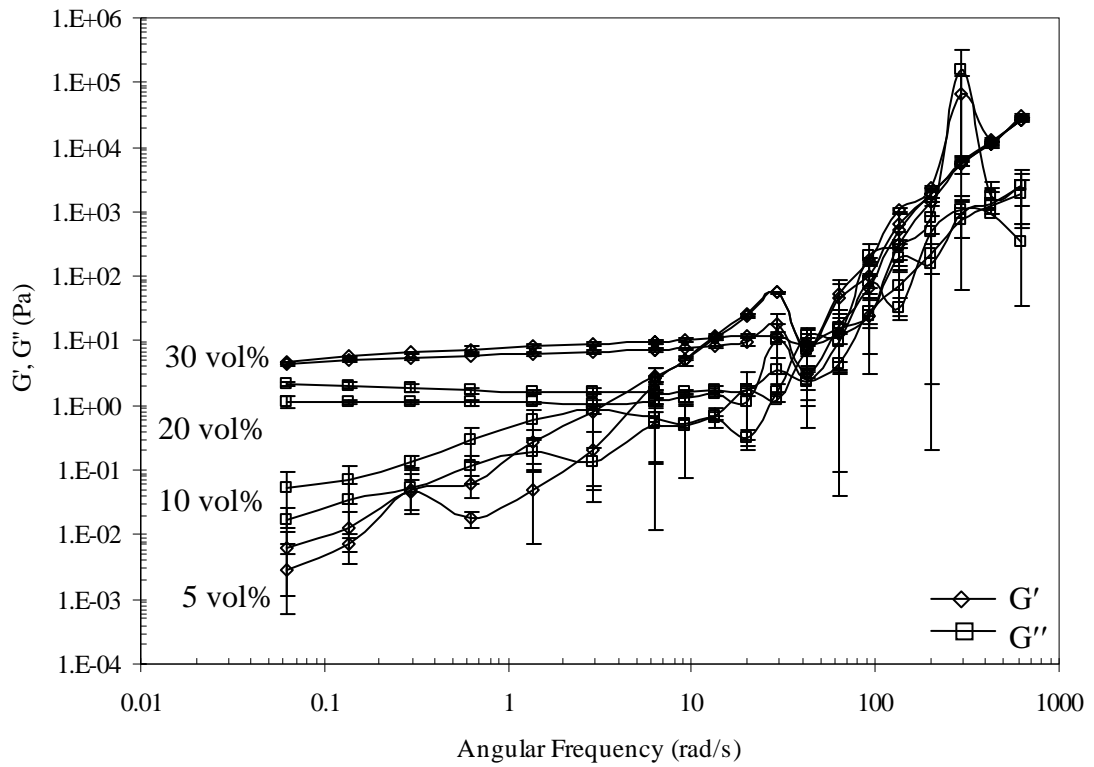


Figure 1. The frequency sweeps of nano alumina dispersions water.

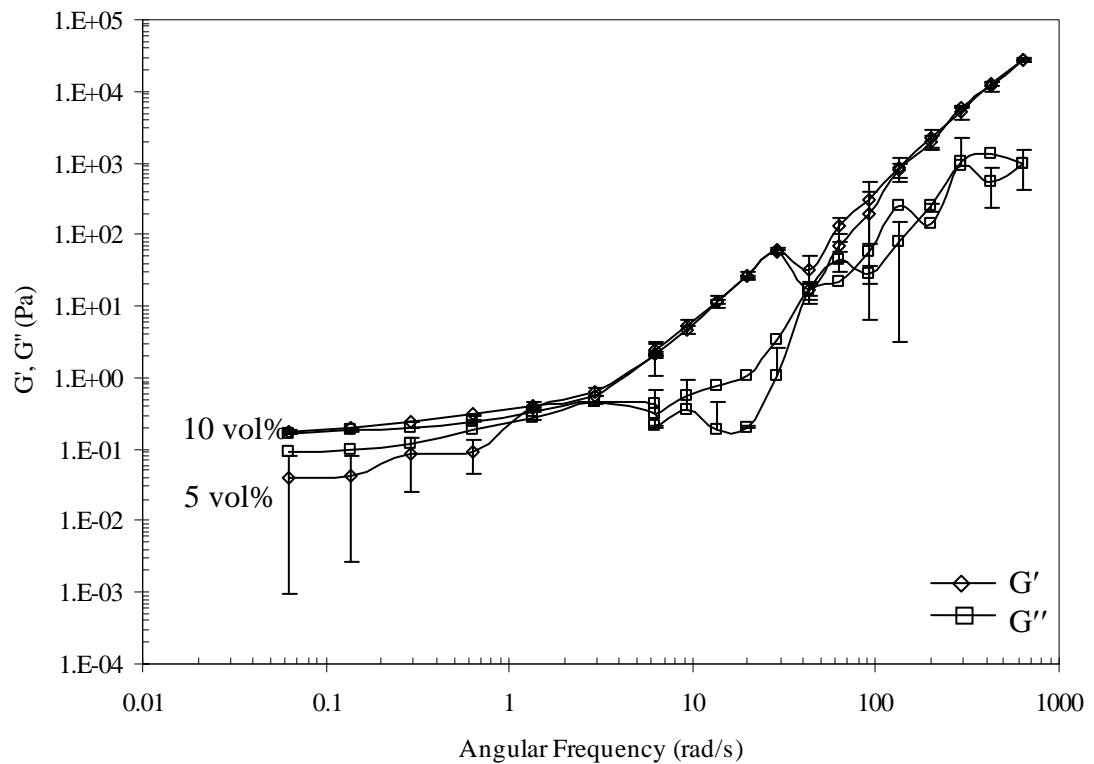


Figure 2. The frequency sweeps of nano alumina dilute dispersions 1 wt% fructose solution.

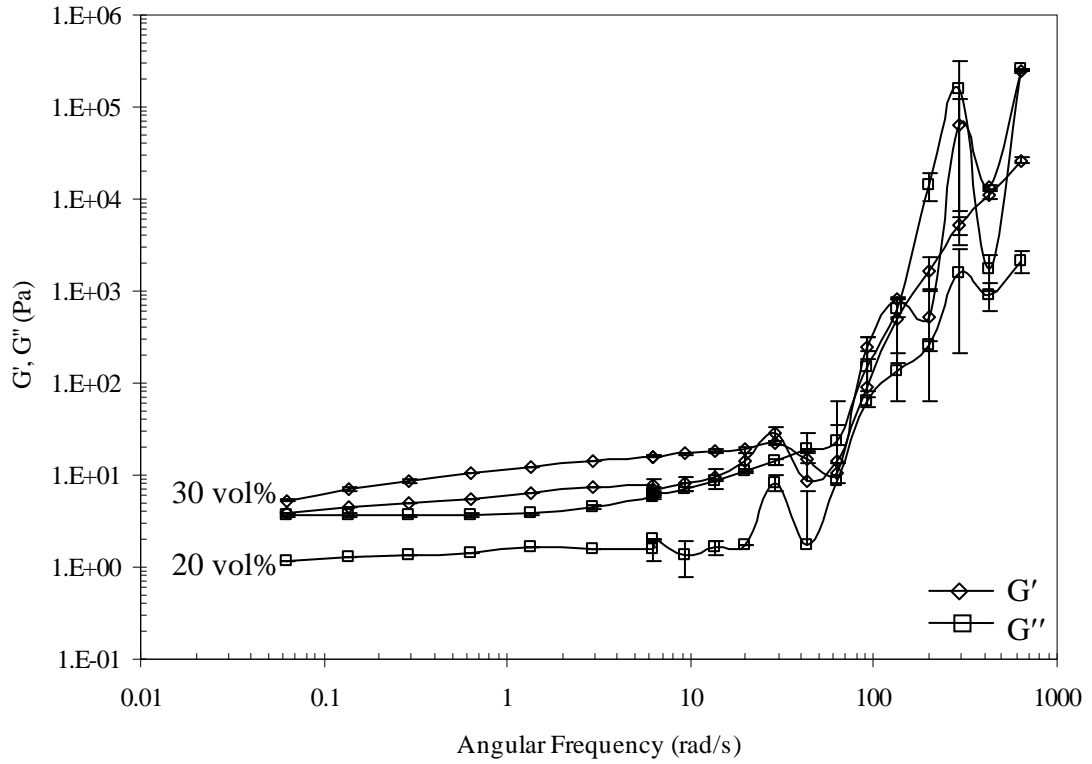


Figure 3. The frequency sweeps of nano alumina concentrated dispersions 1 wt% fructose solution.

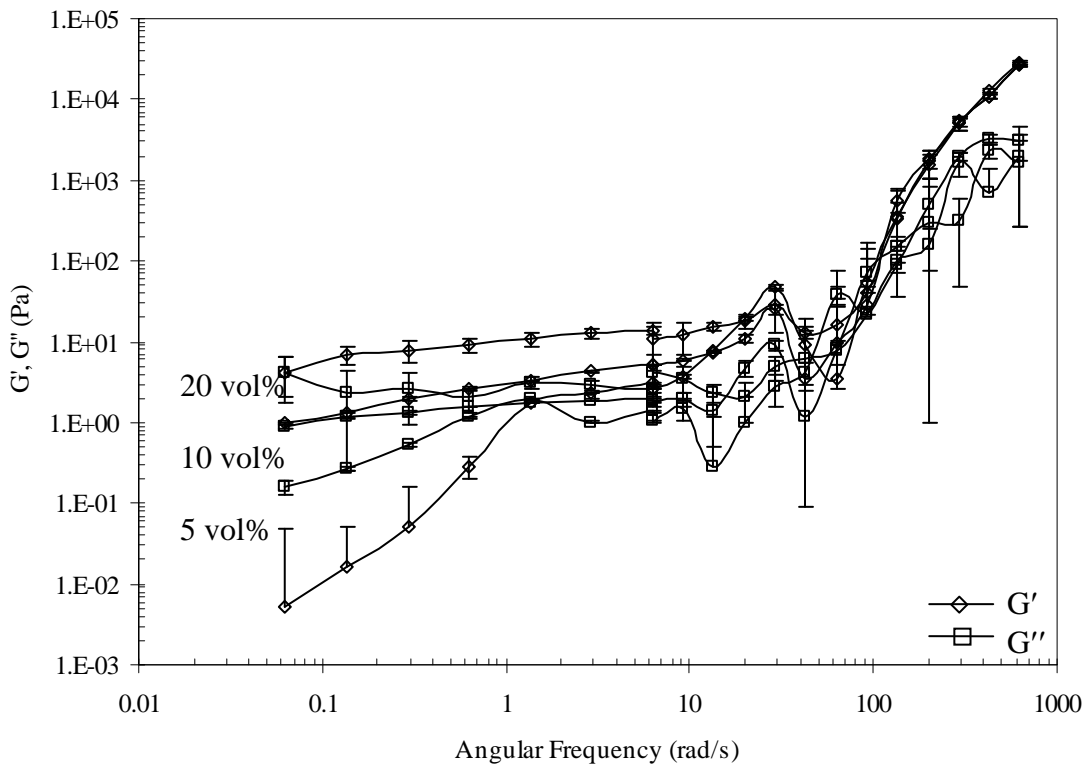


Figure 4. The frequency sweeps of nano alumina dilute dispersions 4 wt% fructose solution.

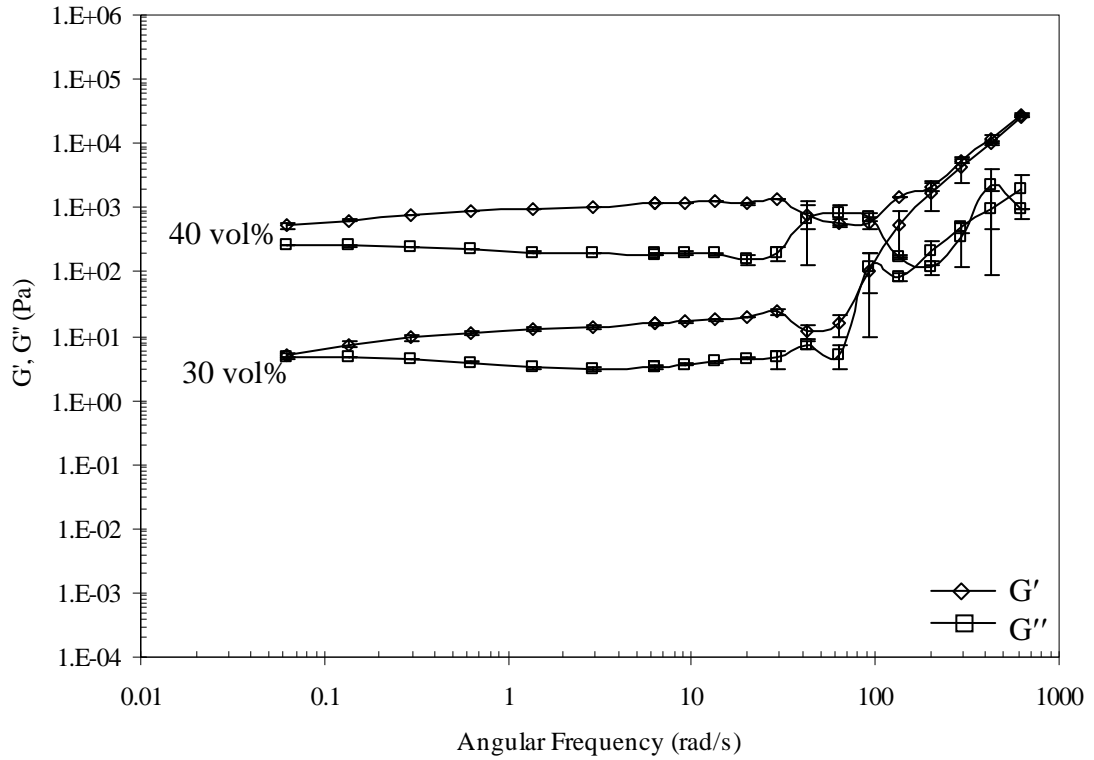


Figure 5. The frequency sweeps of nano alumina concentrated dispersions 4 wt% fructose solution.

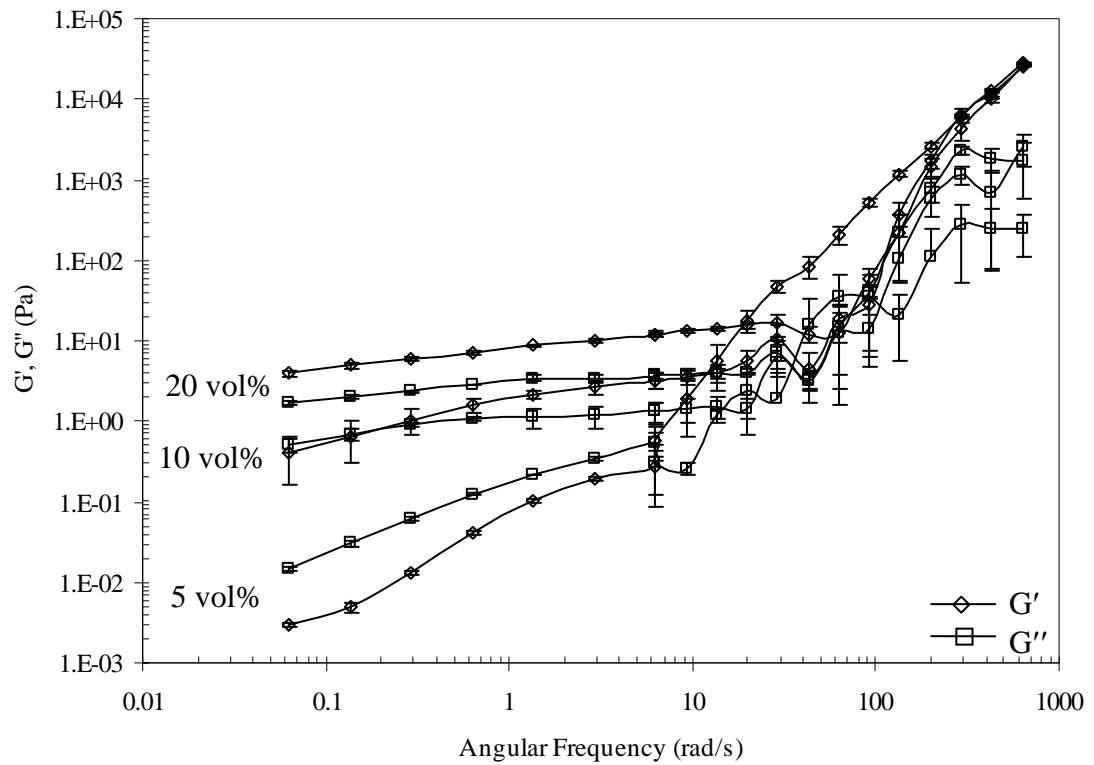


Figure 6. The frequency sweeps of nano alumina dilute dispersions 10 wt% fructose solution.

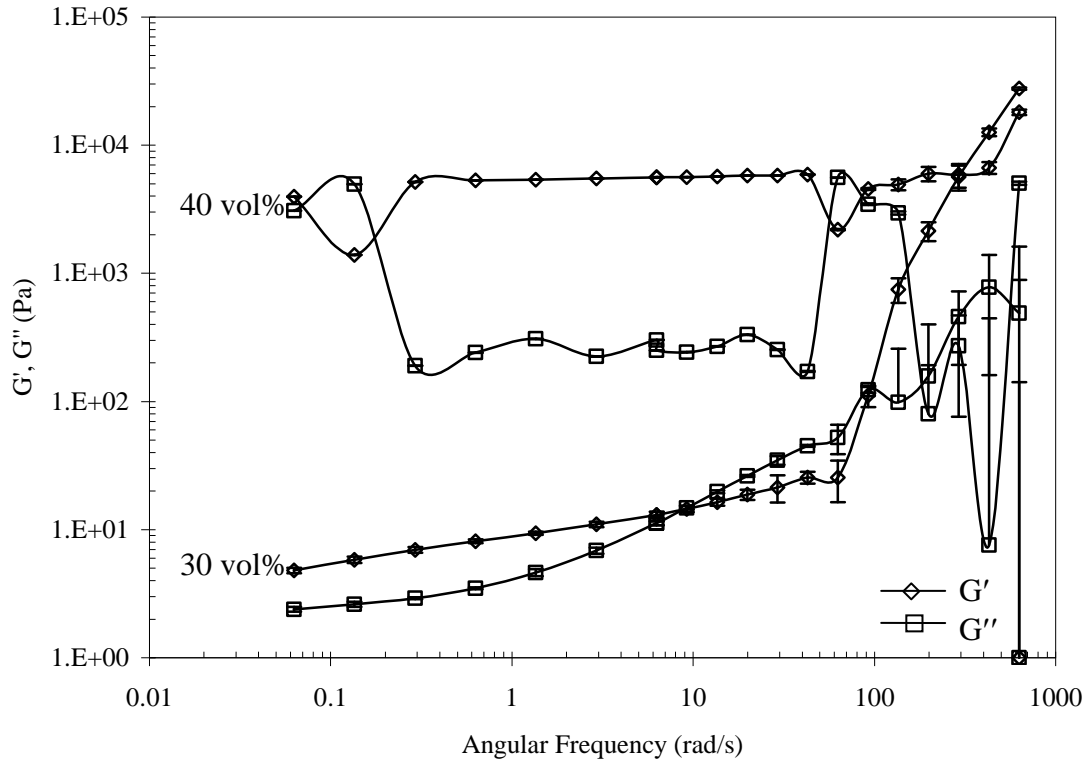


Figure 7. The frequency sweeps of nano alumina concentrated dispersions 10 wt% fructose solution.

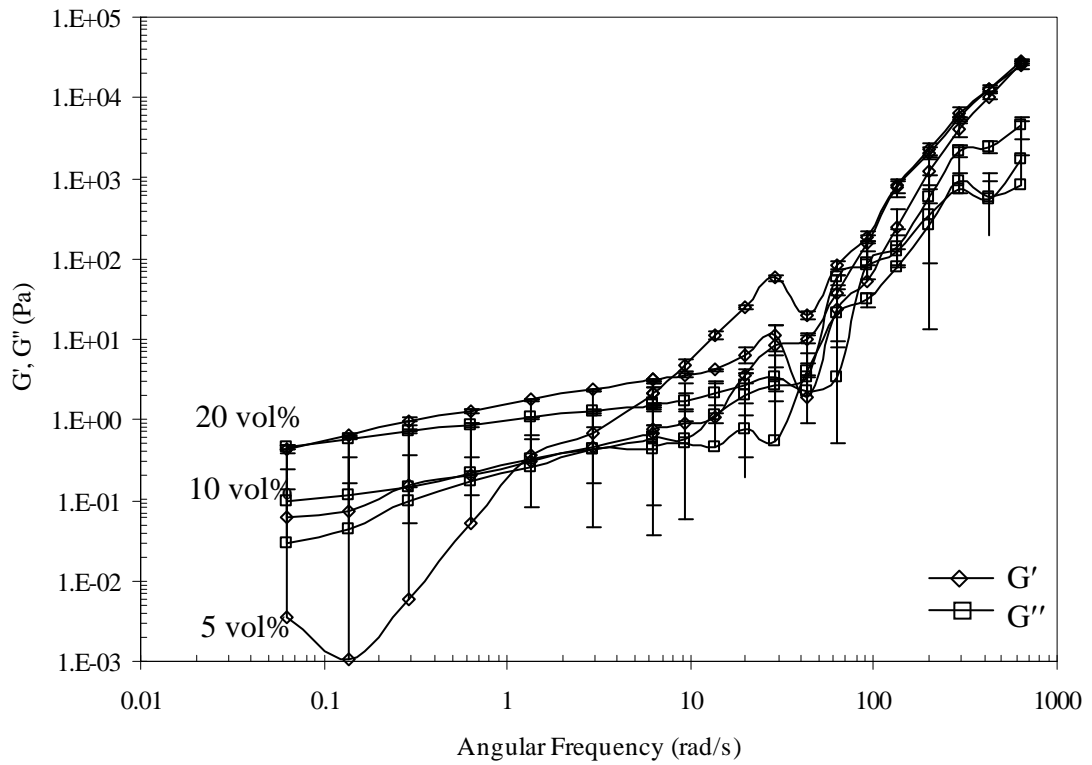


Figure 8. The frequency sweeps of nano alumina dilute dispersions 20 wt% fructose solution.

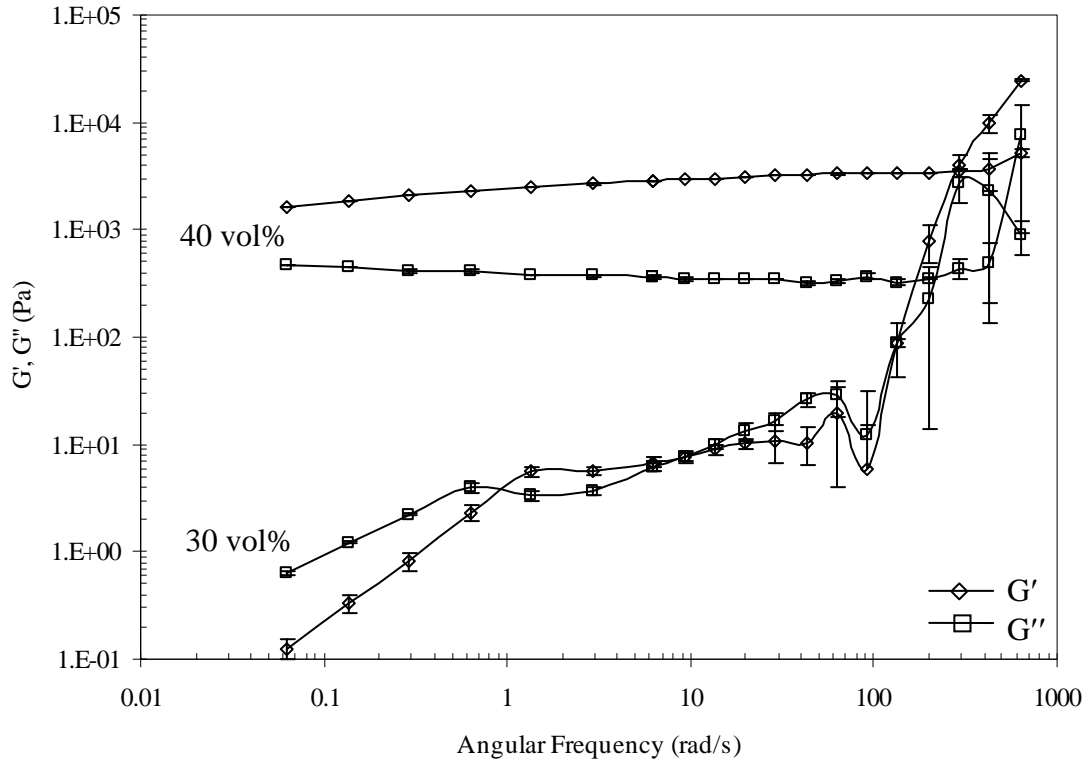


Figure 9. The frequency sweeps of nano alumina concentrated dispersions 20 wt% fructose solution.

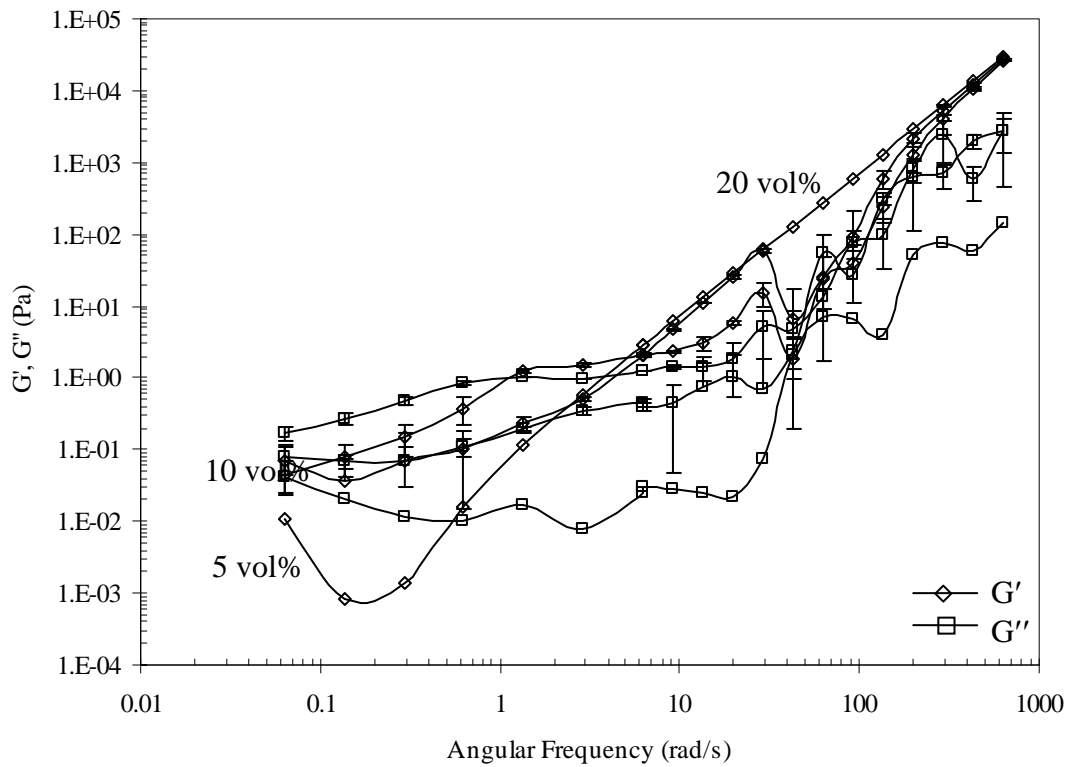


Figure 10. The frequency sweeps of nano alumina dilute dispersions 30 wt% fructose solution.

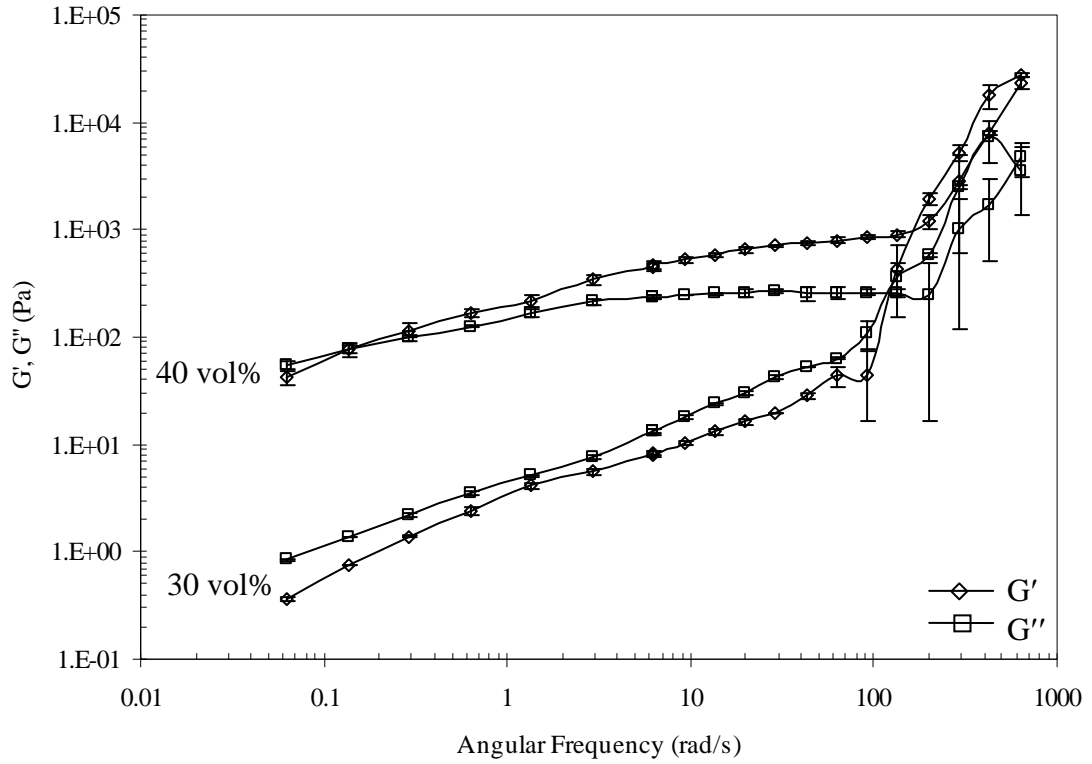


Figure 11. The frequency sweeps of nano alumina concentrated dispersions 30 wt% fructose solution.

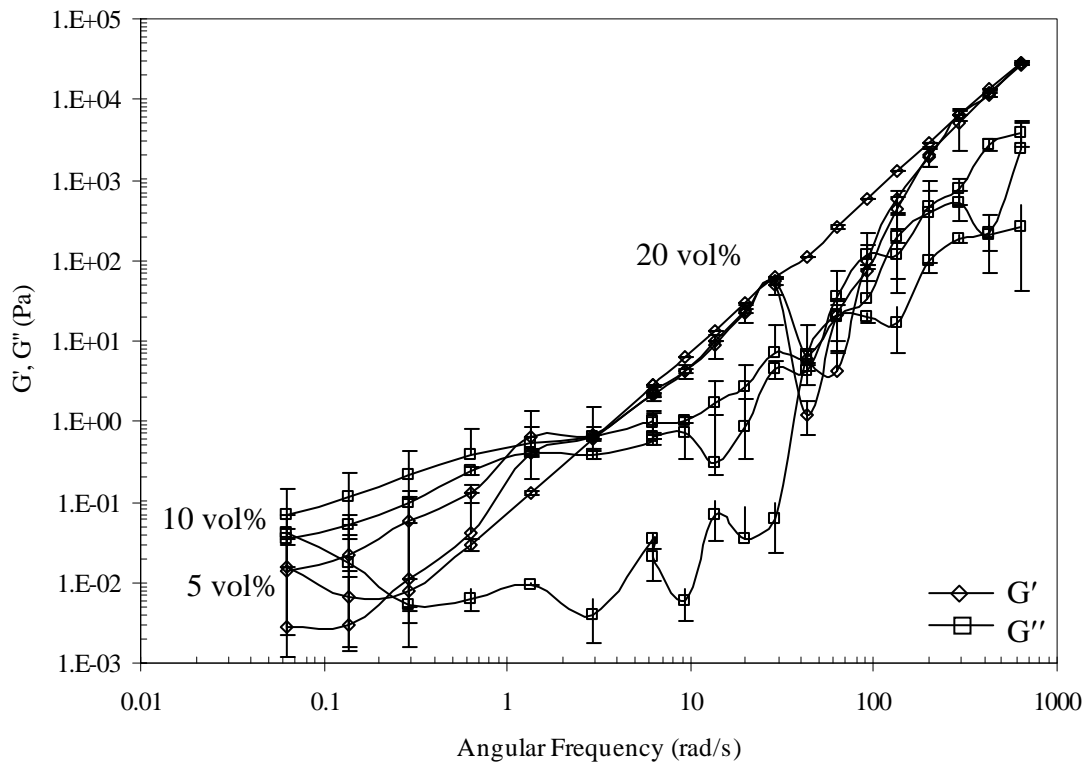


Figure 12. The frequency sweeps of nano alumina dilute dispersions 40 wt% fructose solution.

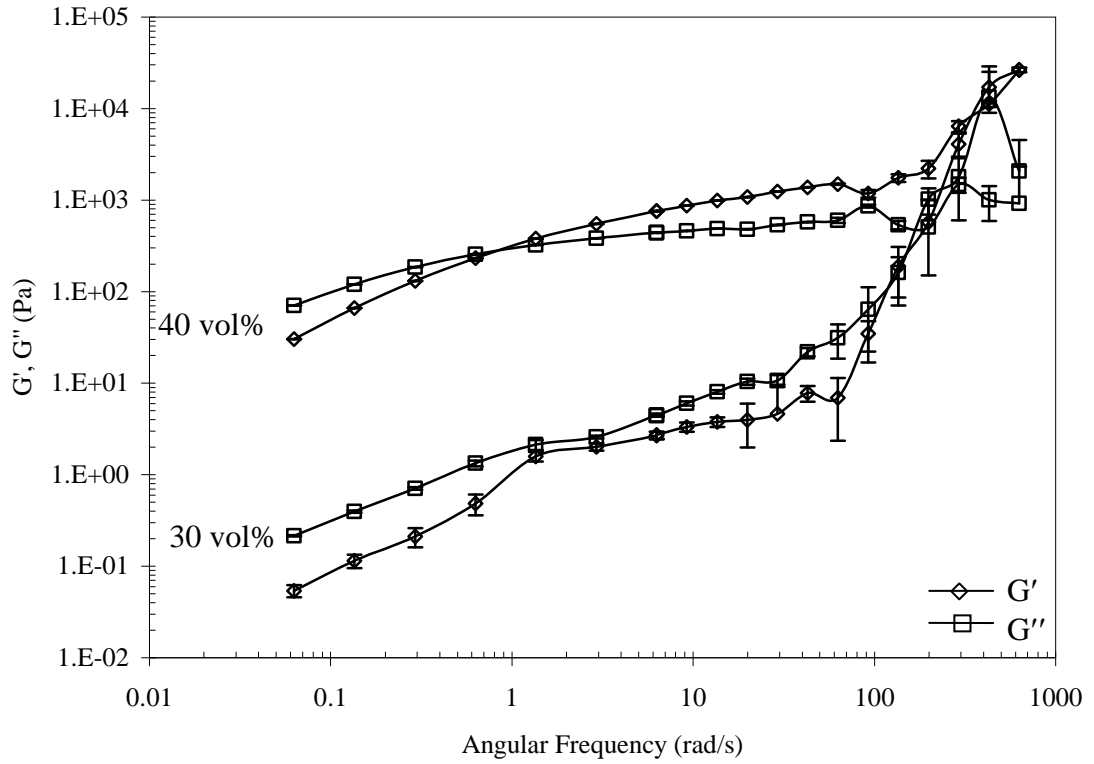


Figure 13. The frequency sweeps of nano alumina concentrated dispersions 40 wt% fructose solution.

APPENDIX D. THE RHEOLOGICAL BEHAVIOR OF NANO TITANIA DISPERSIONS

D.1. The flow and viscosity curves

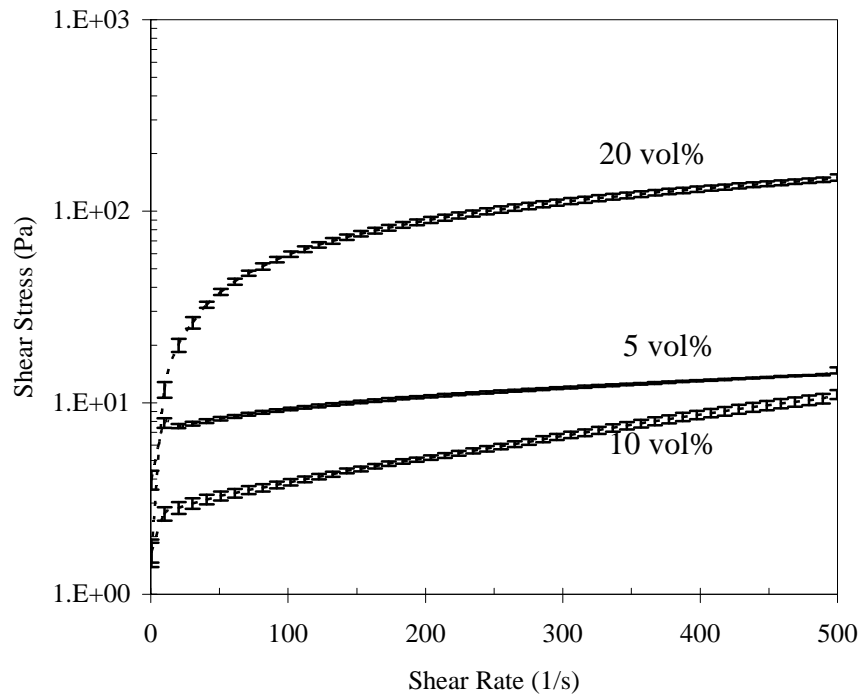


Figure 1. The flow curves of nano titania dispersions without fructose and pH adjustment.

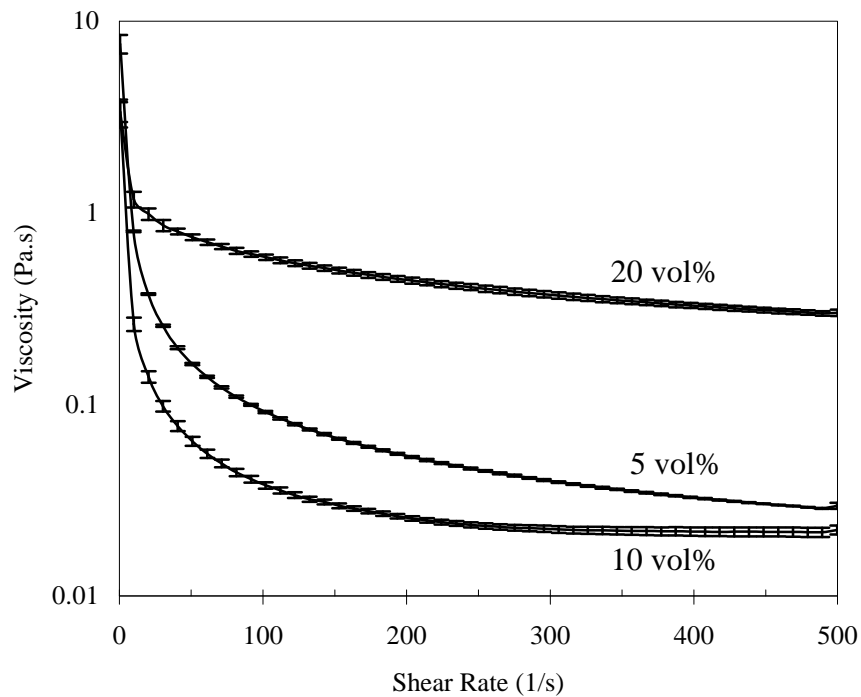


Figure 2. The viscosity curves of nano titania dispersions without fructose.

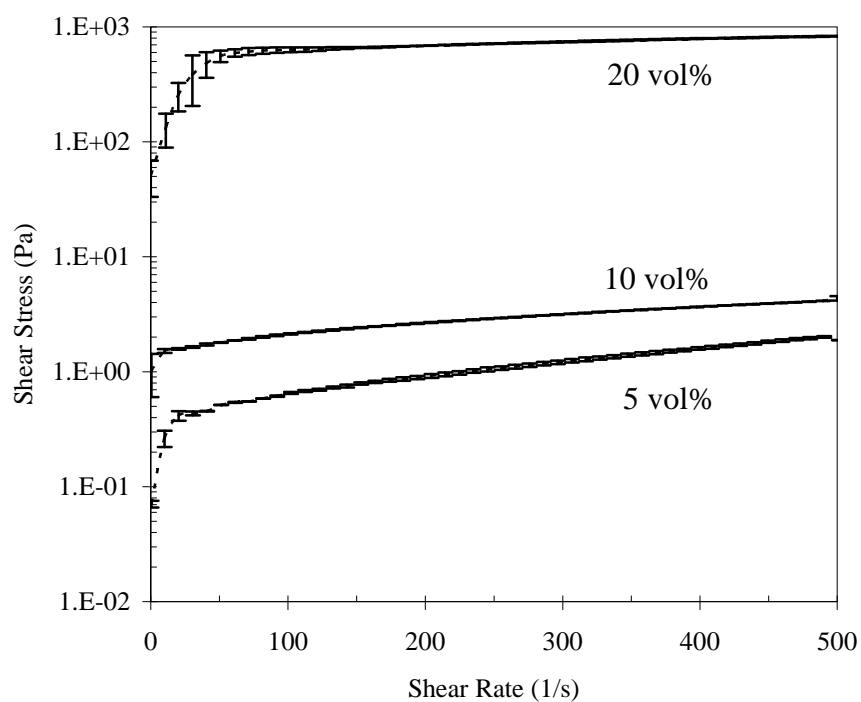


Figure 3. The flow curves of nano titania dispersions without fructose and with pH adjustment.

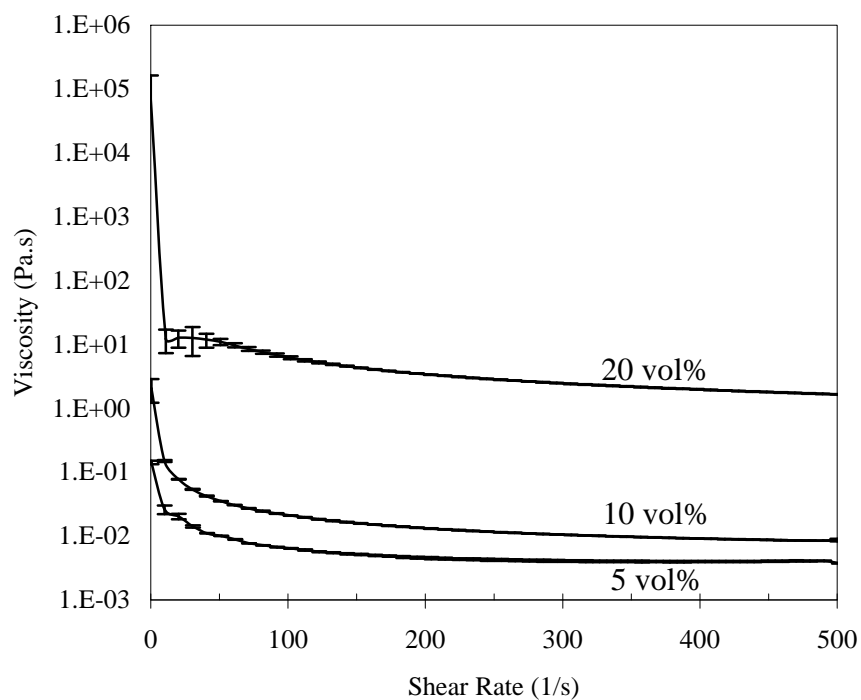


Figure 4. The viscosity curves of nano titania dispersions without fructose and with pH adjustment.

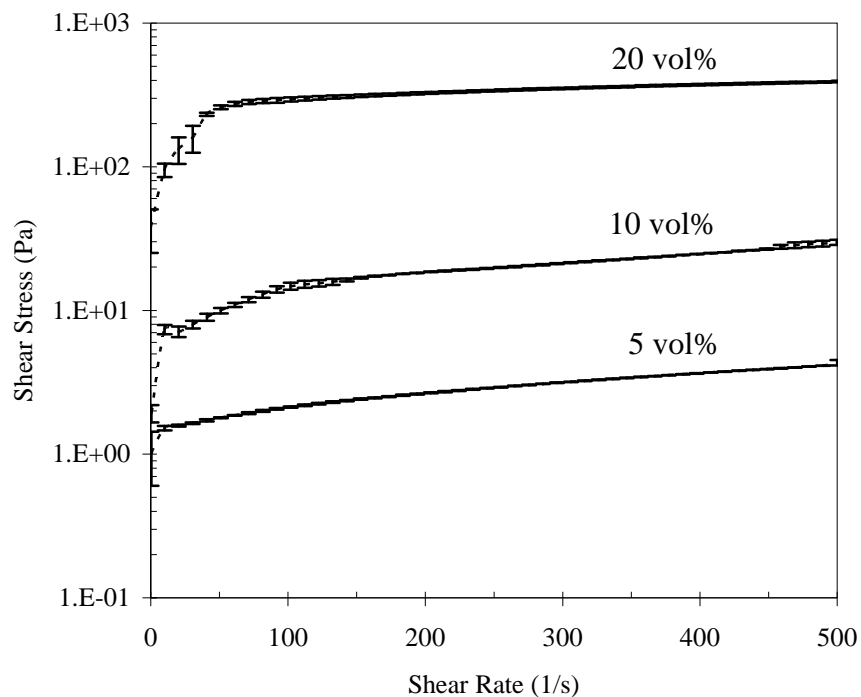


Figure 5. The flow curves of pH adjusted nano titania dispersions in 1wt% fructose solution.

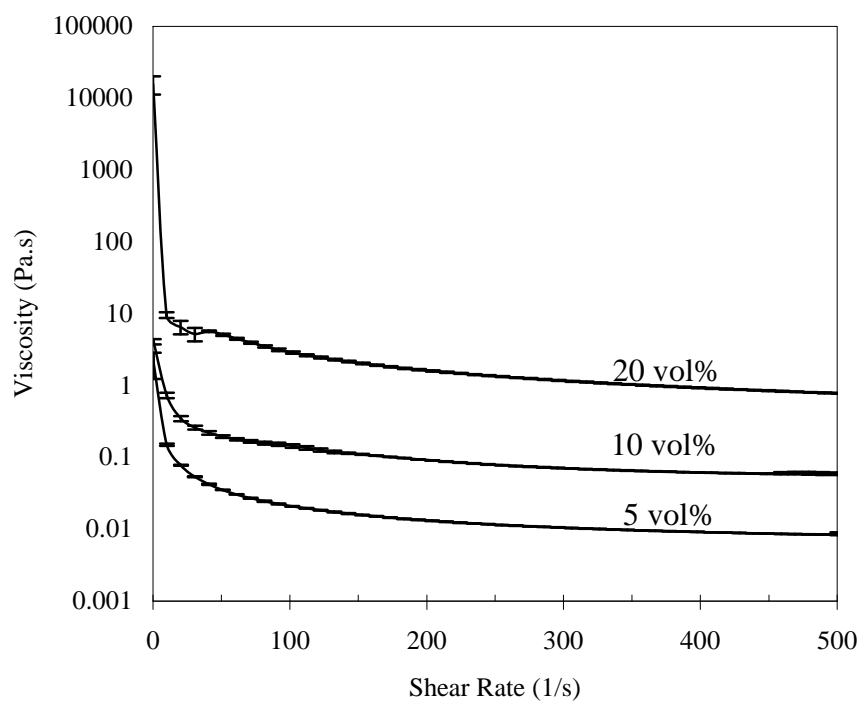


Figure 6. The viscosity curves of pH adjusted nano titania dispersions in 1wt% fructose solution.

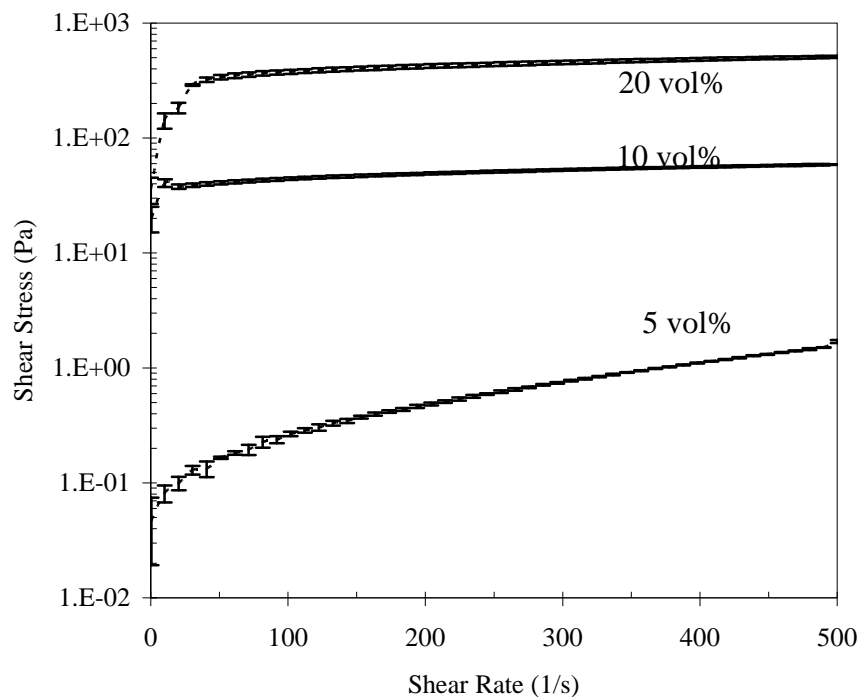


Figure 7. The flow curves of pH adjusted nano titania dispersions in 4 wt% fructose solution.

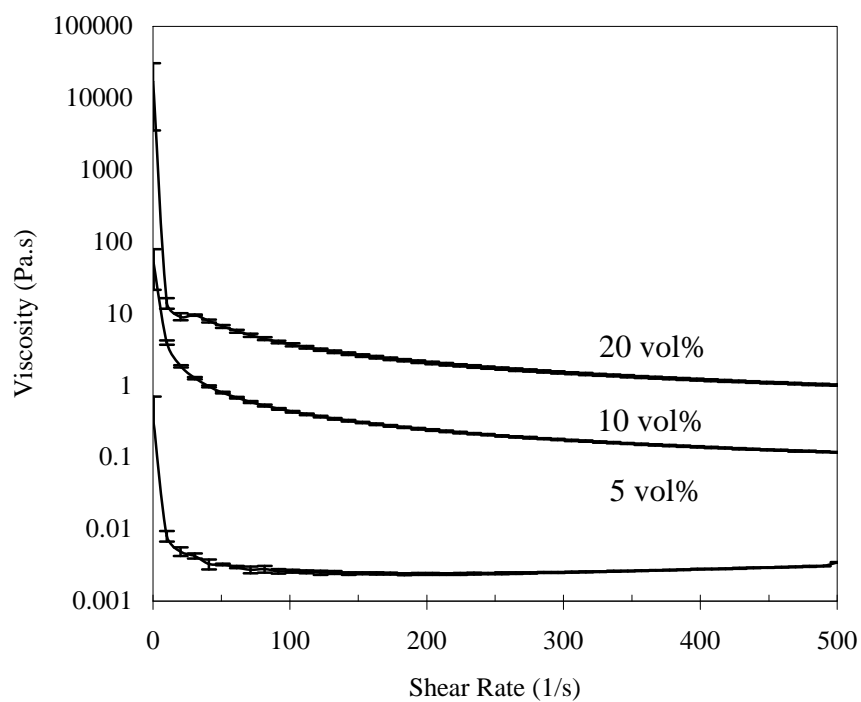


Figure 8. The viscosity curves of pH adjusted nano titania dispersions in 4 wt% fructose solution.

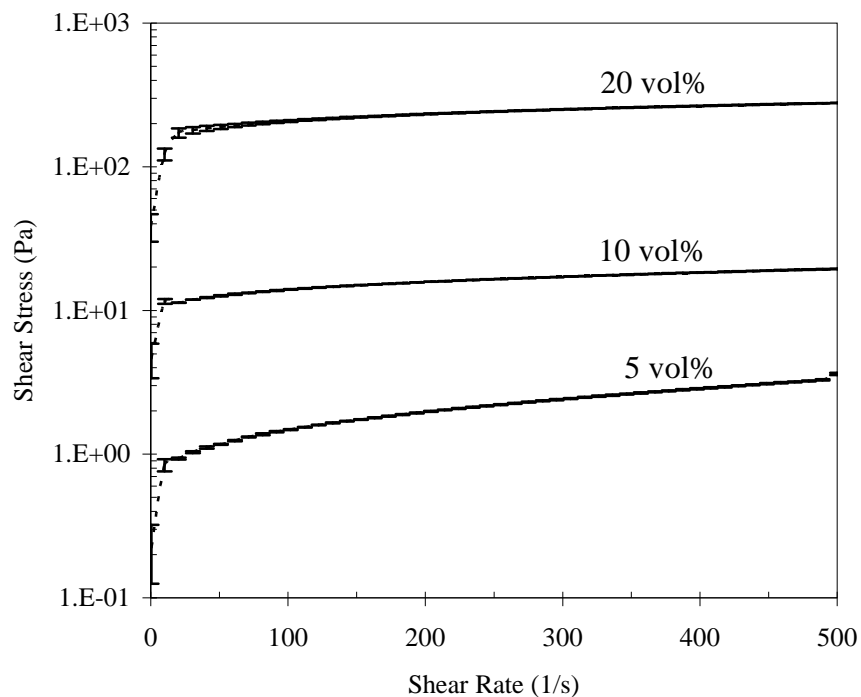


Figure 9. The flow curves of pH adjusted nano titania dispersions in 10wt% fructose solution.

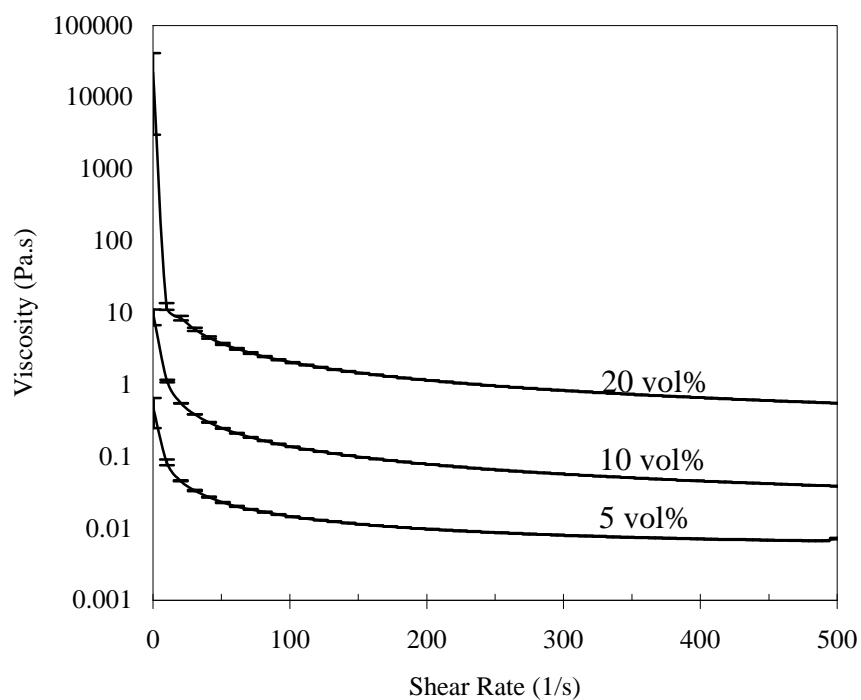


Figure 101. The viscosity curves of pH adjusted nano titania dispersions in 10 wt% fructose solution.

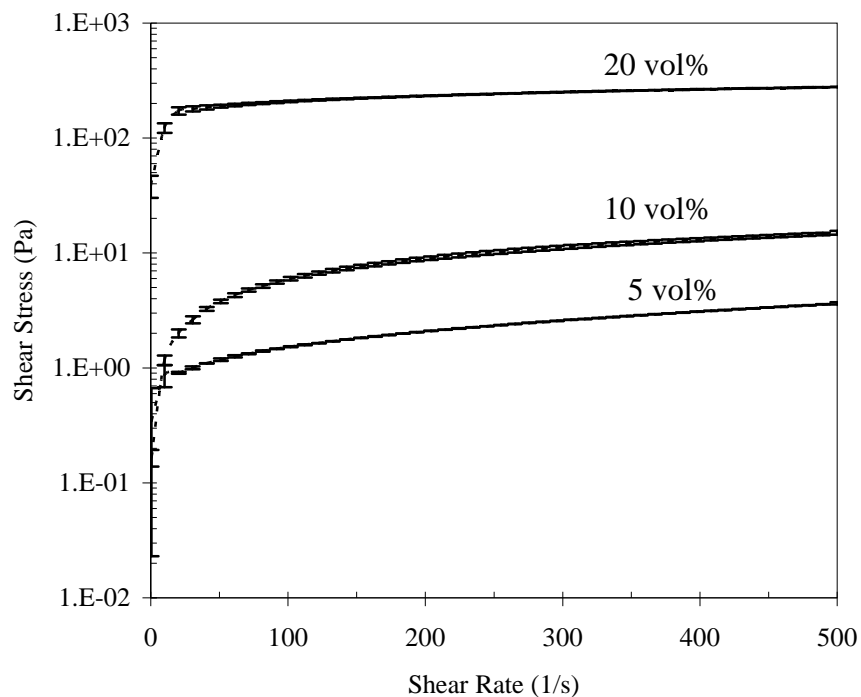


Figure 11. The flow curves of pH adjusted nano titania dispersions in 20wt% fructose solution.

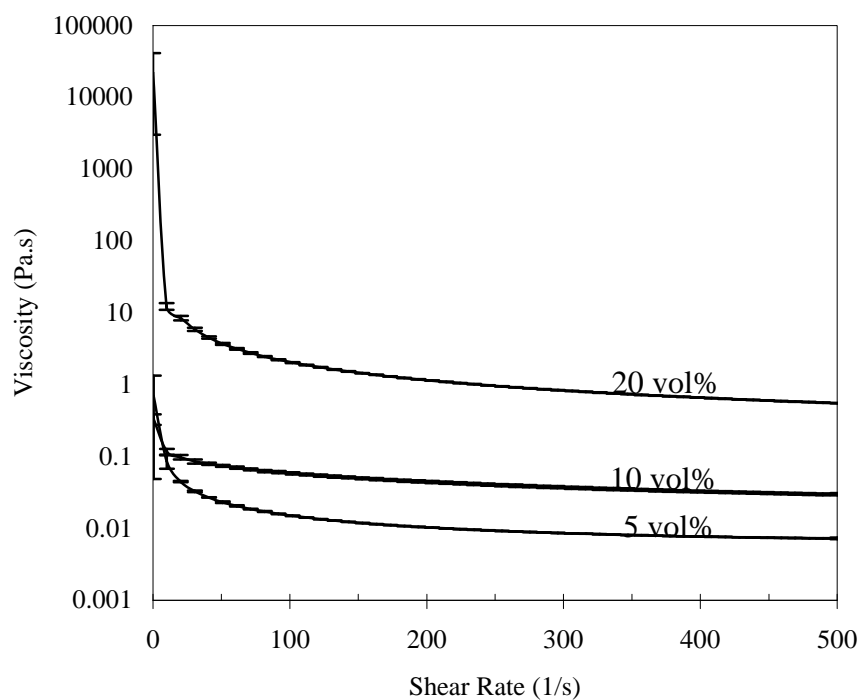


Figure 12. The viscosity curves of pH adjusted nano titania dispersions in 20 wt% fructose solution.

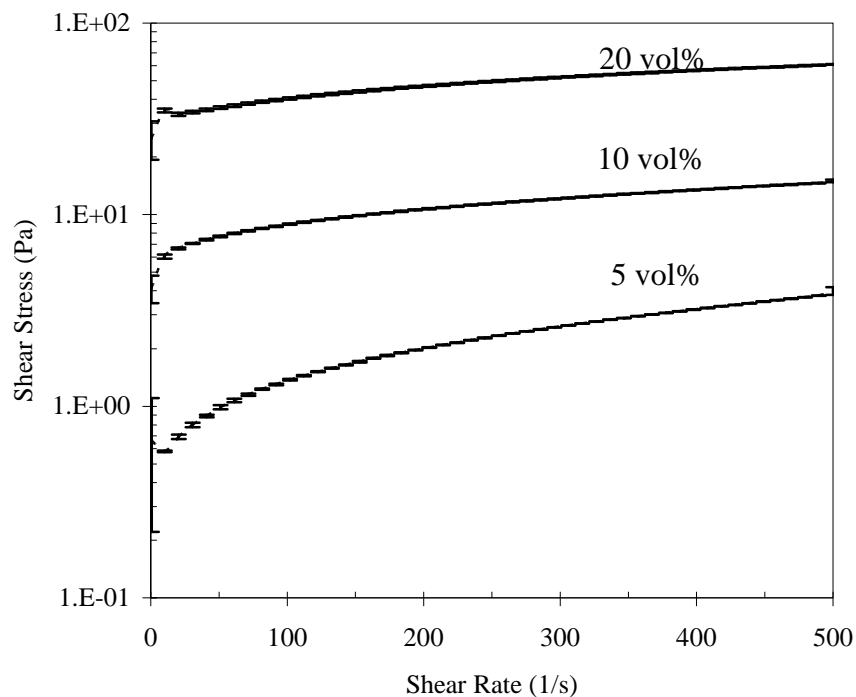


Figure 13. The flow curves of pH adjusted nano titania dispersions in 30wt% fructose solution.

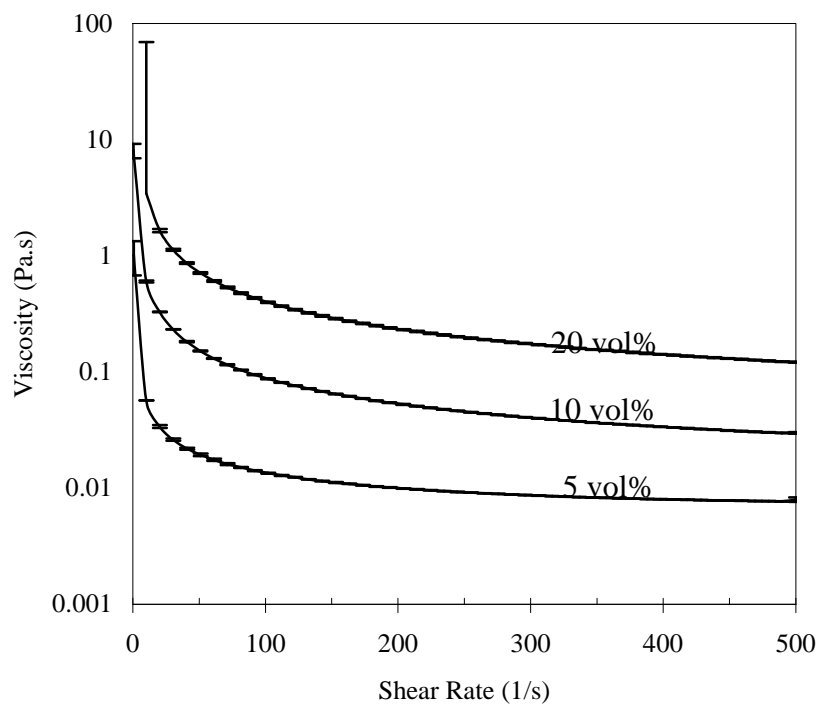


Figure 14. The viscosity curves of pH adjusted nano titania dispersions in 30 wt% fructose solution.

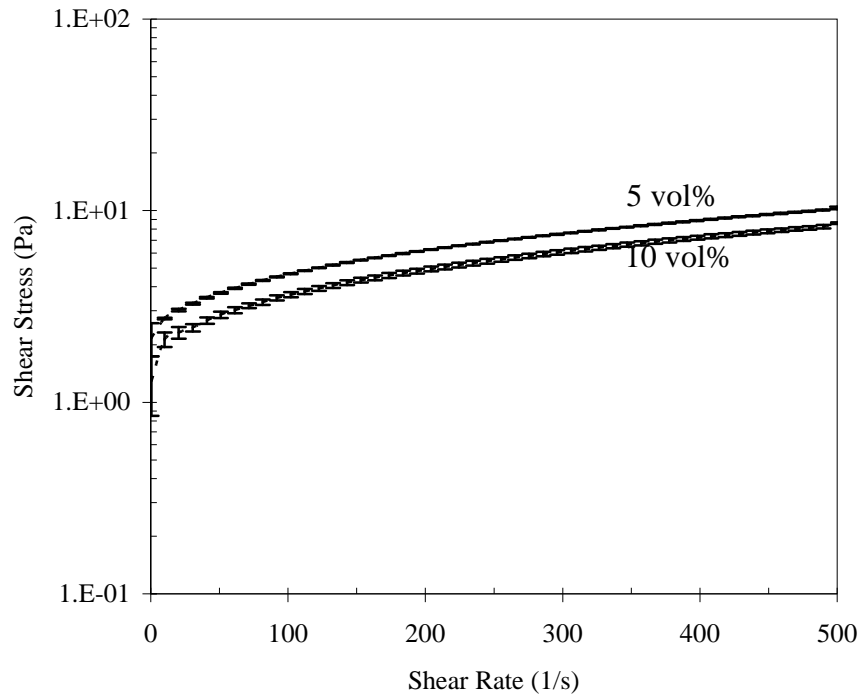


Figure 15. The flow curves of nano pH adjusted titania dispersions in 40wt% fructose solution.

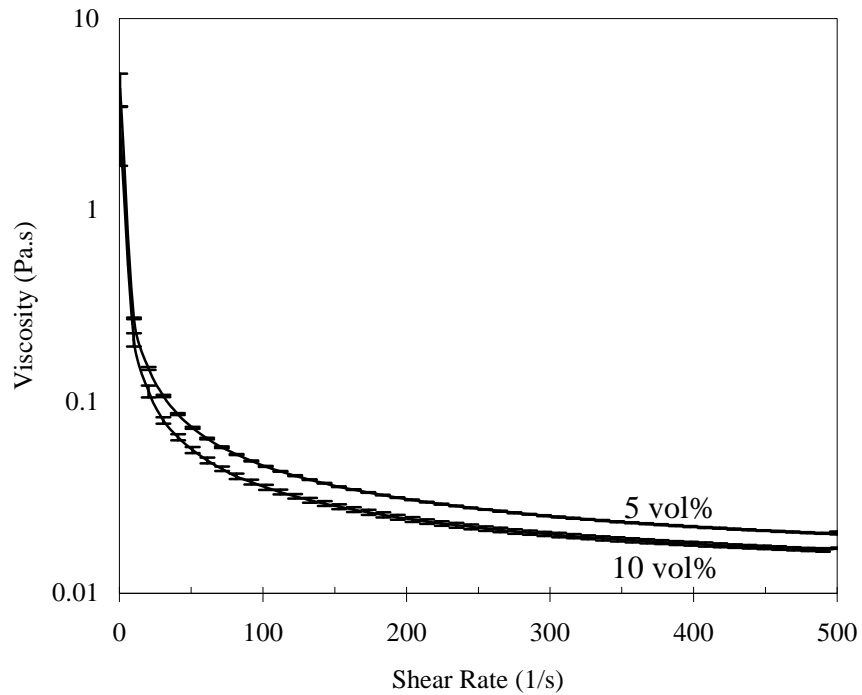


Figure 16. The viscosity curves of pH adjusted nano titania dispersions in 40 wt% fructose solution.

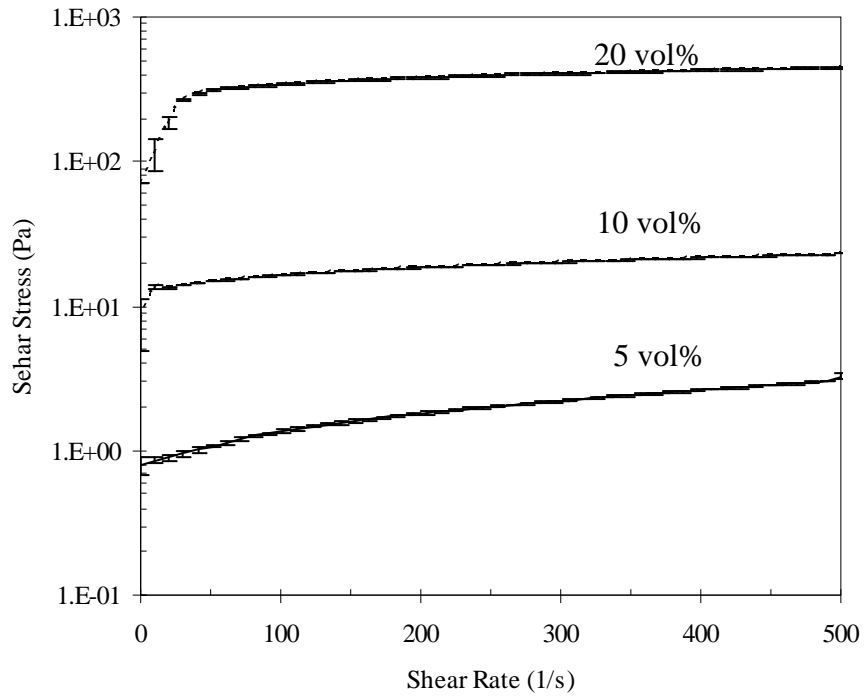


Figure 17. The flow curves of nano titania dispersions in 10wt% fructose solution.

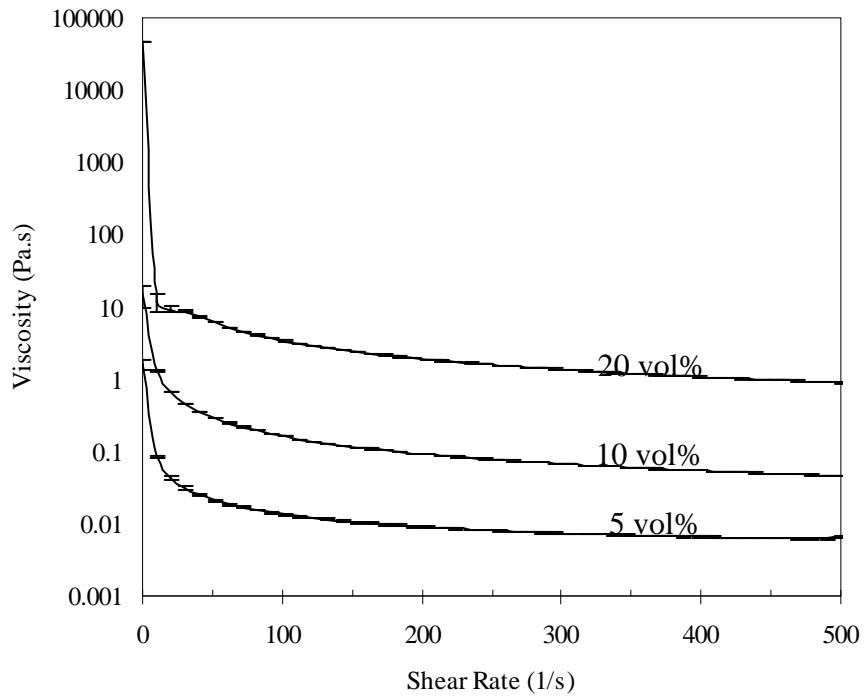


Figure 18. The viscosity curves of nano titania dispersions in 10 wt% fructose solution.

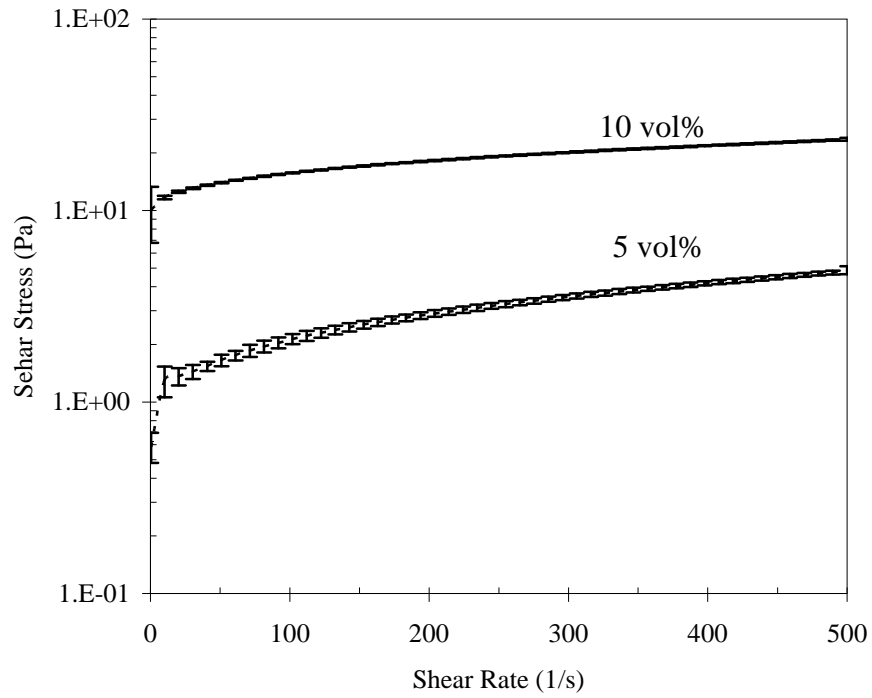


Figure 19. The flow curves of nano titania dispersions in 20wt% fructose solution.

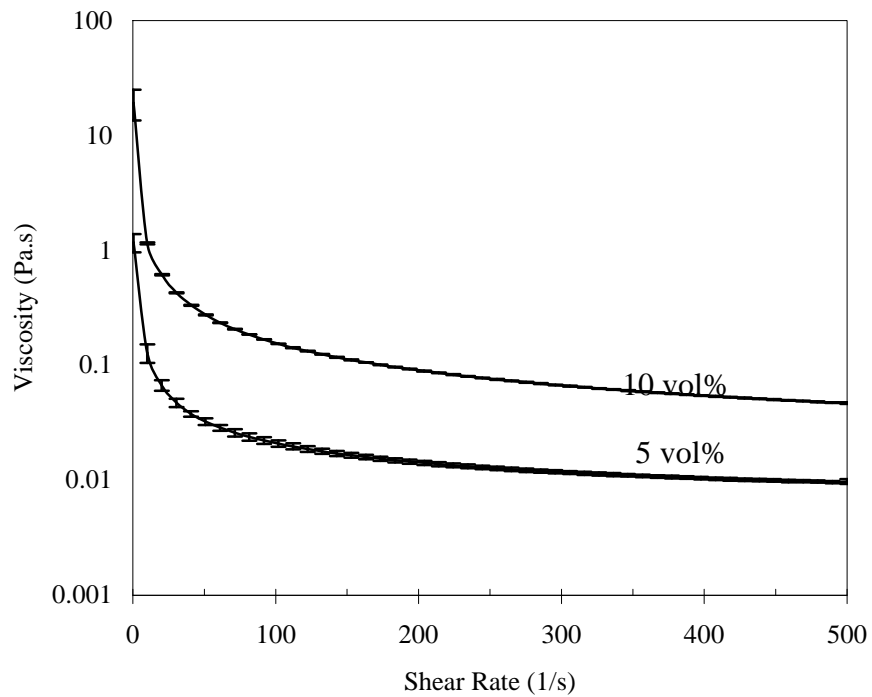


Figure 20. The viscosity curves of nano titania dispersions in 20 wt% fructose solution.

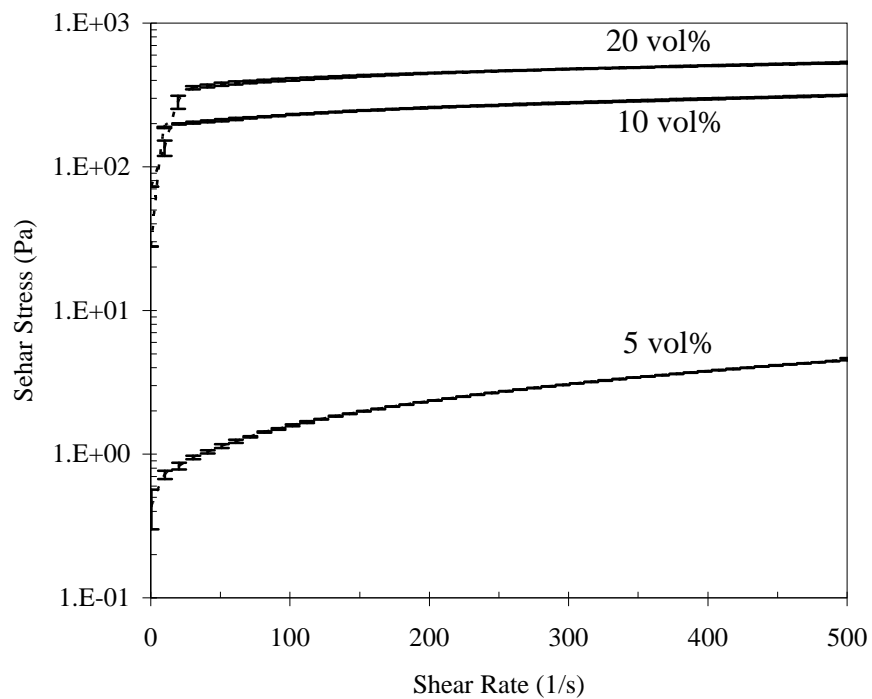


Figure 21. The flow curves of nano titania dispersions in 30wt% fructose solution.

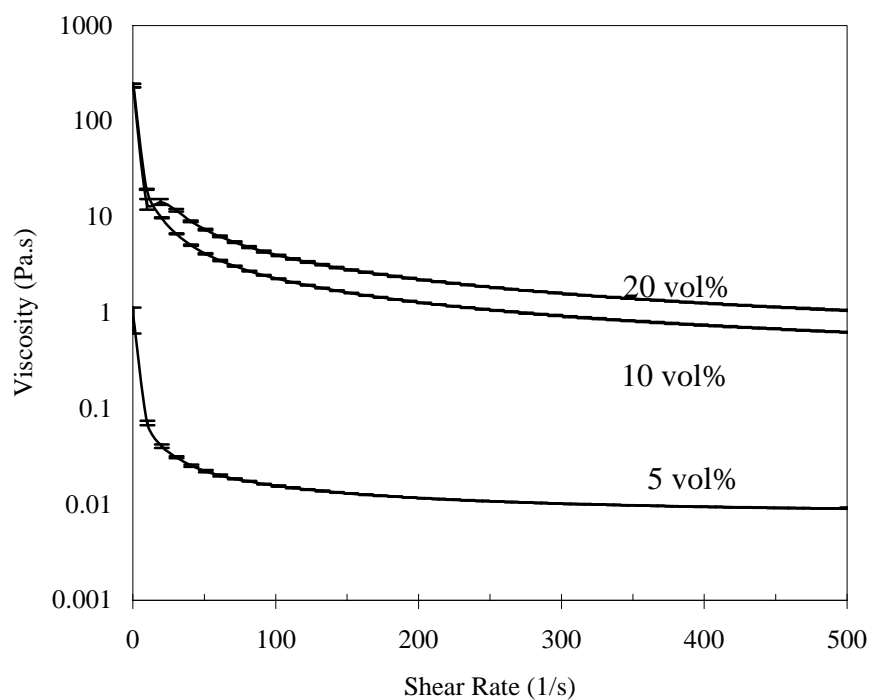


Figure 22. The viscosity curves of nano titania dispersions in 30 wt% fructose solution.

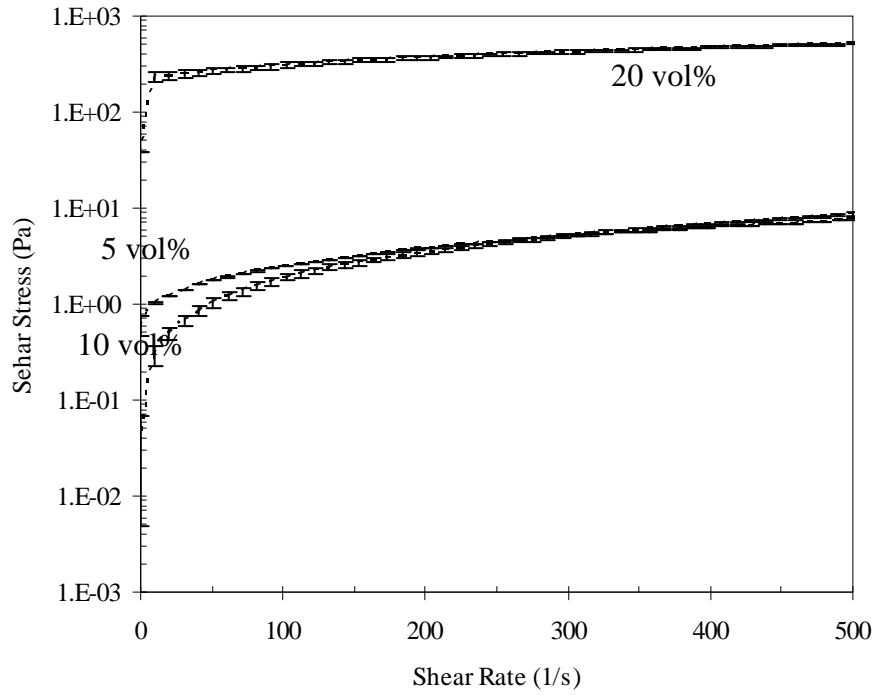


Figure 23. The flow curves of nano titania dispersions in 40wt% fructose solution.

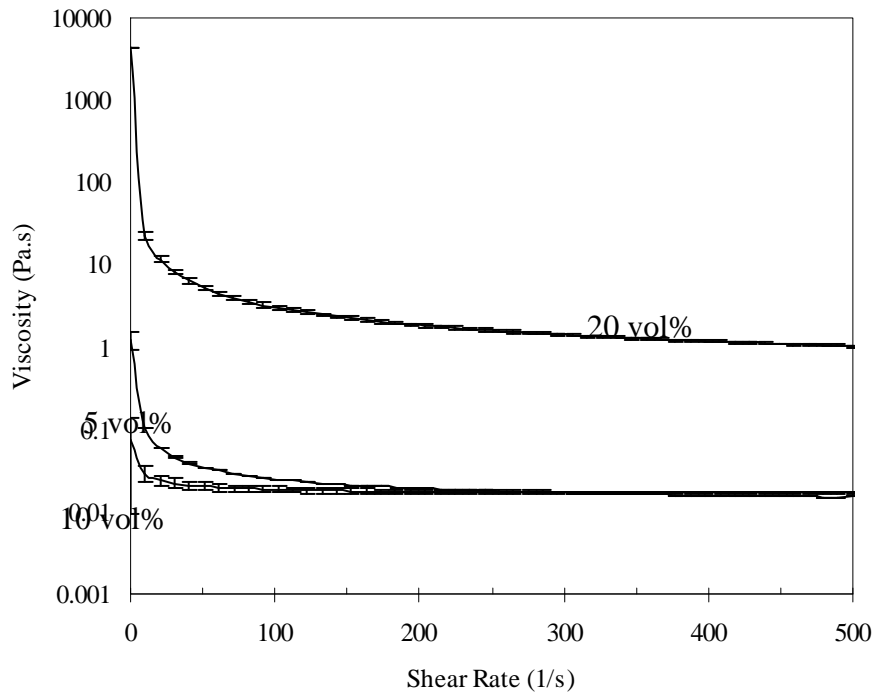


Figure 24. The viscosity curves of nano titania dispersions in 40 wt% fructose solution.

D.2. The thixotropy curves

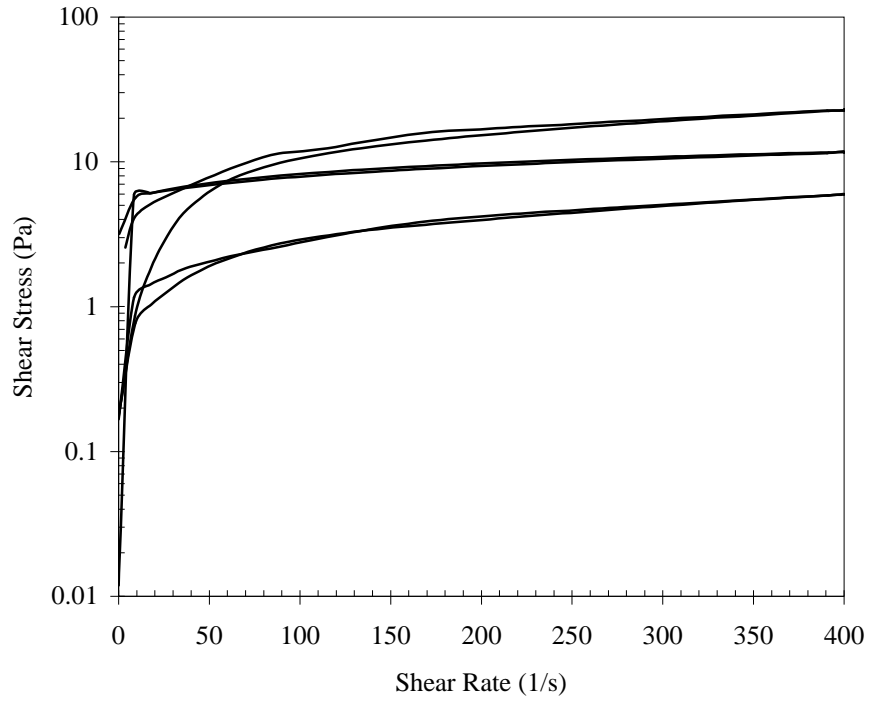


Figure 1. The thixotropy curves of nano titania in water.

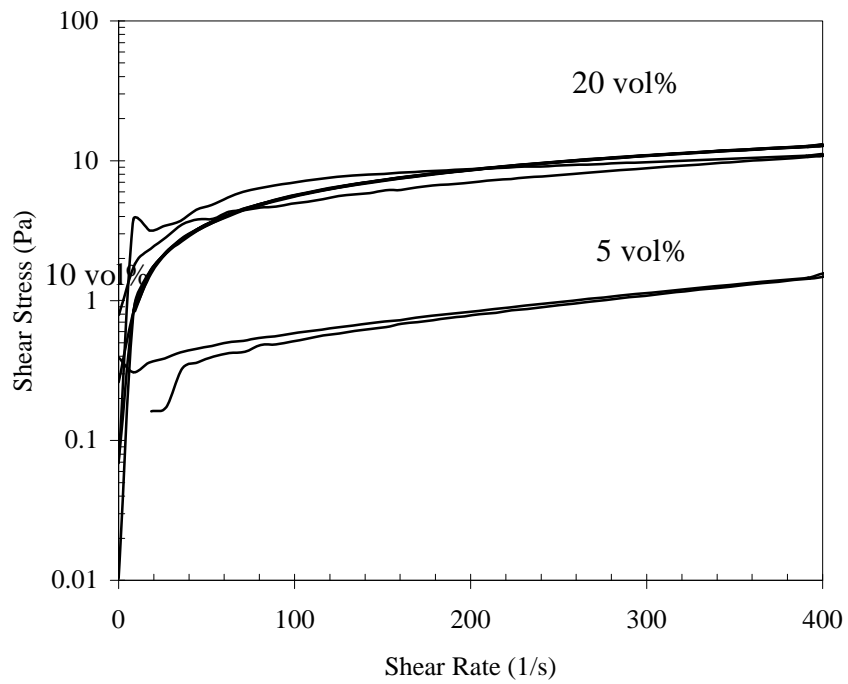


Figure 2. The thixotropy curves of nano titania without fructose and with pH adjustment.

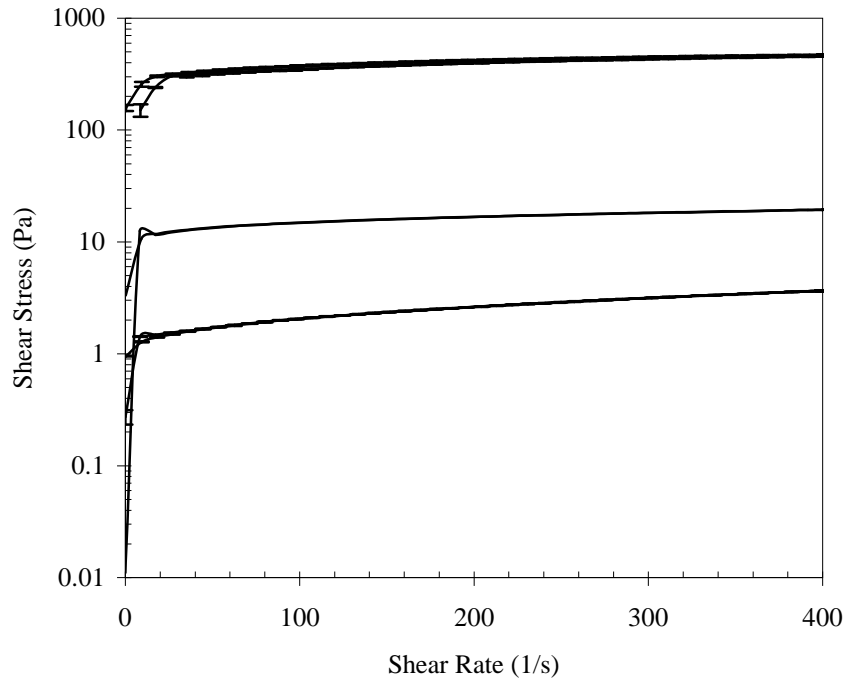


Figure 3. The thixotropy curves of pH adjusted nano titania in 1 wt% fructose solution.

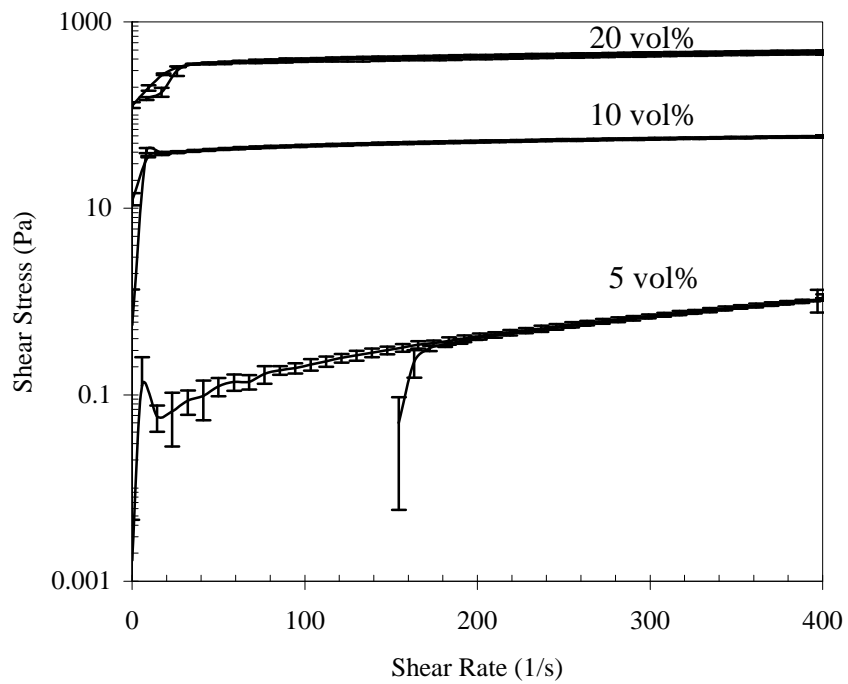


Figure 4. The thixotropy curves of pH adjusted nano titania in 4 wt% fructose solution.

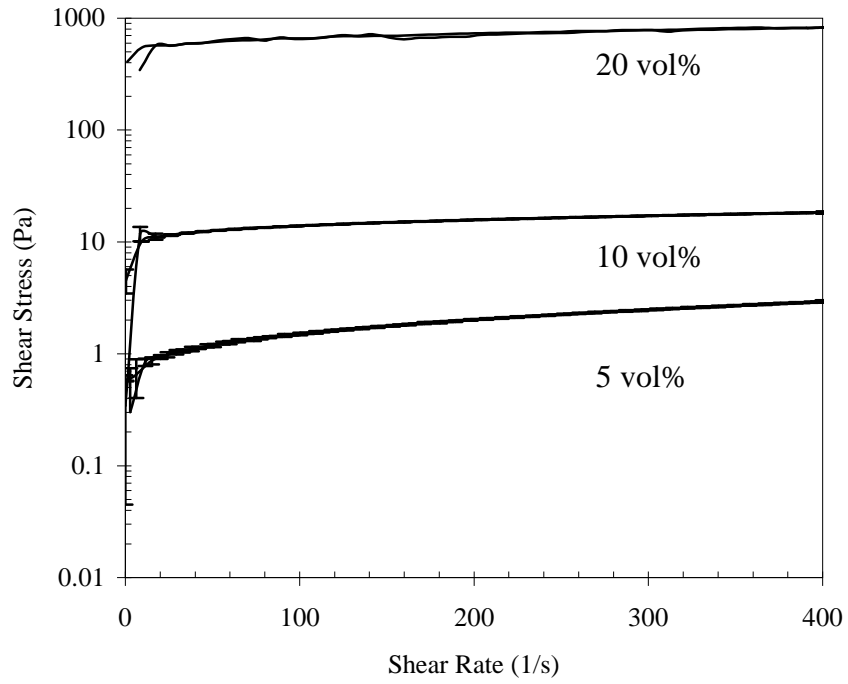


Figure 5. The thixotropy curves of pH adjusted nano titania in 10 wt% fructose solution.

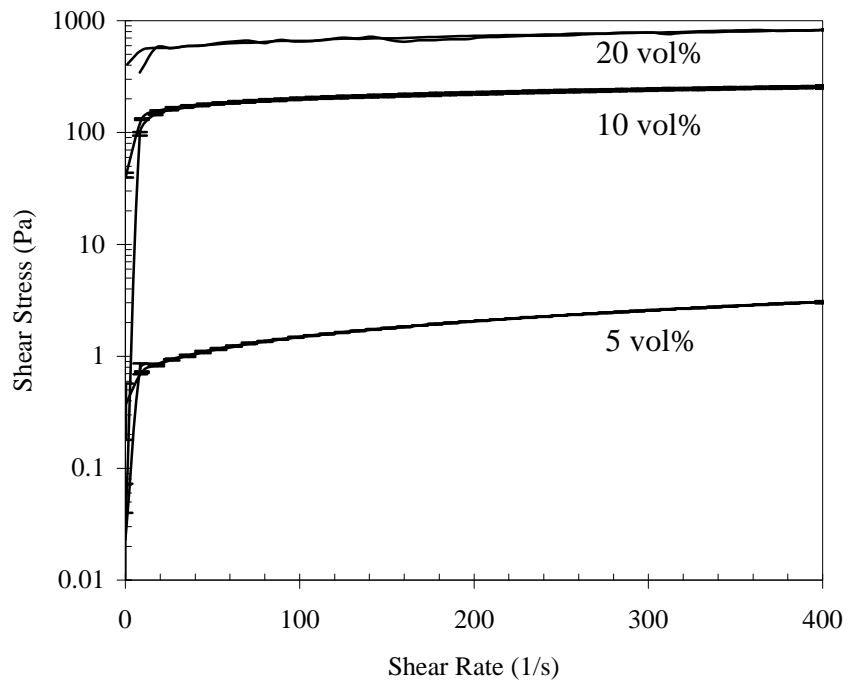


Figure 6. The thixotropy curves of pH adjusted nano titania in 20 wt% fructose solution.

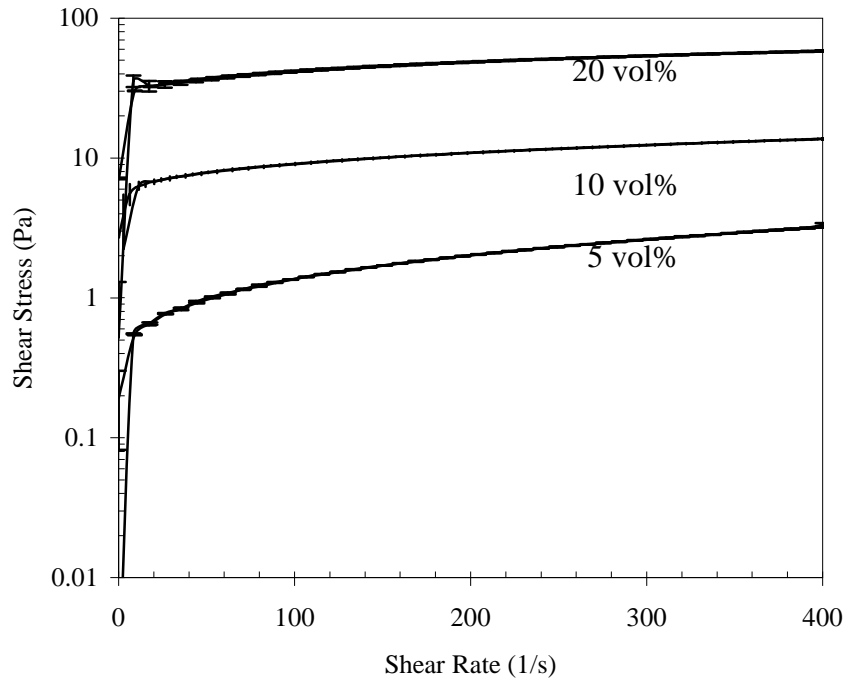


Figure 7. The thixotropy curves of pH adjusted nano titania in 30 wt% fructose solution.

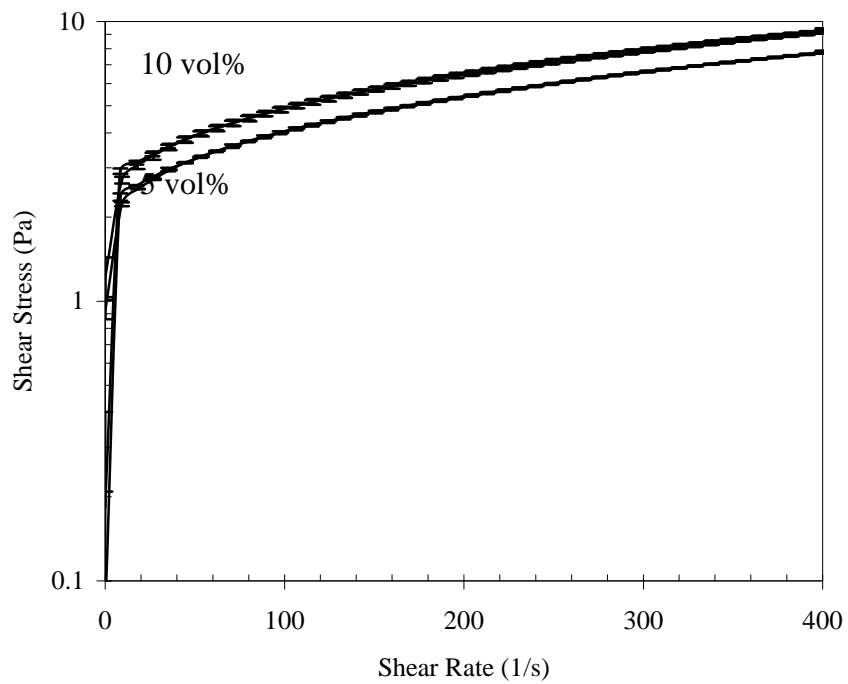


Figure 8. The thixotropy curves of pH adjusted nano titania in 40 wt% fructose solution.

D.3. The stress sweeps

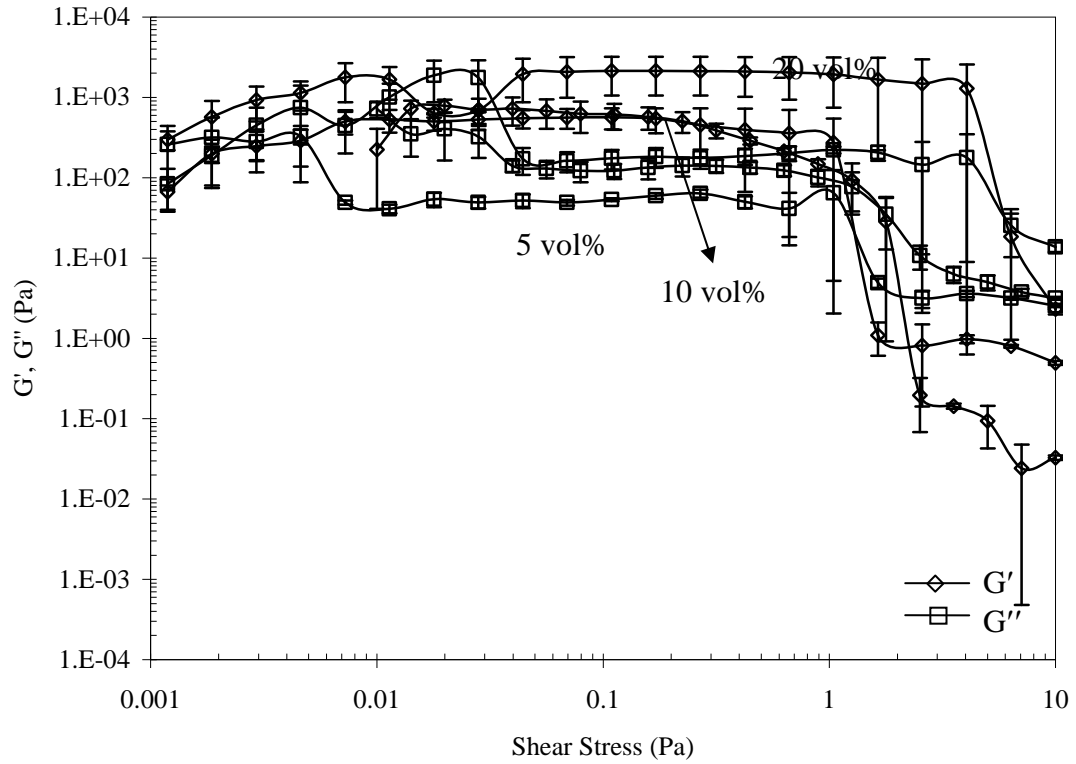


Figure 1. The stress sweeps of nano titania dispersions in water.

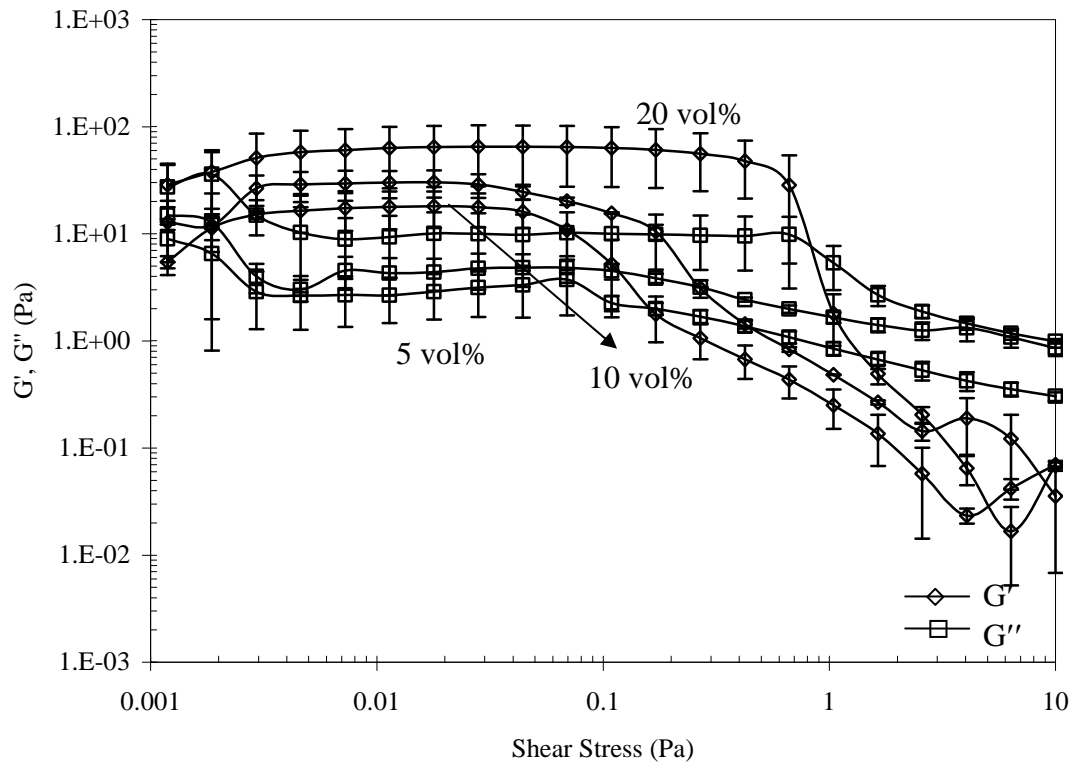


Figure 2. The stress sweeps of nano titania dispersions without fructose and with pH adjustment.

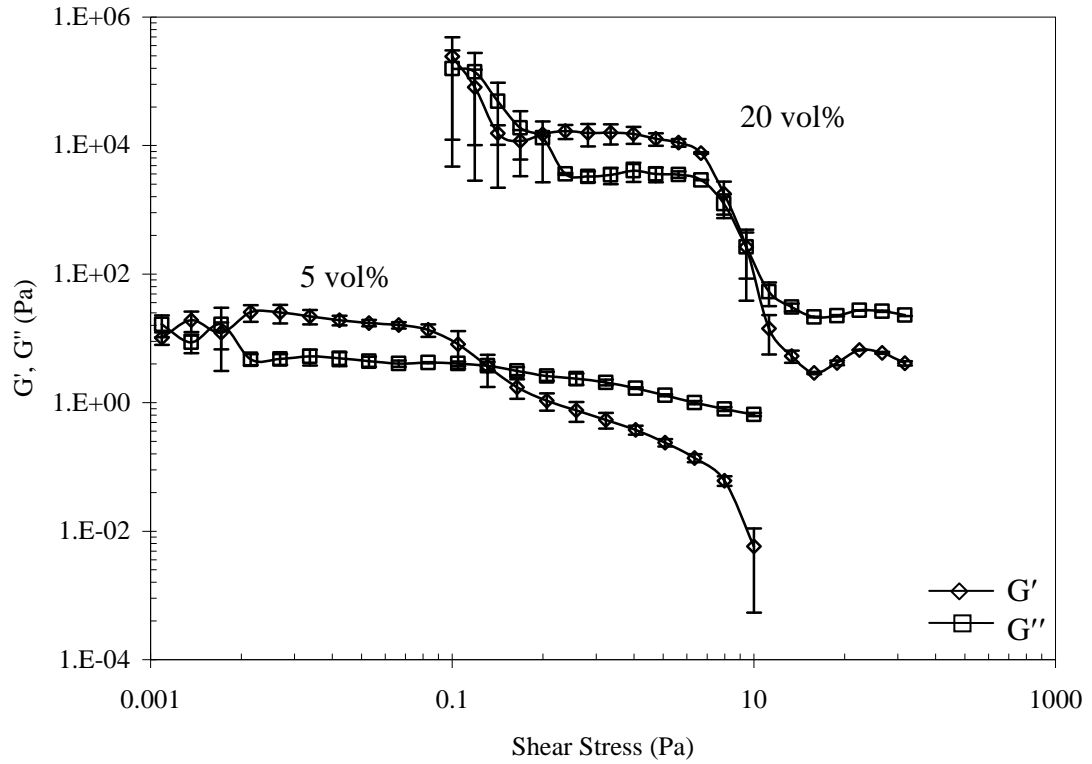


Figure 3. The stress sweeps of pH adjusted nano titania dispersions in 1 wt% fructose solution.

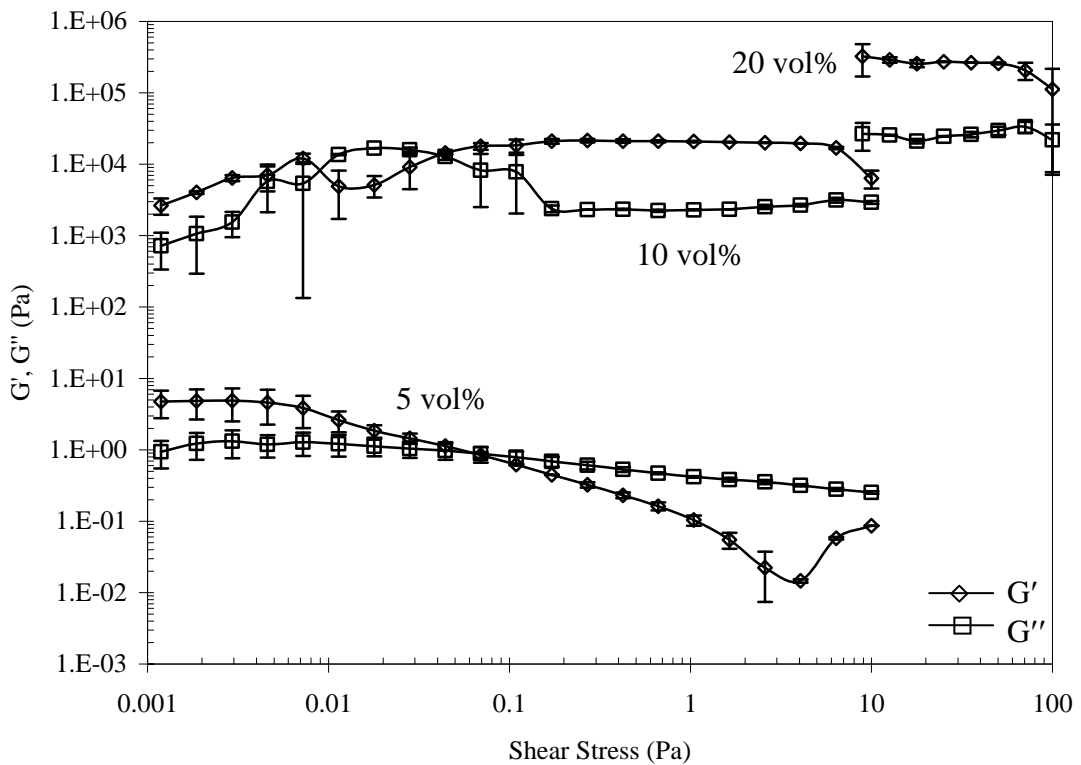


Figure 4. The stress sweeps of pH adjusted nano titania dispersions in 4 wt% fructose solution.

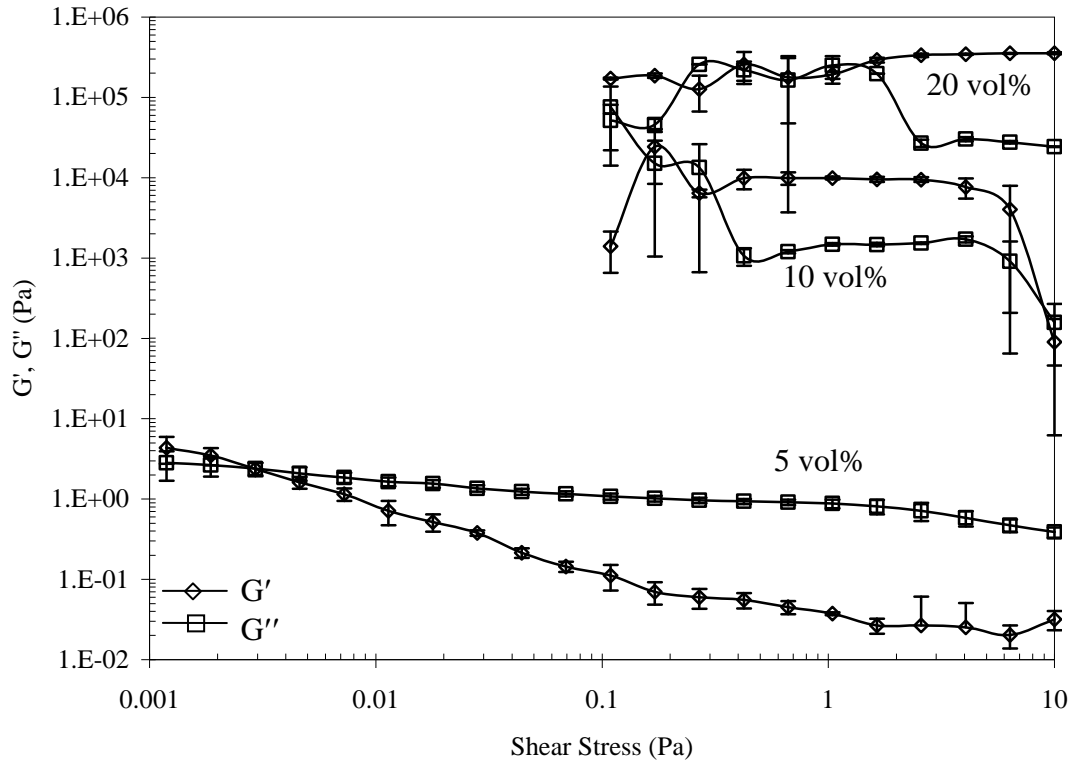


Figure 5. The stress sweeps of pH adjusted nano titania dispersions in 10 wt% fructose solution.

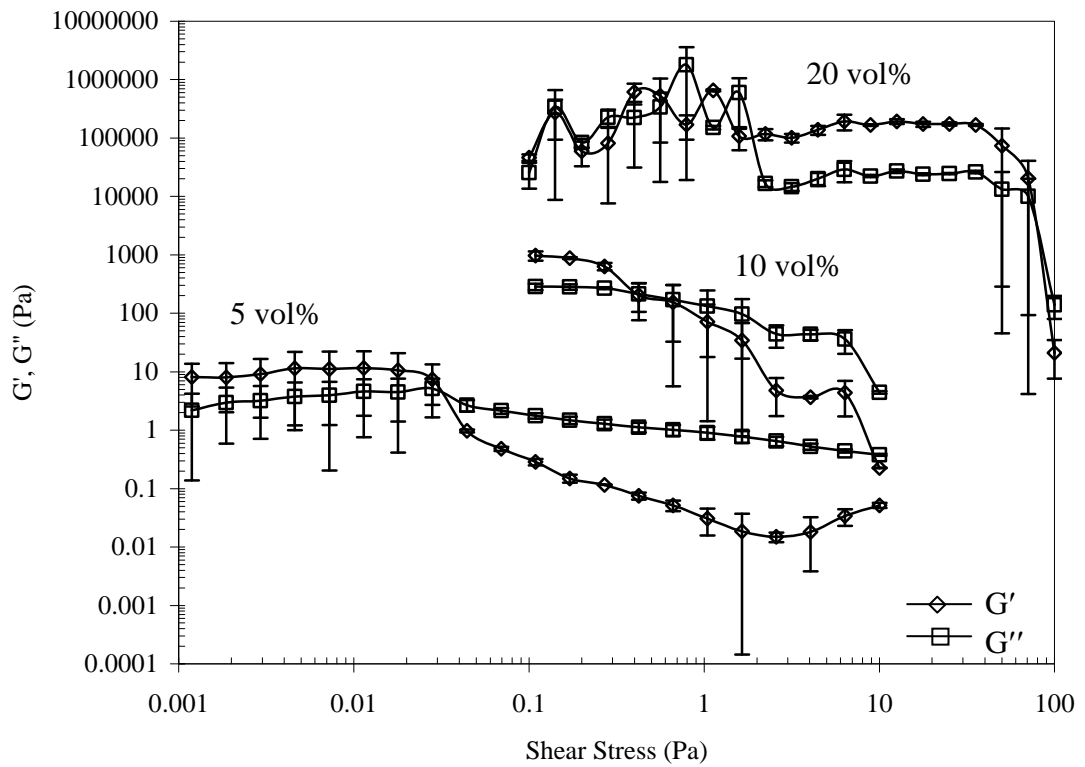


Figure 6. The stress sweeps of pH adjusted nano titania dispersions in 20 wt% fructose solution.

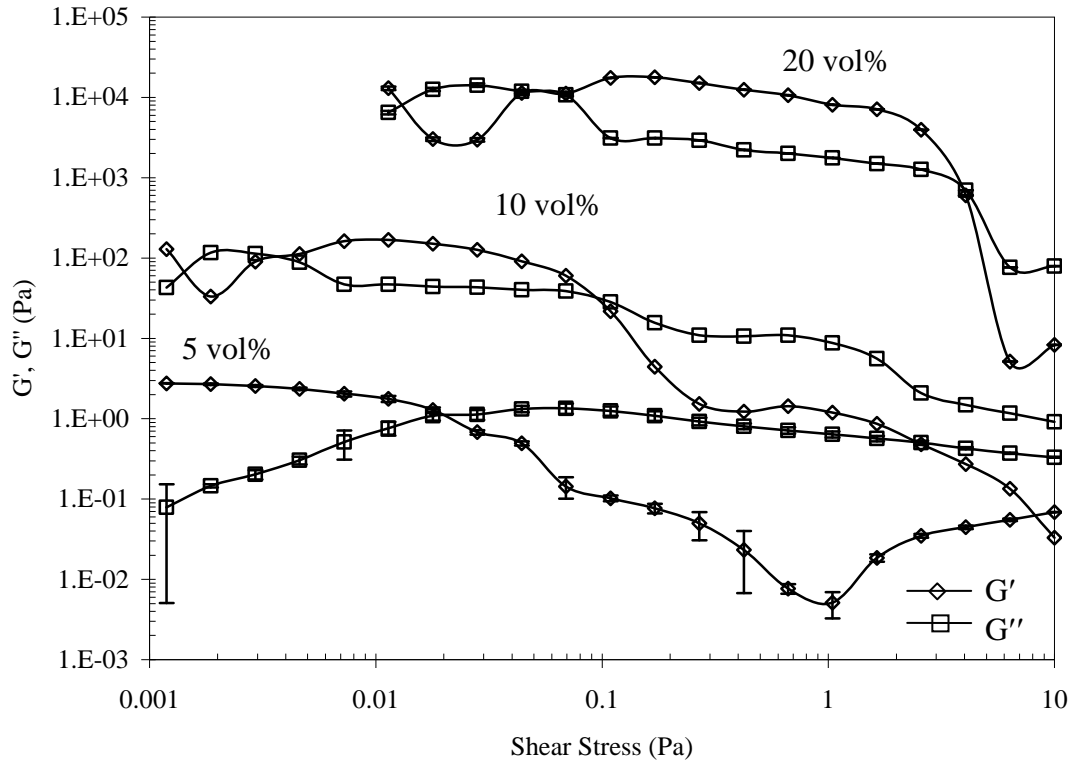


Figure 7. The stress sweeps of pH adjusted nano titania dispersions in 30 wt% fructose solution.

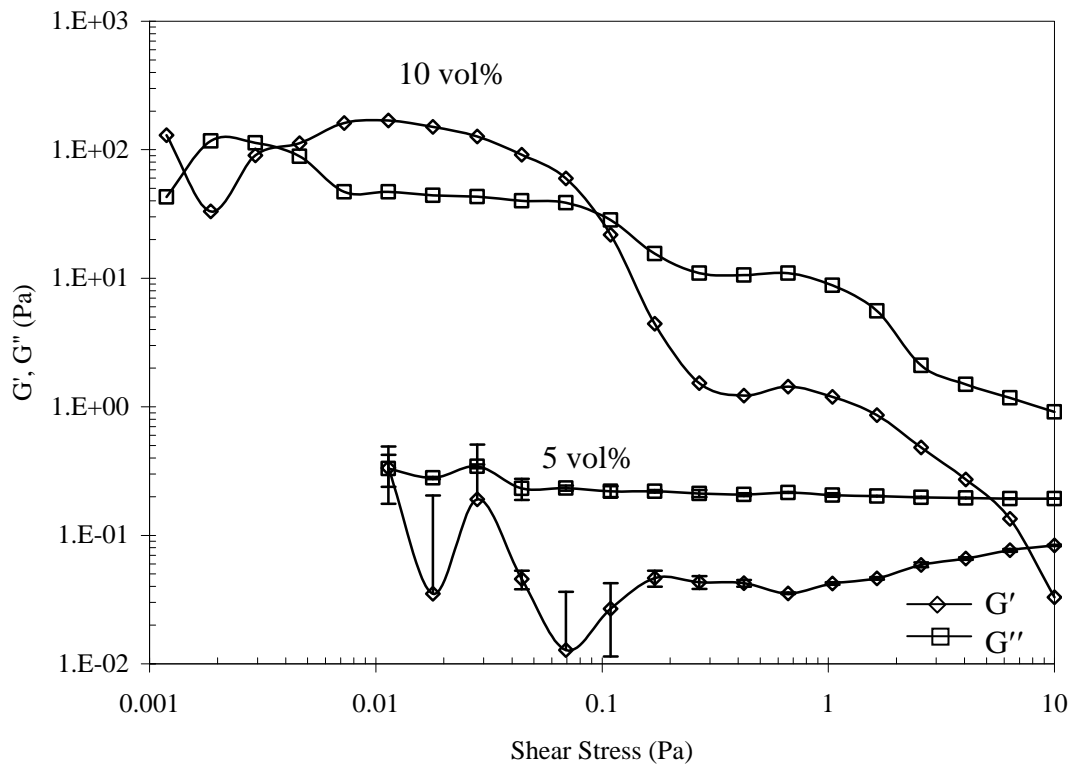


Figure 8. The stress sweeps of pH adjusted nano titania dispersions in 40 wt% fructose solution.

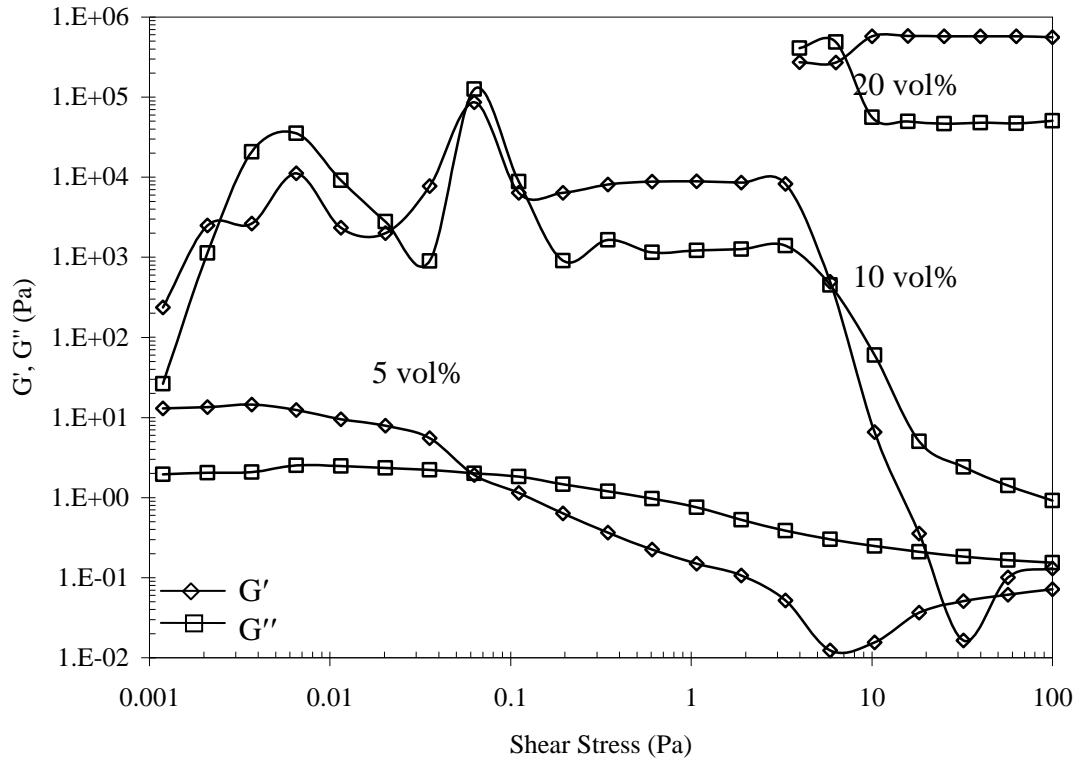


Figure 9. The stress sweeps of nano titania dispersions in 10 wt% fructose solution.

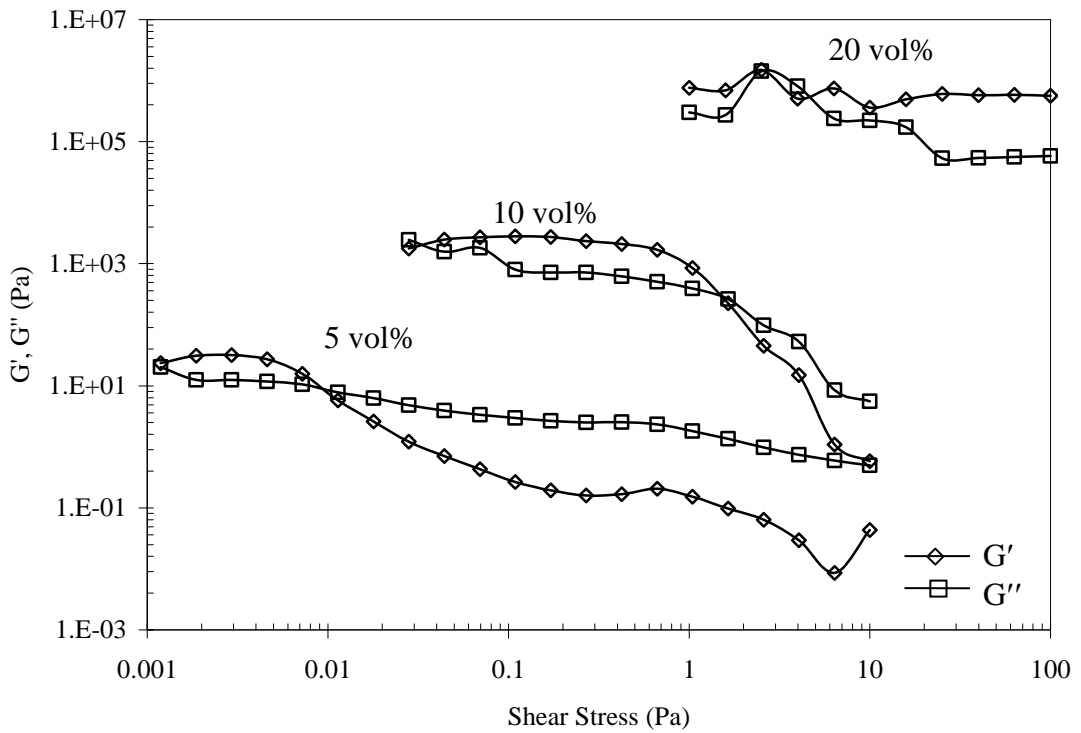


Figure 10. The stress sweeps of nano titania dispersions in 20 wt% fructose solution.

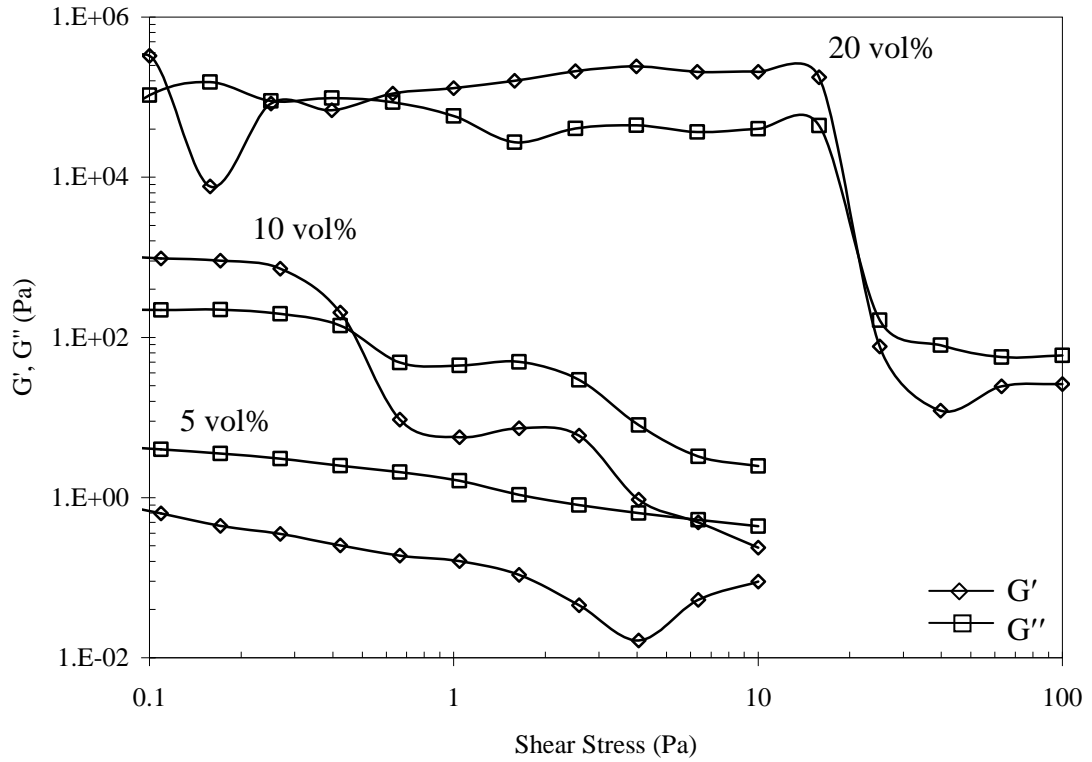


Figure 11. The stress sweeps of nano titania dispersions in 30 wt% fructose solution.

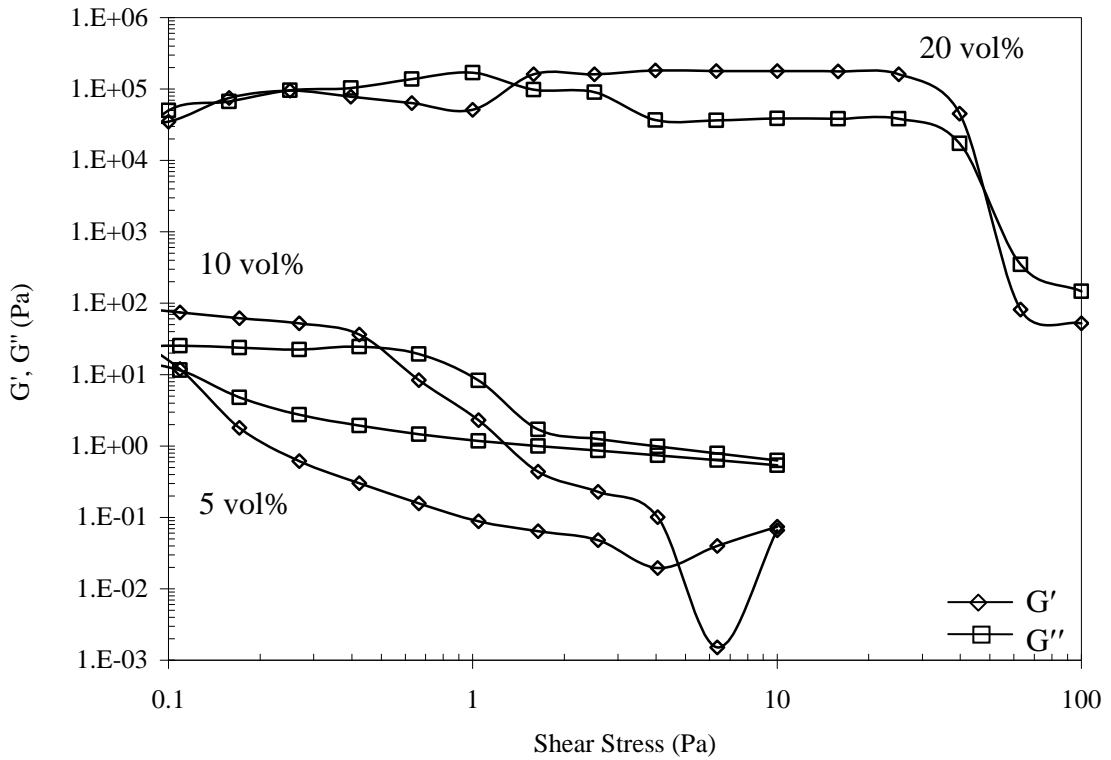


Figure 12. The stress sweeps of nano titania dispersions in 40 wt% fructose solution.

D.4. The frequency sweeps

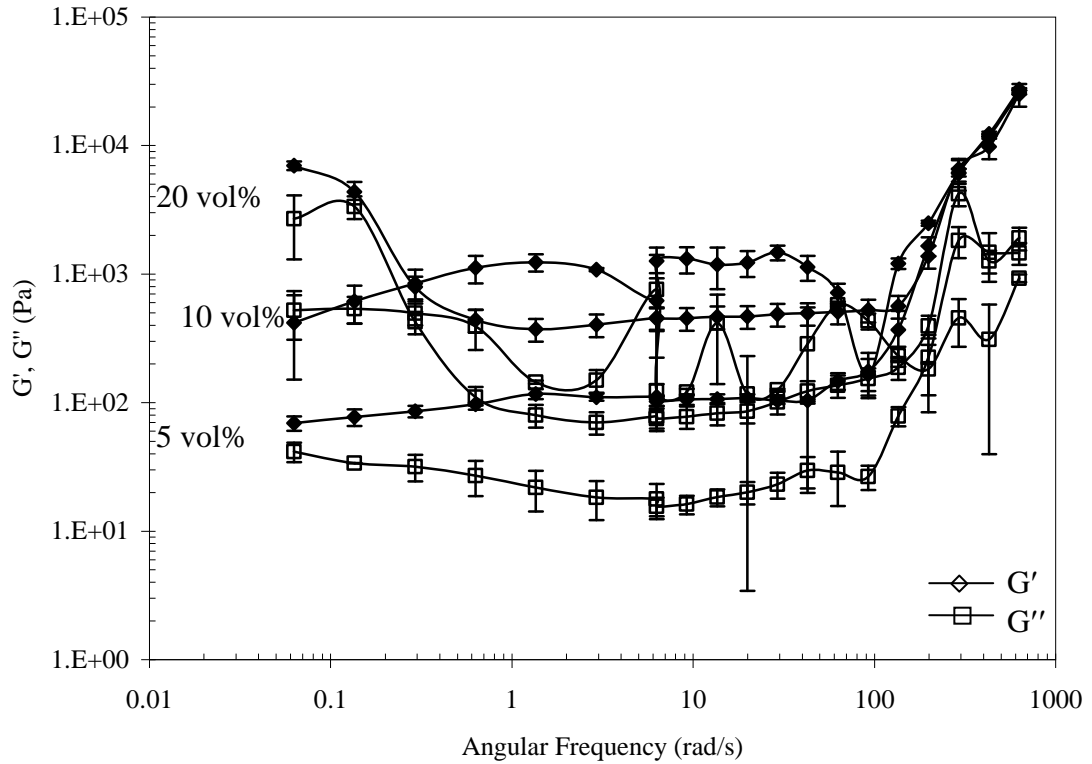


Figure 1. The frequency sweeps of nano titania dispersions in water.

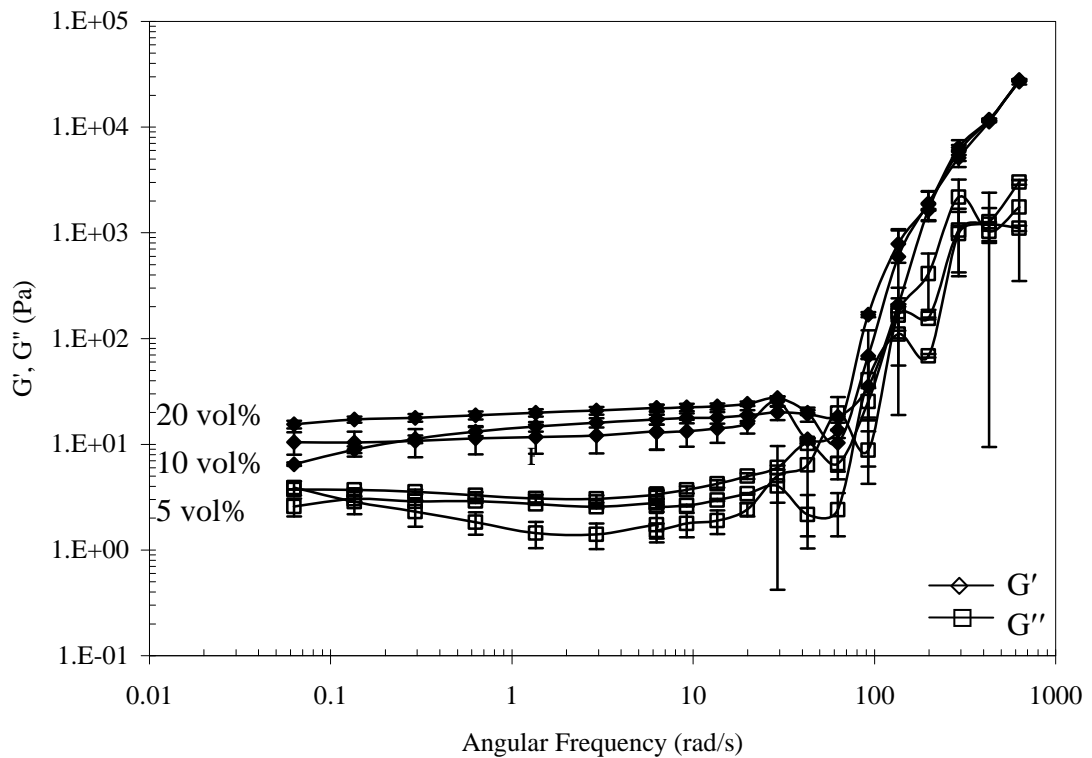


Figure 2. The frequency sweeps of nano titania dispersions without fructose and with pH adjustment.

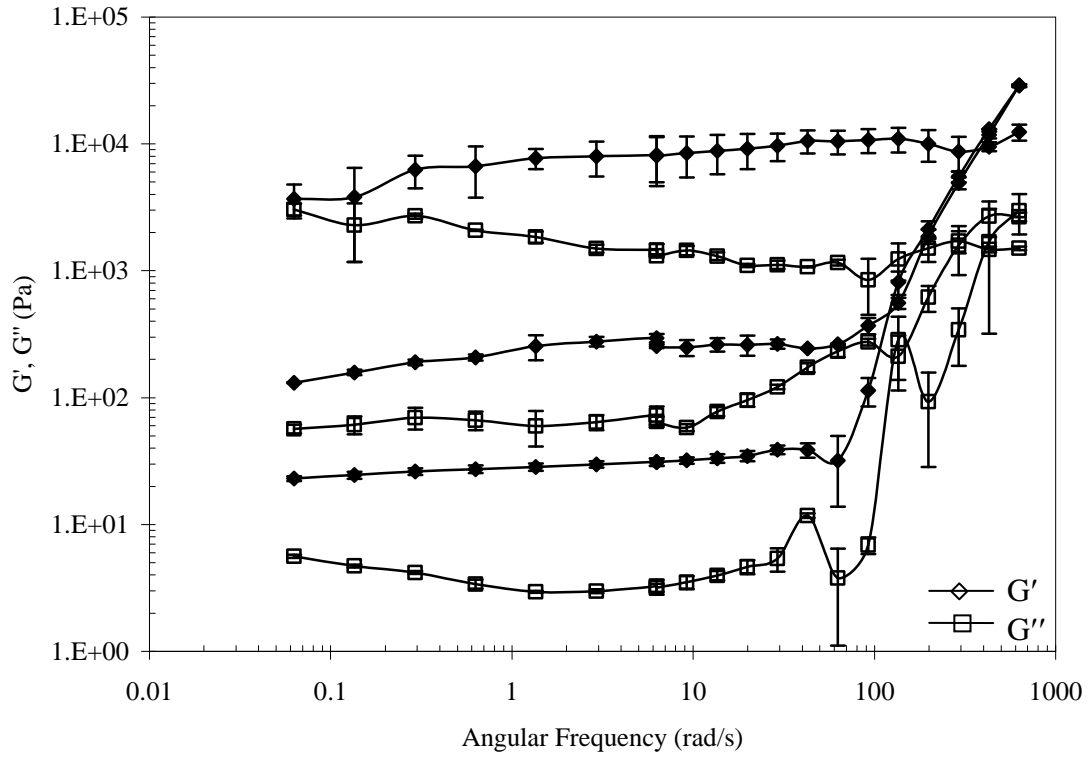


Figure 3. The frequency sweeps of pH adjusted nano titania dispersions in 1 wt% fructose solution.

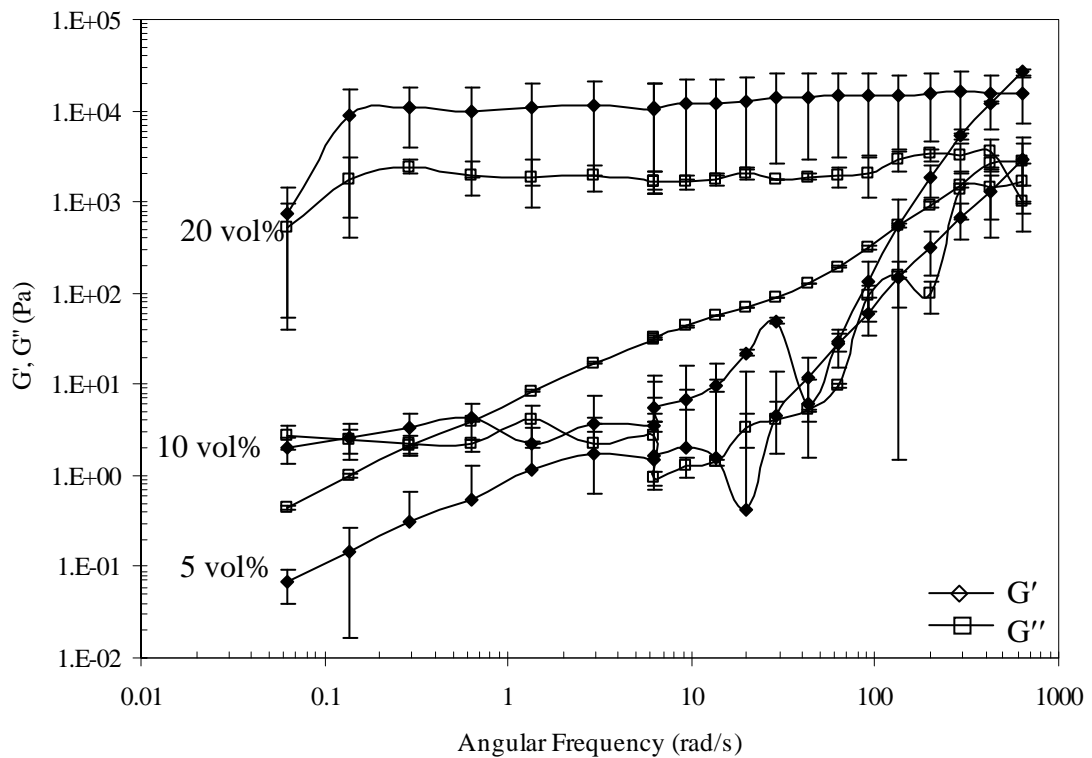


Figure 4. The frequency sweeps of pH adjusted nano titania dispersions in 4 wt% fructose solution.

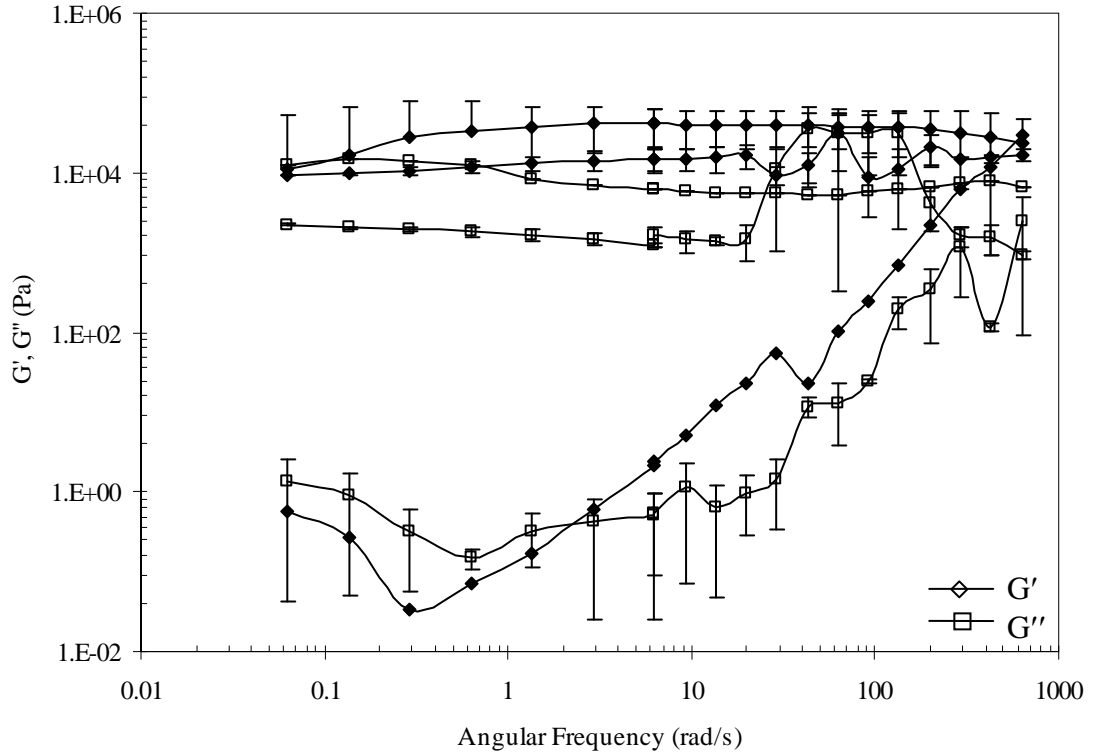


Figure 5. The frequency sweeps of pH adjusted nano titania dispersions in 10 wt% fructose solution.

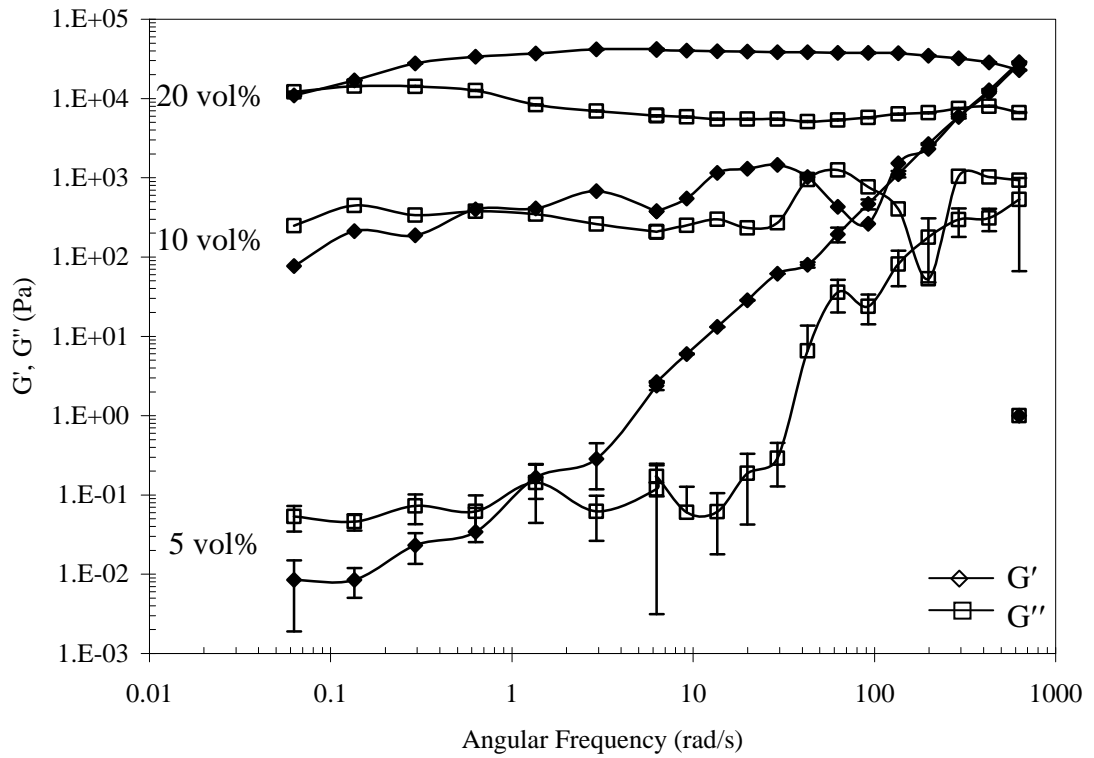


Figure 6. The frequency sweeps of pH adjusted nano titania dispersions in 20 wt% fructose solution.

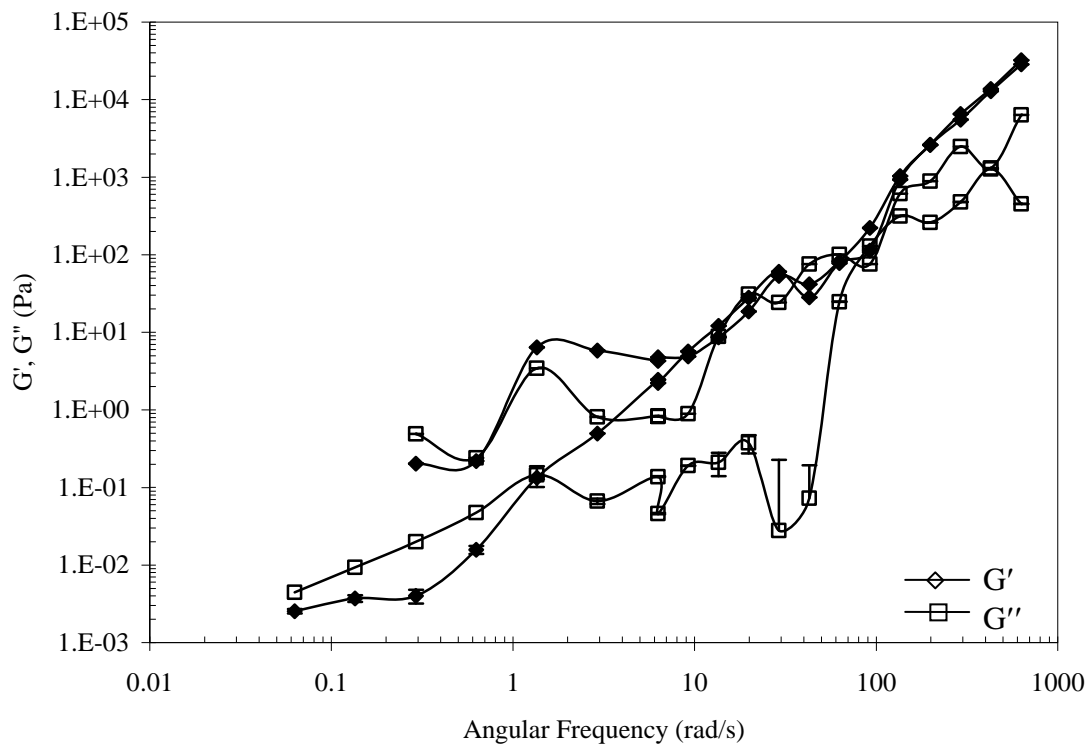


Figure 7. The frequency sweeps of pH adjusted nano titania dispersions in 30 wt% fructose solution.

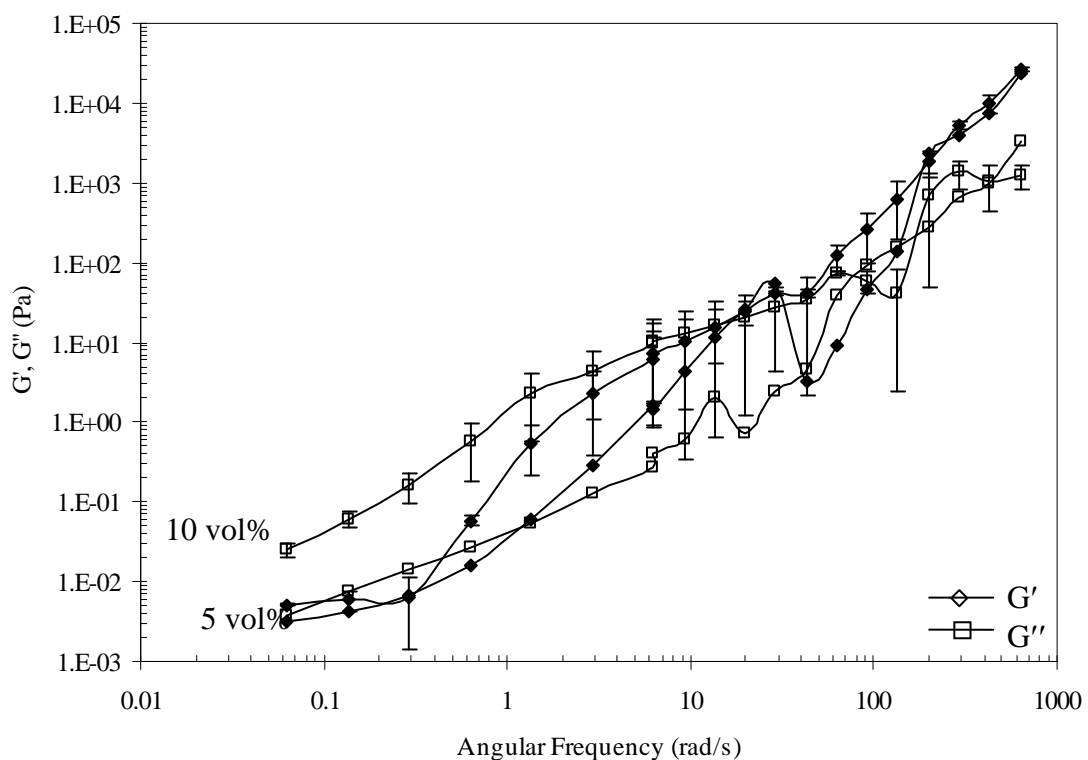


Figure 8. The frequency sweeps of pH adjusted nano titania dispersions in 40 wt% fructose solution.

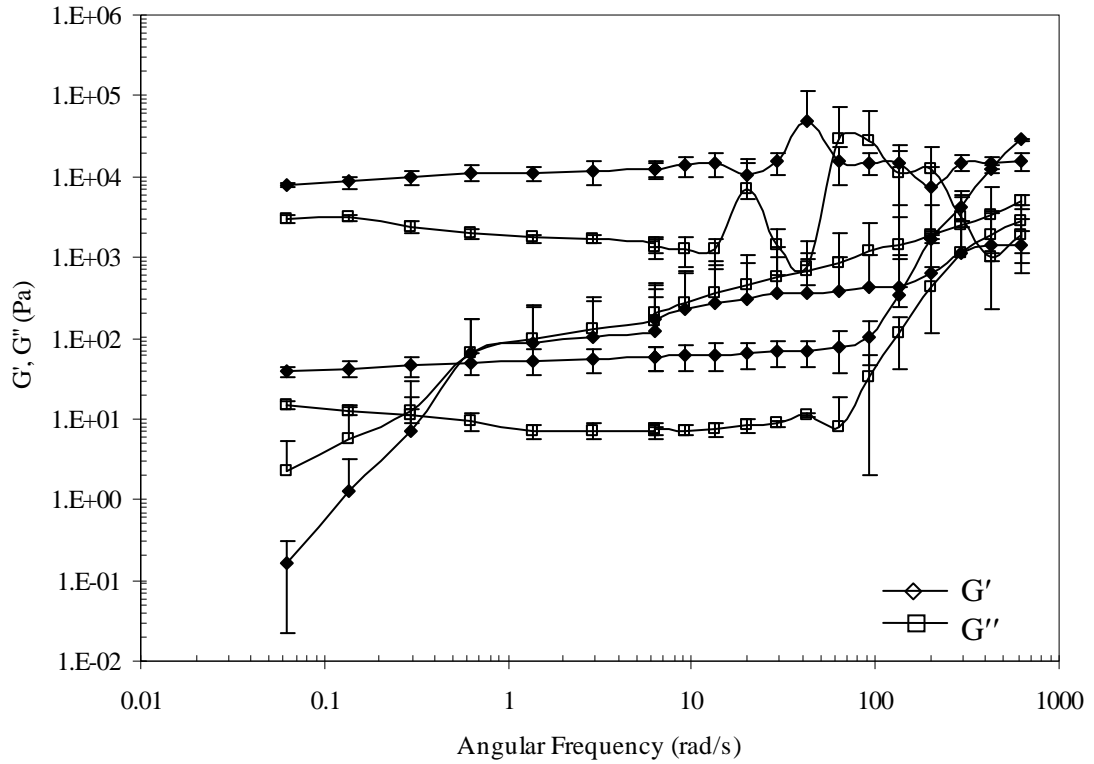


Figure 9. The frequency sweeps of nano titania dispersions in 10 wt% fructose solution.

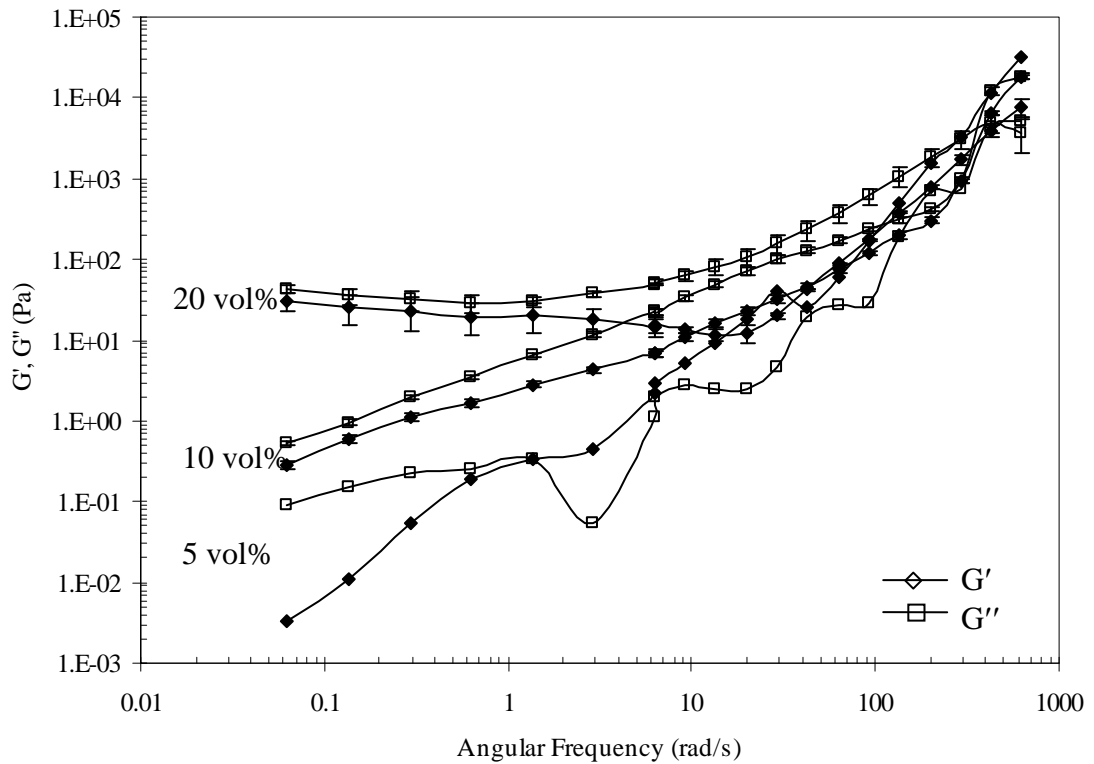


Figure 10. The frequency sweeps of nano titania dispersions in 20 wt% fructose solution.

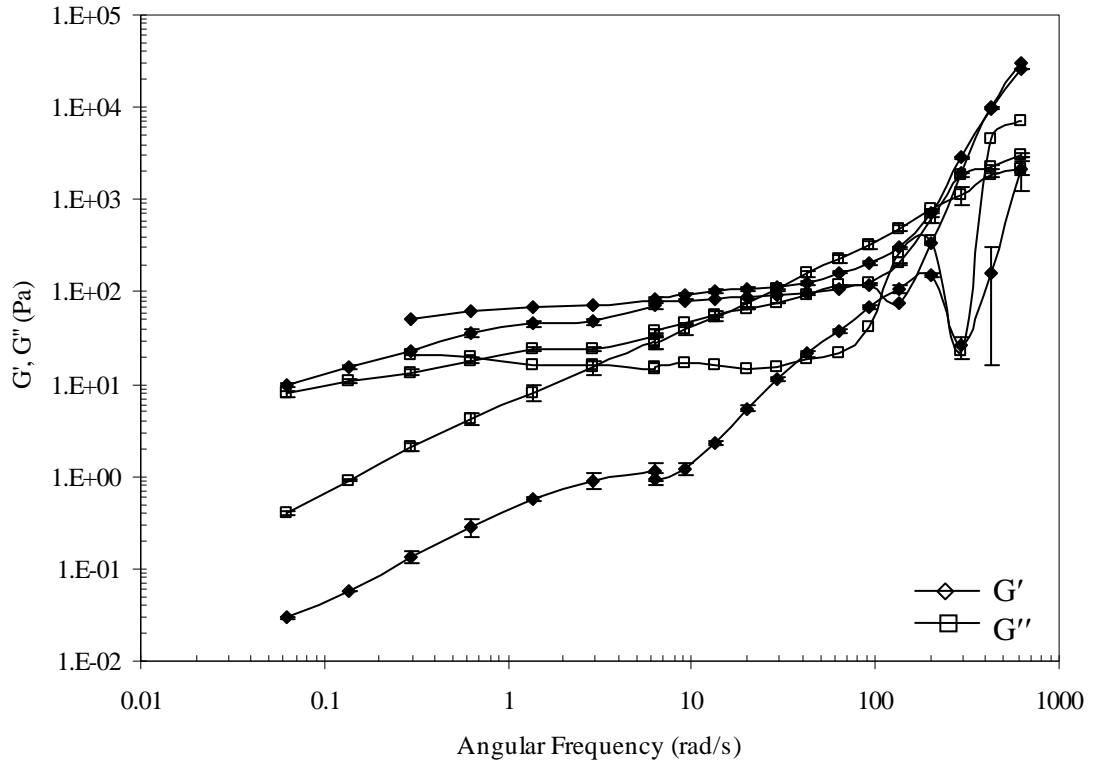


Figure 11. The frequency sweeps of nano titania dispersions in 30 wt% fructose solution.

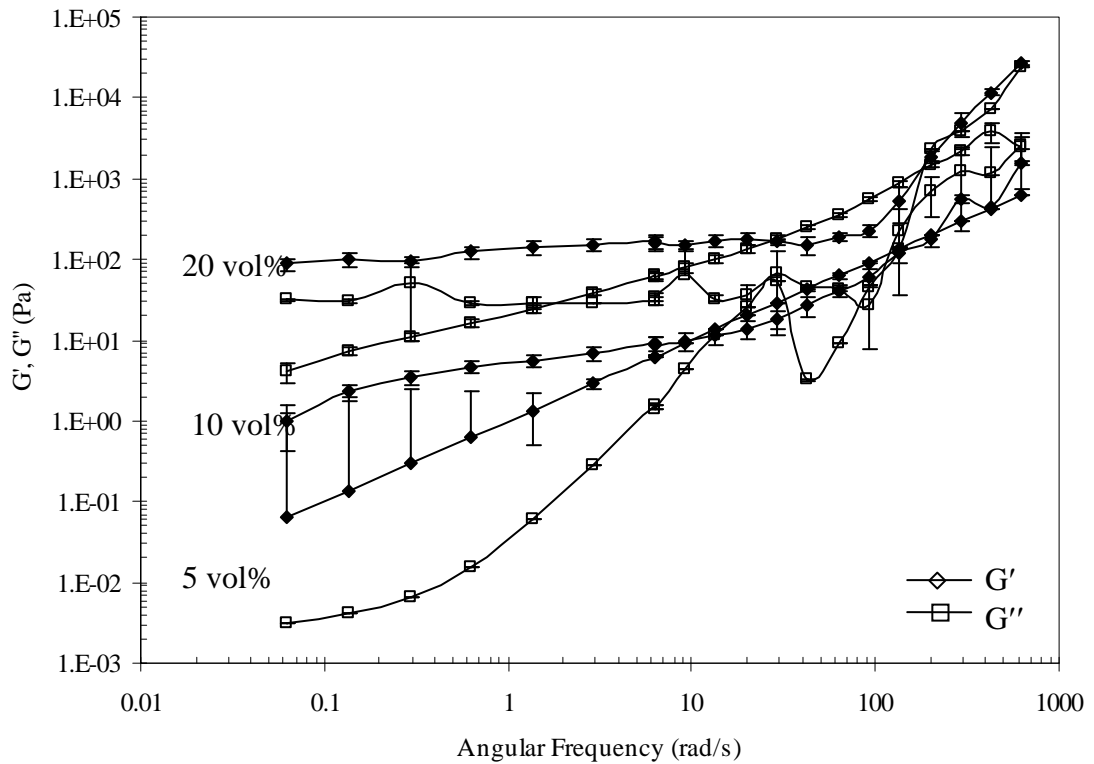


Figure 12. The frequency sweeps of nano titania dispersions in 40 wt% fructose solution.

ÖZLEM ÇAĞLAR DUVARCI

Date of Birth: Feb 07, 1973

Place of Birth: İzmir/Turkey

Citizenship: Turkish

EDUCATION

[1990-1996] B.Sc. (Chemical Engineering)

Ege University

Department of Chemical Engineering, İzmir, Turkey

[1996-1999] M.Sc. (Material Science and Engineering Programme)

İzmir Institute of Technology

Department of Material Science and Engineering, İzmir, Turkey

Dissertation: The Preparation Characterization and Sintering Behavior of Nanocrystalline Ceramics

Advisor: Prof. Dr. Muhsin Çiftçioğlu

İzmir Institute of Technology

[2002-2009] Ph.D. (Chemical Engineering)

Department of Chemical Engineering, İzmir, Turkey

Dissertation: Rheological Behavior of Nanocrystalline/Submicron Ceramic Powder Dispersions

Advisor: Prof. Dr. Muhsin Çiftçioğlu

PUBLICATIONS

Duvarci, Ö.Ç., Çiftçioğlu, M., Güden, M., (2004). Preparation and Microstructural Development of Nanocrystalline Titania and Alumina. *Key Engineering Materials*, 264-268, 2355-2358

Duvarci, Ö.Ç., Akdeniz, Y., Özmihçı, F., Ülkü, S., Balköse, D., Çiftçioğlu, M. (2007) “Thermal behaviour of a zeolitic tuff. *Ceramic International*, Volume 33 (5) 795-801